UNIVERSITY OF BIRMINGHAM

How to formulate for structure and texture via 3D-printing:

Design and characterisation of edible and printable feedstock - dairy gels

by

Kilian Josef Daffner

A thesis submitted to
The University of Birmingham
for the degree of
DOCTOR OF PHILOSOPHY

School of Chemical Engineering
College of Physical and Engineering Sciences
The University of Birmingham
November 2020

Abstract

3D-printing of food is a novel and promising technology capable of creating individualised foods differing in composition, texture, taste or shape. Objects are created layer-by-layer and the most common additive manufacturing technique for food relies on an extrusion process. In order to formulate for structure and texture of food objects via a printing process, in-depth understanding of the solidification mechanism and the material properties is of highest importance. While most of the current research on extrusion printing focuses on pastes and gels, which maintain their shape due to a yield stress, the key challenge of this work lies in a fast, local and irreversible transition of the feedstock from a solution (sol) to a gel. High dairy protein-based materials, which offer health benefits and have high satiating effects, were used to create and tailor novel edible formulations for applications in thermal extrusion printing.

First, characterisation of a solidification mechanism suitable for thermal printing of high dairy protein-based feedstock including a fast sol−gel transition was conducted. Investigation of the pH−temperature (T)-route, cold acidification followed by heating, on the rheometer provided evidence that the temperature–time profile used to trigger gelation was comparable to 3D-printing but without superimposed flow. The sol–gel transition temperature as determined by rheology was used to mimic dynamic conditions during printing by applying a steep temperature gradient. Firm gels were produced and classified regarding their physical properties and status around the sol–gel transition. Formulations showing preferable characteristics, including a low storage modulus G' (~ 0.1 Pa) at low temperatures (2°C) followed by a steep increase of G' during sol–gel transition, were considered to be suitable feedstock for applications in thermal extrusion 3D-printing.

Second, the two main dairy proteins (micellar casein and whey protein) were combined to create and to tailor novel edible casein−whey protein suspensions. These formulations were characterised regarding their potential use for extrusion-based 3D-printing and several design rules

were established. Sol−characteristics at low temperature (2°C) were confirmed, providing a liquid feedstock which could be transferred into a gel via the pH−T-route. The pH at heating during denaturation of the whey proteins as well as the overall protein content were crucial parameters to change the microstructure of casein−whey protein suspensions, e.g. resulting in unwanted pre−gelation (G' > 1 Pa) at too high protein contents. Formulations with depleted casein micelles (CM), caused by desired dissociation of κ-casein at increased pH at heating, showed lower sol−gel transition temperatures and increased aggregation rates. The aggregation rate (represented by the storage modulus G') was proposed as a first good indicator for the printability of high dairy protein-based formulations.

Furthermore, for the creation of more complex and novel edible formulations, dairy fat was added to casein−whey protein suspensions. The additional product parameter, fat, changed the microstructure as the overall total solid content of the formulations increased. Mechanical treatment was necessary to obtain smaller milk fat particles (< 1 µm) covered with protein, which could mimic the protein behaviour and actively contribute as pseudo-proteins to the gelation process via the pH−T-route. With increasing pH at heating, more depleted casein micelles were found on the surface of mechanically treated fat globules, causing a decrease in the sol−gel transition temperature and an increase in the aggregation rate. At a higher pH at heating, more particles contributed to the gelation per unit area and the surface properties of the fat globules covered with certain proteins, e.g. κ-casein depleted CM, were favourable, shown via electrophoresis and a newly developed protocol for low dose transmission electron cryogenic microscopy. Several protein−fat formulations with promising aggregation rates could be printed.

Overall, this thesis demonstrates that high dairy protein-based formulations with and without additional fat can be used as a novel feedstock for thermal extrusion 3D-printing applications via the pH−T-route, if product- and process parameters are precisely adjusted, and all the established design rules are adhered to.

Acknowledgements

With the PhD thesis at hand an interesting and exciting stage of my life comes to an end. At this point, I would like to express a few words of thanks to those people who have contributed to the completion of this thesis at The University of Birmingham, School of ChemEng.

Firstly, I would like to express my sincere gratitude to my primary advisor Dr Tom Mills. I highly appreciate his knowledge and instructive comments in the laboratory as well as his expert guidance throughout countless discussions and meetings. Furthermore, I would like to thank Prof Dr Ian Norton, my second supervisor, for allowing me to be part of his highly reputable group. Many thanks for all the help and guidance throughout my research time, including discussing my work and allowing me so much freedom within my research. I will always be very grateful having had the chance to learn from both of them.

My appreciation also extends to my "mentors", two amazing scientists who supported me so much during my PhD. Firstly, Dr Stefan Nöbel (The University of Hohenheim; Max Rubner-Institute) whom I know now since around five years and who aroused my interest in 3D-printing of food materials. All our discussions, meetings and collaborations helped me so much to better understand my topic and to become a better researcher. Secondly, Prof Dr Sally Gras (The University of Melbourne), who offered me to be a temporary part of her team in The Bio 21 Dairy Research Hub in Melbourne. I highly appreciate all the support, all the discussions about my work, especially about microscopy, and all the reviewing of parts of my work.

I take this opportunity to record my sincere thanks to all the members of the Food Microstructure Group for their encouragement, help and support within the last three years. A special thanks go to Prof Dr Eddie Pelan and Dr Fotis Spyropoulos for all the stimulating discussions around my work. Furthermore, I want to thank my Postdoc Dr Saumil Vadodaria for helping me building up the 3D-printing construction and reviewing parts of the final thesis. Moreover, I want to thank everyone in Prof Dr Gras' group at The University of Melbourne, as I had an absolutely amazing time in "Oz", as well as Prof Dr Eric Hanssen. I'm also very thankful to Dr Heiko Fuhrmeister and Dr Ulrich Metzger (UTM) for providing all my powders. Thanks to all the super friendly staff in ChemEng, especially Lynn and Chris.

I am deeply indebted to my family, especially to my parents. Thank you for the support at any time over the last ten years, especially at The University of Birmingham throughout this PhD, my studies and life in general. I will always appreciate your support and love. Many thanks to my friends Martin, Holger, Horst, Saul, Ben, Patrick and Marcel as well as Ann-Sofie.

Per ardua ad alta.

Per aspera ad astra.

Perseverantia vincit.

Non est ad astra mollis e terris via.

Table of Contents

List of Tables

List of Figures

Abbreviation and nomenclature list

Abbreviations

ABS	acrylonitrile-butadiene-styrene
ALM	additive layered manufacturing
AM	additive manufacturing
CAD	computer aided design
CLSM	confocal laser scanning microscopy
CM	casein micelles(s)
c_p	protein content
cryo-EM	cryogenic transmission electron microscopy
CS	casein
FFF	fused filament fabrication
FTIR	Fourier transform infrared spectroscopy
FDM	fused deposition modelling
FLM	food layered manufacturing
G’	storage modulus
G’’	loss modulus
HME	hot melt extrusion
IEP	isoelectric point
LB	liquid binding
LOM	laminated object manufacturing
MCC	micellar casein concentrate
MF	microfiltration
MFG	milk fat globule
MFGM	milk fat globule membrane
NTC	negative temperature coefficient thermistor
pH−T-route	pH−temperature-route
PLA	polylactic acid
SDS-PAGE	sodium dodecyl sulphate polyacrylamide gel electrophoresis
SEM	scanning electron microscopy
SHASAM	selective hot air sintering
SLA	stereolithography

SLS	selective laser sintering
SME	soft materials extrusion
T	temperature
TEM	transmission electron microscopy
$T_{sol-gel}$	sol−gel transition temperature
WP	whey protein
WPI	whey protein isolate
3D-printing	three-dimensional printing
δ	phase-/loss angle

Nomenclature

A	m^2	Area
d	m	diameter
k	$W\ m^{-1}\ K^{-1}$	Thermal transmission coefficient/ overall heat transfer coefficient
l	m	Length
$\dot{Q}$	W	Heat transfer rate
r	m	Radius of the pipe
Re	-	Reynolds number
dT/dx	$K\ m^{-1}$	Temperature gradient
$\Delta T/\Delta T_M$	K	Logarithmic mean temperature difference
v	$m\ s^{-1}$	Velocity
$\dot{V}$	$m^3\ s^{-1}$	Volume flow
η	$kg\ m^{-1}\ s^{-1}$	Dynamic viscosity
ν	$m^2\ s^{-1}$	Kinematic viscosity
ρ	$kg\ m^{-3}$	Density
τ	Pa	Oscillatory stress
γ	%	Deformation
$\dot{\gamma}$	s^{-1}	Shear rate
ω	$rad\ s^{-1}$	Angular velocity/ frequency
% (w/w)	% (g/100 g)	Percent by weight

1 Chapter:

Introduction

1.1 Project context

"Tea, earl grey, hot" at the touch of a single button. Imagine a replicator machine, capable of turning molecules into drinks or meals, e.g. producing cups of fresh tea. So far, this machine, a "food synthesizer", was only available for use in the famous science fiction television series *Star Trek* from the 1970's. Although research in the area of 3D-printing of food, called food layered manufacturing (FLM), has been conducted for more than ten years and knowledge is increasingly expanded, scientists are far away from reaching such an advanced level of production of food grade materials.

In general, 3D-printing or additive layered manufacturing (ALM) is a digitally controlled, robotic construction technology which deposits materials layer-by-layer to build a three-dimensional object (Wegrzyn et al. 2012). In the 1980's, 3D-printing of plastic-based materials was started and emerged over time, with stereolithography as the first technique (Hull, 1986). Recently, polymers, ceramics, metals or waxes are used for printing purposes in different industries (including motor vehicles, aerospace and medical applications) to manufacture complex parts as a single item. For this traditional 3D-printing approach, geometric complexity and economy at low volume of production are the two main advantages, which also offer great potential for food applications (Lipton et al., 2015). The current research for food printing is driven forward by the consumer's demand for healthier and customised food options but also by the awareness of a more efficient use of available food resources (Severini & Derossi, 2016).

The printing technology itself with food as a feedstock is still considered to be in its infancy, although ongoing research continues and different types of food were printed in the past, including chocolate (Lanaro et al., 2017; Mantihal et al., 2019), dough snacks (Severini et al., 2018), fish surimi gels (Wang et al., 2018), dairy pastes (Lille et al., 2018) or hydrocolloid based materials (Gholamipour-Shirazi et al., 2019; Warner er al., 2019). Several advantages make FLM an attractive production tool for future applications. This includes individualised

food in different shapes, textures and colours with tailorable nutrients based on personal dietary requirements, reduced storage or distribution costs and reduced food waste (Ross et al., 2019). Moreover, 3D-printing could also be applied as a prototyping tool for the development of novel food products (Sun et al., 2015). Up to now, the technology is not sufficiently advanced yet to be used in mass production (like current manufacturing methods) but can still be used at the point of sale or in houses. In an ideal case for prospective applications, FLM offers a chance to tackle obesity and malnutrition via customised nutrition on the one hand but to end world hunger via less food waste on the other.

However, the current formulation engineering approach of research groups strongly varies, with the majority only presenting suitable formulations or process parameters which have resulted in "successful" printing. But to print objects of high quality, the understanding of the interplay between ingredients, process parameters and equipment design (printer set-up) will be necessary (Cheyne et al., 2005). Common issues why certain formulation (e.g. protein/ carbohydrate content) or process parameters (e.g. print speed, extrusion flow rate) resulted in problems during printing (nozzle plugging, inaccurate printing, etc.) did not receive much attention in previous studies. Therefore, advanced knowledge regarding the design of material characteristics (physical, chemical and mechanical), the adjustment of process parameters and how all these key factors cause printing problems, would be necessary to better understand and define printability as well as further develop formulation engineering.

Due to this lack of information in the current literature about potential formulations (feedstock) (Jiang et al., 2019) and their gelation mechanism as well as their in-depth characterisation before printing, the design and understanding of printable food grade materials has to be driven forward (Derossi et al., 2018). FLM of protein-based materials has a great potential for future applications, as proteins provide essential nutrients for a healthy diet but also contribute to structure and texture in the final product (Nöbel et al., 2018). Only little research has been

published on dairy-based materials for printing purposes so far, mainly due to the complex micro - and nanostructure as well as the high moisture content (up to 90%). There is a high demand for fermented concentrated dairy products, rich in protein, such as Greek yogurt, skyr and fresh cheese in general (Jørgensen et al., 2019), with research being published on the health benefits of milk proteins (Fekete et al., 2013). Following this trend, FLM could offer the possibility to manufacture mass-customised protein-rich (gel-like) dairy products with novel textures, e.g. spheres of a few centimetres sold as snacks, via the pH−temperature (T)-route without using a time-consuming fermentation process (Nöbel et al., 2018).

The long-term success of this technology will rely on a detailed understanding of the material characteristics (physical, chemical and mechanical) and how formulations can be easily manipulated and tailored to make them printable, e.g. matching certain (rheological) requirements including being easily extruded and maintaining the shape after being deposited layer-by-layer (Kim et al., 2017) or having a homogenous composition (Godoi et al., 2016). Although ongoing research is conducted to look into a better understanding of potential feedstock and its characteristics, a lot of work has still to be performed to develop a more advanced library of printable food grade materials and to bring printers to everyone's kitchen.

1.2 Objective of the research

Given the clear gaps in the current literature required for a better understanding of the material characteristics, the aim of this thesis is to contribute detailed knowledge as to why certain formulations are suitable for an extrusion-based 3D-printing process, while others are not. Specifically, proteins are of great use as a feedstock for this technology (Nöbel et al., 2018), as their importance for structure and texture in the final product but also their satiating effect, which is stronger than equivalent quantities of energy from either carbohydrate or fat (Morell & Fiszman, 2017), are well known. Therefore, the understanding of a gelation mechanism and the design of dairy protein-based formulations for application in FLM are conducted in this research.

In-depth understanding of the gelation mechanism from rheological characterisation and how to use this data to mimic extrusion behaviour and flowing conditions during potential 3D-printing applications is of highest importance. The sol−gel transition of dairy materials, triggered via the pH−T-route, is one of the most important parameter that has to be characterised, especially to know how to adjust temperatures during extrusion-based thermal printing (Nöbel et al., 2018). For milk proteins, the sol−gel transition temperature (Hammelehle et al. 1997; Koutina et al., 2014; Schäfer et al., 2018; Vasbinder et al. 2003) and the temperature of aggregation (de Kruif & Roefs, 1996) were studied intensively. The latter parameters will be among a few others (heat rate, particle size, zeta-potential and microstructure) that have to be investigated and understood to implement printing of dairy protein-based formulations.

The characterisation of potentially suitable materials via rheological measurements, e.g. critical shear rate (Kern et al., 2018), phase angle (Gholamipour-Shirazi et al., 2019), or storage modulus G' (Warner et al., 2019), should be conducted first. This will help to understand gelation mechanisms specifically for processes like conveying and extrusion or to find shortcut methods to predict printability before printing through "trial and error" is performed. The possibility of combining the two main dairy proteins, casein and whey protein, to induce a fast and irreversible transition from sol to gel offers great potential for 3D-printing purposes. More complex formulations could be designed (addition of fat, lactose, vitamins, etc.), based on the overall understanding of the gelation kinetics and tuning particle characteristics.

Compared to most of the current research focusing on soft matter extrusion of pastes and gels, the uniqueness of this thesis relies on a sol−gel transition behaviour of the feedstock during printing as well as tailoring of the particles in the nanometre range via process parameters. Small changes in these process parameters help to manipulate formulation characteristics, to trigger gelation and to tailor printability. The results for formulation engineering obtained within this study will provide a framework for investigating the printability of any material

printed via the pH−T-route. Therefore, the overall goal of this work is to design and to characterise edible and printable dairy-based formulations via a suitable gelation mechanism for a better understanding of their material properties regarding applications in thermal extrusion-based 3D-printing.

1.3 Thesis structure

This manuscript is composed of seven chapters including an introduction, a literature survey, four results chapters and a conclusion including future work suggestions. Some overlap in the text is present due to peer-reviewed publications. The details of each publication are located on the front page of the relevant chapter.

- **Chapter 1** is the introduction and explains the project context and the goal of this research.
- The current literature is critically reviewed (**Chapter 2**) to inform the reader and provide the necessary background knowledge to better understand the results section. The main dairy ingredients, protein and fat, as well as 3D-printing itself are explained in great details.
- **Chapter 3** includes the results of a collaboration work on the screening of concentration and pH suitable for temperature triggered gelation via the pH−temperature-route for skim milk retentates. The pH−temperature-route was tested and shown to be a suitable mechanisms for application of thermal extrusion 3D-printing of high dairy protein-based formulations. In-depth characterisation of the material characteristics of casein-based feedstock for food layered manufacturing was conducted.
- **Chapter 4** informs about the design and characterisation of casein−whey protein suspensions regarding their application for thermal extrusion-based printability via the pH−temperature-route. Protein-based formulations were prepared to work with a simplified model system and to conduct in-depth characterisation of these materials, with the most promising ones being printed with a customised in-house printer.

- **Chapter 5** is divided into two main sections, with the first one (5.1) focusing on a new screening protocol for transmission electron cryogenic microscopy, developed during research at The University of Melbourne at The Bio 21 Advanced Microscopy Facility. The second one (5.2) presents the results of the characterisation of casein−whey protein suspensions with additional milk fat regarding their extrusion-based printability via the pH−T-route, including further results of the developed microscopy screening protocol. The most promising formulations were related to the aggregation rate and printed.
- **Chapter 6** describes the retrofitting process of a plastic into a 3D food printer including all the hardware/ software changes and informs about the set-up of the printer in detail.
- The final part (**Chapter 7**) provides the conclusion inclusive the main outcomes of this research project and some future work is proposed.

1.4 Publications and presentations

The results of this study have been peer-review published/submitted or presented at conferences:

1.4.1 Publications

1.4.1.1 First author

Daffner, K., Vadodaria, S., Ong, L., Nöbel, S., Gras, S., Norton, I., & Mills, T. (2020). Design and characterization of casein–whey protein suspensions via the pH–temperature-route for application in extrusion-based 3D-Printing. Food Hydrocolloids, 112, 105850.

Daffner, K., Hanssen, E., Norton, I. T., Mills, T., Ong, L., & Gras, G. L. (2020b). Imaging of dairy emulsions via a novel approach of cryogenic transmission electron microscopy using beam exposure. Soft Matter, 16(34), 7888-7892.

Daffner, K., Hanssen, E., Ong, L., Gras, S. L., & Mills, T. (2021). Characterising the influence of milk fat towards an application for extrusion-based 3D-printing of casein−whey protein suspensions via the pH−temperature-route. FOOHYD_106642.

1.4.1.2 Co-author

Nöbel, S., Seifert, B., **Daffner, K.**, Schäfer, J., & Hinrichs, J. (2020). Instantaneous gelation of acid milk gels via customized temperature-time profiles: Screening of concentration and pH suitable for temperature triggered gelation towards 3D-printing. Food Hydrocolloids, 106450.

Wilms, P., **Daffner, K.**, Kern, C., Gras, S.L., Schutyser, M.A.I., Kohlus R. (2021). Optimising the extrusion of food systems for 3D-printing applications. Food Engineering Reviews. (Submitted).

1.4.2 Co-authors and contribution to each chapter

The scientific work presented in this thesis was partly conducted in cooperation with other scientists. Dr. Tom Mills supervised and Prof. Dr. Ian Norton co-supervised the entire thesis.

- Chapter 3: Benjamin Seifert performed most of the rheological experiments. Stefan Nöbel created the graphs. Stefan Nöbel and Kilian Daffner wrote the entire script. Johannes Schäfer, Jörg Hinrichs, Stefan Nöbel and Kilian Daffner corrected the manuscript.

- Chapter 4: Saumil Vadodaria and Tom Mills were involved in the set-up of the food printer. Kilian Daffner wrote the entire script. All co-authors corrected the manuscript.

- Chapter 5.1: Cryo-EM was performed with Eric Hanssen in Melbourne. Kilian Daffner wrote the entire script. All co-authors corrected the manuscript.

- Chapter 5.2: CLSM was performed with Lydia Ong and cryo-EM with Eric Hanssen, both in Melbourne. Jixin Xi performed some of the rheological analysis and zeta-potential measurements. Kilian Daffner wrote the entire script. All co-authors corrected the manuscript.

- Chapter 6: Tom Mills and Saumil Vadodaria were involved in the set-up of the food 3D-printer. Kilian Daffner wrote the entire script.

1.4.3 Presentations

1.4.3.1 Oral presentations (speaker underlined)

Daffner, K., Norton, I., Mills. T. Characterisation of casein-whey protein mixtures differing in pH, protein content and denaturation parameters for extrusion based Food Layered Manufacturing. 8th International Symposium on food rheology and structure, ISFRS 2019, Zurich, Switzerland.

Daffner, K., Norton, I., Mills. T. Extrusion based Food Layered Manufacturing of casein-whey protein mixtures differing in pH, protein content and denaturation parameters. ICEF13 - 13th International Congress on Engineering and Food, 2019, Melbourne, Australia.

1.4.3.2 Poster presentations (presenter underlined)

Daffner, K., Norton, I., Mills. T. Formulation for 3D printing: Creating a plug and play platform for a disruptive UK industry. Establishing formulations for extrusion based 3D-printing of foods. Formulation for 3D Printing Annual review meeting, Nottingham, 2018.

Daffner, K., Norton, I., Mills. T. Formulation for 3D printing: Creating a plug and play platform for a disruptive UK industry. Food Layered Manufacturing of edible and printable materials - Dairy gels. Formulation for 3D Printing Annual review meeting, Nottingham, 2019.

1.5 References

Cheyne, A., Barnes, J., & Wilson, D. I. (2005). Extrusion behaviour of cohesive potato starch pastes: I. Rheological characterisation. Journal of Food Engineering, 66(1), 1-12.

de Kruif, C. G. and Roefs, S. P. F. M. (1996) Skim milk acidification at low temperatures: a model for the stability of casein micelles. Netherlands Milk Dairy Journal 50 113–120.

Derossi, A., Caporizzi, R., Azzollini, D., & Severini, C. (2018). Application of 3D printing for customized food. A case on the development of a fruit-based snack for children. Journal of Food Engineering, 220, 65-75.

Fekete, A. A., Givens, D. I., & Lovegrove, J. A. (2013). The impact of milk proteins and peptides on blood pressure and vascular function: a review of evidence from human intervention studies. Nutrition research reviews, 26(2), 177-190.

Gholamipour-Shirazi, A., Norton, I. T., & Mills, T. (2019). Designing hydrocolloid based food-ink formulations for extrusion 3D printing. Food Hydrocolloids, 95, 161-167.

Godoi, F. C., Prakash, S., & Bhandari, B. R. (2016). 3d printing technologies applied for food design: Status and prospects. Journal of Food Engineering, 179, 44-54.

Hammelehle, B., Schkoda, P. & Kessler, H. G. (1997) Parameters for coagulation properties of direct acidified milk and for the structure of milk gels. Milchwissenschaft 52 671–674.

Hull C.S. (1986). Apparatus for Production of Three-dimensional Objects by Stereolithography. US 4575330 A.

Jiang, H., Zheng, L., Zou, Y., Tong, Z., Han, S., & Wang, S. (2019). 3D food printing: Main components selection by considering rheological properties. Critical reviews in food science and nutrition, 59(14), 2335-2347.

Jørgensen, C. E., Abrahamsen, R. K., Rukke, E. O., Hoffmann, T. K., Johansen, A. G., & Skeie, S. B. (2019). Processing of high-protein yoghurt–A review. International Dairy Journal, 88, 42-59.

Kern, C., Weiss, J., & Hinrichs, J. (2018). Additive layer manufacturing of semi-hard model cheese: Effect of calcium levels on thermo-rheological properties and shear behavior. Journal of Food Engineering, 235, 89-97.

Kim, H. W., Bae, H., & Park, H. J. (2017). Classification of the printability of selected food for 3D printing: Development of an assessment method using hydrocolloids as reference material. Journal of Food Engineering, 215, 23-32.

Koutina, G., Knudsen, J.C., Andersen, U., & Skibsted, L.H. (2014). Temperature effect on calcium and phosphorus equilibria in relation to gel formation during acidification of skim milk. International Dairy Journal, 36, 65–73.

Lanaro, M., Forrestal, D. P., Scheurer, S., Slinger, D. J., Liao, S., Powell, S. K., & Woodruff, M. A. (2017). 3D printing complex chocolate objects: Platform design, optimization and evaluation. Journal of Food Engineering, 215, 13-22.

Lille, M., Nurmela, A., Nordlund, E., Metsä-Kortelainen, S., & Sozer, N. (2018). Applicability of protein and fiber-rich food materials in extrusion-based 3D printing. Journal of Food Engineering, 220, 20-27.

Lipton, J. I., Cutler, M., Nigl, F., Cohen, D., & Lipson, H. (2015). Additive manufacturing for the food industry. Trends in Food Science & Technology, 43(1), 114-123.

Mantihal, S., Prakash, S., Godoi, F. C., & Bhandari, B. (2019). Effect of additives on thermal, rheological and tribological properties of 3D printed dark chocolate. Food research international, 119, 161-169.

Morell, P., & Fiszman, S. (2017). Revisiting the role of protein-induced satiation and satiety. Food Hydrocolloids, 68, 199-210.

Nöbel, S., Seifert, B., Schäfer, J., Daffner, K., & Hinrichs, J. (2018). Oral presentation Food Colloids, Leeds (2018) - Session - Processing of Novel Structures for Functionality. Temperature-triggered gelation of milk concentrates applied to 3D food printing.

Ross, M. M., Kelly, A. L., & Crowley, S. V. (2019). Potential Applications of Dairy Products, Ingredients and Formulations in 3D Printing. In Fundamentals of 3D Food Printing and Applications (pp. 175-206). Academic Press.

Schäfer, J., Läufle, I., Schmidt, C., Atamer, Z., Nöbel, S., Sonne, A., Kohlus, R. & Hinrichs, J. (2018). The sol−gel transition temperature of skim milk concentrated by microfiltration as affected by pH and protein content. International journal of dairy technology, 71(3), 585-592.

Severini, C., & Derossi, A. (2016). Could the 3D printing technology be a useful strategy to obtain customized nutrition?. Journal of clinical gastroenterology, 50(December), S175-S178.

Severini, C., Azzollini, D., Albenzio, M., & Derossi, A. (2018). On printability, quality and nutritional properties of 3D printed cereal based snacks enriched with edible insects. Food Research International, 106, 666-676.

Sun, J., Zhou, W., Huang, D., Fuh, J. Y., & Hong, G. S. (2015). An overview of 3D printing technologies for food fabrication. Food and bioprocess technology, 8(8), 1605-1615.

Vasbinder, A. J., Rollema, H. S., Bot, A., & de Kruif, C. G. (2003). Gelation mechanism of milk as influenced by temperature and pH; Studied by the use of transglutaminase cross-linked casein micelles. Journal of Dairy Science 86 1556-1563.

Wang, L., Zhang, M., Bhandari, B., & Yang, C. (2018). Investigation on fish surimi gel as promising food material for 3D printing. Journal of Food Engineering, 220, 101-108.

Warner, E. L., Norton, I. T., & Mills, T. B. (2019). Comparing the viscoelastic properties of gelatin and different concentrations of kappa-carrageenan mixtures for additive manufacturing applications. Journal of Food Engineering, 246, 58-66.

Wegrzyn, T. F., Golding, M., & Archer, R. H. (2012). Food Layered Manufacture: A new process for constructing solid foods. Trends in Food Science & Technology, 27(2), 66-72.

2 Chapter:

State of the art - literature review

2.1 Background literature: milk proteins, fat globules and gelation characteristics of dairy-based materials

The goal of this chapter is to sum up and review parts of the relevant literature, including an overview of the two main dairy milk constituents, protein and fat. The two proteins, casein and whey protein, their interactions, behaviour after thermal treatment and their emulsifying properties are discussed. Then, the milk fat globules and the secondary milk fat globule (membrane) are reviewed. Finally, the general gelation and aggregation mechanisms of particles is explained, with a focus on casein-based dairy gels and specifically on the pH−temperature (T)-route.

2.1.1 Milk proteins

2.1.1.1 Casein

Bovine milk proteins can be distinguished in two main groups: caseins and whey proteins with a ratio of 4:1. Caseins are formed in the udder of the cow representing an essential nutritional component for the sucking offspring (Horne, 2002). From a technological background in the dairy industry, the caseins, representing the main part of the milk proteins, are the most important component of the raw milk. The texture, sensory and nutritional properties of milk products like liquid milk and fermented products, e.g. cheese or yoghurt, are strongly derived from casein (De Kruif et al., 2012). Caseins form aggregates of colloidal size with a diameter between 50 – 600 nm, the so called casein micelles (CM), which may contain up to thousands of casein molecules (Fox & Bordkorb, 2008; Walstra & Jenness, 1984). The CM are dispersed in a continuous phase of water, salt, lactose and whey proteins.

For casein, four main groups can be distinguished, namely α_{s1}-, α_{s2}-, β- and κ-casein (4:1:3.5:1.5) (Swaisgood, 2003). The casein subfractions differ in the content of phosphate groups, linked to serine through esterification, with α-casein possessing 8 – 10 phosphoserine residues, β-casein five and κ-casein only one. Due to this phosphorylation, caseins can bind certain amounts of calcium ions. This can result in the precipitation of casein but also enables them to bind to calcium phosphate. The single phosphorylated κ-casein does not precipitate, even in the presence of high Ca^{2+}-concentrations (Swaisgood, 2003). All caseins contain hydrophobic amino acids, with β- and κ-caseins having large hydrophobic blocks in their sequences.

For a better understanding of the casein proteins, a few of their properties are shown in *Table 2-1*. Casein molecules carry a net negative charge at the native pH (6.7) of milk due to the deprotonation of amino acid residues, with α-casein having a net charge of –24 mV, β-casein of –13 mV and κ-casein of –3 mV, which varies depending on the solution pH. The average isoelectric point (IEP) of casein is 4.6, at which these proteins precipitate from milk, with exception of κ-casein (higher IEP, see *Table 2-1*). Three main interactions, negative charge, steric

repulsion and surface hydration between the layers of κ-casein around the micelles, stabilise the CM against aggregation (Fox & Mulvihill, 1990; Heertje et al., 1985; Horne, 1986; Walstra, 1990).

Table 2-1: Casein protein fractions and their properties (modified from Walstra & Jenness, 1984; Farrell et al., 2004).

Protein fraction (genetic variation)	Composition in skim milk (g L^{-1})	Molecular weight (g mol^{-1})	Isoelectric point (pH)	Amino acids
α_{s1}-casein	12 – 15	23,615	4.44 – 4.76	199
α_{s2}-casein	3 – 4	25,226	5.0 [1]	207
β-casein	9 – 11	23,983	4.83 – 5.07	209
κ-casein	2 – 4	19,037	5.45 – 5.77	169

[1] Walstra et al., 2006

For the structure of CM different models were developed in the past, including the submicelle (Walstra, 1990), dual binding (Horne, 1998), nanocluster (Holt et al., 2003), and "Dalgleish's" (Dalgleish, 2011) model. All of these models agreed on the presence of κ-casein on the CM surface and colloidal calcium phosphate (CCP) clusters in the core of the micelle. In *Figure 2-1*, the submicelle model is depicted (Walstra, 1990) with submicelles of a size of 10 – 15 nm and consisting of 15 – 20 casein molecules. The core of the CM contains CCP. Two different types of submicelles, with and without κ-casein, exist. The submicelles with α- and κ-caseins are more hydrophilic and therefore located near the outside of the micelle, while the submicelles without κ-casein consist of α- and β-caseins and are located more in the interior of the micelle due to their hydrophobic characteristics.

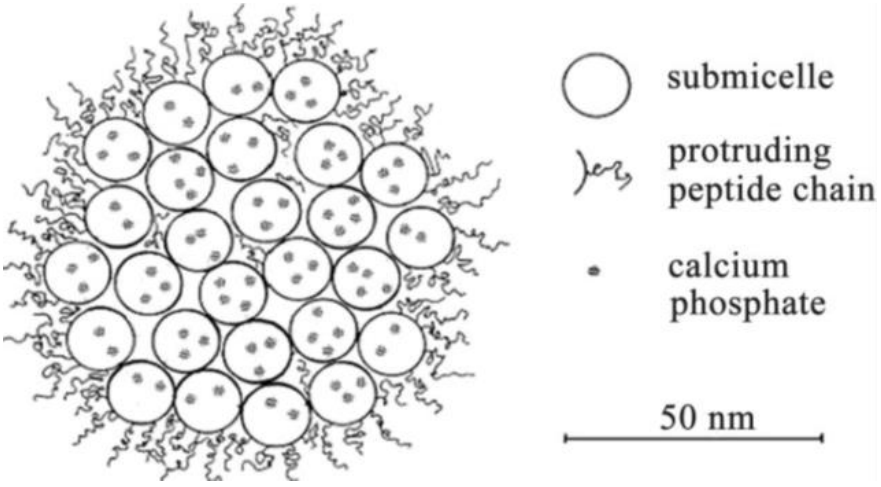

Figure 2-1: Submicelle model according to Walstra (1990).

According to Walstra (1990) the submicelles are kept together by hydrophobic interactions and calcium phosphate linkages. The hairy layer of the micelles is attributed to the hydrophilic glyco-macropeptide part of κ-casein protruding into the continuous phase of the milk. Therefore, κ-casein is responsible for the steric and electro-repulsive stability of the CM, especially for their stability towards aggregation. As a consequence, the CM are present as a stable colloidal dispersion in dairy milk.

The second most popular and accepted model for the structure of CM is the nanocluster model presented by Holt (1992), shown in *Figure 2-2*. According to this model, caseins and calcium phosphate nanoclusters are incorporated into a structure without subunits, suggesting a more homogeneous protein matrix within the micelle. The CM are hold together by interactions between caseins and calcium phosphate, with the hydrophilic part of κ-casein forming the hairy layer and protruding into the serum phase. The word "rheomorphic" was used to describe the caseins, as they are neither globular, nor fibrillar proteins nor molten globules nor random coils. A rheomorphic protein has an open conformation and conformational flexibility (Holt & Sawyer, 1993), evidenced by casein having little α-helical structure via far-UV circular dichroism and Fourier transform infrared spectroscopy.

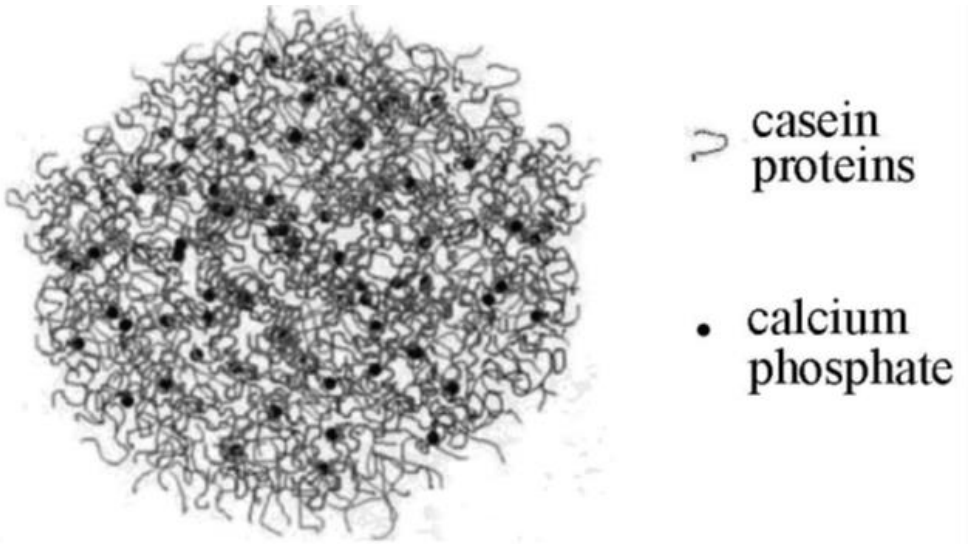

Figure 2-2: Model structure of the casein micelle showing a more-or-less homogeneous protein matrix containing calcium phosphate nanocluster-like particles (•) distributed with a mean spacing of 18 nm. There is no distinct hairy layer, but rheomorphic polypeptide (Holt et al., 1992).

In a previous review, Dalgleish (2011) proposed the role of water in the internal structure of the CM, as most of the previous models consider hydrophobic bonding as the main parameter in maintaining the stability of the sub-micelle/ casein complexes. Dalgleish (2011) suggested an uneven distribution of water in the interior of the CM, with domains or channels of water allowing proteins (e.g. β-casein) to diffuse through the micellar interior. The incompatibility of the hydrophobic character of α_s- and β-caseins in previous models (submicelle, nanocluster and dual binding) with the highly hydrated structure of the CM was explained, as the micelles contain 3 – 4 kg water per kg of protein (de Kruif & Holt, 2003).

In Dalgleish's model, the CM have a relatively sparse hairy layer of κ-casein on their surface, which is dense enough to stabilise (sterically, electrostatically) them against an approach of other CM/particles but also diffuse enough to allow interactions between denatured whey proteins and the para-κ-casein region of κ-casein or to allow β-casein to dissociate from the micelles at low temperatures and to reassociate with the CM on subsequent warming (Anema, 2020). The presence of β-casein in a mobile form interacting with the water molecules due to its high amphiphilic nature was suggested, with approximately 60% of β-casein dissociating out of the CM at low temperatures (4°C), while only small amounts of the other caseins dissociate into the serum (Creamer et al., 1977). All the described models are oversimplified, as the CM are neither hard spheres nor identical in size. For more detailed information about the CM and their (internal) structure it is referred to previous literature of Dalgleish et al. (2004), Horne (2002, 2006), Phadungath (2005), de Kruif et al. (2012) Holt et al. (2013) or latest Anema (2020).

2.1.1.2 Whey proteins

The second group of proteins in bovine milk are the whey proteins which cover about 20% of the total protein content in bovine milk (Fox & McSweeney, 1998). The main whey proteins are β-lactoglobulin (β-lg), α-lactalbumin (α-la), blood serum albumin and immunoglobulins,

with β-lg representing more than 50% (compare *Table 2-2*). The rest of the whey proteins covers around 10%, with different proteins like lactoperoxidase, serum transferrin, enzymes and milk fat globular membrane proteins (Fox & Kelly, 2006). Whey or serum proteins have a relatively high hydrophobicity and compactly folded peptide chains (Walstra et al., 2006). They are typical globular proteins with high levels of secondary and tertiary structures, being responsible for denaturation processes at high temperatures (Dannenberg & Kessler, 1988). For β-lg as the main serum protein, 10 different genetic variants were identified. It has a radius of about 2 nm, an isoelectric point of around 5.2 and contains two disulfide bridges and one free thiol (Hambling et al., 1992).

Table 2-2: Whey protein fractions and their properties (modified from Walstra & Jenness, 1984; Farrell et al., 2004).

Protein fraction	Composition in skim milk (g L^{-1})	Molecular weight (g mol^{-1})	Isoelectric point (pH)	Amino acids
β-lactoglobulin	2−4	18,363	5.13	162
α-lactalbumin	0.6−1.7	14,178	4.2−4.5	123
Serum albumin	0.4	66,399	4.7−4.9	582

The secondary structure contains 15% α-helix, 50% β-sheet and 15-20% reversed turn−β-strands (Creamer et al., 1983). The 3D tertiary structure of the native β-lg with an eight-stranded β-barrel (calyx) formed by β-sheets and flanked by a three turn α-helix is shown in *Figure 2-3*.

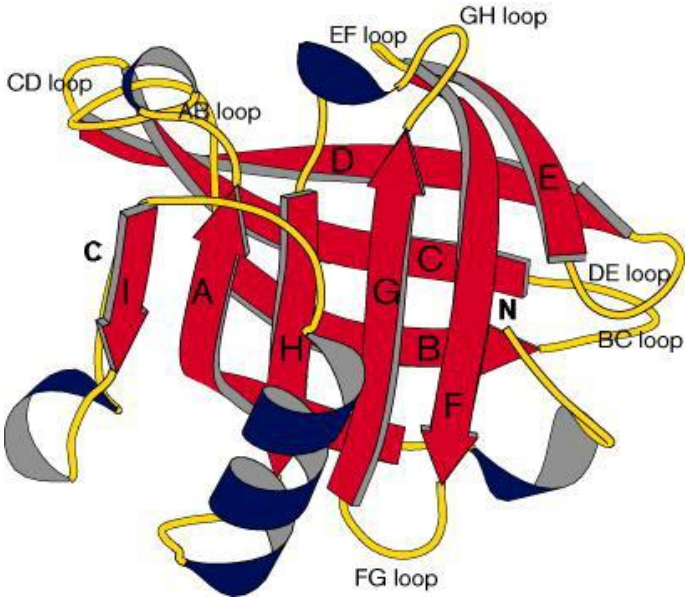

Figure 2-3: Schematic drawing of the structure of β-lactoglobulin (Brownlow et al., 1997).

2.1.1.3 Heat induced casein−whey protein interactions

When milk is heated to temperatures of 70°C and higher, the whey proteins start to unfold, denature irreversibly (Dannenberg & Kessler, 1988) and interact among themselves through hydrophobic bonding and thiol-disulfide exchange reactions (Sawyer, 1969; Smits & Brouwer-shaven, 1980). Denatured whey proteins can also aggregate with κ-casein, if available, resulting in κ-casein−whey protein complexes (Jang, & Swaisgood, 1990; Singh & Creamer, 1991a). κ-casein and β-lg as well as α-la (α-la no free thiol groups) exhibit free thiol groups and/or disulfide bonds allowing intermolecular association via thiol-disulfide exchange reactions. These interactions of the denatured whey proteins, specifically β-lg, with κ-casein on the surface of the CM are of particular interest as the resulting protein complexes influence the functional properties of milk and other dairy products considerably. The latest review, summing up these interactions and how potential heat-induced aggregates influence the milk characteristics, was published by Anema (2020).

Depending on the pH at heating, different types of interactions between denatured whey proteins and CM were found (Anema & Li, 2003a; Anema et al., 2004a; Anema et al., 2004b), while a pH dependent association of the whey proteins with the CM was further confirmed (Anema & Klostermeyer, 1997; Corredig & Dalgleish, 1996; Oldfield et al., 2000). At pH 6.5 at heating, around 70% of the denatured whey proteins were found on the surface of the CM, increasing the original size of the CM by 30 – 35 nm. Vasbinder & de Kruif (2003) proposed that almost all the denatured whey proteins covered the surface of the CM while Anema et al. (2004b) found values between 55 – 85% of whey protein covering the surface of the CM at pH 6.5 at heating, depending on the heating temperature.

With increasing pH at heating (6.9, 7.1), Anema & Li (2003b) and Anema (2007) found a decreased amount of denatured whey protein on the surface of the CM, changing the composition and the surface characteristics of the CM. At those higher pH values at heating, the level of

association decreased with around 30% whey proteins covering the surface of the CM (Anema & Li, 2003a).

κ-casein showed heat-induced, pH-dependent dissociation from the CM accompanied by an increase in the amount of denatured whey proteins remaining in the serum (Singh & Creamer, 1991b). This was confirmed by 80 – 90% of the denatured whey proteins associated with the CM at pH values below 6.7 at heating, whereas only about 20% associated with the CM at pH values above 6.8 at heating (Anema & Klostermeyer, 1997; Oldfield et al., 2000).

These interactions depend on the location of κ-casein which was shown to dissociate from the CM with increasing pH values at heating (Anema & Klostermeyer, 1997; Singh & Fox, 1985). It is not clear why dissociation occurred, but it was found that κ-casein dissociated to the serum at temperatures lower than those required for whey protein denaturation (Anema & Klostermeyer, 1997; Anema, 2008a).

However, there is still ongoing debate over the sequence of events regarding the κ-casein−whey protein interactions. On the one hand, it was proposed that κ-casein dissociated from the CM in early stages during heating and denatured whey proteins interacted with κ-casein in the serum or on the micelle surface, with a preferential serum phase reaction (Anema & Li, 2000; Anema, 2007). This was supported by significant amounts of κ-casein dissociating at temperatures below those necessary for whey protein denaturation (Anema & Klostermeyer, 1997) as well as significant dissociation of κ-casein from the CM in systems which have been depleted of whey proteins (Anema & Li, 2000). On the other hand, it was proposed that denatured whey proteins interacted with CM first, followed by dissociation of the κ-casein−whey protein complexes from the CM (Donato & Dalgleish, 2006; Donato & Guyomarc'h, 2009). This was supported by no increase in the amount of κ-casein−whey protein complexes in the serum after addition of sodium caseinate, indicating that κ-casein−whey protein complexes were formed on the surface of the CM regardless of the pH value at heating (Parker et al., 2005).

2.1.2 Milk fat globules

Bovine milk contains approximately 3 – 5% fat, which is distributed as small, spherical globules in the serum phase (Singh, 2006). The milk fat globules (MFG) have a diameter ranging between 0.1 – 15 μm, with an average of around 3 – 4 μm (Mulder & Walstra, 1974). The inner part of the MFG mainly consists of triglycerides, surrounded by a thin membrane, the so called milk fat globule membrane (MFGM) which hinders the fat globules from coalescing. The MFGM is a complex trilayer membrane (compare *Figure 2-4* and *Figure 2-5*), composed mainly of phospholipids, glycolipids, proteins, lipoproteins and enzymes (Michalski et al., 2002), as shown in *Table 2-3*.

The inner part of the MFG contains milk fat, consisting of 96 – 99% of triglycerides. The structure of a single MFG and the surrounding MFGM are illustrated in *Figure 2-4*. The MFGM consists of a triple layer, shown in *Figure 2-5*. This triple layer includes an inner monolayer of lipids and proteins, a proteinaceous coat located on the inner face of the bilayer membrane, and a bilayer membrane of polar lipids and proteins (Dewettinck et al., 2008). The MFGM proteins were found to account for 25 – 70% of the mass of the membrane material (Deeth, 1997; Fong et al., 2007), while other studies found 25 – 60% (Astaire et al., 2003, Singh, 2006), depending on the isolation method.

Table 2-3: Estimated average composition of milk fat globule membrane (Walstra et al., 1999; Huppertz & Kelly, 2006).

Component	**mg 100 g^{-1} fat globules**	**mg m^{-1} fat surface**	**% of membrane material**
Protein	1800	9.0	70
Phospholipids	650	3.2	25
Cerebrosides	80	0.4	3
Cholesterol	40	0.2	2
Neutral glycerides	+ [a]	+	?
Water	+	+	?
Carotenoids and vitamin A	0.04	2×10^{-4}	-
Iron	0.3	1.5×10^{-3}	+
Copper	0.01	5×10^{-5}	-
Total	*> 2570*	*> 12.8*	*100*

[a] + indicates component is present but concentration has not been determined precisely

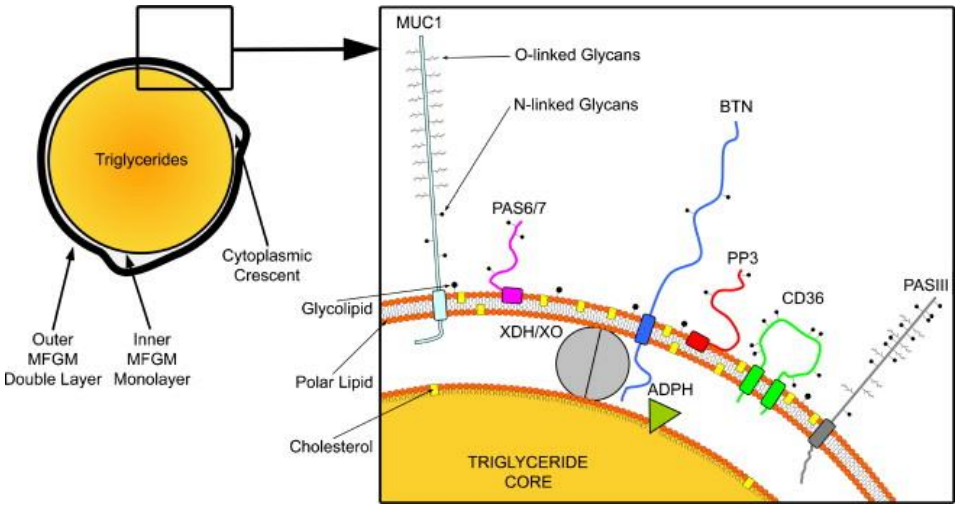

Figure 2-4: Structure of the fat globule with detailed arrangement of the main MFGM proteins. The drawing is highly schematic and sizes are not proportional. A double layer of polar lipids is placed on an inner monolayer of polar lipids. Membrane-specific proteins are distributed along the membrane. ADPH is located in the inner polar lipid layer, XDH/XO is located in between both layers. MUC1, BTN, CD36 and PASIII are located in the outer layer. PAS6/7 and PP3 are only loosely attached at the outside of the MFGM. The choline-containing phospholipids, PC and SM, and the glycolipids, cerebrosides and gangliosides, are largely located on the outside of the membrane, while PE, PS and PI are mainly concentrated on the inner surface of the membrane (Dewettinck et al., 2008).

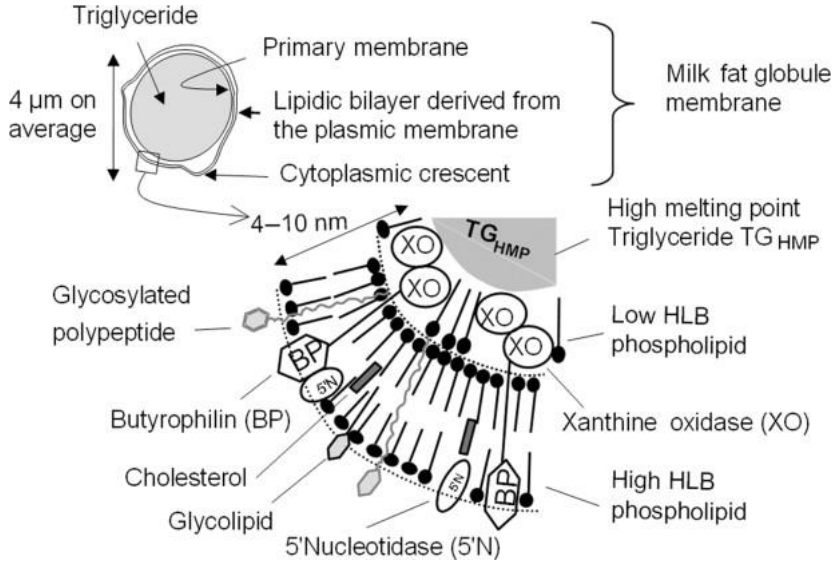

Figure 2-5: Typical structure of the native milk fat globule (Michalski et al., 2005).

The milk fat globule and its membrane are influenced by processes like agitation or cooling, but also during natural creaming and lipolysis. The main process steps altering the MFGM are heat treatment and mechanical input, as shown in *Figure 2-6*. Mechanical input (sonication, micro fluidizing and especially homogenisation) causes a significant reduction of the MFG size and an increase in the interfacial area of the fat particles, changing the composition of the

MFGM. As the native MFGM material is insufficient to cover the larger surface area, proteins from the serum adsorb at the oil−water interface. Depending on the previous treatment of the dairy material, the new MFGM was found to consist of parts of the native MFGM, but mainly casein and also whey protein, if heat was applied before (McPherson & Kitchen, 1983; Ong et al., 2010a; Sharma & Dalgleish, 1993; Walstra & Jenness, 1984).

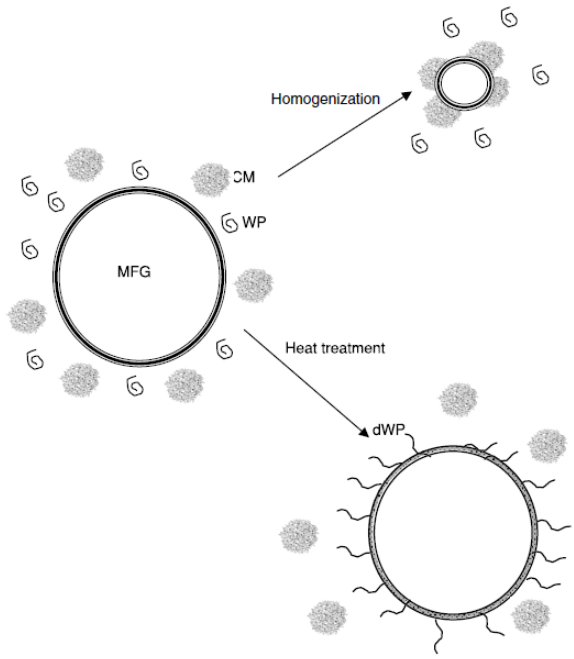

Figure 2-6: Schematic illustration of the relative effects of heating and homogenisation on fat globules in milk. MFG = milk fat globule, CM = casein micelle, WP = whey protein, dWP = denatured whey protein (Huppertz & Kelly, 2006).

After mechanical input, oil droplets were covered and stabilised by a thin layer of proteins adsorbed at the oil−water interface (Dickinson, 1994). During high pressure homogenisation, casein molecules and aggregates adsorbed at the surface of the newly created milk fat globule membrane (MFGM), sterically and electrostatically stabilising the droplets against recoalescence. A mechanical damage of the MFGM caused milk fat globules (MFG) which were found to behave to some extent like CM (Buchheim, 1986). These MFG with protein on the surface could act as pseudo-protein particles during gelation and increased the gel firmness (Ji et al., 2016). Further information about the interfacial properties of casein in emulsions can be found elsewhere (Dickinson, 1999).

Characterising the surface properties, it was reported that the zeta (ζ)-potential (representing the surface charge) of the MFG was around −13.5 mV (Michalski et al., 2002), while it was −13 mV for MFGM phospholipids (Liu et al., 2013). For homogenised MFG, the surface charge increased to around −20 mV, which was explained with CM covering the newly created surface, therefore, approaching the ζ-potential of casein. It was proposed that fully homogenised MFG have a ζ-potential similar to the one of CM, confirming a high surface coverage of fat particles with caseins (Michalski et al., 2002).

After homogenisation, only casein (α, β and κ) and no whey proteins or native membrane proteins (e.g. xanthinoxidase or butyrophilin) were found as proteins attached to the surface of the MFG (Ong et al., 2010a), explained with low heating temperatures and no denaturation of the whey proteins. Similarly, Sharma & Dalgleish (1993) did not find any whey proteins on the surface of the MFG after microfluidisation, if heating was applied at less than 70°C, while Walstra & Jenness (1984) reported whey proteins being part of the newly created surface. Cano-Ruiz & Richter (1997) found no effect of the homogenisation pressure on the composition of the proteins on the surface of the MFG, while 70% of the material was characterised as casein, with the rest being whey and native membrane proteins

It was found that increasing the pH before the heating process (6.3 to 7.3) resulted in increasing amount of α_s- and β-casein, but decreasing amounts of κ-casein and β-lg covering the surface of MFG after mechanical input (Sharma et al., 1996a). Sharma et al. (1996b) found that the amount of κ-casein covering the surface of the MFG was independent of the heat treatment and the order of the two steps, heating and homogenisation. This led to the assumption that the deposition of κ-casein depended only on the homogenisation step. The κ-casein−whey protein complexes in the serum and on the MFG surface were proposed to be similar after heating and homogenisation (Sharma et al., 1996a).

2.1.3 Aggregation and gelation

Aggregation is the process or the result of the formation of aggregates. According to Dickinson & van Vliet (2003) aggregation describes a process where two or more colloidal particles become joined together under the influence of some kind of attractive interparticle colloidal interaction. This process can be induced in three ways for food colloids, by physical processes (e.g. stirring, heating), by chemical change (e.g. acidification, addition of salts or polymers), or by enzymatic action (e.g. renneting). The conversion or rather transition of a stable sol, e.g. skimmed milk, into an aggregated gel network, e.g. yoghurt, involves physico-chemical changes. Aggregation in diluted dispersions or emulsions can be detected experimentally by a larger particle size or an increase in sedimentation or creaming. On the other hand, aggregation for concentrated colloids is detected through rheological properties (Dickinson & van Vliet, 2003).

2.1.3.1 Kinetics of aggregation

The kinetic aspects of aggregation will be discussed on the following pages. It has to be taken into account that most of the theory derived is only valid for ideal cases of diluted dispersions of monodisperse hard spheres. Therefore, most of the food systems don't comply with these restrictions. Fast aggregation appears when interparticle forces are dominated by short-range Van-der-Waals forces. Slow aggregation can be detected in the presence of appreciable potential energy barriers (due to charge-stabilised particles) (Dickinson & van Vliet, 2003). In general, the rate of aggregation is determined by the frequency of collisions and the probability of cohesion during collision. When colloidal particles approach each other, colloidal interaction forces are responsible for aggregation, with two possible ways of aggregation occurring, either due to Brownian motion (perikinetic aggregation) or to velocity gradients/hydrodynamic motions (orthokinetic aggregation).

2.1.3.1.1 Perikinetic fast aggregation

The term perikinetic signifies that the particles encounter each other because of their Brownian motion or diffusion (Walstra, 2003). This theory was proposed in 1916, when Smoluchowski assumed that colloidal particles stick and remain aggregated when encountering each other due to Brownian motion. He considered that particles diffuse to a central particle. Therefore perikinetic aggregation can be ascribed to the Brownian motion of dispersed particles.

According to Smoluchowski (citied by Myers, 1990; Dickinson & Walstra, 1993; Walstra, 2003) the number J_{peri} of encounters per unit volume and time (flux or aggregation rate) [s^{-1}] for equal-sized spheres can be defined as:

$$J_{peri} = 4\,\pi\,D_m\,r\,N \qquad \text{(I)}$$

where D_m is the mutual diffusion coefficient of two particles (for an aggregated sphere equal to the sum of the diffusion coefficient of both spheres) [$m^2\ s^{-1}$], r the collision radius (for a sphere equal the sum of the radii of both spheres) [m] and N the number of particles per unit volume (or particle number concentration) [m^{-3}]. The diffusion coefficient D [$m^2\ s^{-1}$] used in formula (I) is given by the Stokes-Einstein equation:

$$D = \frac{k_B\ T}{3\,\pi\,\eta_0\,d} \qquad \text{(II)}$$

where k_B is the Boltzmann constant [$J\ K^{-1}$], T the absolute temperature [K], η_0 the viscosity of the continuous phase [$Pa{\cdot}s$] and d the diameter of the particle [m]. For equal spheres equation (II) can be transformed into:

$$J_{peri} = \frac{8k_BT}{3\eta_0}\ N \qquad \text{(III)}$$

Assuming that each collision of two particles results in a reduction of the particle number by unity, the change in the number of particles per unit volume with time is obtained by multiplying J by N and dividing by 2 to prevent counting every collision twice: Therefore equation (III) is changed into:

$$-\frac{dN}{dt} = \frac{1}{2} J_{peri}\, N = \frac{4k_B T}{3\eta_0} N^2 \qquad \text{(IV)}$$

Polydispersity tends to enhance the aggregation rate, even for spheres. The reason is that the effects of particle size on collision radius and mutual diffusion coefficient don't exactly cancel in equation (IV). The time which is needed to halve the number of particles, $t_{0.5}$, is given by:

$$t_{0.5} = \frac{2}{J_0} = \frac{3\eta_0}{4k_B T N_0} = \frac{\pi d_0^3 \eta_0}{8k_B T \varphi} \qquad \text{(V)}$$

where J_0, N_0 and d_0 are the initial values of J_{peri}, N and d. The volume fraction, φ, found in formula (V), is described by the following equation:

$$\varphi = \frac{\pi d^3 N}{6} \qquad \text{(VI)}$$

The number of particles as a function of aggregation time is given by:

$$N_t = \frac{N_0}{1 + \frac{t}{t_{0.5}}} \qquad \text{(VII)}$$

The decrease in N with time for an example is shown in *Figure 2-7* (Walstra, 2003):

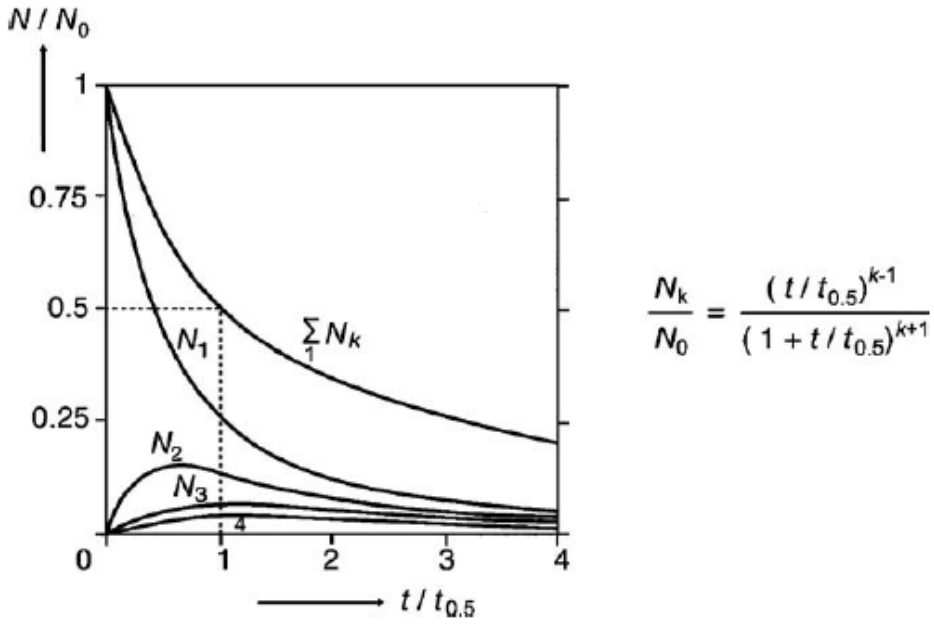

Figure 2-7: Perikinetic aggregation. The relative particle number concentration as a function of the time t after aggregation has started over the halving timet_0.5. N refers to number, N_0 to initial total number, and the subscripts 1, 2, 3, etc. to the numbers of particle monomers, dimers, trimers, etc. The equation for the number of k-mers is also given (Walstra, 2003).

It is important to mention that there are some restrictions. The above presented theory from Smoluchowski (1916) describes the aggregation process of colloidal solutions under following conditions:

- The solution contains a total of N_0 particles at t_0

- All particles are spherical, have the same size and the same aggregation readiness at every time.

- If two particles collide, this implies a fast aggregation and a durable contact

- The newly formed spherical particles from two aggregated particles with the radius r have the radius 2r.

- The aggregation time is independent of the number of non-aggregated particles.

For dispersions not following one or more of these conditions, the theory can be used for the first few aggregation steps, but correction factors have to be considered. Furthermore, the theory from Smoluchowski is not valid in the later stages of aggregation, when the system becomes polydisperse, when interactions between non-spherical aggregates are predominant and when the diffusion coefficient *D* deviates markedly from that of individual particles.

However aggregation kinetics are more intricate than suggested by the perikinetic theory from Smoluchowski. According to Walstra (1993) the formation of fractal aggregates and the presence of small velocity gradients can affect the time needed for aggregation to become perceptible.

2.1.3.1.2 Orthokinetic fast aggregation

The term orthokinetic signifies that particles encounter each other due to velocity gradients in the liquid. For simple shear flow, Smoluchowski's theory assumed that particles stick together and remain aggregated when colliding with each other. *Figure 2-8* depicts this way of aggregation for spheres of equal size, neglecting hydrodynamic interaction forces.

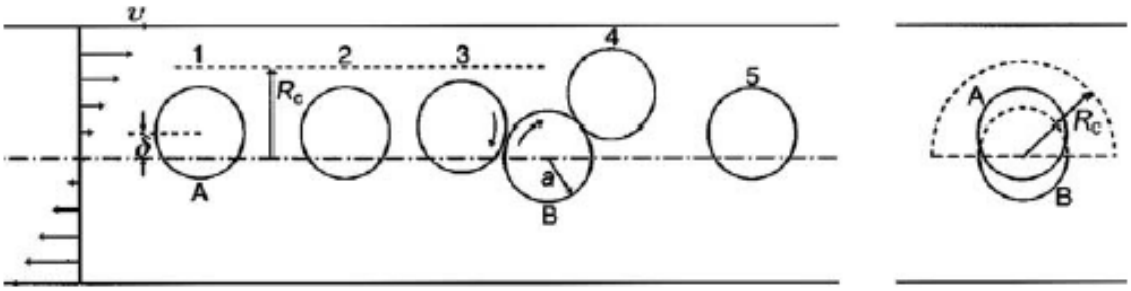

Figure 2-8: Orthokinetic aggregation of particles of equal diameter in simple shear flow, as envisaged by Smoluchowski. At left, the flow velocity profile is shown. Particle A moves from left to right (positions 1 to 5), particle B is in a stationary position, but it does rotate. At right a cross section is given that illustrates the geometry of the half-cylinder containing the centers of the particles to the left of B that will ''collide'' with B (Walstra, 2003).

Particle A meets reference particle B under the condition that its center is in a half cylinder of radius a_c (which equals the collision radius 2a). It can be seen that near position 3, the particles A and B collide and stick. After collision, the newly formed doublet rotates in the shear field.

According to Smoluchowski, the particles fuse into one sphere. Assuming spheres of equal size, the particle number concentration *N* is defined as:

$$-\frac{dN}{dt} = \frac{1}{2} J_{ortho} \mathrm{N} = \frac{2}{3} d^3 \; N^2 \; \dot{\mathrm{y}} = \frac{4}{\pi} \varphi \; \mathrm{N} \; \dot{\mathrm{y}} \qquad \text{(VIII)}$$

where $\dot{y}$ is the velocity gradient (equals the shear rate) [s^{-1}]

For orthokinetic aggregation the time needed to halve the number of particles is given by the following equation:

$$t_{0.5} = \frac{\pi \; ln2}{4\varphi \dot{\mathrm{y}}} \qquad \text{(IX)}$$

The ratio of the initial rates of orthokinetic to perikinetic aggregation is given by:

$$\frac{J_{0,ortho}}{J_{0,peri}} = \frac{d^3 \; \eta_0 \; \dot{\mathrm{y}}}{2 \; k_B \; T} \qquad \text{(X)}$$

It can be shown that orthokinetic aggregation is faster than perikinetic, if the particles are large (above 1 µm). The existence of d^3 in the numerator in equation (X) is only one reason. Another one is that small velocity gradients, induced by temperature fluctuations, lead to significant orthokinetic aggregation for particles above 4 µm. The mechanism of orthokinetic aggregation dominates for particles of micrometer size and larger (Berli et al., 1999). All in all, in food dispersions, orthokinetic aggregation is often more important than perikinetic aggregation.

In reality, slow aggregation takes place more often. This can be ascribed mostly to electrostatic repulsions, hydrodynamic interaction, disaggregation of particle doublets, high volume fractions or sedimentation of the particles. For all mentioned cases, the capture efficiency, α, which represents the probability of two particles sticking closely after encountering, has to be determined.

2.1.3.2 Aggregation and gelation of casein-based dairy gels

The aggregation of the CM can be triggered in different ways. One possibility is the addition of rennet which contains chymosin, a proteolytic enzyme that specifically cleaves κ-casein, causing its C-terminal end to be split off (Horne & Leaver, 1995). While the just mentioned method is popular for dairy products like cheese, for yoghurt the gelation process is induced with the addition of acid. Adding acid (lactic acid bacteria) leads to a reduction of the pH < 5.0, where the net charge of the hairs (κ-casein) is almost zero, the brush collapses and rapid aggregation occurs (Lucey & Singh, 1997).

The different ways used to destabilise the hairy layer of κ-casein are illustrated in *Figure 2-9*. On the left side, the enzymatic clip is shown, where the whole hydrophilic glycomacropeptide is removed, the steric stabilisation repulsion is lost and the CM start to coagulate. In the middle, the effect of alcohol is shown, where the solvent environment is modified and the protein chains are no longer in a good solvent. According to Horne & Leaver (1995) the addition of ethanol induces a conformational collapse of the κ-caseins, which causes the loss of their steric stabilising ability. On the right, the heat induced coagulation of milk can be see, which is explained in more detail in *2.1.1.3*, with the interaction between casein and denatured whey protein.

Figure 2-9: The micellar hairdressing saloon (Horne & Leaver, 1995).

According to Roefs (1986), a gel is defined as one where both the dispersed and the dispersion medium extend themselves continuously throughout the whole system. Gels from dairy products like yoghurt or cheese are casein gels, made from cow milk. Under normal conditions in milk (native pH = 6.7) CM are stabilised by steric and electrostatic repulsion and have a negative charge (Payens, 1979), e.g. shown with a zeta potential of around −15 to −20 mV at 30°C (Dalgleish, 1984).

For colloidal gels in dairy products, e.g. yoghurt, at least three ways of gelation are possible (Horne, 1999). For the formation of acid-induced milk gels, three well-known models are available, namely the adhesive sphere model, the percolation model and the fractal model. All of them were reviewed several times and can be found in literature (Bremer et al., 1989; De Kruif, 1997; Lucey & Singh, 1997).

Gel formation by proteins in general and by casein in particular depends on lots of factors (Roefs, 1986). These influencing factors are the pH value, temperature, ionic strength, ionic composition of the water phase, protein concentration and other difficult to define parameters (e.g. temperature history or mechanical agitation). It is distinguished between the formation of reversible and irreversible gels. Roefs (1986) demonstrated that casein gels are irreversible gels. For the conventional way with a constant temperature and a decreasing pH (T−pH-route), casein gels are enzyme induced (e.g. renneting), acid induced or induced by a combination of the two ways (Dickinson, 2006; van Vliet et al., 2004).

For the other way, the pH−T-route, the coagulation process of CM strongly depends on the temperature (De Kruif & Holt, 2003). As shown in *Figure 2-10*, direct acidification (pH−T-route) at room temperature results in precipitation of the caseins and no gelation appears, whereas low temperatures maintain sol−characteristics. To reach a coagulating system, it is important to know if a gel or a precipitate will be formed. Both possible routes, T−pH-route and pH−T-route are shown in *Figure 2-11*. Whereas the T−pH-route is already understood, well

investigated and many reviews are available for a classical yoghurt production, the focus of this review lies on the pH−T-route, as explained in more detail in the next part of this literature review.

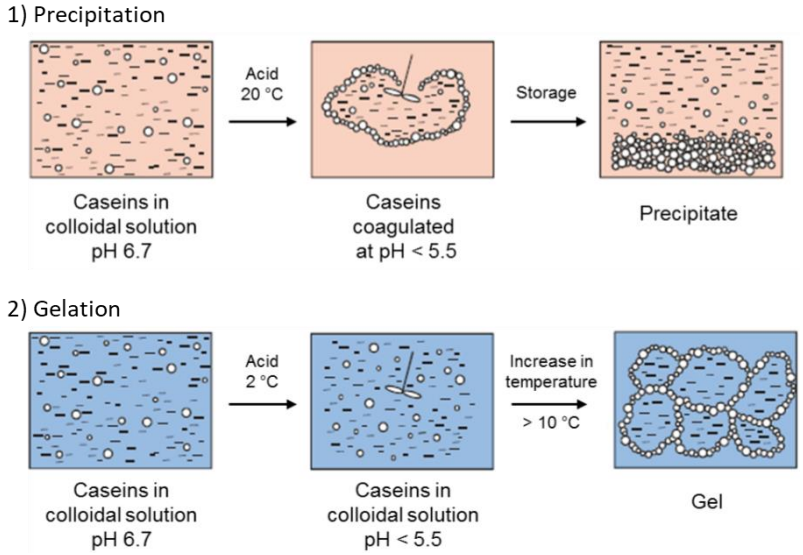

Figure 2-10: Impact of the temperature on the coagulation behaviour of caseins and controlling of (1) the formation of precipitate and (2) the gelation after direct acidification (Kessler, 2002).

2.1.3.3 Aggregation and gelation via the pH−T-route

Casein-based microgels can be induced with mechanical processing, heat treatment, changes in the environmental conditions (e.g. pH) or in the surface properties (interaction with whey proteins) (Loewen et al., 2017). Since one of the prerequisites for 3D-printing is the existence of dynamic conditions, the pH−T-route was found to be suitable for dairy-based materials to convert a material with sol into gel−characteristics (Nöbel et al., 2018). In comparison to the industrial used T−pH-route where fermentation takes several hours, depending on starting temperature, type of culture, culture concentration, etc., the pH−T-route works with a sudden temperature increase of the cold acidified system to trigger gelation of the CM within several minutes or even seconds.

For the pH−T-route, the steps acidification and gelation have to occur separated in space and time. At low temperatures the caseins stayed in colloidal solution at pH values of 4.6 due to weak attractive forces between them. Increasing the temperature (≥ 10°C) resulted in casein

gels formed due to the impact of increasing hydrophobic interactions forces (Horne, 1998). Direct acidification at room temperature caused a sudden coagulation and precipitation of casein without building of a gel structure (*Figure 2-10*). If acidification was conducted at temperatures below 4°C, the casein-suspension stayed stable and no precipitation and gelation occurred. Therefore, the two steps acidification and gel formation occurred separated in time and space and the pH−T-route was found to be suitable for printing of dairy-based materials (Nöbel, 2018).

The deviation in the gelation process from the conventional, well-known T−pH-route, towards the pH−T-route resulted in a higher gelation pH and stronger gels which showed less rearrangements and syneresis (Vasbinder et al., 2003). This was explained with the serum caseins acting as bridging material in the pH−T-route, which contributed to the gel formation. During the T−pH-route, almost no serum casein was released and therefore, could not contribute to the gelation process. At temperatures below 5°C, β-casein, calcium and phosphorus were released from the CM, resulting in bridging and firmer gels due to available serum caseins (Koutina et al., 2014; Nöbel, 2016; Vasbinder et al., 2003), as illustrated in *Figure 2-11*.

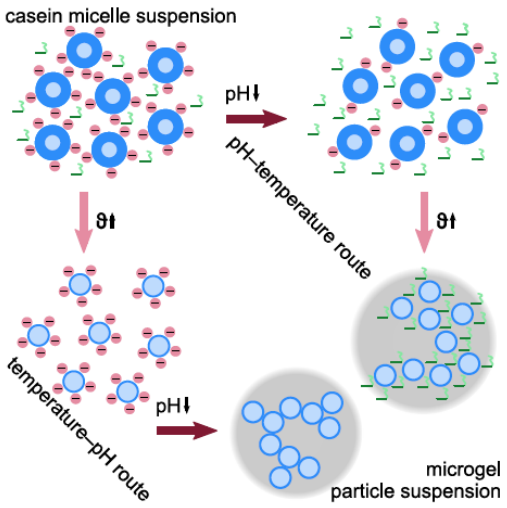

Figure 2-11: Schematic representation of the casein micelle aggregation to microgel particles; temperature–pH route: acidification at moderate or raised temperatures (ϑ ≥ 20°C), casein micelle contains most of the soluble caseins; pH–temperature route: partial dissociation of casein micelle due to β-casein release at lower temperatures (ϑ < 5°C); blue: casein micelle, red: negative surface charge, green: β-casein, grey: microgel particle (Nöbel, 2016).

Roefs (1986) was one of the first who investigated the structure of directly acidified milk gels. As shown in *Figure 2-12*, skim milk solutions with pH adjusted to 4.6 (at 4°C) were heated (30°C) and aged at this temperature (pH−T-route). When the storage modulus G' had reached a value of approximately 400 Nm^{-2}, the temperature was decreased to 4°C and kept at that level for four days. The loss modulus (G'') increased slightly, while G' raised enormously, implying a strong increase in the number or strength of the elastically effective bonds between the protein molecules of different casein particles. During the ageing process at 4°C, G' tended to increase, while G" slightly decreased. This gave the gel a more elastic character. The slight increase of the storage modulus G' was ascribed to retarded temperature reversible protein rearrangements (Roefs, 1986).

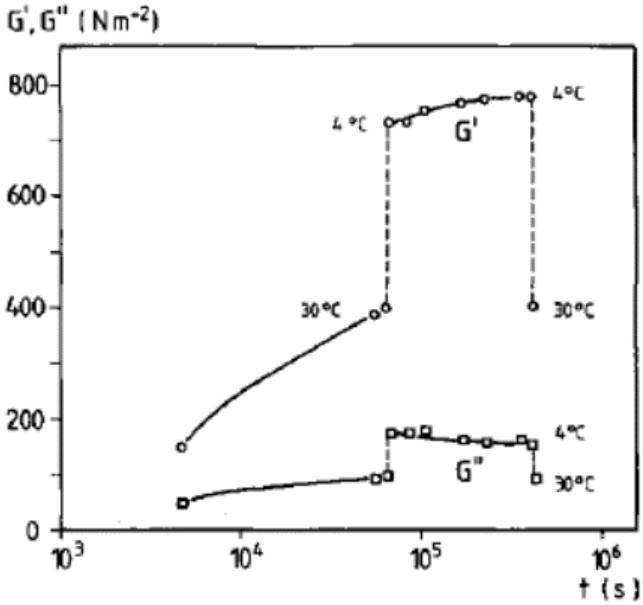

Figure 2-12: Storage modulus G' (o) and loss modulus G" (□) of an acid skim milk gel plotted as a function of the logarithm of ageing time t (s). After heating in the standard manner the gel was aged for 18 h at 30°C, before it was stored 4 days at 4°C. Subsequently it was heated to 30°C. The temperatures are indicated. ω=1.0 rad s^{-1}. (Roefs, 1986).

Acidification in the cold (4°C) followed by a temperature increase to 30 °C (pH−T-route) resulted in gels with a 20 times higher storage modulus G' and a lower permeability compared to milk acidified to the same pH (4.6) at 30°C (T−pH-route) (Van Vliet et al., 1989; van Vliet & Keetels, 1995). This was ascribed to the way the CM are linked together, by straight or by bent strands. It is important to mention that in practice, acidification with microorganisms at these

low temperatures of 4°C or lower (pH−T-route) does not work as the condition are too cold for the bacteria.

For direct acidification, Hammelehle (1994) investigated the influence of different acidifying agents (citric-, lactic- and hydrochloric acid) and found that gels with citric acid showed the highest firmness. Gelation strongly depended on the acidification pH, with lower pH values after direct acidification resulting in earlier gelation (lower temperature). Roefs (1986) also demonstrated that the rate of casein aggregation was an important difference between the direct and the industrial acidification (bacterial). Using direct acidification, the caseins reacted at a certain temperature (around the phase transition temperature), aggregated and built a three-dimensional network.

In the past, cold acidification via the pH−T route was already tested and used for dairy products like yoghurt or cheese (Hammelehle, 1994; Roefs, 1986; Schäfer et al., 2018; Vasbinder et al., 2003). For milk proteins, the sol−gel transition temperature (Hammelehle et al. 1997; Koutina et al. 2016; Schäfer et al., 2018; Vasbinder et al. 2003) and the temperature of aggregation (de Kruif & Roefs, 1996) were studied intensively via the pH−T-route.

A previous study on skim milk retentates produced via microfiltration showed that the sol–gel transition temperature (temperature at which G’ = 1 Pa) decreased significantly with decreasing acidification pH at constant protein content (Schäfer et al., 2018). It was found that sol−gel transition temperatures for acidification pH values between 5.4 and 5.0 decreased significantly with increasing protein content, while they were independent of the protein content at lower acidification pH values (5.0 and 4.8). Smoluchowski’s theory (compare *2.1.3.1.1*) on perikinetic aggregation was used to explain the effect of Brownian motion to trigger collision and coagulation of the protein particles. The independency of the sol−gel transition temperatures at lower acidification pH values (5.0 and 4.8) was proposed to occur due to approaching of the

isoelectric point of the caseins (4.6), and therefore, the net charge being more important for particle aggregation than the number of protein particles per volume.

Other studies which also focused on dairy-based systems, including rehydrated phosphocaseinate powders (Thomar & Nicolai, 2016), reconstituted pasteurised skim milk (Vasbinder & De Kruif, 2003) and micellar casein suspensions with added whey protein isolate (Kharlamova et al., 2019), agreed on sol−gel transition temperatures decreasing with decreasing acidification pH values. Kharlamova et al. (2019) showed that the addition of fractal whey protein isolate aggregates to aqueous suspensions of micellar casein lowered the temperature of gelation (at a fixed micellar casein concentration) and increased the storage modulus G' of the milk gels. A further decrease of the gelation temperature was found if the pH was decreased, the protein concentration increased or $CaCl_2$ was added.

2.2 Background literature: 3D-printing

The second part of the literature review presents information about 3D-printing in general and different techniques, with a focus on extrusion-based printing of food. Current food printing as well as the advantages and disadvantages/challenges of printing with food grade materials are further discussed.

Parts of this review were submitted as

Wilms, P., Daffner, K., Kern, C., Gras, S.L.,Schutyser, M.A.I., Kohlus R. (2021). Optimising the extrusion of food systems for 3D-printing applications. Food Engineering Review.

2.2.1 Basic Knowledge

Additive Manufacturing (AM) is the technical description for a process which is known as rapid prototyping or 3D-printing (ASTM-International, 2012). The word “additive” in this case means that one layer of material is printed after another, resulting in stackable layers forming the finished object or figure. AM is described as a digitally-controlled process, building up objects layer-by-layer, using a phase transition or chemical reaction to fuse 3D-printed layers together (Wegrzyn et al., 2012).

In the ‘80’s of the last century, different types of three-dimensional printing (3D-printing) were invented. After some years of research Charles Hull was the first to use stereolithography in 1986, and is nowadays considered to be the founding father of 3D-printing. Around the same time Scott Crump performed his first trials with fused deposition modelling (FDM) and founded his company Stratasys. Moreover, selective laser sintering (SLS) was invented in the eighties by Carl Deckard. All these technologies as well as other 3D-printing technologies have in common that they use an object image created by Computer Aided Design (CAD) software and print this object layer-by-layer. A lot of other subcategories can be found under the term Rapid Prototyping (RP), including stereolithography (SLA), selective laser sintering (SLS), laminated object manufacturing (LOM), three-dimensional printing (3DP), fused deposition modelling (FDM) or food layered manufacturing (FLM).

In terms of 3D-printing with food as a feed material, FLM describes a new kind of production process that is a translation of the robotics-based AM process into food fabrication. Instead of a wide range of plastic (acrylonitrile butadiene styrene (ABS) or polylactic acid (PLA)) food is used as feed material. In recent years, 3D-printing of food has become more popular and materials like chocolate (Hao et al., 2010; Lanaro et al., 2017; Mantihal et al., 2019), melted cheese (Le Tohic et al., 2018), food protein pastes (Lille et al., 2018), etc. were 3D-printed.

2.2.2 Procedure for 3D-printing of objects

All Rapid Prototyping techniques have in common that a CAD-model, a virtual design of the object, is constructed via a software (.e.g. SketchUp, Tinkercad, etc.) before any production of a 3D-printed object can be conducted. This model is exported in the so called "rapid prototyping" stereolithography (.stl) file format, sliced by a slicing software (e.g. Cura, Repetier, etc.) and the so called "G-code" is created (Godoi et al., 2019). The G-code includes the commands for e.g. the printing and non-printing speed, the temperature of the nozzle or the flow rate/speed of the printer, whereas the geometry and the size of the object are described by the CAD-model. In the Cartesian configuration the 3D-printer moves in x, y and z-axis (left to right, front to back, up and down) (Sun et al., 2018). After the first layer is deposited, the 3D-object is printed by adding one layer on another until the desired structure is achieved (Melchels et al., 2010). For successful printing layers have to be (almost) solidified before new layers are added. Integrity and firmness of the first 3D-printed layer highly influence how further layers are built up on layers (Kirchmajer et al., 2015).

2.2.3 Techniques for 3D-printing

For AM or FLM different ways of printing are used. According to Wegrzyn et al. (2012), the three most relevant techniques are controlled deposition, controlled fusion and controlled cutting with lamination. The technologies applied for 3D-printing are also subdivided due to material properties, e.g. liquid, powder or cell cultures (Godoi et al., 2016). According to the latter author, deposition of liquid materials is done via extrusion or inkjet processes whereas powder-based materials are 3D-printed by deposition followed by the use of a heat source, e.g. a laser or hot air, or a particle binder. Some of the most common 3D-printing technologies are briefly explained within the subsequent sections. Up to now, several reviews are available (Lipton et al.., 2015; Liu et al., 2017, Gholamipour-Shirazi et al., 2020), with one focusing mainly on extrusion-based food printing (Dankar et al., 2018). Currently available commercial extrusion-based food printers were presented in other reviews (Sun et al., 2018; Toh et al., 2018).

2.2.3.1 Fused Deposition Modelling

The first example given for controlled deposition is fused deposition modelling (FDM), also termed fused filament fabrication (FFF). For this technique pastes, gels or molten materials are used and extruded. In earlier days traditional plastic printers started with a solid material (e.g. ABS or PLA), which was transported to a heated nozzle, melted and deposited on the printing platform, where it was re-solidified. Three extrusion mechanisms are possible, namely syringe-based, screw-based and air pressure driven extrusion (Sun et al., 2018). During 3D-printing, one or more extrusion nozzles can be used which work within the Cartesian coordinate space (x-, y- and z-axis) (Wegrzyn et al., 2012). Either the nozzle above the printing platform or the printing platform underneath the nozzle is moved in the y-axis direction.

In general, food grade materials for FLM must be viscous or viscoelastic initially and become a self-supporting gel before the second or more layers are added (Godoi et al., 2016). For ideal printing, the material has to be highly thixotropic, meaning that the viscosity has to become low quickly when applying a shear force but it recovers quickly after the shear force is removed, shown for alginate-based hydrogels (Li et al., 2016). Depending on the material for the extrusion-based printing process, layer-by-layer printing occurs due to accommodation of layers controlled by the rheological properties of the materials, solidification upon cooling or hydrogel-forming extrusion (Godoi et al., 2016). The corresponding techniques are called soft materials extrusion (SME), hot melt extrusion (HME) and hydrogel-forming extrusion, respectively.

For SME, self-supporting layers of the feed material are deposited on the printing bed. A critical process parameter is the viscosity which has to be low enough to ensure extrusion through the nozzle and high enough to allow layer-by-layer deposition. Materials being used in the past were cake frosting (Periard et al., 2007), sugar cookies as well as scallop and turkey-meat purée (Lipton et al., 2010). For a variety of hydrocolloid-based pastes (Gholamipour-Shirazi et al., 2019), different formulations were classified as printable via shortcut methods, if the phase

angle was found in the range of $3 - 15°$ and the relaxation exponent in the range of $0.03 - 0.13$. To print Mickey Mouse models via SME, the design and characterisation of dough formula, differing e.g. in sucrose or butter content, were investigated and those parameters were related to printability (Yang et al., 2018).

For HME, the material is heated slightly above its melting point to fuse to the previous layer (Sun et al., 2015a). So far, the main food material investigated was chocolate (Hao et al., 2010; Lanaro et al., 2017; Mantihal et al., 2019), as it shows sol−characteristics above the melting temperature and solidifies at room temperature. This sol−gel transition of chocolate is triggered via rapid solidification (crystallization; called tempering) after deposition. Examples for shortcut methods for HME were found with semi-hard model cheese (Kern et al., 2018), as the critical shear rate ($10 - 30\ s^{-1}$) increased significantly with decreasing calcium levels and with increasing flowability ($\tan \delta_{60°C}$) and with gelatin-kappa-carrageenan mixtures (Warner et al., 2019), where printing fidelity was related to the magnitude of G', which had to surpass 23 kPa.

For hydrogel-forming extrusion, the first layer needs to have structural integrity before the second layer is deposited (Kirchmajer et al., 2015), with rheological properties and gel forming mechanisms of the feed material being important characteristics influencing the 3D-printing process (Liu et al., 2017). Printing of hydrogels was conducted in recent years to create tissues or organs (Cohen et al., 2008; Song et al., 2010). The three mechanisms for hydrogel printing were chemical linking, ionotropic cross linking and complex coacervate formation (Kirchmajer et al., 2015). The hydrogel material and the surface energy of the printing bed play a crucial role for successful printing due to their influence on the spreading of the feed material.

Up to now, there is still little knowledge available how to correlate material characteristics to critical variables of extrusion-based printing processes as well as to the material structure of the printed object (Severini et al., 2018). Most of the extrusion-based food printing has been conducted with pastes and gels or chocolate, with the latter being one of the most suitable food

grade materials. *Table 2-4* provides some information regarding rheological properties, parameter adjustments for printing and upcoming difficulties during the printing process, which were found within experiments of other research groups. A very detailed table presenting all the work performed in the last ten years in the area of food printing, including the type of printer, can be found in a recent review (Gholamipour-Shirazi et al., 2020).

The formulation engineering approach of research groups varies, with the majority only presenting suitable formulations or process parameters which have resulted in "successful" printing. However, to print objects of high quality, the understanding of the interplay between ingredients, process parameters and equipment design (printer set-up) is necessary (Cheyne et al., 2005). Extrusion-based printers are commercially available (Sun et al., 2018) but most of the research was conducted on customised printers, which complicates comparisons of results. A positive example of "tackling the whole problem" was shown in a recent study, where the calculation of important extrusion-based printing parameters, the application of empirical models (power law behaviour) and the characterisation of material properties (e.g. sol−gel transition) were conducted for alginate-based hydrogels (Li et al., 2016).

Common issues why certain formulation (e.g. protein/ fat content) or process parameters (e.g. print speed, extrusion flow rate) caused problems during printing (e.g. nozzle plugging, inaccurate printing) were not explained in detail in previous studies. Advanced knowledge regarding all the material characteristics (physical, chemical and mechanical) as well as process parameters would be necessary to better define printability and further develop formulation engineering. So far, negative results, including problems and failures during printing, did not receive attention but would be necessary to improve the correlation between formulation engineering, e.g. macronutrient content, pH etc., and the actual extrusion-based printing process, e.g. the effect of shear, temperature, and local temperature changes (Cheyne et al., 2005).

Table 2-4: Examples of previous results of extrusion-based 3D-printing of food materials.

Research group	Technique	Material	Important product parameters	Important process Parameters	Difficulties
Hao et al. (2010)	HME[a]	Chocolate	Viscosity	Nozzle diameter, nozzle height, extrusion rate, nozzle moving speed	Inaccurate parts at non-optimal build height, nozzle aperture diameter
Lanaro et al. (2017)	HME[a]	Chocolate	Viscosity, yield point	Tip to collector distance, printer movement speed, fan speed, fan temperature	Extrusion not always in a consistent strand
Lille et al. (2018)	SME[b]	Protein pastes	Storage modulus (G'), loss modulus (G''), phase angle	Air pressure, printing speed, diameter of the tip	Clogged tip, spreading after printing, thick and dry materials fail to print
Derossi et al. (2018)	SME[b]	Fruit-based snacks	Shear stress, apparent viscosity	Print speed, print flow, height of printed material, infill porosity	printing at low flow: internal structure irregular with interrupted filaments and over porosity fraction printing at high flow: filaments merge each other resulting in increase in thickness of internal structure
Kern et al. (2018)	HME[a]	Semi-hard model cheese	Storage modulus (G'), loss modulus (G''), phase angle, gel−sol transition temperature	Process temperature, shear rate, pressure, wall shear stress	Exceeding a critical shear rate results in extrusion instabilities
Yang et al., (2018)	SME[b]	Baking dough	Storage modulus (G'), loss Modulus (G''), relaxation time (T2)	Nozzle moving speed, extrusion speed	Total solid content exceeded certain threshold, extrusion was deteriorated
Warner et al. (2019)	HME[a]	Gelatin–kappa-carrageenan mixtures	Storage modulus (G'), loss modulus (G''), viscosity, gelling temperature	Printing speed, non-print moving speed	Gelation in nozzle, spreading, broken lines, dragging
Gholamipour-Shirazi et al. (2019)	SME[b]	hydrocolloid-based pastes	Phase angle, relaxation exponent	Diameter and shape of tip/die	Liquid and non-self-supporting materials, too thick samples fail to print
Mantihal et al. (2019)	HME[a]	Chocolate	Melting point, apparent viscosity, yield stress, lubrication properties	Printing speed, extrusion temperature, nozzle diameter	-

[a]) HME = hot melt extrusion
[b]) SME = soft matter extrusion (also called room temperature extrusion)

2.2.3.2 Powder based printing

Powder binding deposition is another way of 3D-printing of food grade materials and is divided into three subtypes (Godoi et al., 2016): Selective Laser Sintering (SLS), Selective hot air sintering and melting (SHASAM) and Liquid binding (LB). All of these technologies have in common that they use a powder and binder to construct 3D figures layer-by-layer. After having spread a layer of powder on the printing plat/bed, the ink-jet head starts to deposit binding materials into the powder. This process is repeated until all layers are completed. Unbound powder has to be removed at the end of 3D-printing. Only little work on powder based printing was published, but Nesquik squares, curry cubes, paprika pyramids and cinnamon cylinders were printed by researchers from TNO using SLS (van der Linden, 2015), shown in *Figure 2-13*.

Figure 2-13: Selective laser sintering of food powders. TNO Nesquik powder (left), sugar (middle) and spice powders (right) (van der Linden, 2015).

During SLS a printing bed or platform is filled with powder (e.g. sugar, sugar-rich powders). Hot air or a laser moves along the x- and y-axes as a sintering source and binds the particles together. As a consequence of this a solid layer can be formed. After the first layer is fused, the powder bed has to be lowered by one layer thickness, and a new layer of particles is deposited on top. This process is repeated continuously as often as it is necessary to build up the 3D object (Godoi et al., 2016, Sun et al, 2015a). While the sintered material forms the 3D-printed object the unsintered powder helps to support the structure. A particular advantage for this technology is the possibility to build up complex structures in a short time without post-curing.

Nonetheless, fabrication processes and machine structure are complicated because many parameters are involved. One main disadvantage of this technique is the compulsory use of a powder or material which can be dried in some way. Therefore, many raw materials cannot be used and manufactured for this printing technology (Sun et al., 2015b).

2.2.3.3 Stereolithography

Stereolithography is the oldest and the least applicable printing technology for 3D-printing of food. During stereolithography a laser cures material into a solid form layer-by-layer. According to its inventor Charles Hull (1986), a movable spot beam of ultraviolet light is used and shines on the surface of a liquid. The whole process is performed until the object is successfully printed. In the non-food industry, resin is mostly used as feed material and is selectively hardened with an ultraviolet laser. Material which was not cured is re-used. According to Godoi et al. (2016), this technology, which uses photo-sensitive materials, is not suitable for 3D-printing of food but could be used in the field of packaging.

2.2.3.4 Jetting-based printing

Inkjet printing is based on a drop deposition process consisting of ejection and detachment. Liquid materials are deposited layer-by-layer with each layer composed of distinct droplets which are either dispensed on a substrate, or a previous layer of the same material, or a powder layer (Vadodaria & Mills, 2020). Piezoelectric inkjet printing, binder jetting, electrostatic jetting, hot-melt jetting and pneumatic jetting are examples for jetting based applications. The application of these techniques for food grade materials is strongly limited as materials have to have very low viscosities (>0.03 Pa s). Moreover, this technology is very hard to scale up into a production of customised food (Vadodaria & Mills, 2020).

2.2.4 3D-printing of food materials

Materials for 3D-printing were classified into different groups (Sun et al., 2015a). The first group included natively printable materials, which can be easily extruded from a syringe. Examples of food grade materials were cake frosting (Periard et al., 2007), cheese (Le Tohic et al., 2018), hummus and chocolate (Lanaro et al., 2017), with the latter shown in *Figure 2-14*. Such natively printable food grade materials can be customised regarding taste, nutritional value and texture (Sun et al., 2015a).

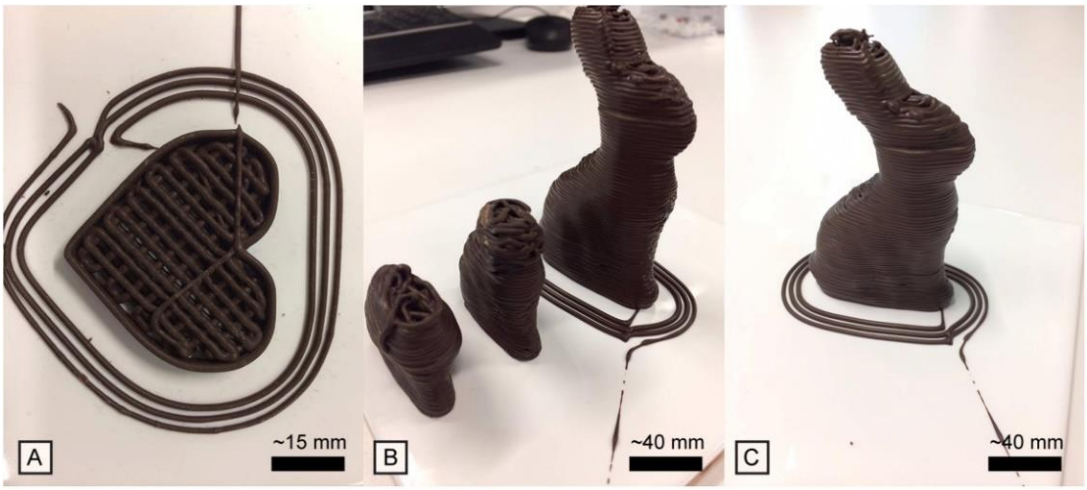

Figure 2-14: 3D-printed Chocolate. (A) No air cooling used, simple 2D structures were made (height is 9 mm). (B) More complex structures were attempted, such as a chocolate bunny without cooling (height is 30 mm and 42 mm). (C) Using cooling, a complex three-dimensional bunny was made (height is 94 mm) (Lanaro et al., 2017).

The second group contained traditional food material consumed in daily life which can normally not be printed due to its composition. Examples given were fruits, vegetables, rice, fish and meat. By adding a defined concentration of hydrocolloids to these solid materials, extrusion was possible according to Sun et al. (2015a). These authors referred e.g. to Cohen et al (2009) who studied hydrocolloids like xanthan gum and gelatin and to Lipton et al. (2010) who worked with cereal paste as well as with turkey (A) and scallop (B), shown in *Figure 2-15*. The latter two products were processed first (puréed) to become an extrudable material. Before printing the transglutaminase was added, causing formation of a new protein matrix over time. Therefore,

Lipton et al. (2010) destroyed the macrostructure of these raw materials, changing texture and taste, and fried or sous-vide cooked the turkey and scallop after printing.

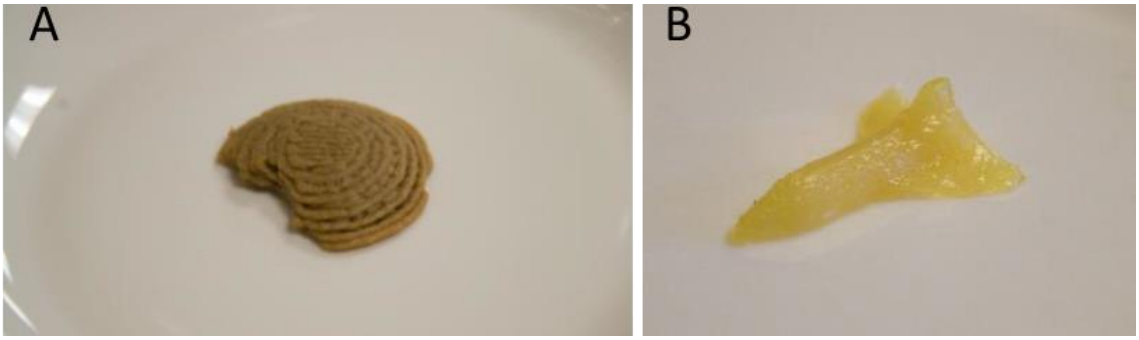

Figure 2-15: A turkey with transglutaminase in a truncated hemisphere (A) and a scallop (B) as a space shuttle were 3D-printed (Lipton et al., 2010).

The third group were alternative ingredients, e.g. extrudable materials mixed with insect powder. The insect flour (dry and grind) was mixed with icing butter, cream cheese or water, gelling agent and flavouring to achieve a consistency of the product which allowed to pass the nozzle. Different concentrations of mealworms were used as another innovative protein source, mixed with wheat flour and helped to modify the printability of the dough (Severini et al., 2018). Depending on the concentration of protein powder added to the flour, the morphological and microstructural characteristics of the final dough changed.

Until now, feed materials like food are restricted for extrusion-based 3D-printing and it has to be considered that a phase transition (e.g. sol to gel) does not work with all types of raw materials due to their multi-complex nano-/ microstructure. Nevertheless, especially hot melt extrusion was used for the creation of personalised chocolate products (Hao et al., 2010; Lanaro et al., 2017; Mantihal et al., 2019). Hao et al. (2010) printed 3D chocolate products in different shapes and sizes, e.g. a logo with letters. These researchers worked with nozzles of circular shape with diameters of 1.0-, 1.25- and 1.5 mm and found several critical parameters influencing the process, namely nozzle aperture diameter, optimum nozzle height from the printing platform, extrusion rate and axis movement speed (compare *Table 2-4*).

Le Tohic et al. (2018) used this technique to print melted cheese with different extrusion rates. 3D-printed cheese was compared to normal industrial processed cheese (25% fat, 18% protein) from a supermarket. It was found that 3D-printed cheese samples had almost 50% less hardness than normal untreated cheese. By using confocal laser scanning microscopy they also showed that higher extrusion flow rates (12 ml min^{-1}) resulted in a smaller fat globule size and a more uniform fat particle size distribution compared to lower extrusion flow rates (4 ml min^{-1}). Le Tohic et al. (2018) attributed this effect to a higher shear rate disrupting more fat globules, which proved that FLM can control the microstructure of the final object.

2.2.5 Advantages of 3D-printing of food

FLM does not only offer many advantages from a production point of view but also for the consumer. For all types of feed materials, complex objects with hollow structures can be printed whereas they cannot be created with traditional machines (Godoi et al., 2016). For traditional printing with plastic, geometric complexity and economy at low volume of production are the two main advantages, which also offer great potential for food applications (Lipton et al., 2015). The geometric complexity is achieved by the use of CAD-software, where almost all shapes can be designed. Changes in the design of a 3D-printed object and engineering are quickly done via a computer programme (Hull, 1986). Therefore, another advantage of this rapid prototyping tool is the short amount of time needed from creating a prototype until 3D-printing of the final object, which is several times faster than the traditional way (Liu et al., 2017; Vancauwenberghe et al., 2017). Hence, 3D-printing could also be applied as a potential prototyping tool for the development of novel food products.

Specifically with food grade materials, printing can offer highly controlled diets, e.g. for athletes or elderly people on the one hand (Ross et al., 2019), and it enables the customised manufacture of new textures and structural elements on the other hand (Lipton, 2017). This could help to improve personalised nutrition via food printing (Lipton, 2017), as many people suffer

diseases like diabetes and could benefit from individualised food. Individualised and customised food in different shapes, textures and colours with tailorable nutrients based on personal dietary requirements could be manufactured.

3D-printed food objects could be printed on-time or even at home. This would result in reduced storage or distribution costs and a reduction of food waste (Ross et al., 2019). Stockrooms as well as storage time could be reduced or avoided, whereas traditional manufacturing products go hand in hand with storage time of some days up to weeks or even months. For small suppliers, 3D-printing of food offers the advantage of objects being freshly created as a point-of-sale application to convince consumers from their range of products (Lipton et al., 2015; Wegrzyn et al., 2012). Compared to mass production in manufacturing plants a more sustainable process is performed due to less material loss. No forms, moulded parts, etc. are used and almost no waste material is produced during the printing process (Holland et al., 2017).

2.2.6 Disadvantages and challenges of 3D-printing of food

Although there are many advantages of FLM, several disadvantages and challenges (still) exist. From a manufacturing point of view, mass production of 3D-printed food products is currently not profitable because production for one single piece takes much longer compared to industrial manufacturing and consumers are unwilling to pay a significantly higher price. At the moment, manufacturing of 3D-printed objects takes up to several minutes or even longer, whereas industrial machines are capable of far quicker production in higher volumes (Lipton et al., 2015). At the moment, only low volumes are printed and prices have to be higher to make 3D-printed objects commercially viable. Therefore, for a more sustainable and profitable production of 3D-printed objects in manufacturing plants, printing processes have to be conducted faster and much cheaper, e.g. running a large number of printers simultaneously. For the customisation of food grade materials in high volumes, a strong interaction of the layers is a key point to manufacture high quality 3D-printed objects (Godoi et al., 2016).

Limited materials being available in the food sector are another challenge, mainly due to the complex microstructure of many raw materials (Godoi et al., 2016). Product groups like fruits and vegetables or meat and fish have to be “destroyed”, e.g. pureed, and then 3D-printed via the help of enzymes or other techniques (Lipton et al., 2015). Hence, the question arises if it is really useful to print these kind of materials.

Another big challenge is the currently available background knowledge of food material properties and the correlation of their physico-chemical characteristics to printing parameters. Before printing a variety of food materials can be performed, detailed background knowledge is necessary regarding the rheological behaviour of the 3D-printed object, e.g. about the viscosity or the phase transition temperature, to know how to adjust parameters at the printer. The composition of the feed material strongly influences the structure and the printability. According to Lille et al. (2018), the biggest challenges in 3D-printing of food materials are rheology of the ingredient mix, structure accuracy, shape stability as well as the printing speed.

Up to now, the accuracy of 3D-printed food objects is limited compared to industrial manufacturing. Many parameters have to be known and adjusted to enhance 3D-printing in a precise manner. Experiments have to be conducted to calculate suitable flow rates, printing speeds, etc. and to better understand the “black box” extrusion-based 3D-printing.

All these factors demonstrate why 3D-printing of food is a complex technology and considerable research will be necessary to overcome these challenges and implement 3D-printing with food materials within a daily usage in everyone’s kitchen.

2.3 References

Anema, S. G. (2020). The whey proteins in milk: thermal denaturation, physical interactions, and effects on the functional properties of milk. In Milk proteins (pp. 325-384). Academic Press.

Anema, S. G., & Klostermeyer, H. (1997). Heat-induced, pH-dependent dissociation of casein micelles on heating reconstituted skim milk at temperatures below 100 C. Journal of Agricultural and Food Chemistry, 45(4), 1108-1115.

Anema, S. G., & Li, Y. (2000). Further studies on the heat-induced, pH-dependent dissociation of casein from the micelles in reconstituted skim milk. LWT-Food Science and Technology, 33(5), 335-343.

Anema, S. G., & Li, Y. (2003a). Association of denatured whey proteins with casein micelles in heated reconstituted skim milk and its effect on casein micelle size. Journal of Dairy Research, 70(1), 73-83.

Anema, S. G., & Li, Y. (2003b). Effect of pH on the association of denatured whey proteins with casein micelles in heated reconstituted skim milk. J. Agric. Food Chem. 51(6), 1640-1646.

Anema, S. G., Lee, S. K., Lowe, E. K., & Klostermeyer, H. (2004a). Rheological properties of acid gels prepared from heated pH-adjusted skim milk. Journal of Agricultural and Food Chemistry, 52(2), 337-343.

Anema, S. G., Lowe, E. K., & Lee, S. K. (2004b). Effect of pH at heating on the acid-induced aggregation of casein micelles in reconstituted skim milk. LWT-Food Science and Technology, 37(7), 779-787.

Anema, S. G. (2007). Role of κ-casein in the association of denatured whey proteins with casein micelles in heated reconstituted skim milk. Journal of agricultural and food chemistry, 55(9), 3635-3642.

Astaire, J. C., Ward, R., German, J. B., & Jimenez-Flores, R. (2003). Concentration of polar MFGM lipids from buttermilk by microfiltration and supercritical fluid extraction. Journal of dairy science, 86(7), 2297-2307.

ASTM-International (2012). Standard terminology for additive manufacturing technologies. In ASTM F2792-10e1 standard, Vol ASTM F2792-10e1 Standard. ASTM International.

Berli, C. L. A., Deiber, J. A., & Anon, M. C. (1999). Heat-induced phenomena in soy protein suspensions. Rheometric data and theoretical interpretation. J Agric Food Chem 47, 893–900.

Bremer, L. G., van Vliet, T., & Walstra, P. (1989). Theoretical and experimental study of the fractal nature of the structure of casein gels. Journal of the Chemical Society, Faraday Transactions 1: Physical Chemistry in Condensed Phases, 85(10), 3359-3372.

Brownlow, S., Cabral, J. H. M., Cooper, R., Flower, D. R., Yewdall, S. J., Polikarpov, I., ... & Sawyer, L. (1997). Bovine β-lactoglobulin at 1.8 Å resolution—still an enigmatic lipocalin. Structure, 5(4), 481-495.

Buchheim, W. (1986). Membranes of milk fat globules ultrastructural biochemical and technological aspects. Kieler Milchwirtschliche Forschungsberichte, 38, 227-246.

Cano-Ruiz, M. E., & Richter, R. L. (1997). Effect of homogenization pressure on the milk fat globule membrane proteins. Journal of Dairy Science, 80(11), 2732-2739.

Cheyne, A., Barnes, J., & Wilson, D. I. (2005). Extrusion behaviour of cohesive potato starch pastes: I. Rheological characterisation. Journal of food engineering, 66(1), 1-12.

Cohen, D. L., Tsavaris, A. M., Lo, W. M., Bonassar, L. J., & Lipson, H. (2008, August). Improved quality of 3D-printed tissue constructs through enhanced mixing of alginate hydrogels. In Proceedings of the 19th Solid Freeform Fabrication Symposium (pp. 4-6).

Cohen, D. L., Lipton, J. I., Cutler, M., Coulter, D., Vesco, A., & Lipson, H. (2009). Hydrocolloid printing: a novel platform for customized food production. In Solid Freeform Fabrication Symposium (pp. 807-818). Austin, TX.

Corredig, M., & Dalgleish, D. G. (1996). Effect of temperature and pH on the interactions of whey proteins with casein micelles in skim milk. Food Research International, 29(1), 49-55.

Creamer, L. K., Berry, G. P., & Mills, O. E. (1977). Study of the dissociation of beta casein from the bovine casein micelle at low temperature. New Zealand Journal of Dairy Science and Technology.

Creamer, L. K., Parry, D. A. D., & Malcolm, G. N. (1983). Secondary structure of bovine β-lactoglobulin B. Archives of Biochemistry and Biophysics, 227(1), 98-105.

Dalgleish, D. G. (2011). On the structural models of bovine casein micelles - review and possible improvements. Soft Matter, 7, 2265-2272.

Dalgleish, D. G., Spagnuolo, P. A., Goff, H. D. (2004). A possible structure of the casein micelle based on high-resolution field-emission scanning electron microscopy. International Dairy Journal 14, 1025–1031.

Dannenberg, F., & Kessler, H. G. (1988). Reaction kinetics of the denaturation of whey proteins in milk. Journal of Food Science, 53(1), 258-263.

Deeth, H. C. (1997). The role of phospholipids in the stability of milk fat globules. Australian Journal of Dairy Technology, 52, 44-46.

Dewettinck, K., Rombaut, R., Thienpont, N., Le, T. T., Messens, K., & Van Camp, J. (2008). Nutritional and technological aspects of milk fat globule membrane material. International dairy journal, 18(5), 436-457.

Dickinson, E. (1994). Protein-stabilized emulsions. Journal of Food Engineering, 22, 59-74.

Dickinson, E. (1999). Caseins in emulsions: interfacial properties and interactions. International Dairy Journal, 9(3-6), 305-312.

Dickinson, E., & van Vliet, T. (2003). Food Colloids, Biopolymers and Materials. Royal Society of Chemistry.

Dickinson, E. (2006). Structure formation in casein-based gels, foams, and emulsions. Colloids and Surfaces A: Physicochem. Eng. Aspects 288, 3-11.

Donato, L., & Dalgleish, D. G. (2006). Effect of the pH of heating on the qualitative and quantitative compositions of the sera of reconstituted skim milks and on the mechanisms of formation of soluble aggregates. Journal of agricultural and food chemistry, 54(20), 7804-7811.

Donato, L., & Guyomarc'h, F. (2009). Formation and properties of the whey protein/$\kappa $-casein complexes in heated skim milk–A review. Dairy Science and Technology, 89(1), 3-29.

Farrell Jr, H. M., Jimenez-Flores, R., Bleck, G. T., Brown, E. M., Butler, J. E., Creamer, L. K., ... & Swaisgood, H. E. (2004). Nomenclature of the proteins of cows' milk—Sixth revision. Journal of dairy science, 87(6), 1641-1674.

Fong, B.Y., Norris, C.S., & MacGibbon, A.K.H.: Protein and lipid composition of bovine milk-fat-globule membrane. In: International Dairy Journal 17 (2007), S.275-288.

Fox, P. F., & McSweeney, P. L. (1998). Dairy chemistry and biochemistry.

Fox, P. F., & Mulvihill, D. M. (1990). Casein. In Food gels (pp. 121-173). Springer, Dordrecht.

Fox, P.F., & Kelly, A.L. (2006). Chemistry and Biochemistry of Milk constituents. In Food Biochemistry & Food Processing, (Blackwell Publishing).

Gholamipour-Shirazi, A., Norton, I. T., & Mills, T. (2019). Designing hydrocolloid based food-ink formulations for extrusion 3D printing. Food Hydrocolloids, 95, 161-167.

Gholamipour-Shirazi, A.; Kamlow, M.-A.; T. Norton, I.; Mills, T. How to Formulate for Structure and Texture via Medium of Additive Manufacturing-A Review. Foods 2020, 9, 497.

Godoi, F. C., Prakash, S., & Bhandari, B. R. (2016). 3d printing technologies applied for food design: Status and prospects. Journal of Food Engineering, 179, 44-54.

Godoi, F. C., Bhandari, B. R., Prakash, S., & Zhang, M. (2019). An introduction to the principles of 3D food printing. In Fundamentals of 3D Food Printing and Applications (pp. 1-18). Academic Press.

Goyanes, A., Buanz, A. B., Basit, A. W., & Gaisford, S. (2014). Fused-filament 3D printing (3DP) for fabrication of tablets. International journal of pharmaceutics, 476(1), 88-92.

Hammelehle B, Schkoda P and Kessler H G (1997) Parameters for coagulation properties of direct acidified milk and for the structure of milk gels. Milchwissenschaft 52 671–674.

Hambling, S. G., Mc Alpine, A. S., & Sawyer, L. (1992). β-lactoglobulin. In P. F. Fox (Ed.), Advanced dairy chemistry -1: Proteins (pp. 141-190). London: Elsevier Applied Science.

Hao, L., Mellor, S., Seaman, O., Henderson, J., Sewell, N., & Sloan, M. (2010). Material characterisation and process development for chocolate additive layer manufacturing. Virtual and Physical Prototyping, 5(2), 57-64.

Heertje, I., Visser, J., & Smits, P. (1985). Structure formation in acid milk gels. Food Structure, 4(2), 10.

Holland, S., Foster, T., MacNaughtan, W., & Tuck, C. (2018). Design and characterisation of food grade powders and inks for microstructure control using 3D printing. Journal of Food Engineering, 220, 12-19.

Holt, C. (1992). Structure and stability of bovine casein micelles. In Advances in protein chemistry (Vol. 43, pp. 63-151). Academic Press.

Holt, C., & Sawyer, L. (1993). Caseins as rheomorphic proteins: interpretation of primary and secondary structures of the α_{S1}-, β-and κ-caseins. Journal of the Chemical Society, Faraday Transactions, 89(15), 2683-2692.

Holt, C., Carver, J. A., Ecroyd, H., & Thorn, D C. (2013). Invited review: Caseins and the casein micelle: Their biological functions, structures, and behavior in foods. Journal of Dairy Science, 96 (10), 6127-6146.

Horne, D. S. (1986). Steric stabilization and casein micelle stability. Journal of Colloid and Interface Science, 111(1), 250-260.

Horne, D. S., & Leaver, J. (1995). Milk proteins on surfaces. Food Hydrocolloids, 9(2), 91-95.

Horne, D. S. (1998). Casein interactions: casting light on the black boxes, the structure in dairy products. International Dairy Journal, 8(3), 171-177.

Horne, D. S. (2002). Casein structure, self-assembly and gelation. Current Opinion in Colloid and Interface Science 7, 456-461.

Horne, D. S. (2006). Casein micelle structure: Models and muddles. Current Opinion Colloid Interface Science 11, 148-153.

Hull, C. W. (1986). U.S. Patent No. 4,575,330. Washington, DC: U.S. Patent and Trademark Office.

Huppertz, T., & Kelly, A. L. (2006). Physical chemistry of milk fat globules. In Advanced Dairy Chemistry Volume 2 Lipids (pp. 173-212). Springer, Boston, MA.

Jang, H. D., & Swaisgood, H. E. (1990). Disulfide bond formation between thermally denatured β-lactoglobulin and κ-casein in casein micelles. Journal of Dairy Science, 73(4), 900-904.

Kern, C., Weiss, J., & Hinrichs, J. (2018). Additive layer manufacturing of semi-hard model cheese: Effect of calcium levels on thermo-rheological properties and shear behavior. Journal of food engineering, 235, 89-97.

Kessler, H. G. (2002). Food and bio process engineering: dairy technology. Verlag A. Kessler.

Kirchmajer, D. M., & Gorkin III, R. (2015). An overview of the suitability of hydrogel-forming polymers for extrusion-based 3D-printing. Journal of Materials Chemistry B, 3(20), 4105-4117.

De Kruif, C. G. (1997). Skim milk acidification. Journal of colloid and interface science, 185, 19-25.

De Kruif C. G., & Roefs S. P. F. M. (1996) Skim milk acidification at low temperatures: a model for the stability of casein micelles. Netherlands Milk Dairy Journal 50 113–120.

De Kruif, C. G., & Holt, C. (2003). Casein micelle structure, functions and interactions. In Advanced Dairy Chemistry-1 Proteins (pp. 233-276). Springer US.

De Kruif, C. G., Huppertz, T., Urban, V. S., Petukhov, A. V. (2012). Casein micelles and their internal structure. Advances in Colloid and Interface Science, 171-172, 36-52.

Kharlamova, A., Nicolai, T., & Chassenieux, C. (2019). Heat-induced gelation of mixtures of casein micelles with whey protein aggregates. Food hydrocolloids, 92, 198-207.

D.M. Kirchmajer, R. Gorkin III, M. in het Panhuis. An overview of the suitability of hydrogel-forming polymers for extrusion-based 3D-printing. Journal of Materials Chemistry B, 3 (20) (2015), 4105-4117.

Koutina, G., Knudsen, J. C., Andersen, U., & Skibsted, L. H. (2014). Temperature effect on calcium and phosphorus equilibria in relation to gel formation during acidification of skim milk. International Dairy Journal, 36, 65–73.

Koutina, G., Christensen, M., Bakman, M., Andersen, U., & Skibsted, L. H. (2016) Calcium induced skim-milk gelation during heating as affected by pH. Dairy Science and Technology 96 79–93.

Lanaro, M., Forrestal, D. P., Scheurer, S., Slinger, D. J., Liao, S., Powell, S. K., & Woodruff, M. A. (2017). 3D printing complex chocolate objects: Platform design, optimization and evaluation. Journal of Food Engineering, 215, 13-22.

Li, H., Liu, S., & Lin, L. (2016). Rheological study on 3D printability of alginate hydrogel and effect of graphene oxide. International Journal of Bioprinting, 2(2), 54-66.

Lille, M., Nurmela, A., Nordlund, E., Metsä-Kortelainen, S., & Sozer, N. (2018). Applicability of protein and fiber-rich food materials in extrusion-based 3D printing. Journal of Food Engineering, 220, 20-27.

Lipton, J., Arnold, D., Nigl, F., Lopez, N., Cohen, D., Norén, N., Lipson, H. (2010). Multi-material food printing with complex internal structure suitable for conventional post-processing. In: 21st Annual International Solid Freeform Fabrication Symposium - an Additive Manufacturing Conference, SFF 2010, pp. 809-815.

Lipton, J. I., Cutler, M., Nigl, F., Cohen, D., & Lipson, H. (2015). Additive manufacturing for the food industry. Trends in Food Science & Technology, 43(1), 114-123.

Lipton, J. I. (2017). Printable food: the technology and its application in human health. Current opinion in biotechnology, 44, 198-201.

Li, H., Liu, S., & Lin, L. (2016). Rheological study on 3D printability of alginate hydrogel and effect of graphene oxide. International Journal of Bioprinting, 2(2), 54-66.

Liu, W., Ye, A., Liu, W., Liu, C., & Singh, H. (2013). Stability during in vitro digestion of lactoferrin-loaded liposomes prepared from milk fat globule membrane-derived phospholipids. Journal of dairy science, 96(4), 2061-2070.

Liu, Z., Zhang, M., Bhandari, B., & Wang, Y. (2017). 3D printing: Printing precision and application in food sector. Trends in Food Science & Technology, 69, 83-94.

Liu, Z., Zhang, M., Bhandari, B., & Yang, C. (2018). Impact of rheological properties of mashed potatoes on 3D printing. Journal of Food Engineering, 220, 76-82.

Loewen, A., Nöbel, S., & Hinrichs, J. (2017). Microgel Particles and Their Effect on the Textural Properties of Foods. https://doi.org/10.1016/B978-0-08-100596-5.21098-6.

Lucey, J. A., & Singh, H. (1997). Formation and physical properties of acid milk gels: a review. Food Research International, Vol. 30, No. 7, 529-542.

Mantihal, S., Prakash, S., Godoi, F. C., & Bhandari, B. (2019). Effect of additives on thermal, rheological and tribological properties of 3D printed dark chocolate. Food research international, 119, 161-169.

McPherson, A. V., & Kitchen, B. J. (1983). Reviews of the progress of dairy science: the bovine milk fat globule membrane–its formation, composition, structure and behaviour in milk and dairy products. Journal of Dairy Research, 50(1), 107-133.

Melchels, F. P., Feijen, J., & Grijpma, D. W. (2010). A review on stereolithography and its applications in biomedical engineering. Biomaterials, 31(24), 6121-6130.

Michalski, M. C., Michel, F., Sainmont, D., & Briard, V. (2002). Apparent ζ-potential as a tool to assess mechanical damages to the milk fat globule membrane. Colloids and Surfaces B: Biointerfaces, 23(1), 23-30.

Michalski, M. C., Briard, V., Michel, F., Tasson, F., & Poulain, P. (2005). Size distribution of fat globules in human colostrum, breast milk, and infant formula. Journal of dairy science, 88(6), 1927-1940.

Melchels, F. P., Feijen, J., & Grijpma, D. W. (2010). A review on stereolithography and its applications in biomedical engineering. Biomaterials, 31(24), 6121-6130.

Mulder, H., & Walstra, P. (1974). The milk fat globule (p. 179). Farnham Royal: Commonwealth Agricultural Bureaux.

Myers, D. (1990). Surfaces, interfaces and colloids. New York etc.: Wiley-Vch.

Nöbel, S. (2016). Dairy Microgel Suspensions: Principles, Phenomena and Models at Different Structural Levels. Verlag Dr. Hut.

Nöbel, S., Seifert, B., Schäfer, J., Daffner, K., & Hinrichs, J. (2018). Oral presentation food colloids. Leeds (2018) - session - Processing of Novel Structures for Functionality. Temperature-triggered gelation of milk concentrates applied to 3D food printing.

Oldfield, D. J., Singh, H., Taylor, M. W., & Pearce, K. N. (2000). Heat-induced interactions of β-lactoglobulin and α-lactalbumin with the casein micelle in pH-adjusted skim milk. International Dairy Journal, 10(8), 509-518.

Parker, E. A., Donato, L., & Dalgleish, D. G. (2005). Effects of added sodium caseinate on the formation of particles in heated milk. Journal of agricultural and food chemistry, 53(21), 8265-8272.

Payens, T. A. J. (1979). Casein micelles: the colloid-chemical approach. Journal of Dairy Research, 46, 291-306.

Periard, D., Schaal, N., Schaal, M., Malone, E., Lipson, H., 2007. Printing food. In: 18th

Solid Freeform Fabrication Symposium, SFF 2007, pp. 564-574.

Phadungath, C. (2005). Casein micelle structure: a concise review. J. Sci. Technol., 27(1), 201-212.

Roefs, S. P. F. M. (1986). Dissertation: Structure of acid casein gels - A study of gels formed after acidification in the cold. University of Wageningen.

Sawyer, W. H. (1969). Complex between β-lactoglobulin and κ-casein. A review. Journal of Dairy Science, 52(9), 1347-1355.

Schäfer, J., Läufle, I., Schmidt, C., Atamer, Z., Nöbel, S., & Sonne, A., et al. (2018). The sol−gel transition temperature of skim milk concentrated by microfiltration as affected by pH and protein content. International Journal of Dairy Technology, 71(3), 585-592.

Severini, C., Azzollini, D., Albenzio, M., & Derossi, A. (2018). On printability, quality and nutritional properties of 3D printed cereal based snacks enriched with edible insects. Food Research International, 106, 666-676.

Sharma, S. K., & Dalgleish, D. G., (1993). Interactions between milk serum proteins and synthetic fat globule membrane during heating of homogenized whole milk. Journal of Agricultural and Food Chemistry, 41(9), 1407-1412.

Sharma, R., Singh, H., & Taylor, M. W. (1996a). Recombined milk: factors affecting the protein coverage and composition of fat globule surface layers. Australian journal of dairy technology, 51(1), 12.

Sharma, R., Singh, H., & Taylor, M. W. (1996b). Composition and structure of fat globule surface layers in recombined milk. Journal of Food Science, 61(1), 28-32.

Singh, H. (2006). The milk fat globule membrane—A biophysical system for food applications. Current opinion in colloid & interface science, 11(2-3), 154-163.

Singh, H., & Fox, P. F. (1985). Heat stability of milk: pH-dependent dissociation of micellar κ-casein on heating milk at ultra high temperatures. Journal of Dairy Research, 52(4), 529-538.

Singh, H., Creamer, L. K. (1991a). Aggregation and dissociation of milk protein complexes in heated reconstituted concentrated skim milks. Journal of Food Science, 56(1), 238-246.

Singh, H., & Creamer, L. K. (1991). Influence of concentration of milk solids on the dissociation of micellar κ-casein on heating reconstituted milk at 120° C. Journal of dairy research, 58(1), 99-105.

Smits, P., & Van Brouwershaven, J. H. (1980). Heat-induced association of β-lactoglobulin and casein micelles. Journal of Dairy Research, 47(3), 313-325.

von Smoluchowski, M. (1916). Versuch einer mathematischen Theorie der Koagulationskinetik kolloider Lösungen. Phys, (17), 557.

Song, S. J., Choi, J., Park, Y. D., Lee, J. J., Hong, S. Y., & Sun, K. (2010). A three-dimensional bioprinting system for use with a hydrogel-based biomaterial and printing parameter characterization. Artificial organs, 34(11), 1044-1048.

Sun, J., Peng, Z., Yan, L. K., Fuh, J. Y. H., & Hong, G. S. (2015a). 3D food printing - An innovative way of mass customization in food fabrication. International Journal of Bioprinting, 1(1), 27-38.

Sun, J., Zhou, W., Huang, D., Fuh, J. Y., & Hong, G. S. (2015b). An overview of 3D printing technologies for food fabrication. Food and bioprocess technology, 8(8), 1605-1615.

Sun, J., Zhou, W., Yan, L., Huang, D., & Lin, L. Y. (2018). Extrusion-based food printing for digitalized food design and nutrition control. Journal of Food Engineering, 220, 1-11.

H. E. Swaisgood, in Advanced Dairy Chemistry-1: Proteins, ed. P. F. Fox and P. L. H. McSweeney, Kluwer Academic/Plenum Press, New York, 2003, ch. 3, part A, pp.139–201.

Toh, W. Y., Li, L., Chua, C. K., & Wong, G. (2018). Comparison of existing 3D food printers.

Le Tohic, C., O'Sullivan, J. J., Drapala, K. P., Chartrin, V., Chan, T., Morrison, A. P., ... & Kelly, A. L. (2018). Effect of 3D printing on the structure and textural properties of processed cheese. Journal of Food Engineering, 220, 56-64.

Thomar, P., & Nicolai, T. (2016). Heat-induced gelation of casein micelles in aqueous suspensions at different pH. Colloids and Surfaces B: Biointerfaces, 146, 801-807.

Vadodaria, S., & Mills, T. (2020). Jetting-based 3D Printing of Edible Materials. Food Hydrocolloids, 105857.

Vancauwenberghe, V., Katalagarianakis, L., Wang, Z., Meerts, M., Hertog, M., Verboven, P., ... & Nicolai, B. (2017). Pectin based food-ink formulations for 3-D printing of customizable porous food simulants. Innovative Food Science & Emerging Technologies, 42, 138-150.

Vasbinder, A. J., & De Kruif, C. G. (2003). Casein–whey protein interactions in heated milk: the influence of pH. International Dairy Journal, 13(8), 669-677.

Vasbinder, A. J., Rollema, H. S., Bot, A., & De Kruif, C. G. (2003). Gelation mechanism of milk as influenced by Temperature and pH; Studied by the use of Transglutaminase cross-linked casein micelles. Journal of Dairy Science 86, 1556-1563.

Van der Linden, D. (2015) 3D Food printing Creating Shapes and Textures. [online]. https://www.tno.nl/media/5517/3d_food_printing_march_2015.pdf. [Accessed 8th April 2020].

Van Vliet, T., Keetels, C. J. A. M. (1995). Effect of preheating of milk on the structure of acidified milk gels. Netherlands Milk & Dairy Journal, 49, 27-35.

Van Vliet, T., Roefs, S. P. F. M., Zoon, P., Walstra, P. (1989). Rheological properties of casein gels. Journal of Dairy Research, 56, 529-534.

Van Vliet, T., Lakemond, C. M.M., & Visschers, R. W. (2004). Rheology and structure of milk protein gels. Current Opinion in Colloid & Interface Science 9, 298-304.

Walstra, P. (1993). Introduction to Aggregation Phenomena. Food colloids and polymers: stability and mechanical properties, 3.

Walstra, P. (1990). On the stability of casein micelles. Journal of Dairy Science, 73(8), 1965-1979.

Walstra, P. (2003). Physical Chemistry of Foods, Marcel Dekker, New York, NY.

Walstra, P., & Jenness, R. (1984). "Dairy Chemistry and Physics". John Wiley & Sons, New York.

Walstra, P., Wouters, J. T., & Geurts, T. J. (2006). Dairy science and technology second edition. FOOD SCIENCE AND TECHNOLOGY-NEW YORK-MARCEL DEKKER-, 147.

Warner, E. L., Norton, I. T., & Mills, T. B. (2019). Comparing the viscoelastic properties of gelatin and different concentrations of kappa-carrageenan mixtures for additive manufacturing applications. Journal of food engineering, 246, 58-66.

Wegrzyn, T. F., Golding, M., & Archer, R. H. (2012). Food Layered Manufacture: A new process for constructing solid foods. Trends in Food Science & Technology, 27(2), 66-72.

Yang, F., Zhang, M., Prakash, S., & Liu, Y. (2018). Physical properties of 3D printed baking dough as affected by different compositions. Innovative food science & emerging technologies, 49, 202-210.

3 Chapter:

Instantaneous gelation of acid milk gels via customised temperature-time profiles: Screening of concentration and pH suitable for temperature triggered gelation towards 3D-printing

This work is peer-review published as follows:

Nöbel, S., Seifert, B., Daffner, K., Schäfer, J., & Hinrichs, J. (2020). Instantaneous gelation of acid milk gels via customized temperature-time profiles: Screening of concentration and pH suitable for temperature triggered gelation towards 3D-printing. Food Hydrocolloids, 106450.

3.1 Abstract

The current interest in manufacturing of individualised food via 3D-printing has identified a need for more information on the understanding and formulation of potential ingredients. This paper proposes a novel approach to use dairy protein-based materials matching the required fast, local and irreversible sol−gel transition. The pH−temperature-route of acid gelation was shown to be a suitable mechanism for extrusion-based 3D-printing applications of skim milk retentates (8.0 – 12.0% (w/w) protein), obtained by microfiltration. pH was adjusted to 4.8 – 5.4 by adding citric acid at 2°C. Sol−gel transition was triggered either by linear temperature ramps (1 K/min) or with temperature−time profiles (ΔT = 15 K, 30 K/min) comparable to 3D-printing but without superimposed flow. Firm and stable gels were produced and characterised by elastic modulus in the rheometer used for gelation, and resistance to penetration and serum binding ability were analysed with individual gel samples. Formulations were classified regarding their sol/gel-status and progression before and during gelation, in particular, a specific softening and occasional pre-gelation. Several gels which showed preferable characteristics, including a low storage modulus G' (~0.1 Pa) during conveying under cold conditions, followed by a steep increase of G' during sol–gel transition, were considered to be a suitable feedstock for application in extrusion-based 3D-printing of skim milk retentates, namely 10.0% (w/w) protein and pH 4.8.

3.2 Introduction

3D-printing, or additive layered manufacturing (ALM), is a digitally controlled, robotic construction technology which deposits materials layer-by-layer to build a three-dimensional shape. 3D-printing of food grade materials (food layered manufacturing, FLM) has been used to print a different range of products. In food research, focus mainly laid on extrusion of gel-based materials (cold extrusion), e.g. hydrocolloid based materials (Gholamipour-Shirazi et al., 2019) or dairy pastes (Lille et al., 2018). Within the food sector, 3D-printing received and still receives increasing attention. On the one hand, it can offer highly controlled diets, e.g. for athletes or elderly people (Godoi et al., 2016), and, on the other hand, it enables the customised manufacture of new textures and structural elements (Lipton, 2017).

There is a high demand for fermented concentrated dairy products, rich in protein such as Greek yoghurt, skyr or fresh cheese (Jørgensen et al., 2019). In the past years, considerable research has been published on the health benefits of milk proteins (Fekete et al., 2013). Following this trend, FLM could offer the possibility to process customised protein rich (gel-like) dairy products with novel textures, e.g. spheres of a few centimeters sold as snacks, directly made of milk concentrate without a time-consuming fermentation (Kern et al., 2018). Only little research has been published on dairy-based materials for printing purposes, mainly due to the complex micro- and nanostructure and the high moisture content (up to 90%). Aiming at a full sol−gel transition of dairy-derived materials, both limited in time and space, to link the raw material layer-by-layer, only a few studies exist, e.g. with sodium caseinate dispersions (Schutyser et al., 2018) or casein−whey protein suspensions (Daffner et al., 2020), all working with dairy powder-based feedstock. In order to create formulations suitable for 3D food printing, they have to match certain (rheological) requirements, including a homogenous composition, being easily extrudable, and maintaining the shape after being deposited layer-by-layer (Godoi et al., 2016; Kim et al., 2017).

The sol−gel transition temperature of dairy materials is one of the most important parameters that has to be characterised, especially to know how to adjust temperatures during 3D-printing. For milk proteins, the sol−gel transition temperature (Hammelehle et al., 1997; Koutina et al., 2014; Schäfer et al., 2018; Thomar et al., 2016; Vasbinder et al., 2003) and the temperature of aggregation (de Kruif & Roefs, 1996) were studied intensively by means of (oscillatory) rheology as well as diffusive wave spectroscopy (DWS) (Vasbinder et al., 2001). In small amplitude oscillatory shear (SAOS) experiments, the point of sol−gel transition is commonly indicated by the crossover where the storage modulus (G') becomes equal or greater than the loss modulus (G''), $G \geq G''$, or expressed in terms of the loss angle, $\tan \delta = G''/G' > 1$. Such definition is applicable during determination of the sol−gel transition time at a fixed temperature to a limited extent, e.g. by Ferrer et al. (2008) and Hemar et al. (2004). Aiming at the evaluation of sol–gel transition as a function of temperature, Hammelehle et al. (1997) and Schäfer et al. (2018) proposed to use a constant threshold of the storage modulus (G') equal to 1 Pa. Temperature will be among other variables (heating rate, particle size, zeta-potential) that have to be considered before implementing 3D-food printing of skim milk retentates. So far, rheological parameters of gelation were mostly studied at rest and low heating rates while all printing processes take place under dynamic conditions. Previous studies which focused on dairy-based systems, including skim milk retentates obtained by microfiltration (MF) (Schäfer et al., 2018) and casein−whey protein suspensions (Daffner et al., 2020), agreed on sol−gel transition temperatures decreasing with decreasing acidification pH and being dependent on previous heat treatment and pH at heating.

Based on our previous studies (Daffner et al., 2020; Nöbel et al., 2018; Schäfer et al., 2018), the pH−temperature (T)-route (Vasbinder et al., 2003) offers great potential for dairy-based 3D-printing under dynamic conditions, including a fast and irreversible transition from sol to gel.

Casein micelles are considered as precursors to form colloidal gels with adjustable fractal structures (Bremer et al., 1990). For the pH−T-route, direct acidification at low temperatures (≤ 10°C) to pH values approaching the IEP of casein (4.6) helped to maintain sol−characteristics due to a reduction of hydrophobic interaction forces (Horne, 1998). Subsequent heating triggered thermal motion of the protein particles, gelation occurred and milk gels were obtained (Daffner et al., 2020; Hammelehle, 1994; Roefs et al., 1990; Roefs & van Vliet, 1990). While the gelation of established products like yogurt and cheese are in scope of dairy research, no quantitative data with specific temperature–time profiles for a tailored perikinetic aggregation of casein micelles, in rest, or orthokinetic aggregation with superimposed flow, e.g. as necessary for extrusion-based printing with fast heating rates, is available.

We hypothesise that 3D-printing of casein-based gels directly from plain milk concentrates and retentates via the pH−T-route could offer a promising approach to produce complex and innovative dairy foods, i.e. for personalised nutrition or mass customisation. For printing purposes, skim milk retentates might be a potential dairy-derived material as soon as the gelation behaviour, final gel firmness and durability can be tailored by extrinsic measures, such as nozzle temperature, offset or volume flow as well as intrinsic measures, particularly protein content and milk pH. Such high protein (10.0% (w/w)) suspensions with sol−characteristics ($G' \leq 0.1$ Pa, $\tan \delta = 90°$) could be transferred into gels under dynamic conditions, which was already shown for powder-based casein−whey protein suspensions via the pH−T-route (Daffner et al., 2020).

The characterisation of potentially suitable materials via rheological measurements, e.g. critical shear rate (Kern et al., 2018), phase angle (Gholamipour-Shirazi et al., 2019), or storage modulus G' (Daffner et al., 2020), should be conducted first to understand gelation mechanisms specifically for processes conveying and extrusion or to find shortcut methods to predict printability before printing through trial and error.

However, to the best of our knowledge, systematic studies investigating the material characteristics of skim milk retentates, obtained by MF, as potential raw material for food layered manufacturing are missing. Thus, for enabling 3D-printing, the entire study focuses on characterising of the gelation of direct acidified plain milk retentates as a temperature-triggered response rather than unravel the details of the gelation mechanism. This chapter analyses the sol−characteristics of the formulations first (section *3.4.1*), to provide crucial information regarding the physico-chemical properties of the feedstock. Results of rheological experiments to determine sol–gel transition temperatures (section *3.4.2*) are used to create individual temperature–time profiles to mimic process steps as expected during extrusion-based 3D-printing applications. Next, formulations of skim milk retentates differing in pH and protein content are screened and classified regarding their response to these customised temperature−time profiles (section *3.4.3*). Finally, the physical properties and durability of freshly prepared gels are analysed (section *3.4.4*).

3.3 Material and methods

3.3.1 Preparation of acidified skim milk retentates

3.3.1.1 Manufacture of MF retentates

Raw bovine milk was obtained from the research station Meiereihof (University of Hohenheim, Stuttgart, Germany) and separated by means of a centrifuge (SA 10-T; Andritz Frautech S.r.l., Schio, Italy) at 60°C into skim milk and cream. The skim milk (≤ 0.1% (w/w) fat; 3.5 ± 0.04% (w/w) protein) was pasteurised (72°C; 32 s) via a plate heat exchanger (KS8FS1545; ATS-Südmo GmbH, Feldkirch, Germany) and cold stored until use. The retentate was manufactured as described by Schäfer et al. (2018): Skim milk was concentrated at 50°C a transmembrane pressure of 0.1 MPa by means of a cross-flow microfiltration plant at pilot scale (Model TFF; Pall GmbH, Dreieich, Germany). The microfiltration plant is equipped with multi-channel gradient of permeability (GP) ceramic membranes (7P19-40 GP Membralox Module, 99.7% α-alumina; Pall Exekia, Bazet, France) featuring channels of 4 mm diameter, a cut-off of 0.1 µm

and a total filtration area of 1.69 m^2. The protein content of the obtained milk retentate was 13.69 ± 0.30% (w/w) and of permeate 0.72 ± 0.01% (w/w). Sodium azide (0.03% (w/w); Carl Roth GmbH & Co. KG, Karlsruhe, Germany) was added to the retentate to prevent microbial spoilage. Retentate and permeate were filled into plastic bags (approx. 200 g), vacuum packed, evacuated and stored at –18°C until use. Retentate manufacture was carried out in duplicate.

3.3.1.2 Protein standardisation and pH adjustment

Retentate and permeate was thawed (in the bags) at 27°C for 25 ± 5 min in a water bath on a daily basis. The retentate was standardised to 8.0, 10.0 and 12.0% (w/w) protein via adding permeate and blending the mixture (approx. 130 g in total) for a few seconds using a magnetic stirrer (RCT basic; IKA Werke GmbH & Co. KG, Staufen, Germany). The different retentate samples were acidified in the same setup as described in detail by Schäfer et al (2018): Approx. 100 g of protein-standardised retentate was cooled down to 2°C in a double-walled beaker (400 mL) connected to a water bath (Ecoline RE 212; Lauda Dr. R. Wobser GmbH & Co. KG, Lauda-Königshofen, Germany). Acidification to pH 5.4, 5.2, 5.0 and 4.8 was carried out within 10 min by adding 1 M citric acid (Carl Roth GmbH & Co. KG, Karlsruhe, Germany) dropwise using piston pipettes (Eppendorf Research plus, Eppendorf AG, Hamburg, Germany). The retentate was stirred continuously on the magnetic stirrer to prevent local aggregation of casein micelles at the retentate−air interface. This step was followed by an equilibration phase of 30 min and, if necessary, readjusting the target pH for a second time. The acidified retentate was either directly transferred to the rheometer or stored in a refrigerator (5°C; max. 4 h) until further gel manufacture. The standardisation and pH adjustment were carried out on a daily basis to provide fresh retentates without pre−gelation. In total, 39 MF retentates were standardised for this study (i = 39).

3.3.1.3 Chemical properties of liquid retentates

The (true) protein, fat, lactose, dry matter and fat-free dry matter contents of microfiltered retentate and permeate (section *3.3.1.1*) as well as for the protein-standardised samples prior to pH-adjustment (section *3.3.1.2*) were determined by the method of Dumas (ISO 14891:2002) using a nitrogen analyser (Dumatherm DT; C. Gerhardt GmbH & Co. KG, Königswinter, Germany) and through Fourier transform infrared spectroscopy (LactoScope FTIR Advanced; Delta Instruments, Drachten, The Netherlands) according to ISO 9622:2013, respectively. The spectrometer was calibrated with standard milk, and a series of retentate and permeate samples as manufactured in the dairy for research and training (University of Hohenheim, Stuttgart, Germany) beforehand. The chemical composition of those reference samples was determined by an accredited lab (ISO 17025; Landwirtschaftliches Zentrum Baden-Württemberg, Wangen, Germany) according to VDLUFA (2010) methods: dry matter (C 35.3), protein (C 30.2), fat (C 15.2.1); and lactose (DIN 10344:2015). All total nitrogen and FTIR analyses were performed at least in triplicate.

3.3.1.4 Physical properties of liquid retentates

Protein-standardised retentates without pH-adjustment (native milk pH 6.8) were physically characterised at two temperatures (10 and 30°C) using an oscillating U-tube density meter (DMA 5000; Anton Paar GmbH, Graz, Austria). The density at 8.0, 10.0 and 12.0% (w/w) was measured six-fold. The apparent shear viscosity for the same protein mass fractions was measured using a stress-controlled AR2000ex rheometer (minimum torque: 0.05 µN m; TA Instruments, New Castle, USA) equipped with a concentric cylinder double gap system (cup: D_i = 40.0 mm; D_o = 44.4 mm; bob: d_i = 40.6 mm, d_o = 44.0 mm; l = 59.5 mm). Temperature sweeps from 10 to 55°C, as relevant to later experiments and 3D food printing, were conducted at a constant shear stress of τ = 0.1 Pa and linear ramp of 1 K/min. Viscosity measurements were performed five-fold.

3.3.2 SAOS during sol−gel transition

3.3.2.1 Quasi steady-state heating (1 K/min)

For the non-destructive determination of the sol−gel transition temperature ($T_{sol-gel}$) of the acidified retentates, a stress-controlled MCR301 rheometer (minimum torque: 0.01 µN m; Anton Paar Germany GmbH, Ostfildern, Germany) was used in a strain-controlled oscillatory mode. A linear temperature sweep with a linear rate of about 1 K/min was recorded with the same double gap geometry und procedure (const. $\gamma = 0.003$ at $\omega = 1$ rad/s) as described in Schäfer et al. (2018). A constant threshold of G' = 1 Pa was applied to extract $T_{sol-gel}$. Measurement of $T_{sol-gel}$ of fresh retentate samples was carried out immediately before further experiments resulting in at least three replicates at each protein and pH level.

3.3.2.2 Fast heating for 3D printing (30 K/min)

To mimic the temperature profile during extrusion-based printing applications, a thin layer (approx. 2.6 mm height) of sample (3.8 ± 0.02 ml) was transferred with a pipette on a Peltier element (10°C), controlled by the AR2000 (minimum torque: 0.1 µN m; section *3.3.1.4*) or an AR2000ex rheometer (minimum torque: 0.05 µN m). A ring ($D_i = 43$ mm, $D_o = 82$ mm) was placed on the Peltier plate and sealed with milking grease to avoid sample loss during gelation (*Figure 3-1*). An acrylic plate geometry (d = 20 mm) was lowered to 2.0 mm gap width allowing continuous oscillatory measurements during gelation. Again, sol–gel transition was detected by G' ≥ 1 Pa or other definition is given where appropriate. If additional temperature recording was needed, a NiCr–Ni thermocouple was immersed to the sample through a small opening and fixed with a piece of foam rubber (*Figure 3-1, inset*). The temperature was continuously recorded with a data logger (Almemo 2390-8; Ahlborn Mess- und Regelungstechnik GmbH, Holzkirchen, Germany). All measurements were done in triplicate for each retentate as freshly prepared per day.

Based on the pre-determined sol−gel transition temperatures from SAOS experiments with 1 K/min (section *3.3.2.1*), the temperature profile was adjusted for each formulation as follows: (a) cooling and equilibration (10°C), (b) linear increase (30 K/min) to a temperature 5 K below the recent sol–gel transition temperature $T_{sol\text{-}gel}$ ($T_{sol\text{-}gel}$ −5 K), (c) holding $T_{sol\text{-}gel}$ −5 K for 10 min, (d) steep temperature increase with a controlled rate of 30 K/min to 10 K above $T_{sol\text{-}gel}$ ($T_{sol\text{-}gel}$ +10 K) that induces the sol–gel transition, (e) holding $T_{sol\text{-}gel}$ +10 K for 90 s, (f) rapid cooling with the maximum achievable rate (> 10 K/min) to 10°C, and (g) holding 10°C for 10 min. During all steps (a – g) the storage and loss moduli were recorded each 15 s by applying a constant strain of $\gamma = 0.003$ at an angular frequency of $\omega = 1$ rad/s (identical to slow heating at 1 K/min).

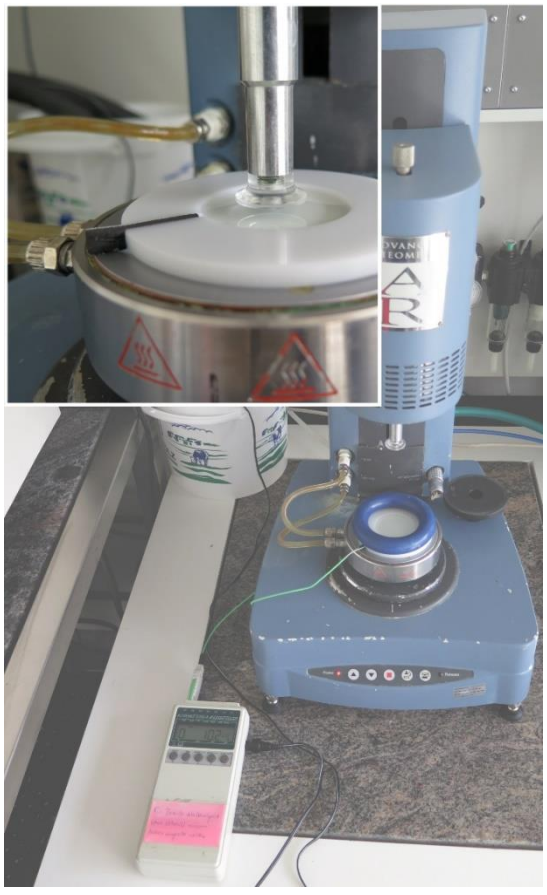

Figure 3-1: Customised experimental set-up to induce a fast and irreversible gelation on a rheometer connected to a Peltier plate; polyoxymethylene-ring (POM) was placed on the Peltier plate and sealed with milking grease to avoid sample loss during gelation; inset: NiCr–Ni thermocouple immersed through the sample to provide continuous temperature logging during gelation.

3.3.3 Physical characterisation of solid gels

3.3.3.1 Destructive stress sweep

Properties of the final gels were characterised by an additional time and stress sweep set at the end of each in-situ time sweep measurements from section *3.3.2.2* above to further examine the firmness induced by the applied temperature-time profile. Temperature was kept at 10°C and finally, the torque was the regulated parameter starting at the instrument's minimum of about 0.1 μNm and increased on a logarithmic scale with 10 points per decade. The yield stress σ_y was determined according to Hoffmann et al. (2014) from the step increase in the ratio of strain and stress amplitudes γ_0/σ_0 due to gel rupture.

3.3.3.2 Penetration test

Uniaxial compression tests were carried out with gels as freshly prepared using the same temperature−time profile as described above (section *3.3.2.2*), but without acrylic plate on the surface of the sample. After equilibrating the sample for 5 min at 10°C, the acrylic plate geometry was moved towards the gel until contact to the surface was registered (normal force > 0.02 N). Then, the actual measurement started and the normal force was recorded while the plunger was moved towards the Peltier plate (velocity: 0.01 mm/s) until the normal force exceeded 4 N, which automatically ended the test. The initial slope of the force–deformation curves, representing the elastic modulus, and the force at the first maximum, representing the gel stiffness at first rupture, was recorded at least three times with fresh gels.

3.3.3.3 Syneresis

Serum binding ability and syneresis was observed at different stages during gelation, cutting of the gel and storage with intact gel samples as described in section *3.3.2.2*. The behaviour of each gel was assessed qualitatively during gelation and it was cut with a spatula into uniform rectangular pieces (15 x 15 mm). Serum loss during cutting was described qualitatively, if applicable. The rectangular piece cut out of each gel was placed on a petri plate (Duran Group GmbH, Wertheim, Germany), sealed with Parafilm (Bemis Company Inc., Neenah, WI, USA)

to prevent water loss during storage, and its shape and position was marked. Petri plates were kept on a metal stand (inclination: 15°) for 24 h at 9°C. Serum release was measured quantitively by soaking up the serum with a paper towel, and the relative amount was calculated as the mass ratio of supernatant to the initial weight of the rectangular piece of sample (0.56 ± 0.04 g). Syneresis was determined from two freshly prepared gels.

3.3.4 Statistical analysis

Statistical analyses were conducted with Matlab 8.5 (R2015a) and its Statistics and Machine Learning Toolbox 10.0. (MathWorks Inc., Natick, MA, USA). Significance levels were set to $\alpha = 0.05$ or given where appropriate. Results are given as arithmetic means and confidence intervals from t-distribution ($\alpha = 0.05$). The number of independent repetitions of the experiments and the overall number of examined samples is expressed as *i* and *n*, respectively.

3.4 Results and discussion

3.4.1 Chemical and physical characterisation of milk retentates

The rheological characteristics of colloidal gels formed from milk proteins depend on intrinsic (e.g. size, shape, availability, protein content) and extrinsic parameters (e.g. temperature, ionic strength, pH) (Dickinson, 2016). Due to the requirement of a fast, local and irreversible sol−gel transition during the printing process (Daffner et al., 2020; Nöbel et al., 2018), the characterisation of formulations in the sol−state provides crucial information regarding the physico-chemical properties (see *Table 3-1*) and the potential printing application.

Too low protein contents, i.e. about 6.0% (w/w) from preliminary tests of this study, prevent a fast aggregation process (Lazzari et al., 2016; Mokoonlall et al., 2016), also not being able to fully entrap the serum phase into the fractal clusters of aggregated casein micelles (Genovese, 2012), while at high protein contents and low temperature a reversible gel-like structure might occur right before printing (Schäfer et al., 2018). Kim et al. (2017) also categorised hydrocolloid based gels from methyl cellulose with a concentration of below 9.0%, similar to the protein

content in case the of skim milk retentates (*Table 3-1*) as not feasible for 3D-printing because of insufficient gelation and stability.

In general, formulations suitable for extrusion-based printing including a sol−gel transition have to be conveyed in sol−state to the nozzle, where a steep locally induced temperature increase will trigger the protein particles to collide and aggregate (Daffner et al., 2020; Roefs & van Vliet, 1990; Schäfer et al., 2018).

To further analyse the sol−characteristics of the formulations at different protein contents, information regarding the dry matter, protein, and fat content, as well as the pH, density, and apparent shear viscosity of raw materials and blended retentates at 10 and 50°C are provided in *Table 3-1*. Retentates were processed in two individual batches without significant differences in protein ($p = 0.0975$; Dumas) and dry matter content ($p = 0.406$; FTIR) and, hence, no blocked experimental design was considered. The effective protein contents and variance of the designated levels of about 8.0, 10.0 and 12.0% were 8.2 ± 0.3, 9.7 ± 0.4, and 12.1 ± 1.2% (FTIR), respectively. In the following, all protein contents given in the text refer to the nominal levels. An increasing protein content from 8.0 to 12.0% (w/w) caused an increase in density and shear viscosity, with the latter decreasing with increasing temperature (*Table 3-1*). The relation between the apparent shear viscosity at a constant shear stress of 0.1 Pa, η (Pa s), and the temperature, T (°C), was fitted using an expanded exponential model (Peleg, 2017):

$$\ln\left(\frac{\eta\,(T)}{\eta\,(T_{ref})}\right) = -\,c_1\,(T - T_{ref}) + c_2\,(T - T_{ref})^2 \qquad \text{(Eq. 1)}$$

where T_{ref} (°C) is a reference temperature, $\eta(T_{ref})$ the apparent viscosity at T_{ref}, and c_1 (1/°C) and c_2 (1/°C^2) freely choose parameters to adjust the quadratic fitting function. For all microfiltered retentates, 8.0 to 12.0% (w/w) protein, and entire temperature range, 5 to 55°C as relevant for conveying and printing, the calculated goodness of fit was high, as the coefficient of determination referring to the fitted viscosity was $r^2 > 0.999$ (data not shown).

Specifically, while applying higher printing temperatures due to high sol–gel transition temperatures, an immediate drop in viscosity at the printing nozzle, e.g. by a factor two (10% protein; 10°C during conveying and approx. 25°C for printing), will counteract the increase in viscosity and stiffness due to gelation, and might result in gel rupture and poor process control. Hence, a low temperature impact, expressed by the factors c_1 and c_2 in Eq. (1), or a small difference between the temperature of conveying and printing is preferred.

A temperature-dependent drop of the viscosity was reported by several authors for skim milk retentates from micro- (Solanki & Rizvi, 2001) and ultrafiltration (Doudiès et al., 2019). Decreasing viscosities beyond the contribution of the solvent water (factor 1.5 from 10°C to 25°C) were caused by the microgel properties of the casein micelles such as a temperature-dependent swelling and the partial migration of β-casein into the serum phase (Dickinson, 2016; Nöbel et al., 2016). Hence, the effect was most pronounced at the highest protein and casein content (*Table 3-1*).

Table 3-1: Compositional and physical properties of the initial and standardised milk permeate and retentates; arithmetic means and confidence intervals calculated from n ≥ 3, i ≥ 1.

Sample	Composition					Physical properties		
	Dumas[a]	FTIR[b]			pH	Density	Apparent viscosity (0.1 Pa)[c]	
	Protein	Protein	Fat	Dry matter	2°C	10°C	10°C	50°C
	% (w/w)	% (w/w)	% (w/w)	% (w/w)	–	kg/m³	mPa s	mPa s
Permeate	0.803 ± 0.044	0.788 ± 0.076	0.036 ± 0.023	6.44 ± 0.01	—	—	—	—
Retentate #1[d]	13.6 ± 0.3	14.0 ± 0.1	0.458 ± 0.005	20.3 ± 0.1	—	—	—	—
Retentate #2[d]	13.4 ± 0.1	14.3 ± 0.4	0.513 ± 0.016	20.4 ± 0.3	—	—	—	—
8% protein	—	8.23 ± 0.27	0.385 ± 0.124	14.0 ± 0.6	6.79 ± 0.01	1049.7 ± 0.1	5.87 ± 0.37[e]	1.60 ± 0.07[e]
10% protein	—	9.67 ± 0.36	0.318 ± 0.071	15.7 ± 0.6	6.80 ± 0.01	1051.5 ± 0.1	9.69 ± 1.27[f]	1.94 ± 0.09[f]
12% protein	—	12.1 ± 1.2	0.525 ± 0.092	18.0 ± 1.5	6.80 ± 0.01	1062.5 ± 0.3	22.0 ± 3.6[g]	2.97 ± 0.16[g]

[a] Protein content was analysed by Dumas (ISO 14891:2002)

[b] Protein, fat and dry matter content were analysed by FTIR (ISO 9622:2013)

[c] Viscosity–temperature relationship was also fitted to an exponential decay model (Eq. (1), Peleg, 2017) covering 5 – 55°C; adj. $r^2 > 0.999$

[d] Retentate #1 and #2 from two individual microfiltration runs

[e] Estimates of the exp. model at 8.0% (w/w) protein: $T_{ref} = 0.0072$°C; $\eta(T_{ref}) = 9.05$ mPas; $c_1 = 0.0462$ 1/°C; $c_2 = 0.0002$ 1/°C²

[f] Estimates of the exp. model at 10%% (w/w) protein: $T_{ref} = 0.0000$°C; $(T_{ref}) = 16.88$ mPas; $c_1 = 0.0605$ 1/°C; $c_2 = 0.0003$ 1/° C²

[g] Estimates of the exp. model at 12%% (w/w) protein: $T_{ref} = 0.0305$°C; $(T_{ref}) = 47.72$ mPas; $c_1 = 0.0845$ 1/°C; $c_2 = 0.0006$ 1/° C²

3.4.2 Instantaneous sol–gel transition

SAOS experiments were performed to determine sol–gel transition temperatures at a quasi steady-state heating with a rate of 1 K/min Schäfer et al. (2018). Choosing this slow rate mainly aimed to ensure a constant temperature distribution within the sample. These values could also serve as a starting point to adjust temperatures in the nozzle, feed tank, or pipe during the fast printing process to intentionally induce a sol−gel transition (Daffner et al., 2020; Nöbel et al., 2018). In *Figure 3-2*, sol–gel transition temperatures $T_{sol-gel}$ of skim milk retentates at different protein contents and pH (the present work) and direct acidified microfiltered skim milk retentates (Schäfer et al., 2018) are shown. A storage modulus of about G' = 1 Pa was used as the threshold to detect the sol−gel transition. Alternative definitions such as the G'–G'' crossover point described above were not considered since literature data on acid-induced gelation is related on the constant threshold (Hammelehle, 1994).

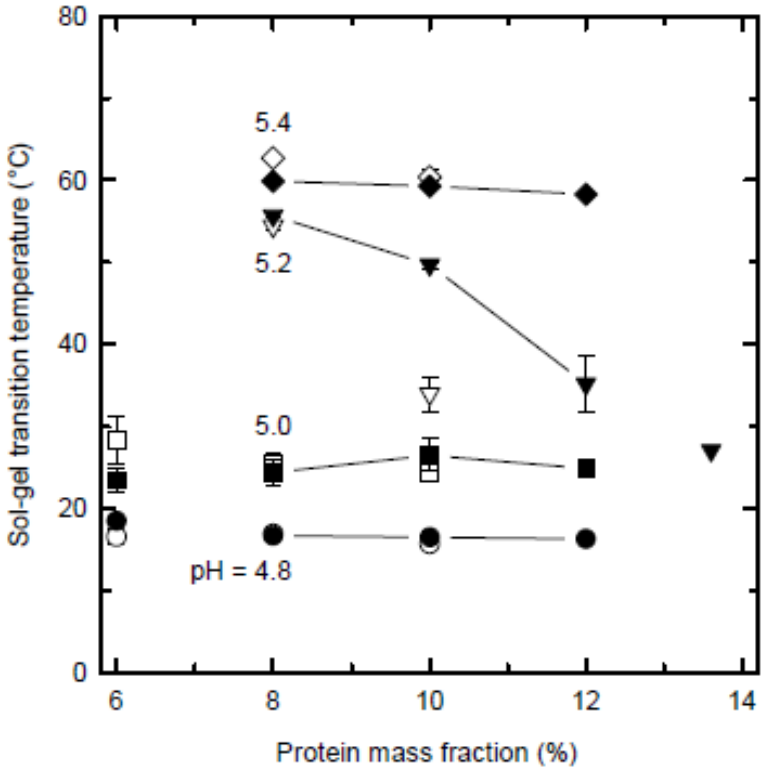

Figure 3-2: Sol−gel transition temperatures as calculated from quasi steady−state heating (1 K/min) of skim milk retentates at different protein levels and pH; threshold for sol–gel transition at G' = 1 Pa; circle: pH 4.8, square: pH 5.0, triangle: pH 5.2, diamond: pH 5.4; open symbols: literature data from Schäfer et al. (2018); average points and standard deviations calculated from i>=2, n>=2; lines connect data points from full factorial design (protein 8.0 − 12.0% (w/w), pH 4.8 − 5.4).

$T_{sol–gel}$ of the skim milk retentates obtained by microfiltration decreased significantly with decreasing acidification pH (5.4 − 4.8) at each protein content level (8.0, 10.0, and 12.0% (w/w)), as shown elsewhere before (Schäfer et al., 2018), and ranged between 16.3 ± 0.3°C and 59.9 ± 2.4°C. *Figure 3-2* demonstrates that $T_{sol–gel}$ of formulations were dependent on the tested protein content at pH 5.4, 5.2 and 5.0, while no dependence was found at pH 4.8, which is in accordance with previous results (Schäfer et al., 2018). For high protein contents, already Schäfer et al. (2018) reported on initial storage moduli G' close to or equal to 1 Pa before a marked sol–gel transition took place. This is in line with results of our study at ≥ 10.0% (w/w) protein and pH > 5.0 (data not shown).

The very different behaviour of formulations acidified to pH 5.2 was proposed to occur due the transition of casein micelles between pH 5.5 and 5.0, as described by Gastaldi et al. (1996). A specific state of micellar fusion occurred, characterised by a pseudo-network of extensively coalesced casein micelles. As this transition state reached a maximum at pH 5.2, we assume that an increasing protein concentration could cause larger aggregation of these coalesced casein micelles, decreasing $T_{sol-gel}$. Furthermore, Gastaldi et al. (1996) observed that casein micelles returned to individual characteristics at a pH lower than 5.0.

An example of a single formulation from skim milk retentates (pH 5.0, 8.0% (w/w)) with immediate gelation during SAOS experiments (quasi steady−state heating at 1 K/min) is shown in *Figure 3-3*. The curve progressions indicate sol–characteristics at low temperatures, with values for the storage moduli < 1 Pa. Slight variations in the temperature onset of the sol−gel transition were explained with experimental variations in the acidification pH and protein content (*Table 3-1*), thermal load to each sample especially due to storage and transfer operations, and an inhomogeneity of temperature gradients within the flat sample (*Figure 3-1*). The interquartile range of $T_{sol–gel}$ calculated for all samples of 8.0% (w/w) protein and pH 5.0 (n = 7) was IQR = 2.1 K. As shown in *Figure 3-3*, all intersections with G' = 1 Pa fell within 1.5 · IQR

(whiskers) as being equivalent to $2 \cdot \sigma$ ($P = 0.95$) expecting normally distributed $T_{sol-gel}$. Considering similar variance for all other formulations (*Figure 3-2*), temperatures of 5 K ($3 \cdot$ IQR, $p \leq 0.01$) below $T_{sol-gel}$ will be used as a sufficiently safe distance to avoid (pre-) gelation.

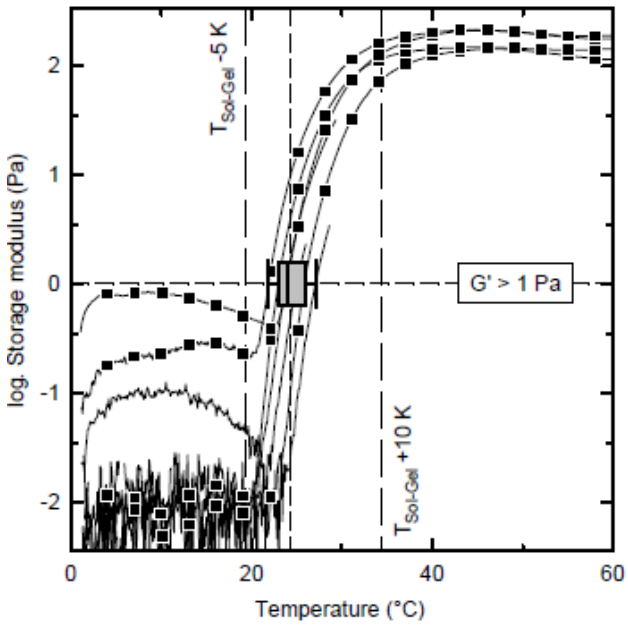

Figure 3-3: Sol−gel transition of skim milk retentates (8.0% (w/w), pH 5.0) during quasi steady-state heating applying 1 K/min; threshold for sol−gel transition at G' = 1 Pa; dashed: region before initial indications of gelation ($T_{sol-gel}$ −5K) or at plateau after gelation ($T_{sol-gel}$ + 10 K); open symbols: measurements as stopped after reaching sol−gel transition (n = 3), closed symbols: measured till 65°C (n =4); box-whisker plot shows means sol−gel transition temperature and 25th/75th-quantiles of all data sets (i=3, n=7).

For the transfer of knowledge from SAOS experiments (quasi steady−state heating at 1 K/min) to a steep temperature increase in a thin layer of sample on a Peltier element (mimicking the temperature profile during extrusion-based 3D-printing applications), the temperature profile was set as follows: during a holding step, each formulation should maintain sol−characteristics, as the temperature was 5 K lower than the sol−gel transition temperature, abbreviated as $T_{sol-gel}$ −5 K. To induce a fast, local and irreversible sol−gel transition, a steep increase (approx. 30 K/min) to a temperature 10 K higher than the sol−gel transition temperature ($T_{sol-gel}$ +10 K) was performed and held for 90 s on the Peltier plate of the rheometer to mimic the printing set-up in the nozzle (total temperature step: $\Delta T = 15$ K). Temperatures even higher than $T_{sol-gel}$ +10 K were not required since thermal energy has to be dissipated as well. Subsequent

cooling to 10°C was conducted as being similar to the temperature on a chilled printing bed after the deposition of the to-be-printed material.

Figure 3-4 (a) illustrates such a temperature−time profile, which was set and recorded by the rheometers temperature probe (dashed line), as well as the one occurring, as measured with an additional thermocouple, immersed into the sample (solid line). The response of the moduli G' and G'' to the temperature changes is shown in *Figure 3-4 (b)*, demonstrating sol−characteristics (G' < 1 Pa) from the start at $T_{sol-gel}$ −5K in the case of the exemplary formulation (pH 4.8, 10.0% (w/w)).

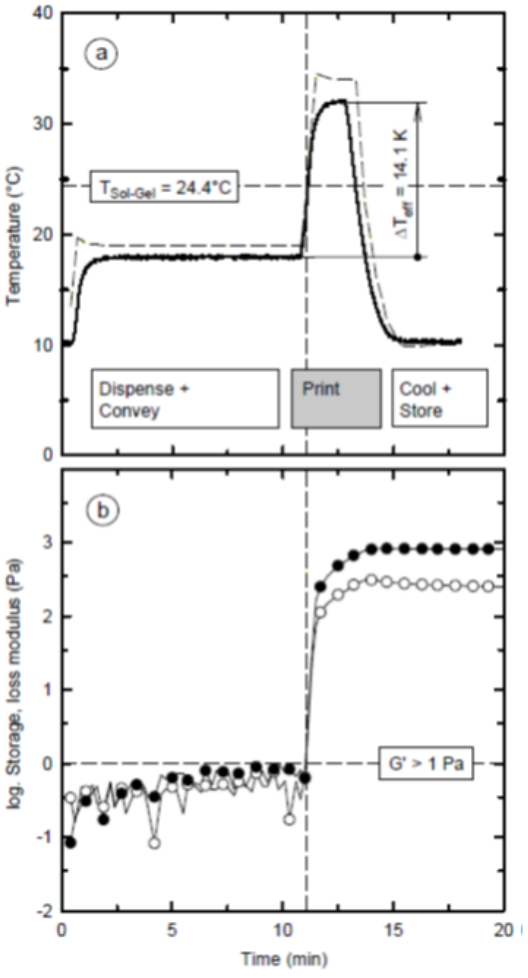

Figure 3-4: Temperature-time profile (a) (immersed thermo couple, solid line) of skim milk retentate (10.0% (w/w), pH 4.8) to mimic a holding step below its sol−gel transition temperature, steep temperature gradient (30 K/min) during printing and subsequent cooling step, dashed plot: temperature measured at the rheometers Peltier element;(b) Storage (closed symbols) and loss modulus (open symbols) of the skim milk retentate as response to the temperature-time profile above, vertical line serves as guide at triggered sol−gel transition (t = 11.1 min).

The high heating rate (30 K/min) on the Peltier element caused immediate gelation within less than 90 s and immediately after $T_{sol-gel}$ = 24.4°C was reached. Storage modulus responded as a strictly monotone increasing function to the stepped temperature–time profile. $T_{sol-gel}$ was in accordance with those obtained from SAOS experiments (*Figure 3-2*). Here, it was demonstrated by a similar onset of the increase of the storage modulus G' at the vertical dashed line in *Figure 3-4 (b)* to *Figure 3-4 (a)* after approx. 11.1 min. In *Figure 3-4 (a)*, $T_{sol-gel}$ for the formulation of 10.0% (w/w) protein and pH 4.8 was passed at the same time.

Matching the results of SAOS experiments (*Figure 3-3*) and on the Peltier element with fast heating (*Figure 3-4*) provided the first evidence that a fast, local and irreversible sol−gel transition of high protein-based formulations of skim milk retentates could be transferred from well-defined laboratory conditions (slow and homogeneous steady-state heating) to dynamic conditions during extrusion-based 3D-printing applications. The proposed temperature−time profile (ΔT = 15 K; $t \leq 90$ s) represents one example on how gelation can be triggered during extrusion-based printing still including a relatively long time due to the thermal inertia. Contrastingly, using the rheometers Peltier element has provided the advantage to study unknown effects in situ such as phase separation and contraction, and to produce sample specimens for further analysing durability.

3.4.3 Screening the concentration−pH-range

Further screening of all formulations in the protein−pH-range (8.0 – 12.0% (w/w), pH 4.8 – 5.4) was performed with the adjusted temperature–time profile ($T_{sol-gel}$ −5K – $T_{sol-gel}$ +10 K – cooling to 10°C). It has to be mentioned that $T_{sol-gel}$ was individually determined on each day of experiment and set points were calculated accordingly. In *Figure 3-5*, all formulations were classified into four groups, according to their gelation behaviour. Formulations within group (a) showed values of G' < 1 Pa and G' < G'', indicating sol−characteristics before the intended sol−gel transition took place. Furthermore, group (a) was characterised by an immediate and

steep increase of G' above 1 Pa (*Figure 3-5 (a)*), indicating a tailored triggering of the gel formation. Thus, group (a) is referred to as the desired gelation behaviour in the following. All formulations with pH 4.8 belong to group (a), independent of the protein content (8.0 – 12.0% (w/w)).

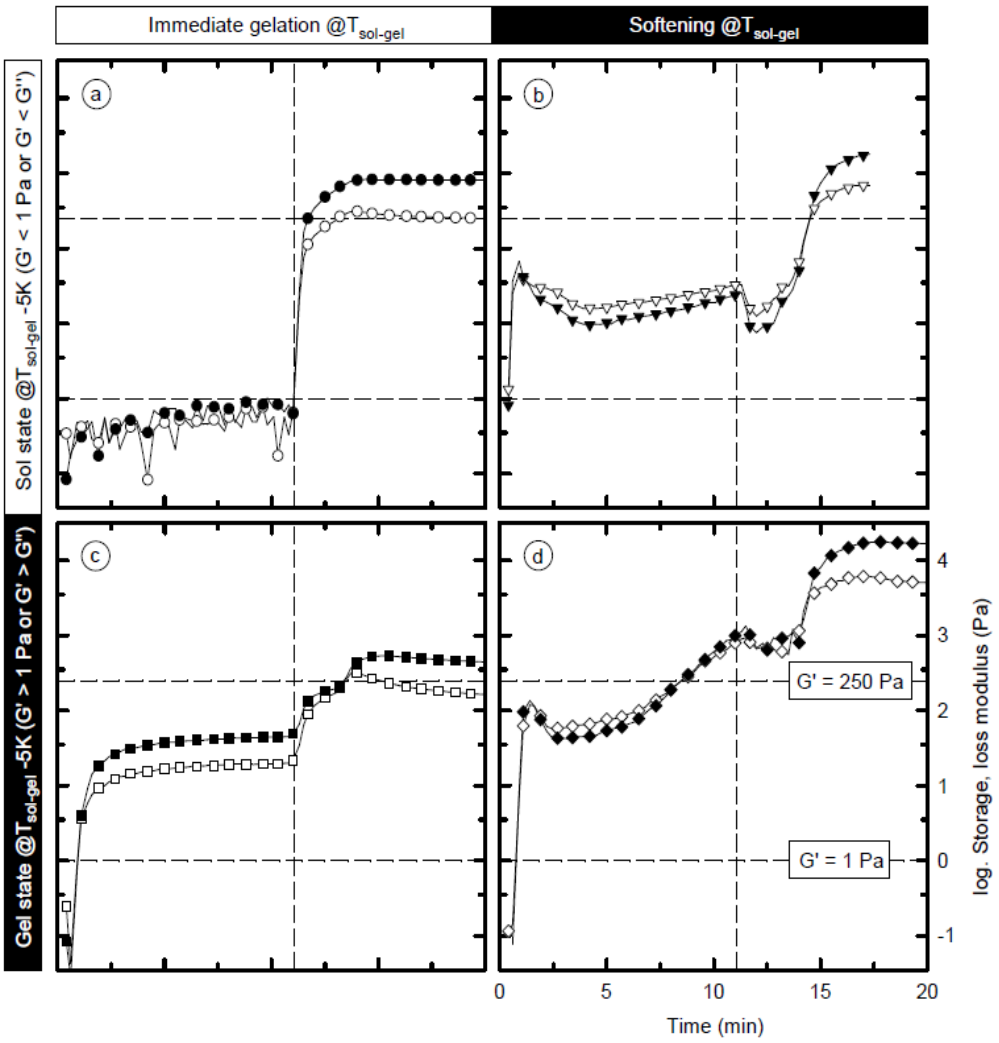

Figure 3-5: Storage (closed symbols) and loss modulus (open symbols) of the different skim milk retentates as response to the same temperature-time profile mimicking 3D food printing (see Figure 3-4a); classified according to their sol/gel-state before steep temperature increase (rows) and gelation/softening during heating (columns); illustrated using the samples (a) 10.0% (w/w) protein, pH 4.8, (b) 8.0% (w/w) protein, pH 5.2, (c) 10.0% (w/w) protein, pH 5.0, and (d) 10.0% (w/w) protein, pH 5.4; vertical line serves as guide at triggered sol−gel transition (t = 11.1 min); upper horizontal dashed line indicates sufficient increase in storage moduli in proportion to $\Delta G'/\Delta T$ > 250 Pa/10 K (Daffner et al., 2020).

Formulations within group (b) still showed sol−characteristics (1 < G' ≤ 10 Pa but G' < G'') before the temperature was increased above $T_{sol-gel}$. In contrast to group (a), group (b) was characterised by a period of short softening (falling moduli) around $T_{sol-gel}$ where immediate gelation was expected. Typically, the drop in the moduli was followed by the final and slower

solidification of the gel. The formulations with 8.0% (w/w) protein at pH 5.2 and 5.4, 10.0% (w/w) protein at pH 5.2, and 12.0% (w/w) protein at pH 5.4 belong to group (b). In the range of pH 5.2 – 5.4, the net charge was slightly reduced as compared to native state and colloidal calcium phosphate dissolved, resulting in swollen but unstable casein micelles (Gastaldi et al., 1996; Nöbel et al., 2016; van Vliet et al., 2004). Also, the lowest bulk viscosity of casein micelles suspensions was observed at pH 5.2 – 5.4 (Gastaldi et al., 1996). These competing effects of increasing attractive forces, decreasing viscosity, and still steric hindering might intensify the response to small temperature changes that became visible as softening. Reducing the temperature dependence, i.e. at lower concentrations (section *3.4.1*), or by decreasing the pH to ≤ 5.0 will overcome this sensitivity and a true bistable (sol- or gel-state) system is expected.

Formulations within group (c) and (d) showed gel−characteristics (G' > 1 Pa or G' > G''), during the first holding step, already before $T_{sol-gel}$ was reached. During and after the steep temperature increase above $T_{sol-gel}$, where gelation was induced, group (c) showed an immediate solidification comparable to group (a) (*Figure 3-5 (c)*). Formulations with 10.0% (w/w) protein at pH 5.0, and 12.0% (w/w) protein at pH 5.0 and 5.2 belong to group (c). Around pH 5.0, on the one hand, attractive forces got dominant and the casein micelles could be easily transferred into a colloidal gel (Gastaldi et al., 1996; Roefs et al., 1990). On the other hand, casein micelle aggregation requires sufficient forces and destabilisation as well as an increasing likelihood of collision due to thermal motion (Nöbel et al., 2016), assuming perikinetic aggregation in rest. The higher the protein content was, the higher the chance for the casein micelles to get in contact, aggregate, and form a gel. Gelation of the small clusters of individual monomeric units was triggered until the entire bulk phase transits from sol to gel (Häbel et al., 2016). Such formulations approaching gelation might be more sensitive to an unequal temperature distribution within the sample specimen and other thermal fluctuations, i.e. during transfer and handling.

Here, in the case of 10.0% (w/w) and 12.0% (w/w) protein, a safer distance with more than 3 · IQR (section *3.4.2*) or based on each sample's $T_{sol-gel}$ variance should be chosen.

Group (d) combines the gel−characteristics during holding with short softening (*Figure 3-5 (d)*), as also observed for group (b). Only formulations with 8.0% (w/w) protein at pH 5.0 and 10.0% (w/w) protein at pH 5.4 belong to group (d). Formulations that showed undesired gelation behaviour (groups b – d) often comply with the minimum aggregation rate of $\Delta G'/\Delta T > 250$ Pa/10 K from Daffner et al. (2020) (*Figure 3-5*; horizontal dashed lines). However, their calculation has limited use since pre-gelation occurred and G‘> 1 Pa was already reached before triggering the proper sol−gel transition in the fast heating step.

Concerning the various gelation profiles in *Figure 3-5*, the sol–gel transition was hard to define in terms of a single rheological feature. An advantage of a constant threshold, for example of about G’ = 1 Pa, is a clear transition from a noisy signal at the sol–state to a stable one during and after gelation. A low signal-to-noise ratio prevents the alternative calculation of the G’–G’’ crossover point as well. Both definitions are hardly applicable where gelation takes place in multiple steps or as an unsteady transition.

In summary, two types of gelation behaviour can be distinguished: (1) formulation with or without pre−gelation at a temperature of –5K below $T_{sol-gel}$ (rows in *Figure 3-5*), and (2) formulations with or without softening at $T_{sol-gel}$ (columns in *Figure 3-5*). While the pre−gelation might occur from an insufficient distance to $T_{sol-gel}$ and its variability, the softening at and during the gelation points to a secondary mechanism that dominates on attractive forces, i.e. due to dropping bulk viscosity. Sole rheological characterisation of the sol−gel transition so far has to be supplemented by observations concerning the gel quality and other mechanical properties.

3.4.4 Physical properties of solid gels

Usage of the rheometer's Peltier element allowed an immediate and steep temperature increase of all formulations, which resulted in stable gels that resemble sliced processed cheese in appearance and texture. The final properties of these freshly prepared gels using the temperature−time profile as described (section *3.3.2.2*) were further analysed by the storage modulus G' (10 min after cooling), the maximum force before destruction (F_{max}) and the elastic modulus, as well as the likelihood of syneresis, as shown in *Table 3-2*. The storage modulus G' ranged between 420 ± 126 Pa (8.0% (w/w), pH 5.0) and $18{,}600 \pm 7{,}500$ Pa (12.0% (w/w), pH 5.4). Final values for G' increased with increasing protein content at all pH, with only one exception (12.0% (w/w), pH 5.2) found. Also, a tendency of G' increasing with increasing pH ≥ 5.0 was observed. Such gels with storage moduli in the range of 500 – 10,000 Pa were expected to be printable due to the low viscosity and, hence, pressure drop during extrusion but still depositing a self-supporting strand (Kim et al., 2017; Lille et al., 2018).

During compressions tests, the values for the elastic modulus, represented by the initial slope of the force–deformation curves, ranged between 1.75 ± 0.95 N/mm (8.0% (w/w) protein, pH 4.8) and 10.0 ± 0.8 N/mm (12.0% (w/w) protein, pH 4.8) in similar fashion as for the shear storage modulus (*Table 3-2)*. The pH and protein content seemed to play no decisive role since no correlation between these parameters was observed. The large variance of the elastic modulus values is explained by the fact that for every measurement a new gel had to be produced. Results of the gel stiffness, represented by the force at the first maximum, were found to be more robust and ranged between 0.409 ± 0.051 N (8.0% (w/w), pH 4.8) and 1.98 ± 0.46 N (12.0% (w/w), pH 4.8). With both increasing pH (≥ 5.0) and protein content, firmer gels were found.

At pH 5.2 and 5.4, inhomogeneous gels were often formed with visible phase separation and small protein aggregates, which were judged as high in syneresis (*Table 3-2).* Hence, instrumental parameters might reflect only (the firm) parts of the gel network and overemphasise the average physical properties of such gels. A general trend towards higher storage or elastic moduli and gel firmness with increasing protein content (8.0 – 12.0% (w/w)) is attributed to increasing $T_{sol-gel}$ of the formulations. For sole protein variation of acid milk gels, rather a linear increase in physical properties was expected (Mokoonlall et al., 2016). The additional gain in gel firmness might occur from the thermal treatment of the acid gels (Hahn et al., 2012) that happened simultaneously, albeit for a short period. Hahn et al. (2012) also described temperature-triggered phase separation and compacting as competing mechanism resulting in firm but coarse gel networks.

Table 3-2: Rheological and physical properties at 10 °C of the final gels (prepared following the procedure in section *3.3.2.2*) after sol–gel transition; arithmetic means and confidence intervals calculated from n ≥ 3, i ≥ 2s.

Sample[a]		Oscillatory rheology		Penetration test		Syneresis		
Protein	pH	G' (1 rad/s)	σ_y	Slope	F_{max}	Gelation[b]	Cutting[b]	Storage[c]
% (w/w)	–	Pa	Pa	N/mm	N	–	–	g_{Serum}/g_{Gel}
8	4.8	426 ± 96	—	1.75 ± 0.95	0.409 ± 0.051	o	+	0.084
8	**5.0**	**420 ± 126**	**219 ± 75**	**5.95 ± 1.38**	**1.60 ± 0.19**	**o**	**o**	**0.019**
8	5.2	914 ± 1670	—	n.d.	n.d.	++	+	—
8	5.4	8490 ± 7720	—	n.d.	n.d.	++	++	n.d.
10	**4.8**	**765 ± 81**	**471 ± 149**	**5.87 ± 0.36**	**1.10 ± 0.39**	**o**	**+**	**n.d.**
10	5.0	463 ± 69	—	2.70 ± 0.36	0.877 ± 0.056	o	o	0.046
10	5.2	1990 ± 700	—	n.d.	n.d.	+	+	n.d.
10	5.4	12100 ± 3600	—	n.d.	n.d.	+	+	n.d.
12	4.8	1210 ± 220	—	10.0 ± 0.8	1.98 ± 0.46	o	+	n.d.
12	**5.0**	**1040 ± 210**	**637 ± 147**	**3.68 ± 1.53**	**1.74 ± 0.43**	**o**	**o**	**n.d.**
12	5.2	1360 ± 270	—	8.71 ± 2.92	3.32 ± 0.26	o	o	n.d.[d]
12	5.4	18600 ± 7500	—	n.d.	n.d.	++	+	n.d.

[a] nominal level from full factorial design (protein 8.0 – 12.0%, pH 4.8 – 5.4), for achieved protein content refer to *Table 3-1*

[b] o, +, ++: qualitative description of no, low, and high syneresis, respectively, during gelation and cutting, as compared between samples

[c] serum release quantified after 24 h storage at 9°C

[d] gel disaggregated completely after 70 h storage at 9°C

bold print: gels with quality sufficient for further assessment and optimisation

n.d.: not detectable at this protein–pH combination/formulation since data too noisy, no clear linear slope, or no serum release due to storage

Considering $T_{sol-gel}$ and the progression of the storage modulus during quasi steady-state heating with a rate of 1 K/min, most of the analysed formulations were suitable for temperature-triggered 3D-printing. The mechanism of the sol−gel transition via the pH−T-route stays the same. In practice, only a few formulations seem to be implementable guided by the following order of criteria: no syneresis > high gel firmness > good reproducibility/low variance. Mapped to all formulations, only a few combinations remain that fitted the criteria and showed convincing gel properties (protein content, pH): 10.0/4.8 > 12.0/5.0 > 8.0/5.0) (*Table 3-2*, bold print). Those samples belong to group (a) of *Figure 3-5* or showed moderate softening as in group (b). An instantaneous and steep increase of the gel firmness already gave a positive indication towards properties in terms of water binding and durability. Although, sole rheological indicators and suitable aggregation rate (Daffner et al., 2020) will not necessarily result in appropriate final gel properties, shown with the soft and watery gel from 8.0% (w/w) protein and pH 4.8 (*Table 3-2).*

Promising candidates, particularly 10.0% (w/w) protein and pH 4.8, can be further optimised for 3D food printing by (a) adjusting the temperature-time profile to the individual $T_{sol-gel}$ and its variation, and (b) moving the holding time at $T_{sol-gel}$ +10 K towards conditions of real printing applications ($t \rightarrow 0$ s). Although, various literature reviewed on the gelation mechanism of acid milk gels (Dickinson, 2016; Lazzari et al., 2016; Vasbinder et al., 2003a), no indication was given how milk gels perform during orthokinetic aggregation in motion apart from the backlash in continuous yogurt manufacture (Driessen et al., 1983). It is straightforward to implement such gelation under dynamic and shearing conditions closer to extrusion-based 3D-printing.

3.5 Conclusion

The gelation behaviour of directly cold acidified plain milk retentates without an additional gelling agent was characterised regarding the potential for extrusion-based 3D-printing applications via the pH–T-route. For the first time, casein micelles' sol–gel transition temperature ($T_{sol-gel}$) as determined by SAOS was further used to mimic extrusion and flowing conditions during potential 3D-printing applications by using a steep temperature gradient ($\Delta T = 15$ K, 30 K/min). From the screening of different concentrations and pH (8.0 – 12.0% (w/w) protein, pH 4.8 – 5.4), only a few formulations showed a fast, local and irreversible transition into durable gels suitable for 3D-printing, although the same colloidal gelation mechanics were assumed.

Milk gels of 10.0% (w/w) protein and pH 4.8 were promising candidates for 3D-printing from a group of formulations characterised by a storage modulus G' below 1 Pa in the cold, a steep increase of G' around $T_{sol-gel}$ and the absence of syneresis and rupture during gelation and storage. In future experiments, our lab group will focus on conveying and printing those high protein-based formulations inclusive sol–gel transition in a printing set-up. Based on our rheological results, the temperatures in certain sections have to be individually adjusted, e.g. keeping the temperature during conveying 5K below $T_{sol-gel}$ to ensure sol–characteristics and avoid pre–gelation. Starting the transition from sol to gel in the nozzle has to be irreversible, triggered via a fast collision and aggregation of the protein particles by an increase in the temperature. This temperature in the nozzle should be high enough to ensure gelation, but as low to prevent clogging in the nozzle. Small changes in the temperature–time profile during conveying will provide new insights if formulations with less promising characteristics could potentially be printed.

3.6 References

Anonymous. (2002). Milk and milk products – Determination of nitrogen content – Routine method using combustion according to the Dumas principle. ISO 14891 IDF 185. Geneva.

Anonymous. (2010). Chemische, physikalische und mikrobiologische Untersuchungsverfahren für Milch, Milchprodukte und Molkereihilfsstoffe. In VDLUFA-Methodenbuch (7th ed.). Darmstadt: VDLUFA-Verlag.

Anonymous. (2013). Milk and milk products – Guidelines for the application of mid-infrared spectrometry. ISO 9622 IDF 141. Geneva.

Anonymous. (2015). Milch und Milcherzeugnisse – Bestimmung des Lactose- und D-Galactosegehalts – Enzymatisches Verfahren. DIN 10344. Berlin.

Anonymous. (2017). General requirements for the competence of testing and calibration laboratories. ISO 17025. Geneva.

Bremer, L. G., Bijsterbosch, B. H., Schrijvers, R., van Vliet, T., & Walstra, P. (1990). On the fractal nature of the structure of acid casein gels. Colloids and Surfaces, 51, 159-170.

Daffner, K., Vadodaria, S., Ong, L., Nöbel, S., Gras, S., Norton, I., & Mills, T. (2020). Design and characterisation of casein–whey protein suspensions via the pH–temperature-route for application in extrusion-based 3D-printing. Food Hydrocolloids, 112, 105850.

Dickinson, E. (2016). Exploring the frontiers of colloidal behaviour where polymers and particles meet. Food Hydrocolloid, 52, 497-509.

Doudiès, F., Arsène, A. S., Garnier-Lambrouin, F., Famelart, M. H., Bouchoux, A., Pignon, F., & Gésan-Guiziou, G. (2019). Major role of voluminosity in the compressibility and sol–gel transition of casein micelle dispersions concentrated at 7° C and 20° C. Foods, 8(12), 652.

Driessen, F. M., Meijer, A., & Ubbels, J. (1983). Continuous manufacture of yogurt. Antonie van Leeuwenhoek, 49(1), 84-85.

Fekete, A. A., Givens, D. I., & Lovegrove, J. A. (2013). The impact of milk proteins and peptides on blood pressure and vascular function: a review of evidence from human intervention studies. Nutrition research reviews, 26(2), 177-190.

Ferrer, M. A., Hill, A. R., & Corredig, M. (2008). Rheological properties of rennet gels containing milk protein concentrates. Journal of Dairy Science, 91(3), 959–969.

Gastaldi, E., Lagaude, A., & De La Fuente, B. T. (1996). Micellar transition state in casein between pH 5.5 and 5.0. Journal of Food Science, 61(1), 59-64.

Genovese, D. B. (2012). Shear rheology of hard-sphere, dispersed, and aggregated suspensions, and filler-matrix composites. Advances in colloid and interface science, 171, 1-16.

Gholamipour-Shirazi, A., Norton, I. T., & Mills, T. (2019). Designing hydrocolloid based food-ink formulations for extrusion 3D printing. Food Hydrocolloids, 95, 161-167.

Godoi, F. C., Prakash, S., & Bhandari, B. R. (2016). 3d printing technologies applied for food design: Status and prospects. Journal of Food Engineering, 179, 44-54.

Häbel, H., Särkkä, A., Rudemo, M., Hamngren Blomqvist, C., Olsson, E., Abrahamsson, C., & Nordin, M. (2016). From static micrographs to particle aggregation dynamics in three dimensions. Journal of Microscopy, Vol. 262, pp. 102–111.

Hahn, C., Sramek, M., Nöbel, S., & Hinrichs, J. (2012). Post-processing of concentrated fermented milk: influence of temperature and holding time on the formation of particle clusters. Dairy Science & Technology, 92(1), 91–107.

Hammelehle, B. (1994). Die Direktsaeuerung von Milch. Untersuchungen zur gezielten Einflussnahme auf Textur und Konsistenz gesäuerter Milchgele. PhD Thesis. München: Technische Universität München/ Weihenstephan.

Hammelehle, B., Schkoda, P., & Kessler, H. G. (1997) Parameters for coagulation properties of direct acidified milk and for the structure of milk gels. Milchwissenschaft 52 671–674.

Hemar, Y., Singh, H., & Horne, D.S. (2004). Determination of early stages of rennet-induced aggregation of casein micelles by diffusing wave spectroscopy and rheological measurements. Current Applied Physics, 4(2-4), 362–365.

Hoffmann, S., Koos, E., & Willenbacher, N. (2014). Using capillary bridges to tune stability and flow behavior of food suspensions. Food Hydrocolloids, Vol. 40, pp. 44–52.

Horne, D. S. (1998). Casein interactions: casting light on the black boxes, the structure in dairy products. International Dairy Journal, 8(3), 171-177.

Jørgensen, C. E., Abrahamsen, R. K., Rukke, E. O., Hoffmann, T. K., Johansen, A. G., & Skeie, S. B. (2019). Processing of high-protein yoghurt–A review. International Dairy Journal, 88, 42-59.

Kern, C., Weiss, J., & Hinrichs, J. (2018). Additive layer manufacturing of semi-hard model cheese: Effect of calcium levels on thermo-rheological properties and shear behavior. Journal of food engineering, 235, 89-97.

Kim, H. W., Bae, H., & Park, H. J. (2017). Classification of the printability of selected food for 3D printing: Development of an assessment method using hydrocolloids as reference material. Journal of Food Engineering, 215, 23-32.

Koutina, G., Knudsen, J.C., Andersen, U., & Skibsted, L.H. (2014). Temperature effect on calcium and phosphorus equilibria in relation to gel formation during acidification of skim milk. International Dairy Journal, 36, 65–73.

de Kruif, C.G., & Roefs, S.P.F.M. (1996). Skim milk acidification at low temperatures: A model for the stability of casein micelles. Netherlands Milk and Dairy Journal, 50(2), 113–120.

Lazzari, S., Nicoud, L., Jaquet, B., Lattuada, M., & Morbidelli, M. (2016). Fractal-like structures in colloid science. Advances in colloid and interface science, 235, 1-13.

Lille, M., Nurmela, A., Nordlund, E., Metsä-Kortelainen, S., & Sozer, N. (2018). Applicability of protein and fiber-rich food materials in extrusion-based 3D printing. Journal of Food Engineering, 220, 20-27.

Lipton, J. I. (2017). Printable food: the technology and its application in human health. Current opinion in biotechnology, 44, 198-201.

Mokoonlall, A., Nöbel, S., & Hinrichs, J. (2016). Post-processing of fermented milk to stirred products: Reviewing the effects on gel structure. Trends in food science & technology, 54, 26-36.

Nöbel, S., Kern, C., Sonne, A., Bähler, B., & Hinrichs, J. (2016). Apparent voluminosity of casein micelles in the temperature range 35–70° C. International Dairy Journal, 59, 80-84.

Nöbel, S., Ross, N.-L., Protte, K., Körzendörfer, A., Hitzmann, B., & Hinrichs, J. (2016). Microgel particle formation in yogurt as influenced by sonication during fermentation. Journal of Food Engineering, 180, 29–38.

Nöbel, S., Seifert, B., Schäfer, J., Daffner, K., & Hinrichs, J. (2018). Oral presentation Food Colloids, Leeds (2018) - Session - Processing of Novel Structures for Functionality. Temperature-triggered gelation of milk concentrates applied to 3D food printing.

Peleg, M. (2017). Temperature–viscosity models reassessed. Critical reviews in food science and nutrition, 58(15), 2663-2672.

Roefs, S. P. F. M., de Groot-Mostert, A. E. A., & Van Vliet, T. (1990a). Structure of acid casein gels 1. Formation and model of gel network. Colloids and surfaces, 50, 141-159.

Roefs, S. P. F. M., & van Vliet, T. (1990). Structure of Acid Casein Gels 2. Dynamic Measurements and Type of Interaction Forces. Colloids and Surfaces, Vol. 50, pp. 161–175.

Schäfer, J., Läufle, I., Schmidt, C., Atamer, Z., Nöbel, S., Sonne, A., Kohlus, R., & Hinrichs, J. (2018a). The sol-gel transition temperature of skim milk concentrated by microfiltration as affected by pH and protein content. International Journal of Dairy Technology, 71(3), 585-592.

Schäfer, J., Bast, R., Atamer, Z., Nöbel, S., Kohlus, R., & Hinrichs, J. (2018b). Concentration of skim milk by means of dynamic filtration using overlapping rotating ceramic membrane disks. International Dairy Journal, 78, 11–19.

Schutyser, M. A. I., Houlder, S., de Wit, M., Buijsse, C. A. P., & Alting, A. C. (2018). Fused deposition modelling of sodium caseinate dispersions. Journal of Food Engineering, 20, 49-55.

Solanki, G., & Rizvi, S. S. (2001). Physico-chemical properties of skim milk retentates from microfiltration. Journal of Dairy Science, 84(11), 2381–2391.

Thomar, P., & Nicolai, T. (2016). Heat-induced gelation of casein micelles in aqueous suspensions at different pH. Colloids and Surfaces B: Biointerfaces, 146, 801–807.

Vasbinder, A. J., van Mil, P. J.J.M., Bot, A., & de Kruif, C. G. (2001). Acid-induced gelation of heat-treated milk studied by diffusing wave spectroscopy. Colloids and Surfaces B: Biointerfaces, 21(1-3), 245–250.

Vasbinder A. J., Rollema H. S., Bot A., & de Kruif C. G. (2003). Gelation mechanism of milk as influenced by temperature and pH; Studied by the use of transglutaminase cross-linked casein micelles. Journal of Dairy Science 86 1556-1563.

van Vliet, T., Lakemond, C. M., & Visschers, R. W. (2004). Rheology and structure of milk protein gels. Current Opinion in Colloid & Interface Science, 9(5), 298-304.

4 Chapter:

Design and characterisation of casein−whey protein suspensions via the pH−temperature-route for application in extrusion-based 3D-printing

This work is peer-review published as follows:

Daffner, K., Vadodaria, S., Ong, L., Nöbel, S., Gras, S., Norton, I., & Mills, T. (2020). Design and characterisation of casein–whey protein suspensions via the pH–temperature-route for application in extrusion-based 3D-printing. Food Hydrocolloids, 112, 105850.

4.1 Abstract

The current interest in individualised food through additive manufacturing has identified a need for more information on the formulation and printability of potential ingredients. Here, the effect of formulation parameters of casein−whey protein suspensions like the pH (4.8 – 5.4) as well as the casein content (8.0 – 12.0% (w/w)) mixed with whey protein (2.0 – 3.0% (w/w)) and the effect of pre-processing parameters including the denaturation of whey proteins (80°C, 10 min; adjusted pH 6.55, 6.9 and 7.1) on the gel formation via the pH−temperature (T)-route was studied. Rheological measurements showed that the sol−gel transition temperature (G' = 1 Pa) decreased and the aggregation rate of the casein−whey protein suspensions increased with increasing pH value at heating. The aggregation rate was considered to be a key parameter predicting the printability of formulations. By reaching or exceeding a certain aggregation rate (250 Pa/ 10 K), casein−whey protein suspensions were found to be printable resulting in firm and stable gels.

4.2 Introduction

3D-printing is a new trend in the food sector that is receiving increasing attention. In addition to the traditional additive manufacturing process with plastic or metal as feed material, 3D-printing can be conducted as food layered manufacturing (FLM). In general, 3D-printing is an additive manufacturing technology with a layer-by-layer deposition of the material to form an object that cannot be created with conventional techniques. Technologies like controlled fusion and controlled deposition are amongst the most popular for FLM (Wegrzyn et al., 2012). Although most FLM technologies are still being researched, different food materials have successfully been printed. The complex microstructure of food and the sol−gel transition of food ingredients (e.g. crystallization of cocoa butter from liquid to solid to manufacture chocolate or protein-based gelation for dairy products) are just two of the challenges that must be addressed to implement food for 3D-printing, which could result in highly customised products for individuals (Ross et al., 2019). The design of edible, printable and individualised casein−whey protein suspensions and the assessment of suspension printability is therefore a step towards the printing of more types of food.

Recent studies have shown that dairy-based materials can be used for 3D-printing, with the first being processed cheese (Le Tohic et al., 2018). A significant decrease (49%) of the hardness for melted and printed cheese was found compared to untreated cheese. Moreover, sodium caseinate, which showed reversible gelation characteristics, was used for extrusion-based printing (Schutyser et al., 2018). The addition of pectin, sucrose and starch facilitated the printing process. Nöbel et al. (2018) used cold acidified concentrates from milk microfiltration differing in pH (4.8 – 5.4) and protein content (8.0 – 12.0% (w/w)) which were heated in an extrusion-based 3D-printer to induce a sol−gel transition. At pH 4.8, firm and homogeneous milk gels were printed, while milk gels at pH 5.0 were not mechanically stable after printing. For further information about 3D-printed dairy-based materials, a review (Voon et al., 2019) is recommended.

Bovine milk contains about 34 g L^{-1} proteins in the form of casein and whey protein. Casein represents around 80% of the protein content and consists of four main types (α_{s1}- (40%), α_{s2}- (10%), β- (35%) and κ-casein (15%)) which together with colloidal calcium phosphate form complexes called casein micelles (CM). The hydrodynamic diameter of the CM is about 200 nm and the zeta-potential is about –19 mV at the native pH of 6.7 (Anema & Klostermeyer, 1996). Three main interactions, negative charge, steric repulsion and surface hydration between the layers of κ-casein around the micelles, stabilise the CM against aggregation (Heertje et al., 1985; Horne, 1986).

The whey proteins are globular proteins with defined secondary and tertiary structure. At temperatures around 70°C, they denature and interact or undergo aggregation reactions with κ-casein, especially β-lactoglobulin (Anema, 2008a), mainly via thiol-disulfide exchange reactions. Depending on the pH at heating, different types of interaction between denatured whey proteins and CM occur (Anema et al., 2004a; Anema et al., 2004b). When heating at pH 6.5, around 70% of the denatured whey proteins were attached to the surface of the CM, increasing its diameter up to 30 – 35 nm. With increased heating at pH 6.7, the level of association decreased with around 30% whey proteins covering the CM (Anema & Li, 2003a). This interaction depended on the location of κ-casein, which dissociated from the CM with increasing pH at heating (Singh & Fox, 1985; Anema & Klostermeyer, 1997). It is unclear why dissociation occurred, although κ-casein dissociated into the serum at temperatures lower than required for whey protein denaturation (Anema & Klostermeyer, 1997; Anema, 2008a).

During a traditional fermentation process for dairy products at constant temperature, gelation of milk occurs due to a reduction of the pH value by lactic acid bacteria and following the decrease of the net charge of the CM. While the fermentation process (T–pH-route) takes several hours under steady conditions, the alternative pH−temperature (T)-route can be used for immediate solidification during heat up of milk concentrates that have been pre-acidified in the

cold. For the pH−T-route, the two steps of acidification and gelation, which normally overlap in the fermentation processes (T-pH), occur separately, showing great potential for 3D-printing under dynamic conditions (Nöbel et al., 2018). Cold pre-acidification of milk up to pH 4.6 at less than 4 °C reduced the hydrophobic interactions and helped to maintain solution (sol)-characteristics. Subsequent heating of the acidified material caused collision and aggregation of the CM and gelation occurred (Roefs, 1986; Schäfer et al., 2018). Vasbinder et al. (Vasbinder et al., 2003) also found that firmer gels were obtained via the pH−T-route compared to the T-pH-route at the same concentration. Recent studies (Silva et al., 2018; Kharlamova et al., 2019) showed the effect of adding native as well as denatured whey protein on the gelation behaviour of casein micelles via the pH−T-route. Kharlamova et al. (2019) showed that the addition of fractal whey protein isolate aggregates to aqueous suspensions of micellar casein lowered the temperature of gelation (at a fixed micellar casein concentration) and increased the storage modulus G' of the milk gels. A further decrease of the gelation temperature was found, if the pH was decreased, the protein concentration increased or $CaCl_2$ added.

The success of 3D-printing as a method to produce highly individualised and tailored nutrition for specific requirements will strongly depend on the food materials and the printability of the recipes. To the best of our knowledge, no prior studies have investigated the usage of micellar casein combined with whey protein for extrusion-based 3D-printing via the pH−T route, inclusive a tailored sol−gel transition. Casein-based microgels can be induced with mechanical processing, heat treatment, changes in the environmental conditions (e.g. pH) or in surface properties (interaction with whey proteins) (Loewen et al., 2017). We hypothesised that by altering one of the pre-processing parameters, e.g. the pH during heat treatment, tailoring of the surface characteristics of the CM causes changes in the sol−gel transition temperature and thus, increases the aggregation rate. Either weaker or firmer printable gels for tailored nutrition can

potentially be provided by this method. Four parameters, the protein content, casein−whey protein ratio, heating - and acidification pH of the casein−whey protein suspensions were adjusted to investigate the material characteristics and to correlate these properties with printability.

4.3 Material and methods

4.3.1 Material

Micellar casein concentrate (MCC 85) was provided by Sachsenmilch Milk & Whey Ingredients (Sachsenmilch Leppersdorf GmbH, Wachau, Germany). As specified by the manufacturer, MCC 85 was composed of 85% (w/w) protein in dry matter, with a 9:1 ratio of casein to whey protein. This specific batch of MCC 85 contained 87.60% (w/w) protein in dry matter, 1.45% (w/w) fat, 2.48% (w/w) lactose and 7.44% (w/w) ash. GermanProt 9000 - Whey protein isolate (WPI) was provided by the same manufacturer. This specific batch was composed of 93.74% (w/w) protein in dry matter, 0.23% (w/w) fat, 0.61% (w/w) of lactose and 3.16% (w/w) of ash. Citric acid (1M) (Sigma Aldrich, UK) was prepared by mixing with Milli-Q water (Elix® 5 distillation apparatus, Millipore®, USA) and sodium hydroxide (1M) was bought from Sigma Aldrich (UK) and used for pH adjustment.

4.3.2 Sample preparation

Solutions of micellar casein were prepared using deionised water and agitated at a constant speed for 5 h at 40°C to disperse the powder, with the procedure shown in *Figure 4-1*. The suspensions were cooled to room temperature and stored at 4°C overnight to allow hydration of the caseins, with starting pH values of 6.7 ± 0.05. Three different casein contents (8.0-, 10.0- or 12.0% (w/w)) were tested. To adjust the casein to whey protein ratio to 4:1 and to keep impurities (high lactose content, for example in skim milk powder) as low as possible, powdered whey protein isolate was added to all three micellar casein contents. A total amount of 2.0-, 2.5- or 3.0% (w/w) of whey protein was mixed with casein, dispersed in deionised water

and heated at 40°C for 5 h. A high pressure homogeniser (Panda NS1001L-2K, Gea Niro Soavi, Parma, Italy) was used to ensure a homogenous distribution of the particles (one pass, 500 bar).

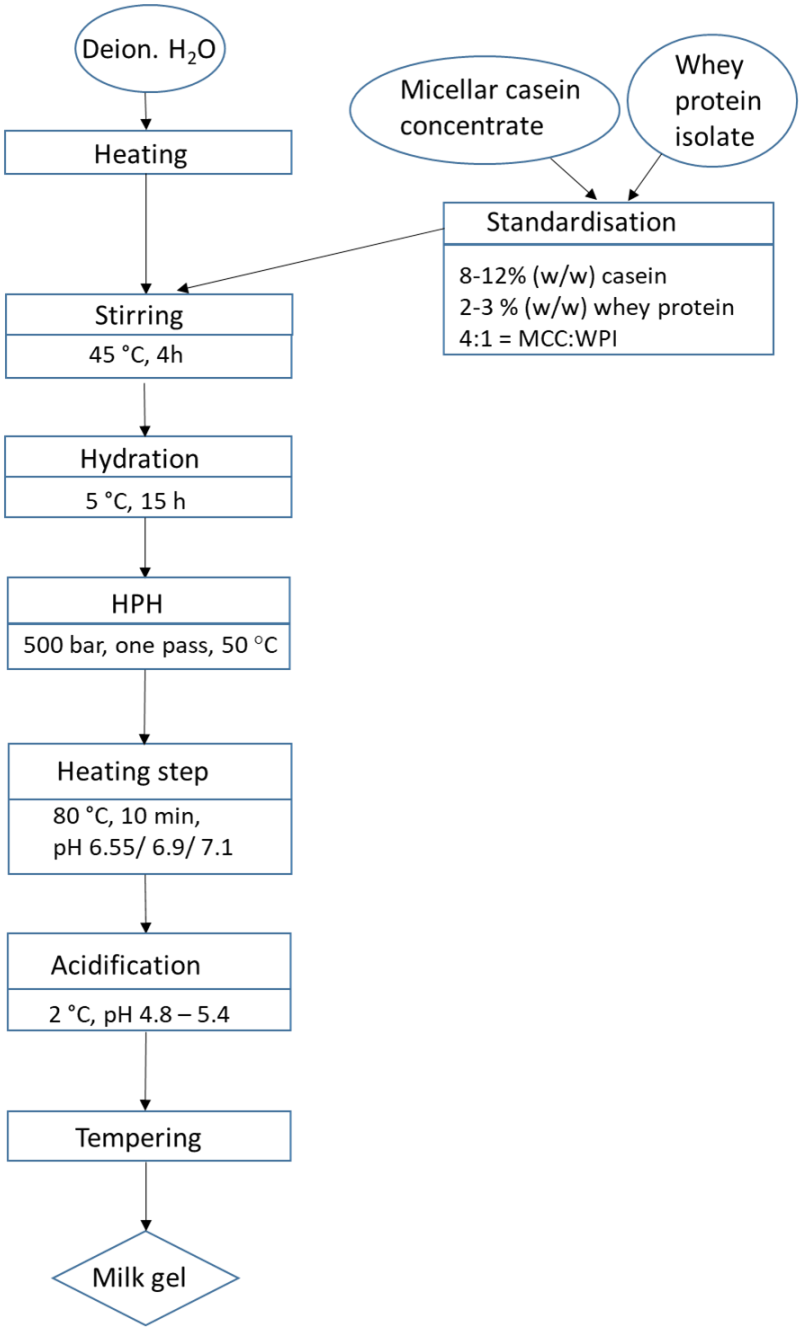

Figure 4-1: Flow chart for the preparation of casein-whey protein suspensions for application in extrusion 3D-printing.

The influence of the denaturation of whey proteins on the sol−gel transition temperature and the aggregation rate was tested as follows. The pH of the casein−whey protein suspensions was adjusted to 6.55 (1M citric acid) or to 6.9/7.1 (1M NaOH) before heat treatment. The bottles containing the suspensions were indirectly heated (80°C, 10 min) in a water bath on a stirring

plate to ensure denaturation (degree of denaturation$_{\beta\text{-LG}} \geq 80\%$; as estimated from Kessler, 2002) of the whey proteins. After heating, samples were filled in a double-walled beaker connected to a water bath at 2°C. Cold acidification was performed dropwise with citric acid under agitation. After decreasing the pH value (5.4 – 4.8), the solution was equilibrated for 30 min and the pH was readjusted, if changes occurred (Schäfer et al., 2018; Nöbel et al., 2018).

4.3.3 Rheology

Rheological measurements were conducted by a Kinexus Pro rheometer (Malvern Instruments, UK) with a cup (D = 27.17 mm, depth = 63.5)-vane (d = 61 mm, height = 25 mm)-geometry. For dynamic oscillatory measurements, temperature sweeps were performed from 2 – 60°C with a heating rate of 1 K/min. The samples were pre-sheared with a shear rate of 100 s^{-1}, followed by an equilibration time for 300 s with no shearing. The oscillation step was performed with a deformation of 0.3% and a frequency of 1 rad/s to ensure a non-destructive measurement in the linear viscoelastic region of the final gel. During measurements the storage modulus (G'), the loss modulus (G''), the phase angle ($tan\ \delta$) and the temperature were monitored. The sol−gel transition temperature was determined when G' reached a value of 1 Pa (Nöbel et al., 2018; Schäfer et al., 2018).

4.3.4 Zeta-potential and particle size measurements

The particle size and the zeta (ζ)-potential were determined using a Zetasizer (Malvern Instruments, UK). For particle size measurements, samples were prepared at native pH (6.7) by diluting them with deionised water and measured at 20°C. Casein−whey protein suspensions were analysed in the exact same way after the denaturation step at different pH values (6.55, 6.9, 7.1). Refraction indices of 1.33 (water) and 1.57 (casein) were adjusted for the volume-based particle size distribution (Griffin & Griffin, 1985), calculated via the Mie theory. Averaged particle sizes were presented by the intensity weighted mean hydrodynamic diameter z-average.

After a stepwise (0.2 units) decrease of the pH to lower values than the native pH (6.7) by means of 1M citric acid, the ζ-potential was measured and plotted against the solution pH. Before every experiment, samples were diluted with deionised water. The temperature of each sample, the water (diluent) and within the zetasizer was adjusted to 2°C to ensure no pre-gelation or precipitation of the caseins during measurements.

4.3.5 SDS-PAGE

4.3.5.1 Preparation of the samples via centrifugation

After heating (80°C, 10 min) at different pH values (6.55, 6.9 and 7.1) with continuous rocking, an amount of 1.5 ml for each sample was placed in small plastic tubes. Serum proteins were defined as the particles that did not sediment from the sample during a centrifugation step (Type 5424, Eppendorf, North Ryde, Australia) at 21.000g at 20°C for 1 h (Anema, 2007). The supernatants were analysed on the same day.

4.3.5.2 Sodium dodecyl sulphate polyacrylamide gel electrophoresis (SDS-PAGE)

SDS-PAGE was performed using precast Bis-Tris 12% polyacrylamide gels and an electrophoresis system (Invitrogen, Mount Waverley, Australia). Centrifugal supernatants were diluted (1:25) with deionised water and mixed (10 µl) with 5 µl of LDS (Sigma Aldrich, UK), 2 µl of reducing agent (Sigma Aldrich, UK) and 5 µl of β-mercaptoethanol (Bio-Rad Laboratories Ltd., UK). Each of the non-heated reference samples was diluted in a similar way and the same amount of reagents was added. All samples were heated at 100°C for 3 min prior to loading. The gels were run at 115 V for 90 min and a solution containing 0.025% w/v Coomassie (Bio-Rad Laboratories Ltd., Watford, UK), 40% w/w methanol and 7.5% w/w acetic acid was used for staining for 90 min and a 7.5% w/w acetic acid solution was used for de-staining the gels overnight. Gels were visualised using a Fuji Film Intelligent Dark Box II with Fuji Film LAS-3000 V2.2 software (Brookvale, Australia). The proteins were identified by comparison to the

molecular weight (Mw 10 – 250 kDa) of protein standards (Precision Plus, Kaleidoscope, Bio-Rad, Australia).

4.3.6 Microscopy

4.3.6.1 Scanning electron microscopy (SEM) preparation

For comparison of the different pre-process treatments regarding the casein micelle structure, all four formulations (micellar casein concentrate without any heating, micellar casein concentrate plus whey protein heated at a pH of 6.55, 6.9 and 7.1 at 80°C for 10 min) were used. The preparation process was done mainly following the procedure of Dalgleish et al. (2004), who presented the micellar surface of the casein particles with a cold field-emission ultra-high resolution scanning electron microscope (FESEM).

One drop of each sample was placed on a poly-lysine coated glass slide in a humidity chamber to prevent drying. Samples were allowed to settle for an hour and were fixed in 2.5% glutaraldehyde in phosphate buffer. The buffer was removed after two minutes. After an hour the primary fixative was removed, the sample was rinsed with the phosphate buffer and the secondary fixative, 1% osmium tetroxide in phosphate buffer, was added for an hour. After removing the secondary fixative, all the samples were rinsed three times with buffer and then dehydrated using a graded ethanol series: 70%, 90%, 95% and 100% EtOH (elapsed time per solution was five minutes). The 95% EtOH step was repeated twice and the 100% EtOH three times. Following dehydration the samples were fixed onto stubs using conductive copper tape and were sputter-coated with gold. All three samples were stored in a desiccator at ambient temperature until they were used for imaging.

4.3.6.2 Imaging

The samples were imaged using an environmental-SEM (FEI/Philips XL30 ESEM-FEG, Philips, UK). Between 15kV and 20kV were applied for the acceleration voltage and magnifications of up to 50.000 x were used.

4.3.7 Set-up of a customised 3D-printer

A customised printer was created to print dairy materials via the pH−T-route, including a sol−gel transition, similar to Nöbel et al. (2018). A commercially available plastic printer (Creality Ender 3 Printer; Creality, Shenzhen, China) was retrofitted (shown in *Figure 4-2*). For better control of the additional weight of the new parts, the motor and the syringe with the double walled cooling jacket were fixed on the top of the printer. The stepper motor, connected to a screw plunger, controlled and powered the syringe to perform the extrusion-based printing. Two stainless steel bars held all the parts in line and several computer-aided design (CAD)-printed parts supported the straight attachment of the motor.

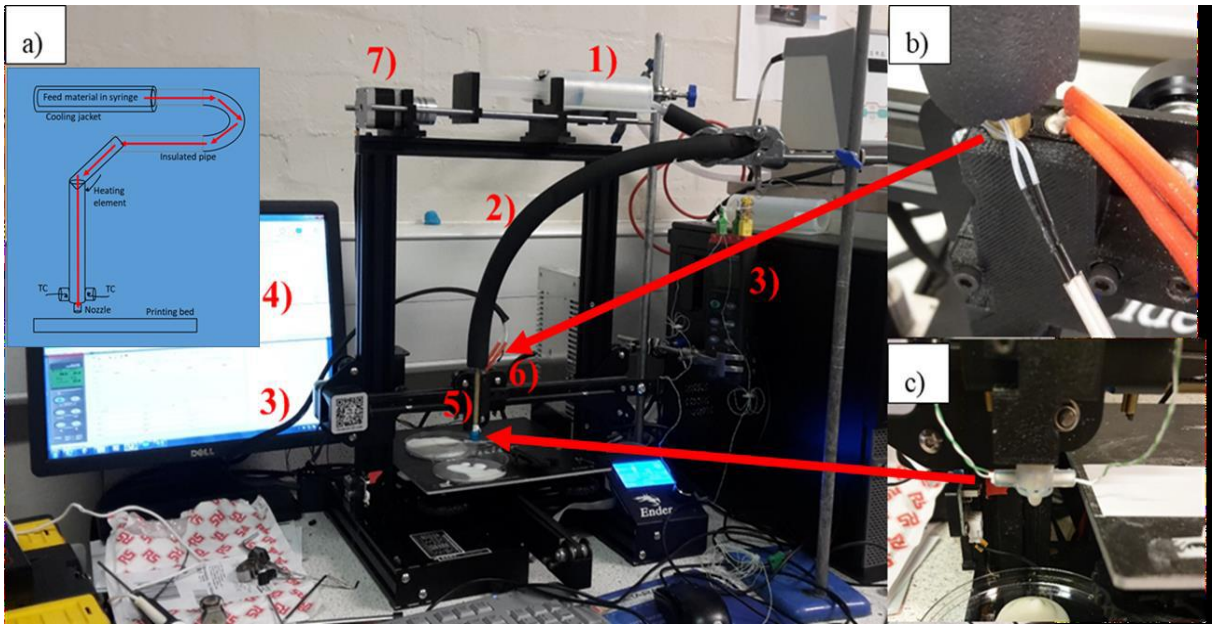

Figure 4-2: Set-up of the customised 3D-Food printer after the retrofitting process including 1) syringe in double walled cooling jacket, 2) insulated pipe for transport of feed material to nozzle, 3) thermometer, thermocouples (TC) and software, 4) firmware of Ender 3 printer, 5) nozzle with die at the end, 6) heating element for nozzle and 7) stepper motor. b) Heating element in contact with the copper pipe. c) Nozzle with dye and thermocouples at the end. The small inset image in (a) shows a simplified schematic of the set-up with the flow direction of the feed material in red.

Before the printing process, the syringe was loaded with 60 ml of the cold acidified casein−whey protein suspension. To maintain sol−characteristics, a temperature of 2°C was maintained within the syringe cooling jacket, connected to a water bath. Materials were transported via a pipe to the copper nozzle (plastic dye at the end, 1.15 mm in diameter), heated with the heating element and a sol−gel transition was induced. The software used to control the printer

was Repetier. To create a printed object, a CAD model (25 x 25 x 3 mm rectangle slice) of the object was created in the software. The printing line speed was set to 20 mm/s. The layer height was adjusted to 1 mm for all three layers, which were printed above each other. This resulted in an overall height of around 3mm for every printed rectangle. Before each print, the bed level had to be calibrated manually. Printing was performed on a hydrophobic printing paper (10 x 10 cm; Legamaster International B.V., The Netherlands) to prevent spreading of the first layer.

4.3.8 Statistics

The data plotted in the publication includes the average of at least three measurements accompanied by error bars that consist of the standard deviation of the mean. In the case where mean values of an observation are compared between samples the data have been subjected to analysis of variance (ANOVA) in order to determine significant differences. Data analysis was conducted with Sigma Plot 12.5 (Systat Software Inc., San Jose, CA, USA). Individual samples were compared with Student's t-test and a level of significance of $p < 0.05$ was chosen.

4.4 Results and discussion

4.4.1 Physico-chemical characterisation of the sol−state

4.4.1.1 Particle size

The rheological characteristics of colloidal gels formed from milk proteins depend on intrinsic (e.g. size, shape, availability, protein content) and extrinsic parameters (e.g. temperature, ionic strength, pH) (Dickinson, 2016). The size of the CM was considered to be a crucial parameter influencing the printing characteristics of the starting material, due to the requirement of a fast and irreversible sol−gel transition during the printing process (Nöbel et al., 2018). Smaller particles (nanometre range) move faster due to Brownian motion, which can result in a faster aggregation process and be expected to provide denser and hence, firmer gels during printing. The volume-based distribution of the casein−whey protein suspensions is shown in *Figure 4-3*, with protein particles ranging between 50 – 650 nm.

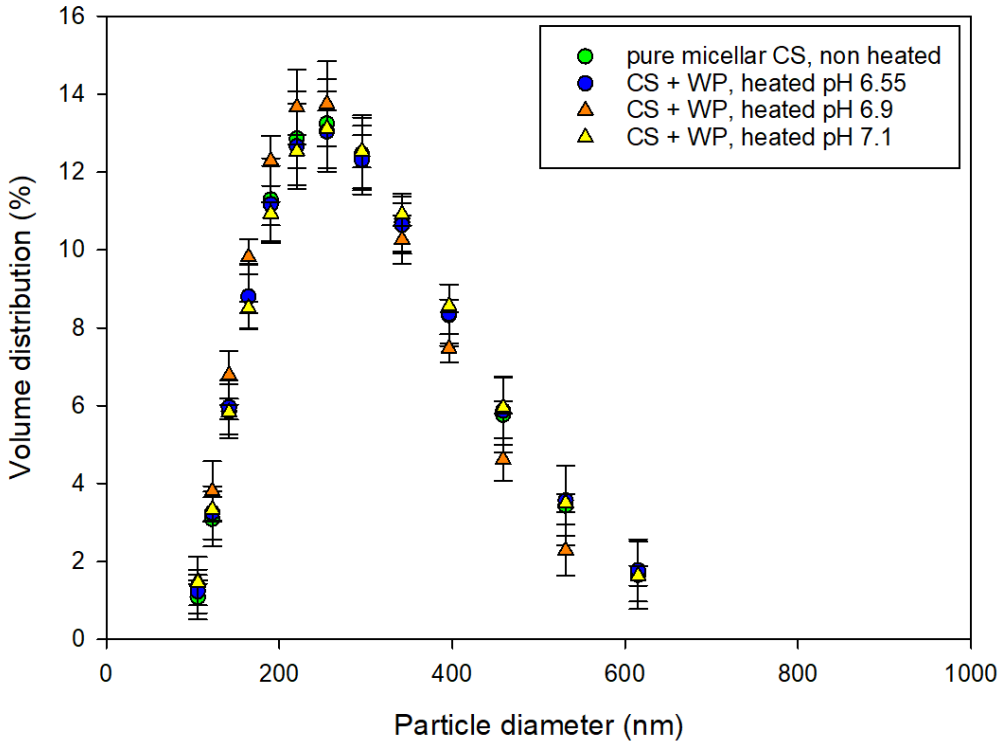

Figure 4-3: Particle size distribution for non-heated CS (○/green), heated (pH 6.55) CS + WP (●/blue), heated (pH 6.9) CS + WP (▲ /orange) and heated (pH 7.1) CS + WP (Δ/yellow) casein−whey protein suspensions.

After a homogenisation step, performed to avoid any aggregates that may have formed during hydration overnight, the average intensity weighted diameter (z-average) of the protein particles in all formulations, independent of the pH at heating, was around 230 – 240 nm. Anema et al. (2004b) measured the size of CM in reconstituted skim milk and found a similar value of around 215 nm for unheated milk at pH 6.5. Heating at the same pH for 30 min at 80°C, 90°C and 100°C resulted in an increase of the size of 15-, 30- and 40 nm respectively. This small increase in the size of the CM was explained by the interaction of the denatured whey proteins, especially β-lactoglobulin, with κ-casein on the surface of the CM via thiol-disulfide bond exchange reactions as well as hydrophobic and ionic interactions. Due to higher temperatures and a longer heating time, it is proposed that Anema et al. (2004b) were able to show a significant decrease in the size of the CM at higher pH at heating compared to results in this study. The range of sizes of particles was confirmed with SEM (showing the raspberry structure of the CM) and cryo-EM images (see *Supplementary Figure 4-1*).

4.4.1.2 Zeta-Potential

The ζ-potential as a function of the pH of pure, non-heated micellar casein - and heated (pH 6.55, 6.9, 7.1) casein−whey protein suspensions is shown in *Figure 4-4*. The ζ-potential of each formulation was averaged for all the protein particles captured within this sample. Independent of the type of formulation, an almost linear decrease of the ζ-potential with decreasing acidification pH was found. A significant downshift of up to 5 mV of the ζ-potential of heated casein−whey protein suspensions over the whole range of pH values was evident compared to the non-heated sample. Heating resulted in physical and chemical changes, e.g. precipitation of calcium phosphate and dephosphorylation of caseins, which altered the ζ-potential of the CM (Fox, 1981; Singh & Creamer, 1992). No significant changes in the ζ-potential over all acidification pH values were found for any of the pH adjusted conditions performed before the heating step (6.55, 6.9, 7.1). Anema & Klostermeyer (1996) found that CM heated at pH 6.6

showed a higher (more negative) ζ-potential than CM heated at pH 7.1, although only very small differences were found below pH 6.0 and no measure of variation was provided in their publication. Darling & Dickinson (1979) reported the same almost linear decrease in the ζ-potential of CM when the pH was reduced, although significantly lower values were found. At pH 4.75, Anema & Klostermeyer (1996) found a ζ-potential of –13.5 mV (30°C) for heated milk samples (120°C, 6 min) which was very similar compared –13.1 mV ± 1.3 mV at pH 4.8 for non-heated, pure casein suspensions in our study. This was not in accordance with the results of Darling & Dickson (1979) who found a value of 0 mV at the IEP of casein (4.6). It has been suggested that an increasing ζ-potential was caused by a dissociation of colloidal calcium phosphate, which increased with decreasing pH up to a complete solubilisation at around pH 5.3 (Dalgleish & Law, 1988). As a result, ionic calcium binds to the surface of the CM, thereby reducing the electrophoretic mobility and decreasing the ζ-potential of CM (Dalgleish, 1984). Anema & Klostermeyer (1996) proposed that this binding of the calcium to the CM shields their negative charges, resulting in a decrease of the ζ-potential.

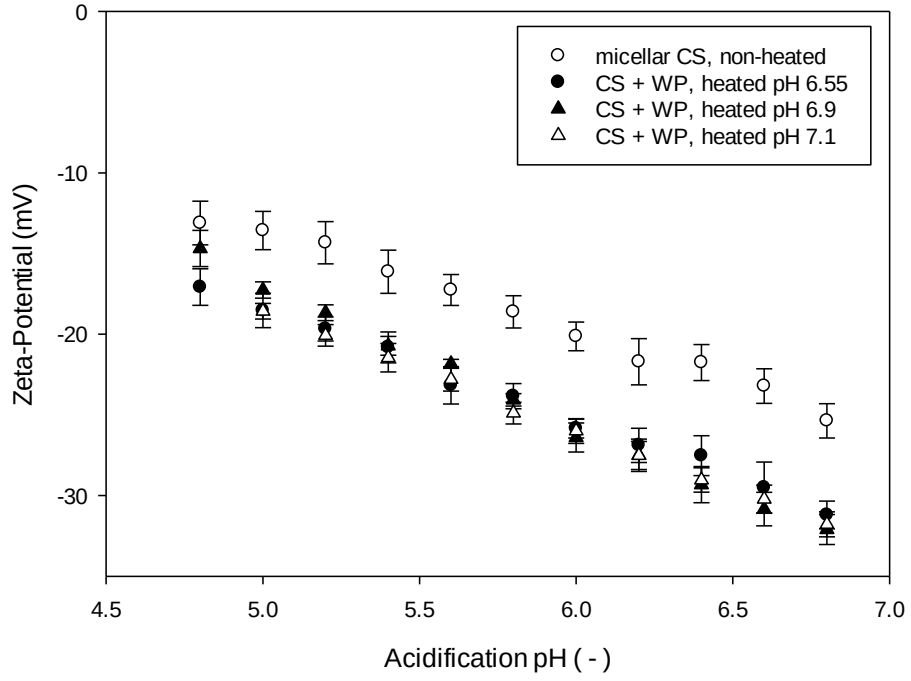

Figure 4-4: Changes in the ζ-potential with decreasing pH of non-heated micellar CS (○), heated (pH 6.55) CS + WP (●), heated (pH 7.1) CS + WP (Δ) and heated (pH 6.9) CS + WP (▲) suspensions (casein to whey protein ratio of 4:1). Measurements were performed at a temperature of 3°C for the sample, the diluent (deionised water) and within the zetasizer.

4.4.1.3 SDS-PAGE

Figure 4-5 shows the SDS-PAGE analysis of the supernatants obtained from non-heated (6.55, 6.9, 7.1) and heated (6.55, 6.9, 7.1) casein−whey protein suspensions following centrifugation, with a main focus on the disintegration of the casein micelle. Heat treatment at pH 6.55 resulted in a significantly lower amount of whey proteins in the supernatant, confirming other results with whey protein (mainly β-lactoglobulin) covering the surface and being bound to the CM at this pH (Anema et al., 2004a; Anema, 2007). Increasing the pH at heating to 6.9 and 7.1 caused increasing amounts of κ-casein dissociating from the CM into the serum, resulting in additional free κ-casein−whey protein complexes in the serum and decreased levels of CM covered with whey proteins, evidenced by the same amount of whey proteins in the supernatant.

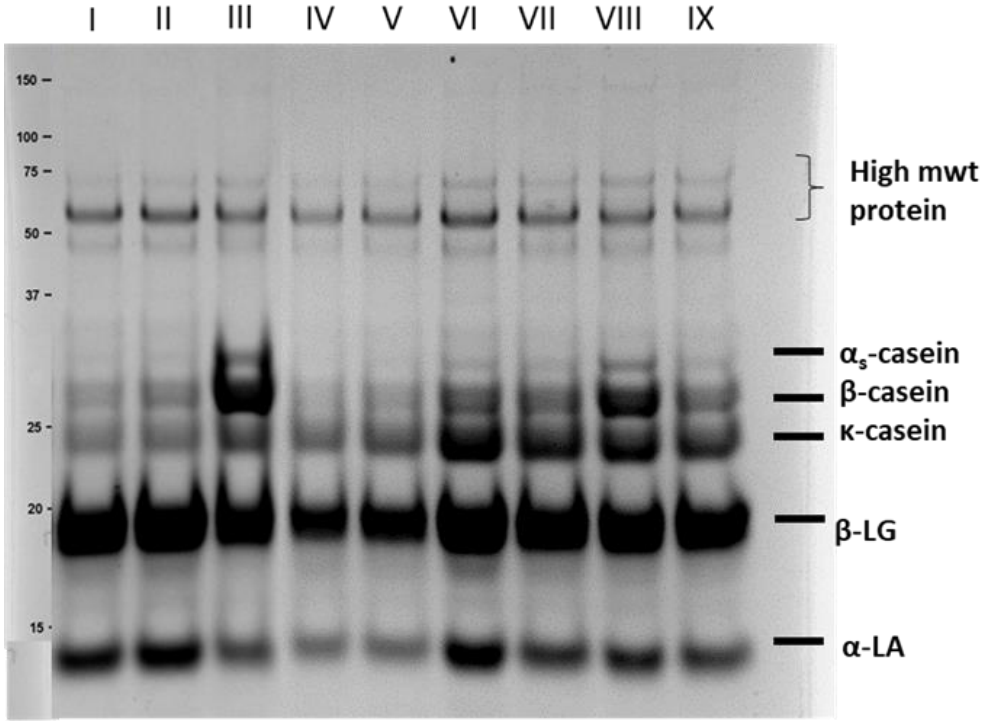

Figure 4-5: SDS-PAGE analysis of serum phase proteins with - and without thermal treatment (80°C, 10 min). Lane I-III: non-heated, pH 6.55, 6.9 and 7.1 (from left to right). Lane IV-V: heated, pH 6.55; Lane VI-VII, heated, pH 6.9 and Lane VIII-IX, heated, pH 7.1.

Our results are consistent with Anema (2008a), who demonstrated the pH dependent dissociation of κ-casein on heating. It is estimated that a less significant difference in κ-casein dissociation between the lower and the higher pH at heating compared to other results (Anema, 2007;

Anema, 2008a; Anema, 2008b) was due to a lower heating temperature during our denaturation process, but could also be explained with a lower protein concentration used in the studies of Anema (2008a). Singh & Creamer (1991) found that the dissociation of κ-casein from the CM depended on two parameters, the pH and the total solids content of the sample before a heating process. Both parameters, higher pH values at heating (6.5 – 7.1) and higher proteins concentration, caused an increase in the extent of dissociation out of the CM.

4.4.2 Rheological characterisation of the sol−gel transition

The gelation behaviour of casein-based milk concentrates at different acidification pH-protein combinations showed promising results for extrusion-based 3D-printing (Nöbel et al., 2018). The sol−gel transition temperatures were obtained by temperature sweeps from the point when the storage modulus G' equalled 1 Pa (Schäfer et al., 2018; Nöbel et al., 2018). This value could be further used to adjust the temperature in the nozzle during the printing process to intentionally induce a sol−gel transition. In *Figure 4-6* (B-D) the sol−gel transition temperatures of cold acidified casein−whey protein suspensions after a heating step at different pH values (6.55, 6.9, 7.1) are illustrated. For comparison, the result of a pure micellar casein sample (no addition of whey protein, no heating step) is provided in each subfigure and discussed first. *Figure 4-6* (A) depicts the sol−gel transition temperature of micellar casein suspensions differing in the protein content as function of the acidification pH, which was chosen according to previous results (Nöbel et al., 2018).

For casein suspensions a linear relationship between the acidification pH and the sol−gel transition temperature (G' = 1 Pa) was found. As shown in *Figure 4-6* (A), the CM stayed in colloidal solution below the coagulation line and direct acidification followed by heating resulted in gelation of the CM. Above the coagulation line, spontaneous coagulation occurred during acidification and the casein precipitated (Hammelehle et al., 1997; Schäfer et al., 2018). The coagulation line depends on the composition (pH, protein content) and the pre-treatment

(e.g. heating time, -temperature and - pH). At all protein contents, sol−gel transition temperatures decreased significantly with decreasing acidification pH, as observed elsewhere for microfiltrated skim milk retentates (Schäfer et al., 2018), rehydrated phosphocaseinate powders (Thomar & Nicolai, 2016), reconstituted pasteurised skim milk (Vasbinder & De Kruif, 2003) and micellar casein suspensions with added whey protein isolate (Kharlamova et al., 2019).

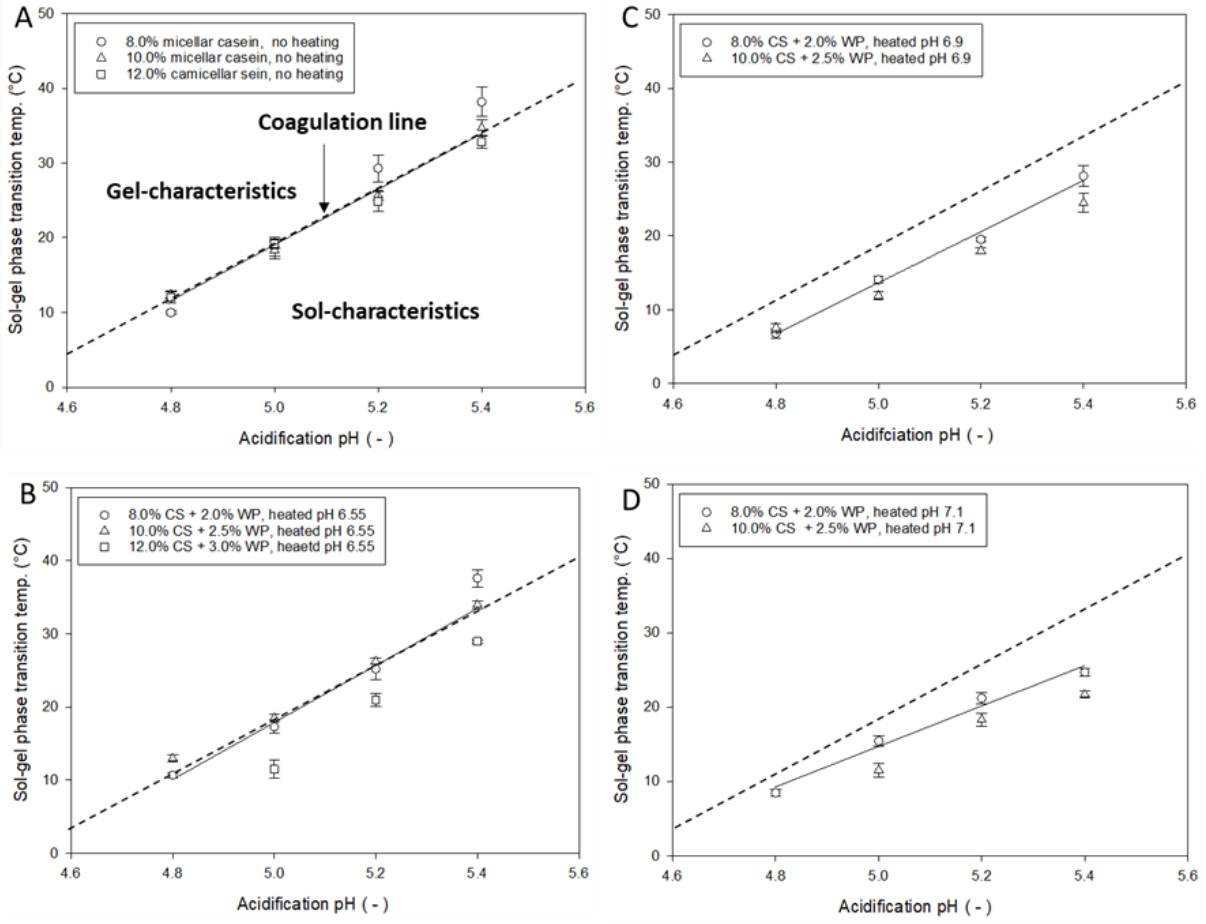

Figure 4-6: Sol−gel transition temperatures of cold acidified micellar casein - (9:1 ratio of CS to WP, (A)) and casein−whey protein suspensions (4:1 ratio of CS to WP, B-D) at a heating rate of 1 K/min. With no heating step (A) and a heating step at 80°C for 10 min at pH 6.55 (B), pH 6.9 (C) and pH 7.1 (D). The dashed line in all images represents the coagulation line for pure micellar casein from (A) and is shown for comparison.

The sol−gel transition temperatures for heated (pH 6.55) casein−whey protein suspensions also decreased with decreasing acidification pH (*Figure 4-6*, B). Suspensions at the highest protein content showed significantly lower sol−gel transition temperatures at pH 5.0, 5.2 and 5.4 compared to lower protein concentrations, while pre−gelation was found at pH 4.8 (G' > 1 Pa). This

significant decrease of the sol−gel transition temperature at higher protein contents was proposed to appear with an increased amount of particles per unit volume, actively contributing to the gelation process. The mixed casein (8.0 – 10.0% (w/w)) - whey protein (2.0 – 2.5% (w/w)) suspension that was heated at pH 6.55 showed a similar coagulation line during acidification when compared to the non-heated casein sample.

For all casein−whey protein suspensions after pH 6.9 at heating, independent of the acidification pH, no sol−gel transition temperatures were obtained at the highest protein concentration (12.0% (w/w) CS and 3.0% (w/w) WP). At an acidification pH of 5.3, CM started to collide and aggregate, resulting in bigger particles, which caused unintended pre−gelation. This was evidenced by an increase of the storage modulus (G' > 1 Pa) prior to heating, preventing any sol−gel transition. For the highest pH at heating (7.1), all sol−gel transition temperatures of the formulations with the medium protein content were found below the coagulation line of pure micellar casein, indicating the dependency of the gelation point on the protein content during acidification. *Figure 4-6* (C) and (D) clearly showed that heating at a higher pH (6.9, 7.1) caused a shift of the coagulation line towards higher acidification pH values, explained with earlier acid induced coagulation of the surface-modified protein particles, confirming results of Hammelehle (1994).

4.4.3 Influence of the aggregation rate on printability

The aggregation rate (Pa/ 10 K), represented by the evolution of the storage moduli G' during linear temperature ramps, was chosen to be an important parameter to characterise the formulations differing in product - (pH and protein content) and pre-process parameters (pH at heating) regarding their printability (three layers printed). The aggregation rate was the parameter which was analysed when comparing the increase of the storage modulus G' from the sol−gel transition temperature (G' =1 Pa) until the next 10 K, as demonstrated with a casein−whey protein suspension in *Figure 4-7*. This specific value of ten degrees above the sol−gel transition temperature was chosen to compare how fast and how strong a three-dimensional network was built after the sol−gel transition temperature was reached. A fast aggregation rate of the CM was considered as a prerequisite for a sol−gel transition from sol to gel to obtain a firm gel network, supporting its own weight during an extrusion-based layer-by-layer printing process.

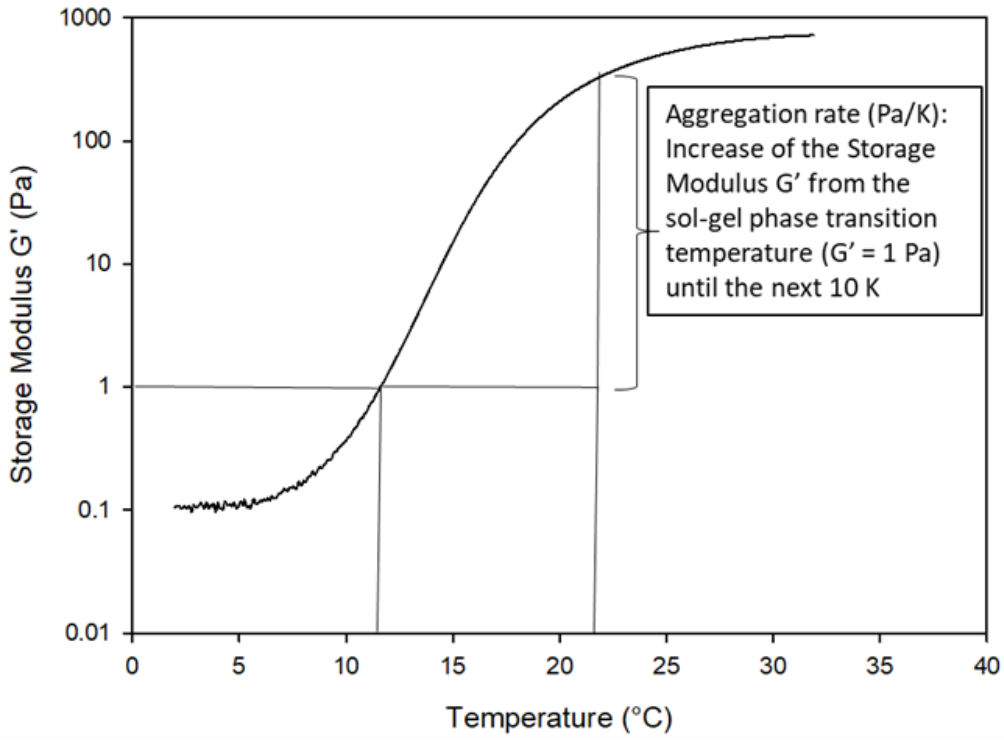

Figure 4-7: Example of a temperature sweep to illustrate how the aggregation rate (Pa/ 10 K) was defined. A casein−whey protein suspension (4:1 ratio, 8.0% (w/w) CS and 2.0% (w/w) WP) was heated at pH 6.9 (80°C, 10 min), cold acidified at 2°C to pH 5.0 and heated in a rheometer (heating rate of 1 K/min). A sol−gel transition temperature (G' = 1 Pa) was obtained at 11.92°C. The aggregation rate was calculated from the moduli increase between 11.92°C to 21.92°C.

In a previous study (Nöbel et al., 2018), pure casein-based suspensions were found to be printable at an acidification pH of 4.8, showing firm and homogeneous characteristics, while milk gels at pH 5.0 were not mechanically stable after the extrusion-based printing process. Within our study, only the aggregation rate of a non-heated, pure micellar casein-based suspensions (*Figure 4-8*) was shown for comparison with casein−whey protein suspensions, but no printing was performed for these samples. An increase in the casein content from lowest - (8.0% (w/w)) to highest values (12.0% (w/w)) resulted in significantly firmer gels, regardless of the acidification pH value.

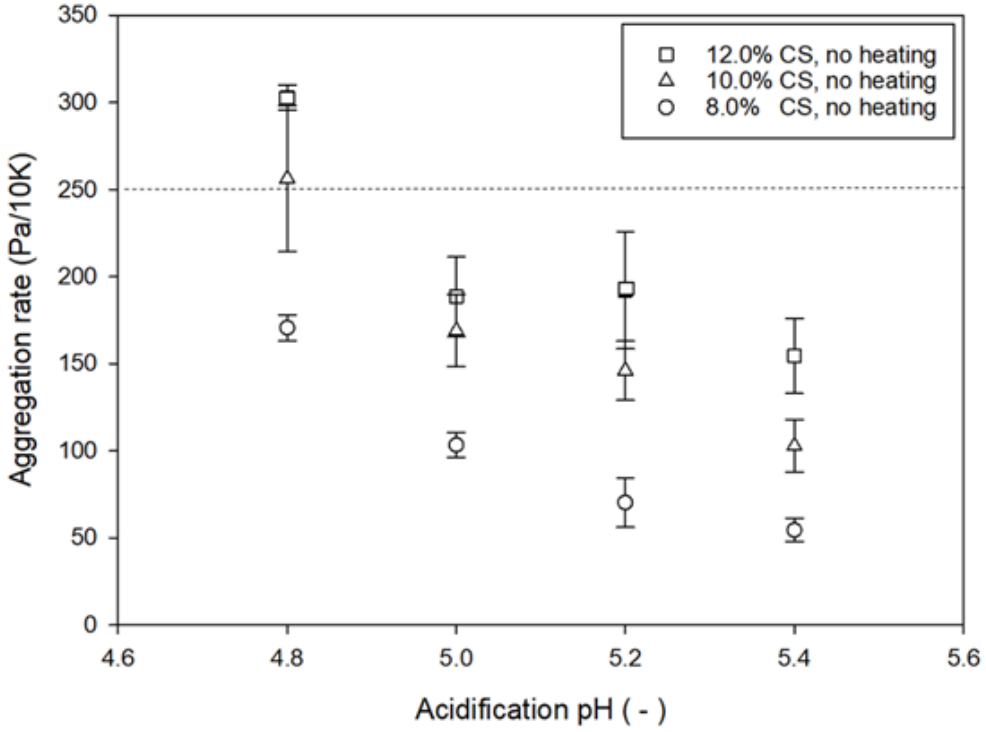

Figure 4-8: Aggregation rate (Pa/ 10 K) for non-heated, micellar casein suspensions at different pH values (4.8 – 5.4) and casein contents (8.0 – 12.0% (w/w)) at 10°C after/higher than sol−gel transition temperature obtained by temperature sweeps (heating rate of 1 K/min). The dotted line indicates the threshold where above 250 Pa/ 10 K the gels produced were stable after the printing process.

The aggregation rate of casein−whey protein suspensions after a heating step (at pH 6.55, 6.9, 7.1) is illustrated in Fig 8-10 and related to the printability by means of inset pictures. The aggregation rate of the casein−whey protein suspensions, that significantly depended on the protein content, the acidification - and the pH values at heating, was compared to the 3D-

printed images (25 x 25 x 3 mm, 3 layers). At the lowest pH at heating (6.55), the aggregation rate increased with decreasing pH and increasing protein content, apart from the highest protein content where the aggregation rate was not determined because of pre−gelation behaviour (*Figure 4-9*). All casein−whey protein suspensions at an acidification pH value of 4.8 showed firm and stable gels after the printing process, while higher acidification pH values (≥ 5.0) resulted in spreading of the material over the printing bed and no stable three-layered printing process.

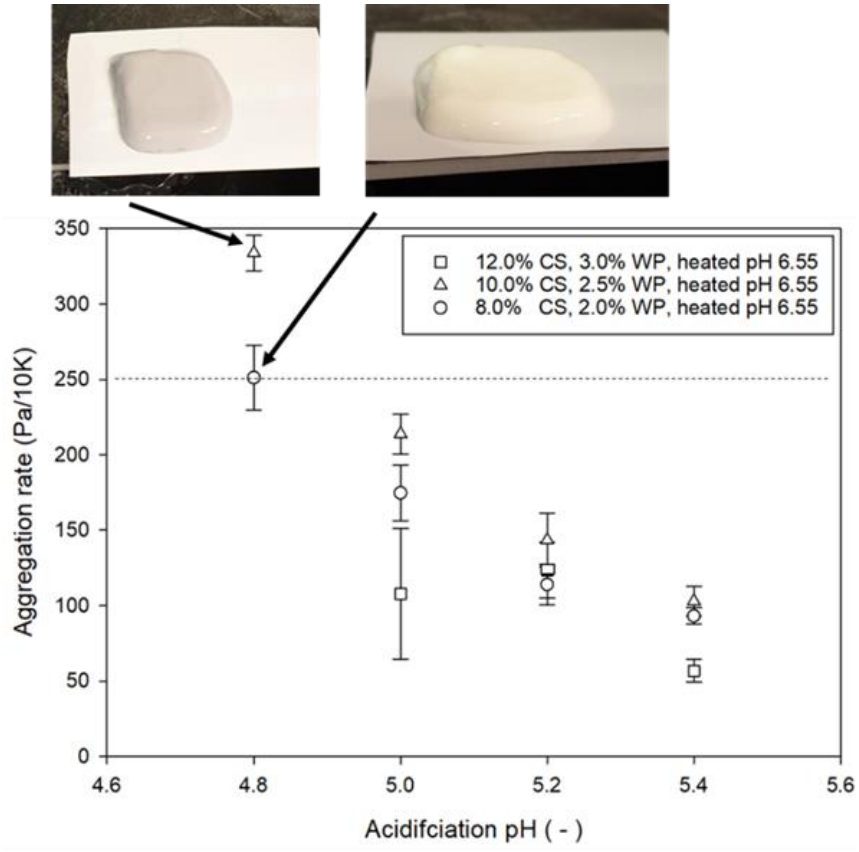

Figure 4-9: Aggregation rate (Pa/ 10 K) at different pH values (4.8 – 5.4) for casein−whey protein suspensions after a heating step (80°C, 10 min) at pH 6.55 at 10°C after/higher than the sol−gel transition temperatures obtained by temperature sweeps (heating rate of 1 K/min). Printed images are shown to relate the aggregation rate to printability. The dotted line indicates the threshold where above 250 Pa/ 10 K the gels produced were stable after the printing process.

An almost linear increase in the aggregation rate with decreasing acidification pH and increasing protein content was found after a heating step at pH 6.9 and pH 7.1 (*Figure 4-10* and *Figure 4-11*). All casein−whey protein suspensions with an aggregation rate higher than a chosen threshold of about 250 Pa/ 10 K showed firm gels after the printing process and maintained their shape. For the most promising formulation (pH 4.8, 10.0% (w/w) CS, 2.5% (w/w) WP,

heated pH 6.9; compare *Figure 4-10*) regarding the fastest aggregation from oscillatory measurements (315.5 ± 27.2 Pa/ 10 K), pre−gelation occurred during real printing processes. The clogged nozzle did not allow printing due to a low sol−gel transition temperature of 7.6 ± 0.6°C (*Figure 4-6*, C) and high absolute protein content of the sample. Slight fluctuations in the temperature during conveying may have induced this unintended gelation.

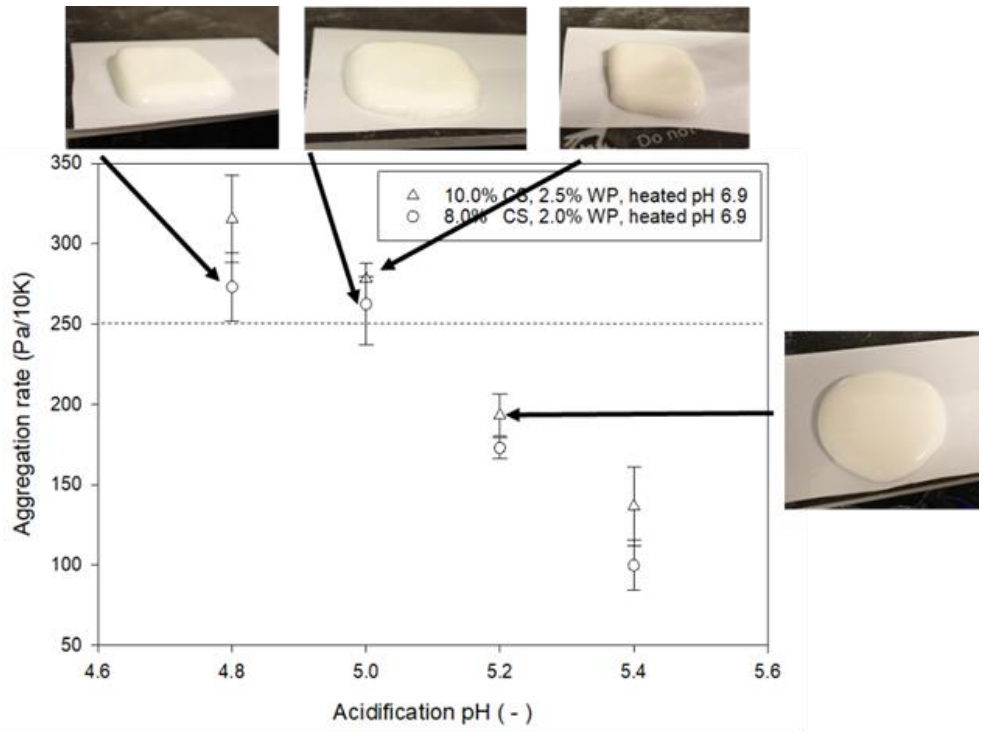

Figure 4-10: Aggregation rate (Pa/ 10 K) at different p values (4.8 – 5.4) for casein−whey protein suspensions after a heating step (80°C, 10 min) at pH 6.9 at 10°C after/higher than the sol−gel transition temperatures obtained by temperature sweeps (heating rate of 1 K/min). Printed images are shown to relate the aggregation rate to printability. The dotted line indicates the threshold where above 250 Pa/ 10 K the gels produced were stable after the printing process.

The aggregation rate of the casein−whey protein suspensions after a pH of 7.1 at heating increased with decreasing acidification pH, showing significantly lower values at the higher acidification pH values (5.2, 5.4) and lower protein content (*Figure 4-11*). The increase in the aggregation rate at the fixed lower protein content with decreasing pH was in accordance with the results of formulations heated at pH 6.9 (*Figure 4-10*) although a tendency to a faster aggregation at a pH of 7.1 at heating was found. Similarly to formulations after a pH of 6.9 at heating, unintended pre-gelation occurred at an acidification pH of 4.8 during printing (low sol−gel

transition temperature of 8.5°C; *Figure 4-6*, (D)) and no printing could be conducted, independent of the protein content.

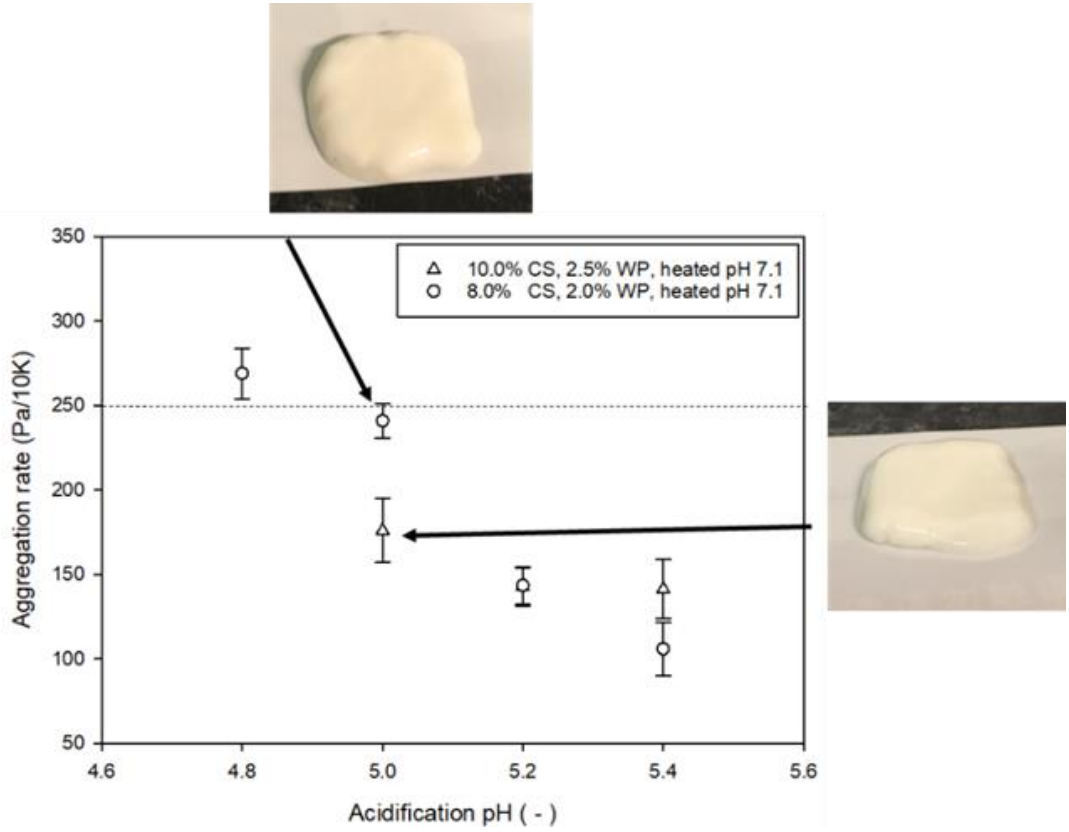

Figure 4-11: Aggregation rate (Pa/ 10 K) at different pH values (4.8 – 5.4) for casein−whey protein suspensions after a heating step (80°C, 10 min) at pH 7.1 at 10°C after/higher than the sol−gel transition temperatures obtained by temperature sweeps (heating rate of 1 K/min). Printed images are shown to relate the aggregation rate to printability. The dotted line indicates the threshold where above 250 Pa/ 10 K the gels produced were stable after the printing process.

4.4.4 Tailored casein micelle surface characteristics for printability

For the aggregation rate, a value of 250 Pa/ 10 K was proposed to predict the printability the best for formulations in the concentration and temperature range investigated in this study. Images of printed gels are shown in Fig 4.9–4.11. We found that formulations with an acidification pH of 5.0 were printable only by addition of whey protein and a heating step at higher pH values (≥ 6.9). Standardisation of such formulations to a micellar casein to whey protein ratio of 4:1 with the addition of whey protein isolate and a small change in the pH value (6.9, 7.1) before heating resulted in κ-casein depleted CM with less steric repulsion forces and more κ-casein−whey protein complexes in the serum (*Figure 4-12*). This intended tailoring of the surface

characteristics of the CM and the increased number of particles per unit volume allowed us to print casein−whey protein suspensions at both acidification pH values, 4.8 and 5.0, with the latter found not to be printable for non-heated, pure casein-based systems (Nöbel et al., 2018).

The pH sensitive CM are the main particles contributing to a gelation process of dairy gels, if they coagulate (*Figure 4-4*). An intended modification of the surface characteristics (κ-casein depleted CM, pH value at heating ≥ 6.9) resulted in suitable casein−whey protein suspensions for extrusion-based 3D-printing. After a heating step, denatured whey proteins contributed to the three-dimensional network, decreased the sol−gel transition temperature (≥ pH 6.9 at heating) and increased the aggregation rate (≤ acidification pH values of 5.0) of milk gels. In this study, the aggregation rate (*Figure 4-9*) of casein−whey protein suspensions after heating at pH 6.55 increased only for formulations examined at an acidification pH of 4.8, while the sol−gel transition temperature (*Figure 4-6*, B) did not change compared to pure non-heated, micellar casein-based samples. The results from the literature and this study suggest that the number of particles contributing to the aggregation did not increase during a heating step at pH 6.55. At this pH, Vasbinder et al. (2003b) proposed that almost all the denatured whey proteins covered the surface of the CM while Anema et al. (2004b) found values between 55 – 85% of whey protein covering the surface of the CM for pH 6.5 at heating, depending on the heating temperature.

As the pH at heating was increased (6.9, 7.1), Anema & Li (2003b) and Anema (2007) found a decreased amount of denatured whey protein on the surface of the CM, changing the composition and the surface characteristics of the CM. Results of SDS-PAGE in our study confirmed a dissociation of κ-casein from the CM into the serum at higher pH values at heating (*Figure 4-5*). At higher pH values at heating, denatured β-lactoglobulin and κ-casein formed complexes in the serum, apart from covering the CM, reducing the concentration of free κ-casein in the serum phase (*Figure 4-12*). The dissociation of κ-casein into the serum suggests that the density

of the hairy layer covering the surface of the CM was reduced, which facilitated the collapse of the remaining κ-casein, if the acidification pH was lowered. Therefore, aggregation of the CM at lower temperatures may occur due to less steric repulsion forces provided by a weaker hairy layer of κ-casein, while electrostatic repulsion forces did not change after heating at different pH values (*Figure 4-4*). A similar explanation was provided by Lakemond & Van Vliet (2008), who heated skim milk at different pH values and proposed that CM heated at higher pH (6.9) collided and aggregated faster than CM heated at lower pH (6.2), due to a higher steric hindrance occurring at a lower pH at heating. These results showed the effect of small changes in the pH before the heat treatment on the type of casein−whey protein complexes and κ-casein dissociation out of the CM and how these changes resulted in more promising material characteristics for a 3D-printing process of casein−whey protein suspensions. A simple schematic model is proposed in *Figure 4-12* based on microstructural observations of proteins in this study, which illustrates the differences of gel structures after the 3D-printing process.

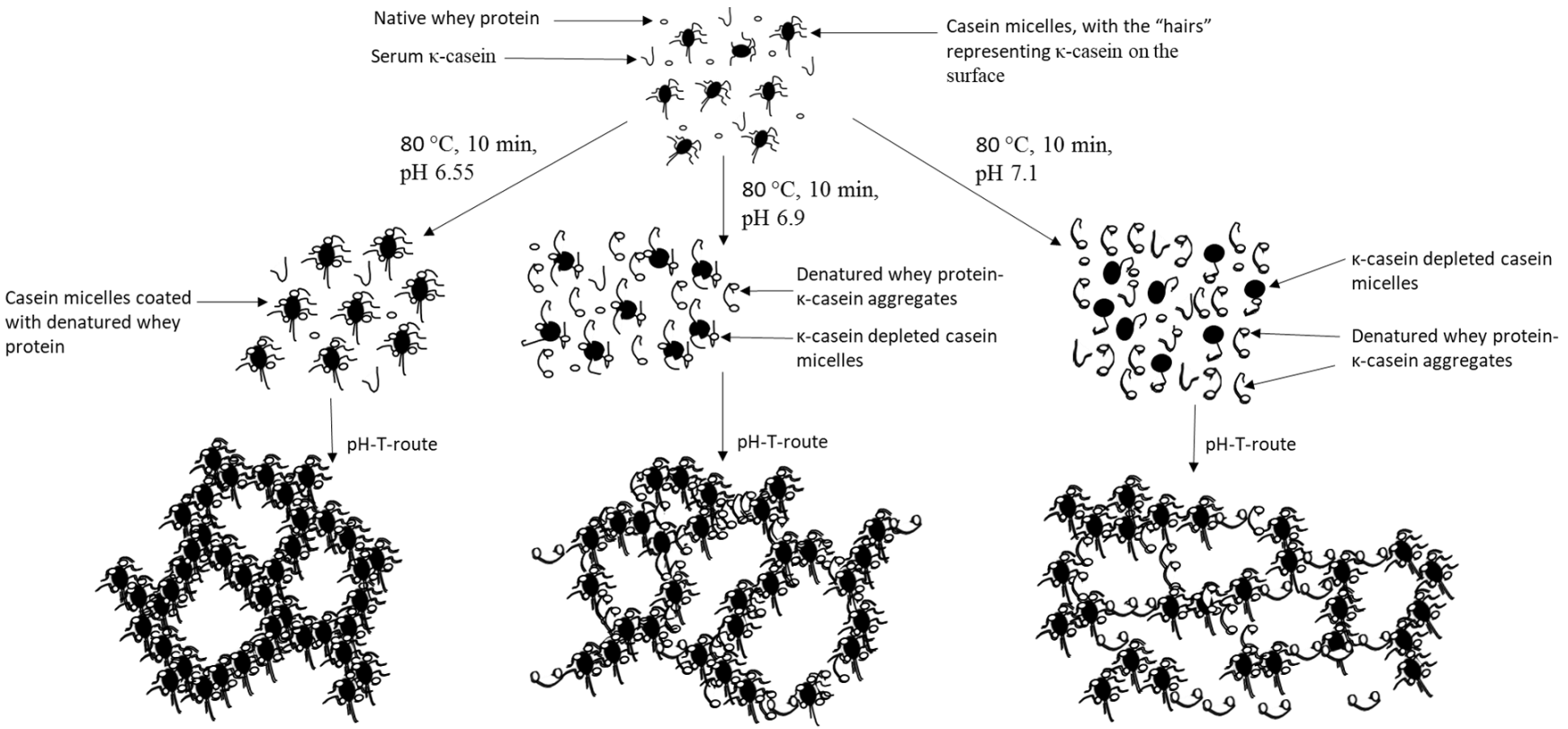

Figure 4-12: Schematic representation depicting the interactions of casein−whey protein formulations depending on the pH value during the heating step and explaining the differences of gels after a printing process.

4.5 Conclusion

Casein−whey protein suspensions differing in product - and pre-process parameters were investigated regarding their potential use for extrusion-based 3D-printing for tailored nutrition. This study demonstrated the influence of different pH values during heat treatment and the use of the acidification pH to manipulate the sol−gel transition temperature and the aggregation rate of casein−whey protein suspensions, if gelation was applied via the pH−T-route. Sol−characteristics at cold temperatures were confirmed with rheological - and zeta-potential measurements, providing a liquid feed material for a layer-by-layer printing process inclusive a full transition from sol to gel.

Depending on the location of κ-casein, denatured whey protein was either mainly bound to the surface of the CM (pH 6.55) or mostly found as complexes with κ-casein in the serum phase (pH 6.9, 7.1) which significantly modified the surface characteristics of the CM. These higher pH values at heating, causing κ-casein depleted CM, decreased the sol−gel transition temperature and increased the aggregation rate. The latter property was proposed as a good indicator for the printability of the formulations used within this study, if values of 250 Pa/ 10 K for the aggregation rate (represented by the storage modulus G') were recorded during a linear temperature ramp. The aggregation rate will be a good prospective indicator, but has to be investigated for each material and related to printing characteristics, as currently no quantitative and analytical method is available to objectively predict printability.

Lower acidification pH and higher protein concentrations of the cold acidified casein−whey protein suspensions resulted in an increase in the aggregation rate. Extrusion-based 3D-printing showed firm and stable gels at acidification pH values of 4.8 and 5.0, with more suitable formulations found after higher pH values at heating. Future studies focusing on more complex systems including different calcium/protein concentrations, fat or lactose will provide more

options for tailored and individualised nutrition via printing and will allow to design and understand more formulations.

4.6 Appendix

4.6.1 Supplementary data 1

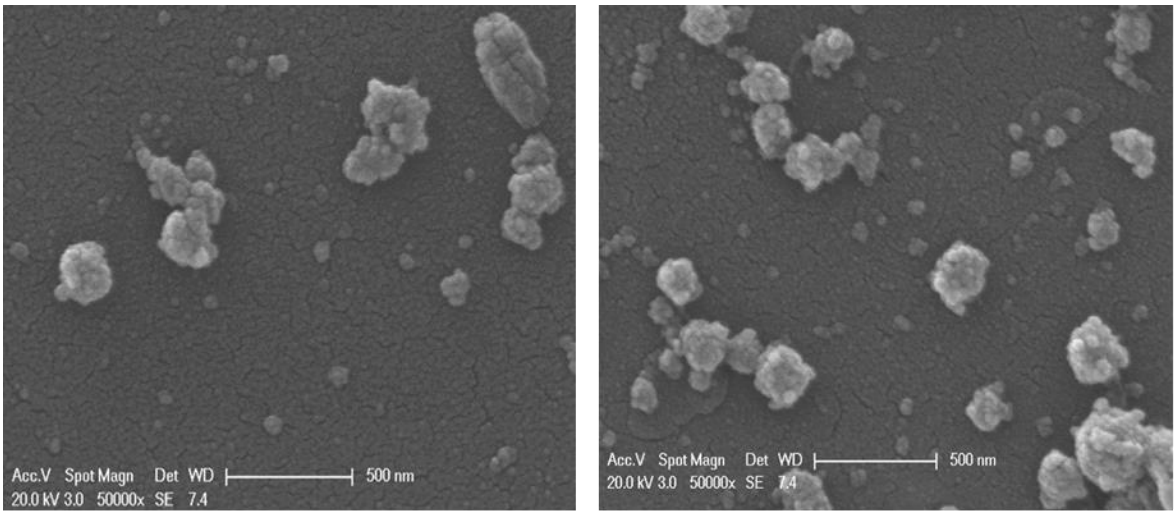

Supplementary Figure 4-1: Electron micrograph of only casein micelles in pure micellar casein - (left) and casein−whey protein suspension (pH 6.9 at heating, 10 min, 80°C; right), made using scanning electron microscopy.

4.6.2 Supplementary data 2

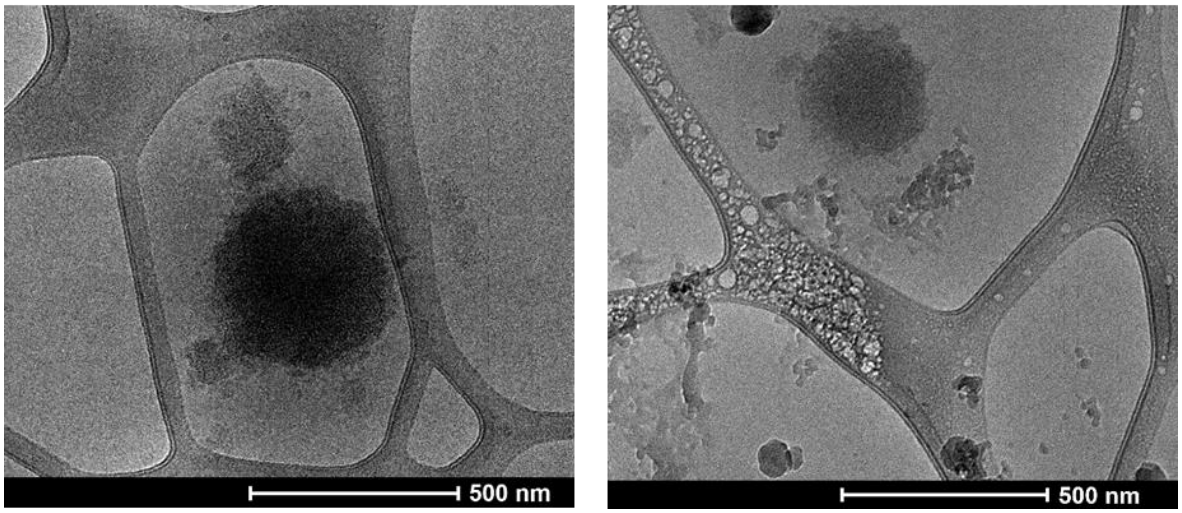

Supplementary Figure 4-2: Electron micrograph of casein micelles in casein−whey protein suspension (pH 6.55 at heating, 10 min, 80°C) made using cryo-EM, left and right.

4.7 References

Anema, S. G. (2007). Role of κ-casein in the association of denatured whey proteins with casein micelles in heated reconstituted skim milk. Journal of agricultural and food chemistry, 55(9), 3635-3642.

Anema, S. G. (2008a). On heating milk, the dissociation of κ-casein from the casein micelles can precede interactions with the denatured whey proteins. Journal of dairy research, 75(4), 415-421.

Anema, S. G. (2008b). Effect of milk solids concentration on the gels formed by the acidification of heated pH-adjusted skim milk. Food Chemistry, 108(1), 110-118.

Anema, S. G., & Klostermeyer, H. (1996). ζ-Potentials of casein micelles from reconstituted skim milk heated at 120 °C. International Dairy Journal. 6(7), 673-687.

Anema, S. G., & Klostermeyer, H. (1997). Heat-induced, pH-dependent dissociation of casein micelles on heating reconstituted skim milk at temperatures below 100 C. Journal of Agricultural and Food Chemistry, 45(4), 1108-1115.

Anema, S. G., & Li, Y. (2003a). Association of denatured whey proteins with casein micelles in heated reconstituted skim milk and its effect on casein micelle size. Journal of Dairy Research, 70(1), 73-83.

Anema, S. G., & Li, Y. (2003b). Effect of pH on the association of denatured whey proteins with casein micelles in heated reconstituted skim milk. J. Agric. Food Chem. 51(6), 1640-1646.

Anema, S. G., Lee, S. K., Lowe, E. K., & Klostermeyer, H. (2004a). Rheological properties of acid gels prepared from heated pH-adjusted skim milk. Journal of Agricultural and Food Chemistry, 52(2), 337-343.

Anema, S. G., Lowe, E. K., & Lee, S. K. (2004b). Effect of pH at heating on the acid-induced aggregation of casein micelles in reconstituted skim milk. LWT-Food Science and Technology, 37(7), 779-787.

Dalgleish, D. G. (1984). Measurement of electrophoretic mobilities and zeta-potentials of particles from milk using laser Doppler electrophoresis. Journal of Dairy Research, 51(3), 425-438.

Dalgleish, D. G., & Law, A. J. (1988). pH-induced dissociation of bovine casein micelles. I. Analysis of liberated caseins. Journal of Dairy Research, 55(4), 529-538.

Darling, D. F., & Dickson, J. (1979). Electrophoretic mobility of casein micelles. J. Dairy Res. 46(3), 441-451.

Dickinson, E. (2016). Exploring the frontiers of colloidal behaviour where polymers and particles meet. Food Hydrocolloid, 52, 497-509.

Fox, P.F. (1981). Heat-induced changes in milk preceding coagulation. Journal of Dairy Science, 64, 2127-2137.

Griffin, M. C. A., & Griffin, W. G. (1985). A simple turbidimetric method for the determination of the refractive index of large colloidal particles applied to casein micelles. Journal of colloid and interface science, 104(2), 409-415.

Hammelehle, B. (1994). Die Direktsaeuerung von Milch. Untersuchungen zur gezielten Einflussnahme auf Textur und Konsistenz gesäuerter Milchgele. PhD Thesis. Muenchen: Technische Universitaet Muenchen/ Weihenstephan.

Hammelehle, B., Schkoda, P., & Kessler, H. G. (1997). Parameters for coagulation properties of direct acidified milk and for the structure of milk gels. Milchwissenschaft, 52(12), 671-674.

Heertje, I., Visser, J., & Smits, P. (1985). Structure formation in acid milk gels. Food Structure, 4(2), 10.

Horne, D. S. (1986). Steric stabilization and casein micelle stability. Journal of Colloid and Interface Science, 111(1), 250-260.

Kharlamova, A., Nicolai, T., & Chassenieux, C. (2019). Heat-induced gelation of mixtures of casein micelles with whey protein aggregates. Food hydrocolloids, 92, 198-207.

Kessler, H. G. (2002). Food and bio process engineering. Dairy Technology, 5th edition (Verlag A. Kessler, Munich, Germany).

Lakemond, C. M., & van Vliet, T. (2008). Acid skim milk gels: the gelation process as affected by preheating pH. International Dairy Journal, 18(5), 574-584.

Loewen, A., Nöbel, S., & Hinrichs, J. (2017). Microgel Particles and Their Effect on the Textural Properties of Foods. https://doi.org/10.1016/B978-0-08-100596-5.21098-6.

Nöbel, S., Seifert, B., Schäfer, J., Daffner, K., & Hinrichs, J. (2018). Oral presentation Food Colloids, Leeds (2018) - Session - Processing of Novel Structures for Functionality. Temperature-triggered gelation of milk concentrates applied to 3D food printing.

Roefs, P. F. M. (1986). Structure of acid casein gels: A study of gels formed after acidification in the cold (Doctoral dissertation, Roefs). Wageningen University & Research Centre.

Ross, M. M., Kelly, A. L., & Crowley, S. V. (2019). Potential Applications of Dairy Products, Ingredients and Formulations in 3D Printing. In Fundamentals of 3D Food Printing and Applications (pp. 175-206). Academic Press.

Schäfer, J., Läufle, I., Schmidt, C., Atamer, Z., Nöbel, S., Sonne, A., Kohlus, R., & Hinrichs, J. (2018). The sol–gel transition temperature of skim milk concentrated by microfiltration as affected by pH and protein content. International Journal of Dairy Technology, 71(3), 585-592.

Schutyser, M. A. I., Houlder, S., de Wit, M., Buijsse, C. A. P., & Alting, A. C. (2018). Fused deposition modelling of sodium caseinate dispersions. Journal of Food Engineering, 20, 49-55.

Silva, J. V., Balakrishnan, G., Schmitt, C., Chassenieux, C., & Nicolai, T. (2018). Heat-induced gelation of aqueous micellar casein suspensions as affected by globular protein addition. Food hydrocolloids, 82, 258-267.

Singh, H., & Fox, P. F. (1985). Heat stability of milk: pH-dependent dissociation of micellar κ-casein on heating milk at ultra high temperatures. Journal of Dairy Research, 52(4), 529-538.

H. Singh & L. K. Creamer (1991). Influence of concentration of milk solids on the dissociation of micellar k-casein on heating reconstituted milk at 120°C. Journal of Dairy Research 58, 99-104.

Singh, H., & Creamer, L.K. (1992). Heat stability of milk. In Advanced Dairy Chemistry-I. Proteins, ed. P.F. Fox. Elsevier Applied Science, London, pp. 621-656.

Thomar, P., & Nicolai, T. (2016). Heat-induced gelation of casein micelles in aqueous suspensions at different pH. Colloids and Surfaces B: Biointerfaces, 146, 801-807.

Le Tohic, C., O'Sullivan, J. J., Drapala, K. P., Chartrin, V., Chan, T., Morrison, A. P., & Kelly, A. L. (2018). Effect of 3D printing on the structure and textural properties of processed cheese. Journal of Food Engineering, 220, 56-64.

Vasbinder, A. J., Rollema, H. S., Bot, A., & De Kruif, C. G. (2003). Gelation mechanism of milk as influenced by temperature and pH; studied by the use of transglutaminase cross-linked casein micelles. Journal of Dairy Science, 86(5), 1556-1563.

Vasbinder, A. J., & De Kruif, C. G. (2003). Casein–whey protein interactions in heated milk: the influence of pH. International Dairy Journal, 13(8), 669-677.

Voon, S. L., An, J., Wong, G., Zhang, Y., & Chua, C. K. (2019). 3D food printing: a categorised review of inks and their development. Virtual and Physical Prototyping, 14(3), 203-218.

Wegrzyn, T. F., Golding, M., & Archer, R. H. (2012). Food Layered Manufacture: A new process for constructing solid foods. Trends in Food Science & Technology, 27(2), 66-72.

5 Chapter:

Design, characterisation and understanding of protein-fat formulations towards an applications for 3D-printing

Chapter 5 is divided into two main sections, with the first one (5.1) focusing on a new screening protocol for microscopy, and the second one (5.2) presenting the results of the characterisation of casein-whey protein suspensions with additional milk fat regarding their extrusion-based printability via the pH−T-route.

Chapter 5

5.1 Imaging of dairy emulsions via a novel approach of transmission electron cryogenic microscopy using beam exposure

This work is peer-review published as follows:

Daffner, K., Hanssen, E., Norton, I. T., Mills, T., Ong, L., & Gras, G. L. (2020). Imaging of dairy emulsions via a novel approach of cryogenic transmission electron microscopy using beam exposure. Soft Matter, 16(34), 7888-7892.

5.1.1 Abstract

Emulsions containing both small fat and protein particles are difficult to differentiate but low dose transmission electron cryogenic microscopy can visualise and distinguish between these droplets or particles. A controlled increase in electron dose caused the sample to bubble and visibly degrade at < 25 $e^-/Å^2$ for fat globules and at > 150 $e^-/Å^2$ for protein particles, allowing particle differentiation. This technique may be useful for the development of nanoemulsions, as well as nanostructured and 3D printed foods.

5.1.2 Introduction

Protein and fat particles are typically easy to differentiate when the particles are large in size or substantially different in appearance. The two major components in bovine milk, the casein micelles (CM) and the milk fat globules (MFG), for example, can be distinguished in their native forms using chemical staining and confocal laser scanning (CLSM) (Lopez et al., 2008; Ong et al., 2010a). Differences in the size and appearance of native CM (mean ~ 150 nm) (Fox & Brodkorb, 2008) and native MFG (mean ~4 µm) can also be visualised using scanning electron microscopy (SEM) (Dalgleish et al., 2004) and transmission electron microscopy (TEM) (Dalgleish et al., 1996; McMahon & Oommen, 2008; Ong et al., 2010b). These microscopy techniques are less effective, however, when examining nanoparticles or nanoemulsions, where the particles are similar in size and appearance, as the particles also have low differential contrast. Given the recent increased interest in nanoemulsions, including for 3D-printing of food (Daffner et al., 2020), there is a need for microscopy methods that can both image and distinguish between protein and fat particles. This will allow the visualisation of dairy emulsions at a nanoscale.

Transmission electron cryogenic microscopy (cryo-EM) offers the high magnification and resolution needed to image nanoemulsions but also provides insights that may be useful for distinguishing between protein and fat particles. During imaging protein and fat particles are embedded in vitreous ice. Exposure of the sample to the electron beam causes damage to the vitreous ice layer, the embedded protein and fat particles and the supporting carbon film and prolonged exposure can cause hydrated specimens to appear to boil (Chen et al., 2008). This effect is called “bubbling” and is mainly caused by the radiolysis of water molecules, which results in free radical formation and pockets of hydrogen gas forming within the specimen (Chen et al., 2008; Leapman & Sun, 1995). This behaviour of samples during prolonged beam exposure,

whilst typically viewed as an unwanted effect, can potentially be utilised to provide further complementary information about particles present in the sample.

In this study, the potential of cryo-EM to both visualise and differentiate between protein and fat particles was assessed. A dairy emulsion consisting of small protein (50 − 650 nm) and milk fat particles (< 1 µm), generated by mechanical input, was used as a model system to assess the potential utility of the proposed approach as a new screening protocol. While it is well known that a high-energy electron beam can damage samples during imaging, this work tests the hypothesis that radiation damage at longer beam exposures would provide a better way of differentiating between protein and fat particles based on differences in density and carbon content.

5.1.3 Material and methods

5.1.3.1 Material

The model dairy samples examined included micellar casein−whey protein suspensions mixed with fat that were thermally treated and mechanically processed, to denature the whey proteins and generate small particles that adhere together, are difficult to distinguish by microscopy. These preparations are also useful formulations for potential 3D-printing of food. The casein concentrate (MCC 85) and German Prot 9000 - Whey protein isolate (WPI) were provided from Sachsenmilch Milk & Whey Ingredients (Sachsenmilch Leppersdorf GmbH, Wachau, Germany). Exact specifications by the manufacturer are provided elsewhere (section *4.3.1*). Cream (dairy fat) was bought from a supermarket (Meander Valley Dairy, Coles, Melbourne, Australia) and 100 ml contained 56.0% (w/w) fat, 2.6% (w/w) lactose, 1.6% (w/w) protein and 0.018% (w/w) salt. Citric acid (1M) (Sigma Aldrich, UK) was prepared by mixing it with Milli-Q water (Elix® 5 distillation apparatus, Millipore®, USA) and sodium hydroxide (1M) was bought from Sigma Aldrich (UK) to adjust the pH value.

5.1.3.2 Sample preparation

Casein−whey protein suspensions containing protein and fat particles of a similar size were prepared following the procedure in *4.3.2*. Cream (2.5% (w/w) total fat) was weighed and directly added with a spoon to glass bottles containing the protein suspension (8.0% (w/w) casein plus 2.0% (w/w) whey protein), with a pH of 6.7 ± 0.1. All samples were indirectly heated in a water bath under continuous rocking at 80°C for 10 min to ensure denaturation of the whey proteins (degree of denaturation β-LG ≥ 80%; estimated (Kessler et al., 2002)). After heating, samples were subjected to a pre-homogenisation step (50.0 ± 2.0°C) using a high intensity ultrasonic vibracell processor (Vibra Cell 750, Sonics, USA) operating in a continuous mode, at 750 W and 20 kHz. The power output was set at 95% of the nominal power and sonication was conducted over a controlled period of time (2 min) with 4 s on and 2 s off (3 min all in all). Directly after the pre-homogenisation step, each sample was single-passed through a high-pressure valve homogeniser (Panda NS1001L-2K, Gea Niro Soavi, Parma Italy) at 500 bar at 50.0 ± 2.0°C.

5.1.3.3 Transmission electron cryogenic microscopy (cryo-EM)

Thermally (80°C, 10 min) and mechanically (sonication and homogenisation) treated protein-fat samples were prepared for cryo-EM and diluted 1:10 with deionised water. Pure casein-whey protein suspensions were prepared at the same concentration. A Formvar lacey carbon film mounted on a 300 mesh copper grids (ProSciTech, Australia) was glow discharged for 15 s and used as a hydrophilic support on which the samples (3 µl) were adsorbed. After 10 s, the grids were plunged in liquid ethane using a Vitrobot (FEI Company, Eindhoven, Netherlands) to freeze the sample. The grids were observed on a Tecnai G2 F30 (FEI Company, Eindhoven, Netherlands) operating at 200 kV and no objective aperture, equipped with a CETA CMOS 4kx4k detector (FEI company, Eindhoven, Netherlands). For every sample, a series of micrographs of increasing dose was recorded with a defocus value of −6.66 µm.

5.1.3.4 Image analysis

Micrographs were high pass filtered to 5 nm to decrease noise due to low dose imaging. Pixels within each protein or fat particle were determined to be either grey or light (non-grey), where light pixels were defined as having a grey value less than 90% (a threshold selected to account for noise and X-ray heating of the detector plate). The fraction of light pixels in each particle was determined at each time interval from 7.5 $e^-/Å^2$ (1.5 s of exposure) in steps of 25 $e^-/Å^2$ electron dose (5 second exposure). Five images containing multiple particles were used for each dataset and for each particle type, with 16 fat and 12 protein particles counted in total.

5.1.4 Results and discussion

Within this study, a novel approach was developed to image and distinguish between protein and milk fat particles of similar size that display similar electron contrast when observed by cryo-EM. The particles were around 230 nm for protein and showed a size range between $30 - 955$ nm for fat particles. Milk protein can be observed by cryo-EM imaging following rapid freezing, which allows the particles to be observed without chemical fixatives, dehydration and embedding (*Figure 5-1*). The appearance (size, shape) of these particles found in our study is consistent with prior studies of milk components by cryo-EM (McMahon & Oommen, 2008) which allows greater detail than that possible with lower resolution techniques, such as confocal laser scanning microscopy. Cryo-EM has also been used in the past (Cano-Ruiz & Richter, 1997; Sharma & Dalgleish, 1993; Walstra & Jenness, 1984) to observe casein and whey proteins on the surface of the MFG after mechanical and thermal input to the system. The amount of protein present was found to strongly depend on several processing and formulation parameters including: homogenisation pressure, heat treatment and casein-fat ratio.

For protein−fat mixtures used within the present study, cryo-EM images were recorded in steps of 25 $e^-/Å^2$ (exposure time of 5 s) to analyse dose-dependent change to particles (both protein

and fat) and to detect differences in electron damage. Images of protein samples were taken first to provide a baseline. Heat treated casein−whey protein suspensions without milk fat are shown in *Figure 5-1*. Several CM were visible and did not show any visible time-dependent damage at a dose up to 150 $e^-/Å^2$, while gas bubbles were found on the holey carbon film at an electron dose of 30 $e^-/Å^2$, demonstrating the effect of "specimen bubbling" (Chen et al., 2008). Damage within the protein particles was evident after a total dose of 150 $e^-/Å^2$, with the appearance of "bubbles" occurring homogeneously throughout the protein particle.

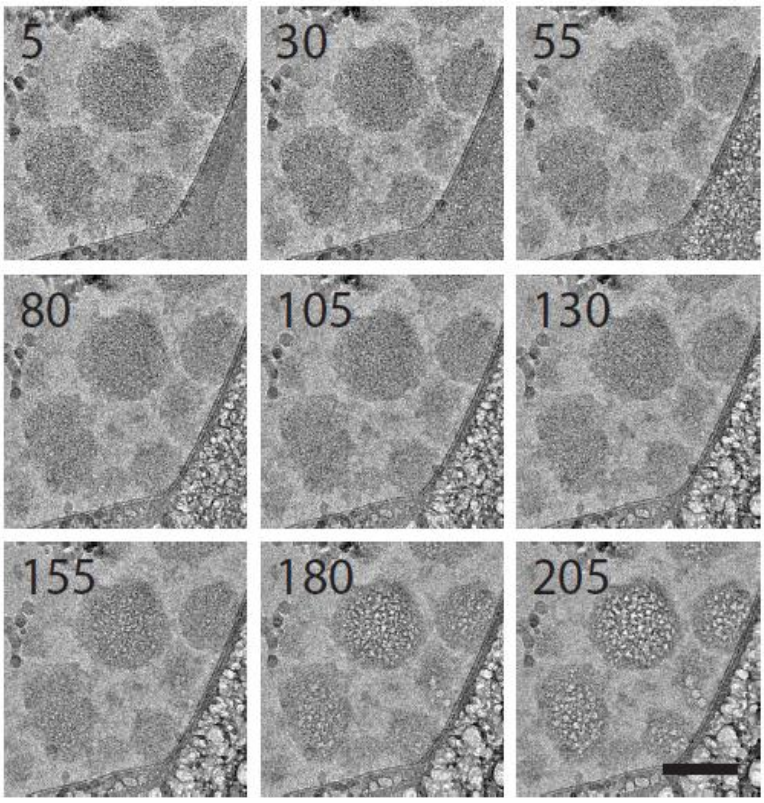

Figure 5-1: Cryo-EM images of the microstructure and radiation induced damage to protein particles within samples of thermally treated casein−whey protein suspensions. The first visible radiation damage was observed on the holey carbon support at a dose of around 30 $e^-/Å^2$, while protein particles did not show any damage up to a dose of 155 $e^-/Å^2$. Protein suspensions (8.0 and 2.0% (w/w); 4:1 CS to WP ratio) were thermally treated (80°C, 10 min) and diluted 1:10 with deionised water (final protein concentration of 1.0% (w/w)). The scale bar is 200 nm in length.

The visible decay of particles in response to electron dose was used to assess protein and fat particles. Specifically, the fraction of light pixels in each particle (which occurred due to radiation damage) was measured as a function of exposure to increasing steps of 25 $e^-/Å^2$ of electrons (5 seconds exposure) from an initial dose of 7.5 $e^-/Å^2$ (3 s of exposure).

In samples containing only protein (*Figure 5-1*), the particles did not show any visible damage or significant increase in the fraction of light pixels until a dose of 150 $e^-/Å^2$. In samples containing both fat and protein (*Figure 5-2*), the fat could easily be differentiated by the rapid decay of circular fat particles, with a significant increase in the fraction of light pixels at 20 $e^-/Å^2$, while the protein particles displayed a decay similar to the protein-only control. These differences likely arise from dissimilar densities and carbon contents within the two components.

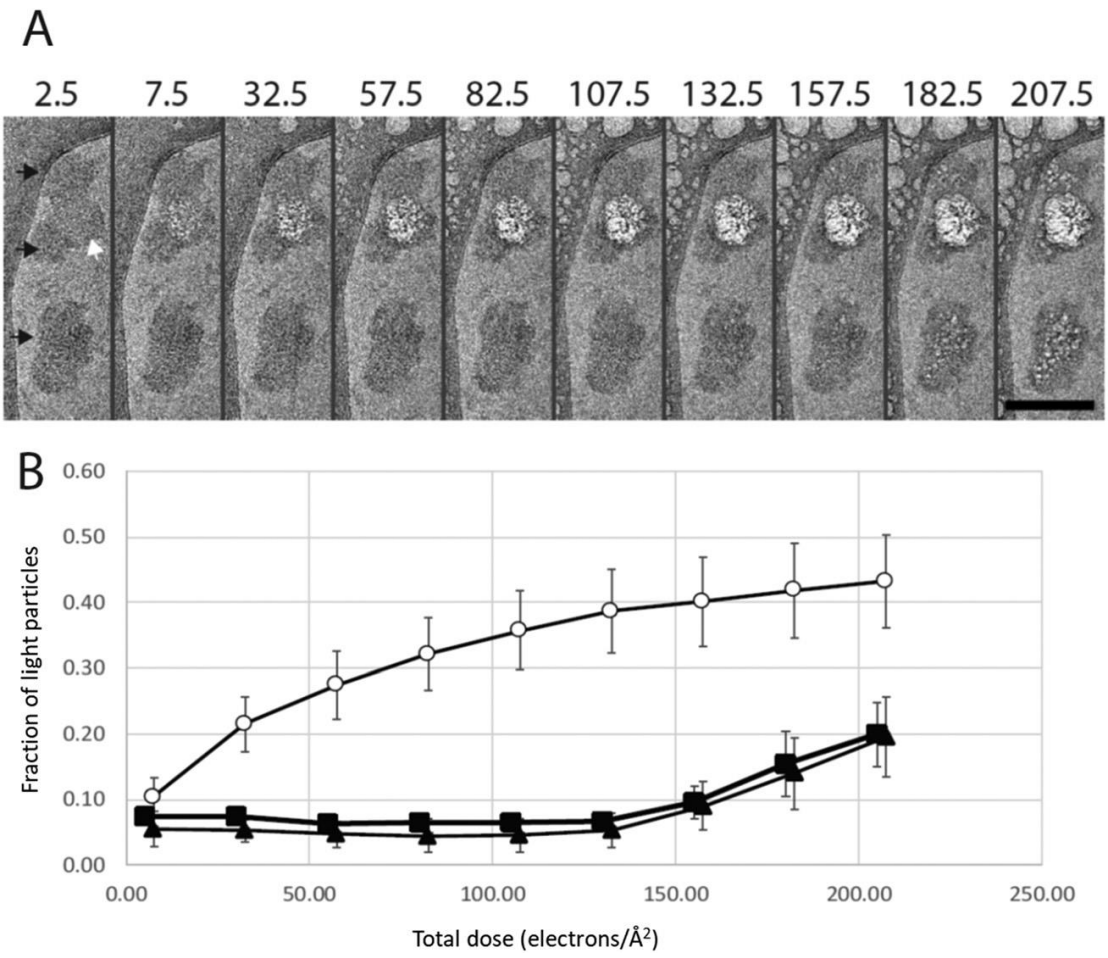

Figure 5-2: Qualitative damage to protein and fat particles, as visualised by cryo-EM with increased beam exposure. A: Images of three protein particles (dark triangles) and one fat particle (white triangle) that illustrate changes in particle colour intensity as a function of total electron dose. Samples were exposed to a dose of 2.5 $e^-/Å^2$ (1 s exposure) for initial sample visualisation. The effect of electron dose was then assessed from 7.5 $e^-/Å^2$ (3 s exposure) in steps of electron dose of 25 $e^-/Å^2$ (5 s exposure). The composition of the particles shown on the far left is assigned based on the damage due to cryo-EM exposure shown in the right images. B: Quantitative damage to protein and fat particles was measured as the fraction of light (or non-grey) pixels within each particle as a function of total electron dose, from an initial exposure of 7.5 $e^-/Å^2$. The fraction of light pixels was measured for samples containing only protein, which were used as a control (black squares) or samples containing both protein and fat, where the protein particles (dark triangles) were identified due to their similar decay to the protein only control, while the fat particles (hollow circles) decayed rapidly, resulting in a significant increase in the fraction of light pixels.

The potential broader utility of this technique could be the characterisation of MFG after heating and homogenisation, which generates a range of small nanometre sized particles that are otherwise difficult to differentiate. Several small fat particles are shown in *Figure 5-3*, which are covered by small protein nanoparticles. In this circumstance, controlled electron exposure can be used to differentiate between the small coating protein particles and the MFG using a final dose of 120.12 $e^-/Å^2$ with steps of 28.60 $e^-/Å^2$. With increasing beam exposure, the MFG were severely damaged (as indicated by the change in colour intensity; see *Figure 5-2*) which allowed visual distinction from the proteins. Therefore, *Figure 5-3* clearly shows several MFG in the nanometre range (30 – 50 nm) with different types of proteins on their surface, where the new technique allows MFG to be identified within the population of particles despite their small size. The surface of the MFG appears to be surrounded by CM or protein subunits consisting of casein monomers and whey protein aggregates. Such intact casein micelle-like particles have previously been found to partially cover the surface of larger MFG (~ 1.3 and ~ 1.1 µm in diameter) after heating at 50, 65 and 79°C and homogenisation at 4 and 7 MPa, shown by TEM (Ye et al., 2008). Additionally, a magnified image of several fat particles surrounded by protein is shown in *Figure 5-4*.

Electrophoresis of the proteins isolated from the surface of larger MFG droplets (560 nm in diameter) in homogenised cream has also confirmed that casein monomers or subunits of CM associate with the surface of fat (Sharma et al., 1996). These observations are consistent with the identification of protein on the surface of the smaller nanometre sized MFG in the present study and suggest that they may also be CM.

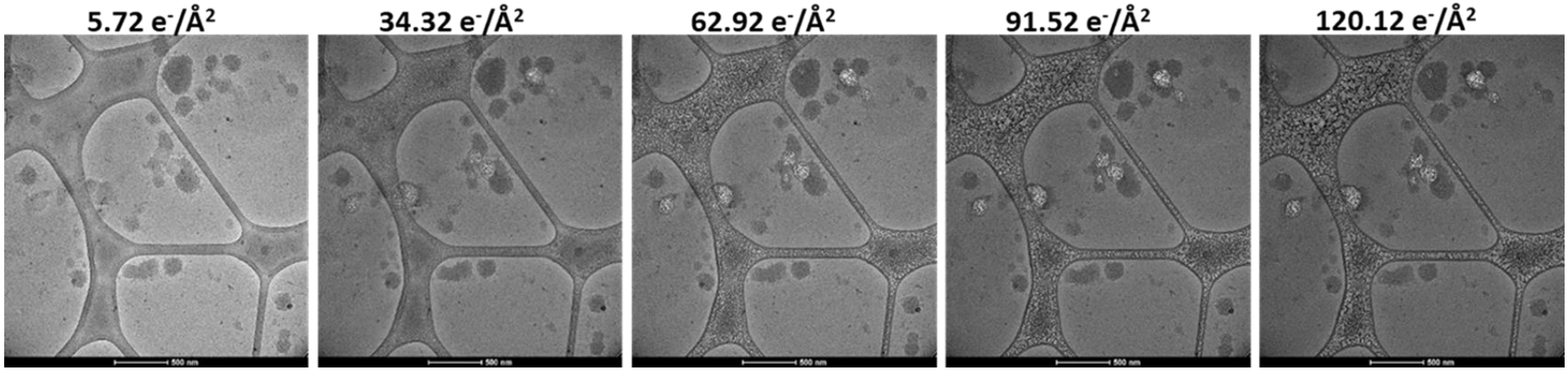

Figure 5-3: Cryo-EM images of the microstructure and radiation induced damage to protein and fat particles within suspensions of thermally and mechanically treated casein−whey protein with added milk fat. Images were taken in steps of 25 $e^-/Å^2$ (5 s exposure), with the total electron dose indicated at the top of images. The increasing contrast due to radiation damage was used to distinguish between protein and fat particles, with fat particles showing clearly visible radiation damage from a dose of 34.32 $e^-/Å^2$. The suspensions of casein whey protein (8.0- and 2.0% (w/w)) were prepared by sonication and homogenisation, followed by the addition of 2.5% (w/w) milk fat and dilution 1:10 with deionised water. The scale bar is 500 nm in length.

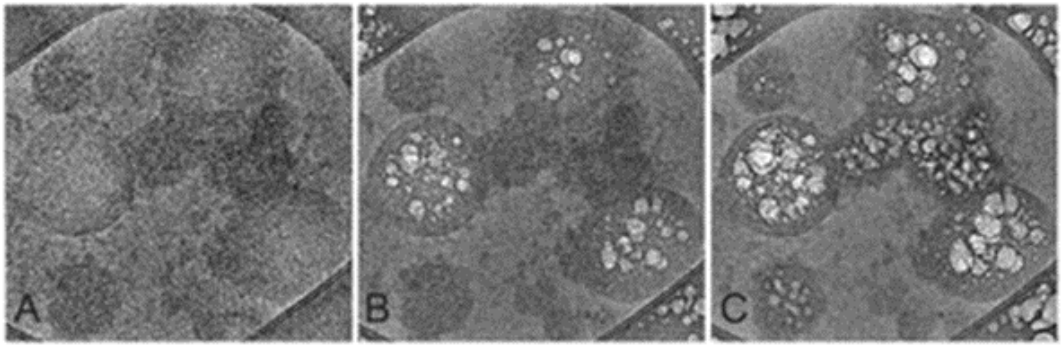

Figure 5-4: Graphical abstract showing a zoom in on protein and fat particles with increasing beam exposure. A) Electron dose of 2.5 $e^-/Å^2$ with no visible radiation damage for protein and fat particles. B) Electron dose of 82.5 $e^-/Å^2$ with visible radiation damage for fat particles, while protein particles remain unchanged. C) Electron dose of 182.5 $e^-/Å^2$ with visible damage for protein and fat particles.

5.1.5 Conclusion

A new method using transmission electron cryogenic microscopy was developed to image emulsions and differentiate between small fat and protein particles. This technique was demonstrated using casein−whey protein suspensions with nano sized milk fat droplets generated by thermal and mechanical treatment. At a constant low beam intensity, differences in time-dependent electron radiation damage allowed distinction between fat and protein particles. Intentional beam exposure (with a final electron dose up to 120.12 $e^-/Å^2$) caused severe damage to milk fat globules and a lightening of image pixels, while proteins remained intact with little change in pixel intensity within the same timeframe. The bubbling effect and the rate of change in pixel intensity were used to identify different particle types. The technique allows small spherical fat globules to be identified within complex dairy emulsions, where they are covered by casein micelles and protein subunits (e.g. casein subfractions or denatured whey protein (i.e. aggregates)).

The protocol developed will have potential for application in the characterisation of nanoemulsions, including bioactive or nutraceutical formulations, or in the development of novel structured foods, such as in 3D printing, where the similar size of fat and protein particles or droplets makes differentiation difficult. It may also be able to distinguish other compositional differences in density, help to facilitate the development and optimisation of products based on complex nanoemulsions.

5.1.6 References

Cano-Ruiz, M. E. & Richter, R. L. (1997). Effect of homogenization pressure on the milk fat globule membrane proteins. Journal of Dairy Science, 80(11), 2732-2739.

Chen, J. Z., Sachse, C., Xu, C., Mielke, T., Spahn, C. M., & Grigorieff, N. (2008). A dose-rate effect in single-particle electron microscopy. Journal of structural biology, 161(1), 92-100.

Daffner, K., Vadodaria, S., Ong, L., Nöbel, S., Gras, S., Norton, I., & Mills, T. (2020). Design and characterisation of casein–whey protein suspensions via the pH–temperature-route for application in extrusion-based 3D-printing. Food Hydrocolloids, 112, 105850.

Dalgleish, D.G., Tosh, S.M., & West, S. (1996). Beyond homogenization: the formation of very small emulsion droplets during the processing of milk by a microfluidizer. Netherlands Milk Dairy J. 50, 135-148.

Dalgleish, D. G., Spagnuolo, P. A., & Goff, H. D. (2004). A possible structure of the casein micelle based on high-resolution field-emission scanning electron microscopy. International Dairy Journal, 14(12), 1025-1031.

Fox, P. F. & Brodkorb, A. (2008). The casein micelle: Historical aspects, current concepts and significance. International Dairy Journal, 18(7), 677-684.

Kessler, H. G. (2002). Food and bio process engineering. Dairy Technology, 5th edition (Verlag A. Kessler, Munich, Germany).

Leapman, R. D. & Sun, S. (1995). Cryo-electron energy loss spectroscopy: observations on vitrified hydrated specimens and radiation damage. Ultramicroscopy, 59(1-4), 71-79.

Lopez, C., Briard-Bion, V., Menard, O., Rousseau, F., Pradel, P., & Besle, J. M. (2008). Phospholipid, sphingolipid, and fatty acid compositions of the milk fat globule membrane are modified by diet. Journal of Agricultural and Food Chemistry, 56(13), 5226-5236.

McMahon, D. J. & Oommen, B. S. (2008). Supramolecular structure of the casein micelle. Journal of Dairy Science, 91(5), 1709-1721.

Ong, L., Dagastine, R. R., Kentish, S. E., & Gras, S. L. (2010a). The effect of milk processing on the microstructure of the milk fat globule and rennet induced gel observed using confocal laser scanning microscopy. Journal of food science, 75(3), E135-E145.

Ong, L., Dagastine, R. R., Kentish, S. E., & Gras, S. L. (2010b). Transmission electron microscopy imaging of the microstructure of milk in cheddar cheese production under different processing conditions. Australian Journal of Dairy Technology, 65(3), 222.

Sharma, S. K. & Dalgleish, D. G. (1993). Interactions between milk serum proteins and synthetic fat globule membrane during heating of homogenized whole milk. Journal of Agricultural and Food Chemistry, 41(9), 1407-1412.

Sharma, R., Singh, H., & Taylor, M. W. (1996). Recombined milk: factors affecting the protein coverage and composition of fat globule surface layers. Australian journal of dairy technology, 51(1), 12.

Ye, A., Anema, S. G., & Singh, H. (2008). Changes in the surface protein of the fat globules during homogenization and heat treatment of concentrated milk. Journal of dairy research, 75(3), 347-353.

Walstra, P. & Jenness, R. (1984). Dairy chemistry & physics. John Wiley & Sons. New York.

5.2 Characterising the influence of milk fat towards an application for extrusion-based 3D-printing of casein−whey protein suspensions via the pH−temperature-route

This work is peer-review published as follows:

Daffner, K., Hanssen, E., Ong, L., Gras, S. L., & Mills, T. (2021). Characterising the influence of milk fat towards an application for extrusion-based 3D-printing of casein−whey protein suspensions via the pH−temperature-route. FOOHYD_106642.

5.2.1 Abstract

This study presents the design and characterisation of casein−whey protein suspensions (8.0/10.0% (w/w) casein and 2.0/2.5% (w/w) whey protein) mixed with dairy fat (1.0, 2.5 and 5.0% (w/w) total fat) processed via the pH−temperature-route in preparation for 3D-printing. Mechanical treatment was applied to significantly decrease the particle size of the milk fat globules and increase surface area, creating small fat globules (< 1 µm) covered with proteins, which could act as pseudo protein particles during gelation. Different proteins covered the fat globule surface after mechanical treatment, as a result of differences in the pH adjusted just prior to heating (6.55, 6.9 or 7.1). The protein-fat suspensions appeared similar by transmission electron cryogenic microscopy and the zeta-potential of all particles was unchanged by the pH at heating, with a similar charge to the solution (~ −20 mV) occurring after acidification (pH 4.8/5.0) at low temperatures (2°C). A low pH at heating (6.55) resulted in increased sol−gel transition temperatures (G' = 1 Pa) and a decreased rate of aggregation for protein−fat suspensions. A higher pH at heating (6.9 and 7.1) caused an increased rate of aggregation (aggregation rate ≥ 250 Pa/ 10 K), resulting in materials more promising for application in extrusion-based printing. 3D-printing of formulations into small rectangles, inclusive of a sol−gel transition in a heated nozzle, was conducted to relate the aggregation rate towards printability.

5.2.2 Introduction

3D-printing, or additive manufacturing (AM), is a robotic construction technology that deposits materials layer-by-layer to build a three-dimensional object and that gains more and more interest in the area of foods (Wegrzyn, Golding, & Archer, 2012). 3D-printing of food, or food layered manufacturing (FLM), has been recently used to print a different range of food grade materials, including chocolate (Lanaro et al., 2017), hydrocolloid-based materials (Gholamipour-Shirazi et al., 2019) or processed cheese (Le Tohic et al., 2017), although the first food being printed was already in 2006 (Malone & Lipson, 2006). This printing technology offers advantages such as individualised products, flexibility with respect to nutritional content and also the potential to reduce waste and storage or distribution costs of the final product compared to conventional mass production of food (Godoi et al., 2016; Ross et al., 2019).

While the actual printing of food and characterisation following printing has received considerable attention, few experiments have considered defining the desirable material properties for optimal printing (Derossi et al., 2018). Food grade materials have complex nano- and microstructure as well as altered properties associated with liquid to solid phase transition, complicating their use in printing. A greater understanding of material properties will enable the design of useful formulations and is perhaps one of the most important steps in the printing of a range of edible foods. Edible and printable formulations need to match several requirements. For example, they should ideally be of homogenous composition, have suitable flow properties and enable printability in a layer-by-layer manner (Godoi et al., 2016; Kim et al., 2017).

There is a high demand for fermented concentrated dairy products, rich in protein and fat, such as Greek yogurt or fresh cheese (Jørgensen et al., 2019), and FLM has the potential to produce dairy-based products for tailored nutrition. Nöbel et al. (2018) were the first to implement a pH−temperature (T)-route, including cold acidification followed by heating, for printing of milk concentrates inclusive of a sol−gel transition, which resulted in small printed spheres. For the

pH−T-route, direct acidification at cold temperatures (≤ 10°C) to pH values approaching the isoelectric point (IEP) of casein (4.6) helped to maintain solution (sol)−characteristics due to a reduction of hydrophobic interaction forces (Horne, 1998). Increased temperatures then resulted in increasing hydrophobic interaction forces and particle aggregation (Hammelehle, 1994; Roefs, 1986; Schäfer et al., 2018). Pre-chilled acidified concentrates from milk microfiltration differing in pH (4.8 – 5.4) and casein content (8.0 – 12.0% (w/w)) have also been investigated and characterised for their suitability for 3D-printing (Nöbel et al., 2018; Nöbel et al., 2020). Formulations at pH 4.8 formed firm and homogeneous milk gels when printed. In contrast, the milk gels at pH 5.0 were not mechanically stable after printing, illustrating the importance of pH as a process variable to alter printed food properties.

Recently, casein−whey protein suspensions differing in their protein content, acidification - and the pH at which heating was conducted were also characterised via the pH−T-route (Daffner et al., 2020a). It would be of high interest to see whether dairy fat could be added to such formulations and how this would change the microstructure and suitability of the dairy-based feedstock regarding printing. It is established that the rheological behaviour of dairy products like cheese, yoghurt or mayonnaise is influenced by the presence of emulsified fat (Dickinson, 2012). Mechanical input causes oil droplets being covered and stabilised by a thin layer of proteins adsorbed at the oil−water interface (Dickinson, 1994). During high pressure homogenisation, CM and casein molecules also adsorb at the surface of the newly created milk fat globule membrane (MFGM), sterically and electrostatically stabilising the droplets against recoalescence (McClements, 2004). Homogenisation has also been shown to cause milk fat globules (MFG) to behave to some extent like CM (Buchheim, 1986).

The surface properties are a further characteristic of the MFG that can influence printability. The zeta (ζ)-potential of MFG is reported to be around −13.5 mV (Michalski et al., 2002a), with

the MFGM phospholipids having a similar potential of −13 mV (Liu et al., 2013). This ζ-potential increases to around −20 mV for homogenised MFG due to CM covering the newly created surface, approaching the ζ-potential of the protein casein. These results led to the assumption that the electrophoretic mobility of casein in the serum and casein adsorbed on the surface of the MFG were the same (Michalski et al., 2002a). When included in dairy gels, the MFG with a surface covered by casein and whey protein causes an increase in firmness, essentially increasing the apparent protein concentration (Aguilera & Kessler, 1988; Hammelehle, 1994; Ji et al. 2016; Van Vliet & Dentener-Kikkert, 1982).

MFG with protein on the surface were shown to act as pseudo-protein particles during gelation and increase gel firmness (Ji et al., 2016). The aim of this study was to develop novel printable formulations for tailored nutrition by adding dairy fat to casein−whey protein suspensions for application in extrusion-based FLM via the pH−T-route. Adjusting the pH before heating was expected to cause a change in the types of protein covering the surface of the MFG after mechanical input. We hypothesise that this change in the surface properties of the MFG influences the overall formulation characteristics, tailoring the sol−gel transition temperature and manipulating the aggregation rate, with the latter property recently related towards printability (Daffner et al., 2020a). Several parameters including the protein and the fat content, as well as the pH during heating and cold acidification, were adjusted to design and characterise novel formulations towards printing applications.

5.2.3 Material and methods

5.2.3.1 Material

Micellar casein concentrate (MCC 85) and German Prot 9000 - Whey protein isolate (WPI) were provided from Sachsenmilch Milk & Whey Ingredients (Sachsenmilch Leppersdorf GmbH, Wachau, Germany). The manufacturer specifications are provided in section *4.3.1*. Cream (dairy fat) was bought from a local supermarket (Sainsbury’s, Birmingham, UK) and

100 mL contained 47.5% (w/w) fat, 1.5% (w/w) lactose, 1.5% (w/w) protein and 0.05% (w/w) salt. For pH adjustment, citric acid (1M) (Sigma Aldrich, UK) was prepared in Milli-Q water (Elix® 5 distillation apparatus, Millipore®, USA) and sodium hydroxide (1M) was bought from Sigma Aldrich (UK).

5.2.3.2 Sample preparation

Casein−whey protein suspensions (4:1 ratio, casein to whey protein) were prepared following the procedure in *4.3.2*. After a full hydration of the proteins overnight, fat was added to the protein suspensions (with a starting pH of 6.7 ± 0.1) to obtain final fat concentrations of 1.0, 2.5 or 5.0% (w/w). Before the heat treatment, the pH was adjusted to 6.55 (with 1 M citric acid) or either 6.9 or 7.1 (with 1 M NaOH). The protein−fat suspensions were indirectly heated in a water bath on a stirring plate at 80°C for 10 min to ensure denaturation of the whey proteins (degree of denaturation $_{\beta\text{-LG}} \geq 80\%$; estimated from Kessler, 2002) of the whey proteins. After heating, the protein−fat suspensions were subjected to pre-homogenisation at 50.0 ± 2.0°C using a high intensity ultrasonic vibracell processor (Vibra Cell 750, Sonics, USA) operating in a continuous mode, at 750 W and 20 kHz. The power output was set at 95% of the nominal power and sonication was conducted for 2 min, with 4 seconds on and 2 seconds off (3 min in total). Directly after pre-homogenisation, each sample was single-passed through a high-pressure valve homogeniser (Panda NS1001L-2K, Gea Niro Soavi, Parma, Italy) at 500 bars and 50.0 ± 2.0°C. All formulations were cold acidified at 2°C to pH values of 4.8 or 5.0, as described in section *4.3.2*. The whole preparation of these casein−whey protein suspensions with additional dairy fat is shown in a flowchart in *Figure 5-5*.

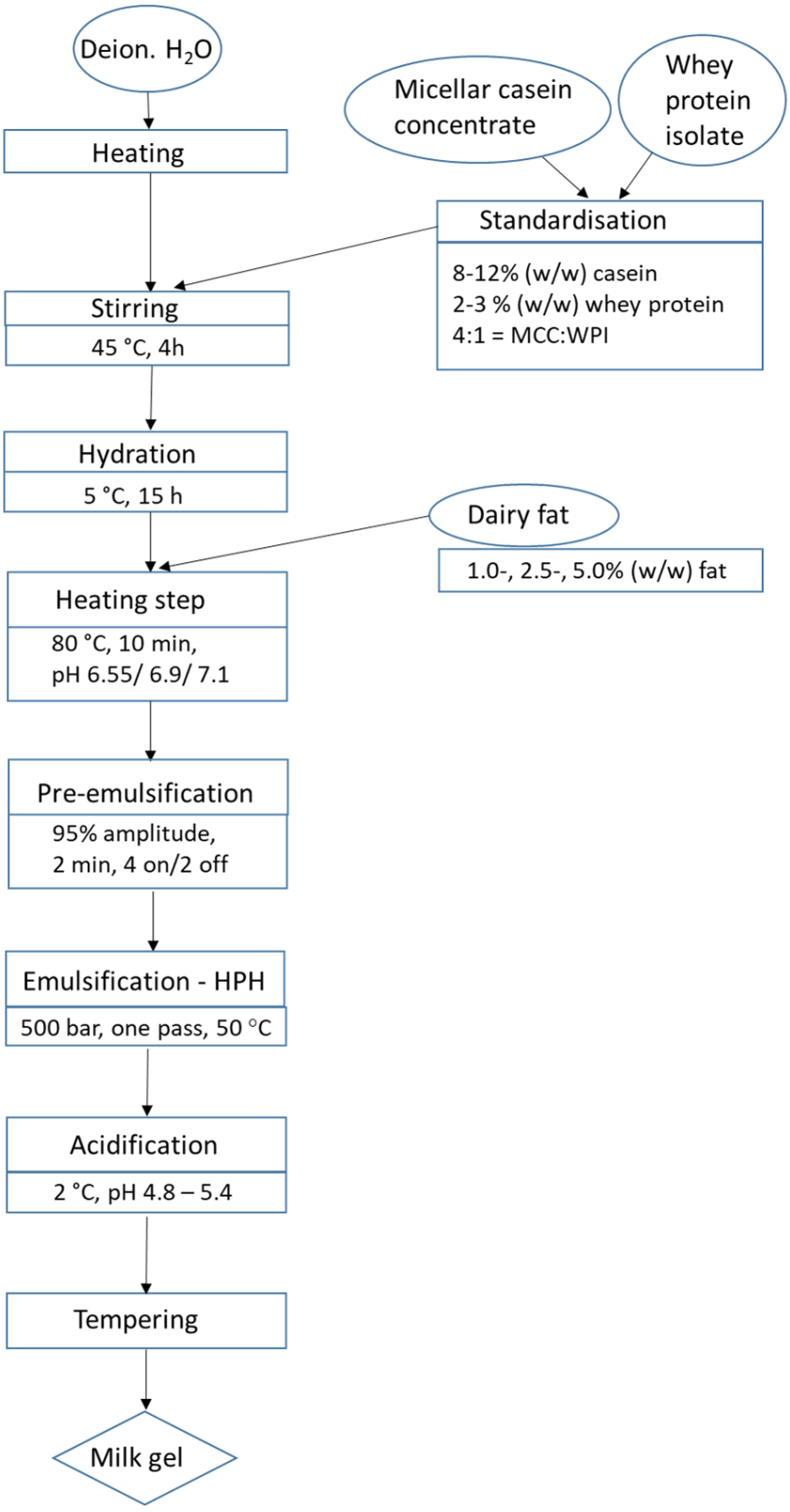

Figure 5-5: Flow chart for the preparation of casein-whey protein suspensions mixed with additional dairy fat for applications towards extrusion-based 3D-printing.

5.2.3.3 Rheology

Rheological measurements were conducted by a Kinexus Pro rheometer (Malvern Instruments, UK) with a cup (D = 27.17 mm, depth = 63.5) and vane (d = 61 mm, height = 25 mm)-geometry. For dynamic oscillatory measurements, temperature sweeps were performed from 2 – 60°C with a heating rate of 1 K/min, following the procedure in section *4.3.3*. The sol−gel transition temperature was determined when G' reached a value of 1 Pa (Daffner et al., 2020a; Schäfer et al., 2018, Nöbel et al., 2018; Nöbel et al., 2020).

5.2.3.4 Zeta-potential and particle size measurements

The particle size and the zeta (ζ)-potential were determined using a Mastersizer 2000 (Malvern Instruments, UK) and a Zetasizer (Malvern Instruments, UK). A drop of the untreated dairy fat was placed into the circulating cell which contained deionised water and the particles in the micro range were measured at 20°C. Refraction indices of 1.46 and 1.33 were set for milk fat and water respectively. After homogenisation, the Zetasizer was used to characterise the formulations to give particle size distribution in the nanometre range. Samples were diluted 100 times with deionised water before experiments and ζ-potential measurements were performed over a range of pH values (6.8 to 4.8), as described in section *4.3.4*.

5.2.3.5 Microscopy

5.2.3.5.1 CLSM

5.2.3.5.1.1 Preparation of samples

Thermally and mechanically treated protein−fat suspensions were prepared for CLSM, mainly following the procedure of Ong et al. (2010a). A volume of 10 µl each of fast green FCF solution (1 mg/ml in MilliQ water, Sigma-Aldrich, St. Louis, U.S.A.) and Nile red solution (1 mg/ml in 100% dimethyl sulfoxide, Sigma-Aldrich, St. Louis, U.S.A.) was added to 480 µl of the sample that included protein and fat particles. The stained sample was diluted 1:5 with agarose

solution (40°C, 0.25g/50 ml Milli Q water) to reduce particle movement due to Brownian motion, as shown in previous literature (Lopez et al., 2010; Devnani et al., 2020). The fat specific stain Nile red only stained the fat core of the MFG and did not provide any information about the MFGM (Ong et al., 2010a). According to the procedure of Ong et al. (2010a), a 10 µl aliquot of the stained sample was transferred to a cavity slide (0.7 mm in depth) (ProSciTech, Thuringowa, Australia), covered with a glass coverslip (0.17 mm thick) and secured with nail polish (Maybelline LLC, U.S.A.). The sample was then inverted for analysis by CLSM.

5.2.3.5.1.2 CLSM procedure

The microstructure of the samples was observed using an inverted confocal scanning laser microscope (Leica SP8; Leica Microsystems, Heidelberg, Germany) powered by Ar/Kr and He/Ne lasers. All samples were viewed using an oil immersion 63 x lens (1.32 Numerical Aperture) and the pinhole diameter was maintained at 1 Airy Unit. All the wavelengths were adjusted according to Ong et al. (2010a).

5.2.3.5.1.3 Image analysis of CLSM micrographs

Image analysis of CLSM micrographs was performed with LAS X software (LAS X Core Offline version for Life Science, Leica Microsystems). Images were restored by a deconvolution process conducted with Huygens Essential 3.7 software (Scientific Volume Imaging, Netherlands).

5.2.3.5.2 Cryogenic transmission electron microscopy and image analysis

Thermally (80°C, 10 min; adjusted pH 6.55/ 6.9/ 7.1) and mechanically (sonication and homogenisation) treated protein−fat suspensions were prepared for cryo-EM, following the protocol in section *5.1.3.3*. Samples were diluted 1:10 with deionised water to ensure an optimal number of particles for imaging. Next, a Formvar lacey carbon film mounted on a 300 mesh copper grids (ProSciTech, Australia) was glow discharged to have a hydrophilic support on which the samples (3 µl) were adsorbed. To freeze the sample the grids were then plunged in liquid ethane

using a Vitrobot (FEI Compa-ny, Eindhoven, Netherlands). The grids were observed on a Tecnai G2 F30 (FEI Company, Eindhoven, Netherlands) operating at 200 kV with no objective aperture, equipped with a CETA CMOS 4kx4k detector (FEI company, Eindhoven, Netherlands). A series of micrographs of increasing dose was recorded for all samples with a defocus value of −6.66 µm. High pass filtering and differentiation of the fat and protein particles was performed as described in section *5.1.3.4*.

5.2.3.6 SDS-PAGE

5.2.3.6.1 Separation and washing of the MFG surface proteins

The proteins on the surface of the MFG after thermal and mechanical treatment were analysed via SDS-PAGE following the isolation procedure of Sharma et al. (1996a/ 1996b) and Ye et al. (2002), with a few changes. This procedure involved centrifugation (Thermo Sorvall RC-6-Plus; Thermo Scientific, Asheville, USA) of the samples to recover the cream layer first, followed by a washing step to remove serum proteins, and determination of the different types of casein and whey protein covering the fat globule surface layer (Sharma & Dalgleish, 1993). To increase the difference in the density between fat and serum phase, 8.6 g of sucrose was added per 30 g of sample, followed by centrifugation at 18.000 g for 20 min at 20°C to separate the cream. After decanting the supernatant containing excess proteins in solution, not bound to the fat globule membrane, the cream layer at the top of the sample was washed with deionised water and centrifuged at 18.000 g for 20 min at 20°C to remove any further unbound proteins. The washing step was repeated two times, as no further changes in protein content were found when monitoring the supernatant with SDS-PAGE.

5.2.3.6.2 Isolation and analysis of the fat globule surface protein components

The identity of the proteins covering the MFG was determined with SDS-PAGE, using pre-cast Bis-Tris 4 – 12/ 12% polyacrylamide gels (Invitrogen, Mulgrave, Victoria, Australia). The washed cream layers were dispersed (1:25) in a buffer (0.5 M Tris, 2% SDS, 0.5% β-mercaptoethanol, pH adjusted to 6.8) to displace the protein from the FGM (Sharma et al., 1996a). Samples were heated at 90°C for 5 min and centrifuged (2500 g, 20 min, 20°C) to remove the fat from the sample. Subnatants (10 µl) were mixed with 5 µl NUPAGE 4x LDS sample buffer, 2 µl NUPAGE 10x reducing agent containing 0.5 M DTT and 5 µl β-mercaptoethanol. Samples were heated (100°C, 3 min) and 10 µl of each sample was loaded into the gels. The gels were run, stained, de-stained and visualised as described in section *4.3.5.2*.

5.2.3.7 Set-up of a customised 3D-printer

The retrofitted set-up explained in section *4.3.7* was used for extrusion-based 3D-printing of small rectangles (25 x 25 x 3 mm; 3 layers above each other).

5.2.3.8 Statistics

The data plotted in the publication includes the average of at least three measurements accompanied by error bars that consist of the standard deviation of the mean. In the case where mean values of an observation are compared between samples the data have been subjected to analysis of variance (ANOVA) in order to determine significant differences. Data analysis was conducted with Sigma Plot 12.5 (Systat Software Inc., San Jose, CA, USA). Individual samples were compared with Student's t-test and a level of significance of $p < 0.05$ was chosen.

5.2.4 Results and discussion

5.2.4.1 Physico-chemical characterisation of the sol−state

The pH−T-route was selected for the creation of promising protein-based formulations with added dairy fat for extrusion-based 3D-printing. Mechanical damage of the MFG in the preparation is necessary to decrease the size and to cover the increased surface area of the MFG with proteins. Previous studies have shown casein and whey proteins to cover more than 40% of the newly created secondary milk fat globule membrane (SFGM), resulting in a significant increase in the storage modulus G‘, shown for acid- and rennet-induced milk gels (Michalski et al., 2002b). Better gel properties were achieved, if the heating step, which denatures whey proteins, was conducted before the homogenisation step (Hammelehle, 1994), allowing the denatured whey proteins to interact with the MFG, as well as with the CM, increasing the number of particles contributing to the overall gelation process.

The goal of this study was to identify if those smaller MFG could behave like CM and actively contribute to the protein-based gelation process as structure promoters (Buchheim, 1986; Ji et al., 2016; Michalski et al., 2002c), thereby enhancing printability. The particle size, zeta-potential and surface coverage of the newly created SFGM (SDS-PAGE, microscopy), sol−gel transition temperature and aggregation kinetics were investigated, building on a prior study of protein-based systems (Daffner et al., 2020a).

5.2.4.1.1 Zeta-potential and surface characteristics

Casein−whey protein suspensions were mixed with fat and heated at different pH, treated by mechanical input and then cooled to 2°C, followed by acidification. The ζ-potential of the resulting samples is shown in *Figure 5-6*, where the data represents an average of all protein and fat particles captured within the sample. An almost linear increase of the ζ-potential was found with decreasing pH during acidification and this trend was independent of the pH value adjusted before heating. A non-heated micellar casein suspension without any whey protein and fat was also included for comparison (Daffner et al., 2020a).

At an acidification pH of 4.8 and 5.0, the ζ-potential of casein−whey protein suspensions with fat was around –20 mV. This demonstrated that sol−characteristics of all formulations, independent of the pH at heating, were maintained at an acidification temperature of 2°C and electrostatic repulsion forces between particles were dominant.

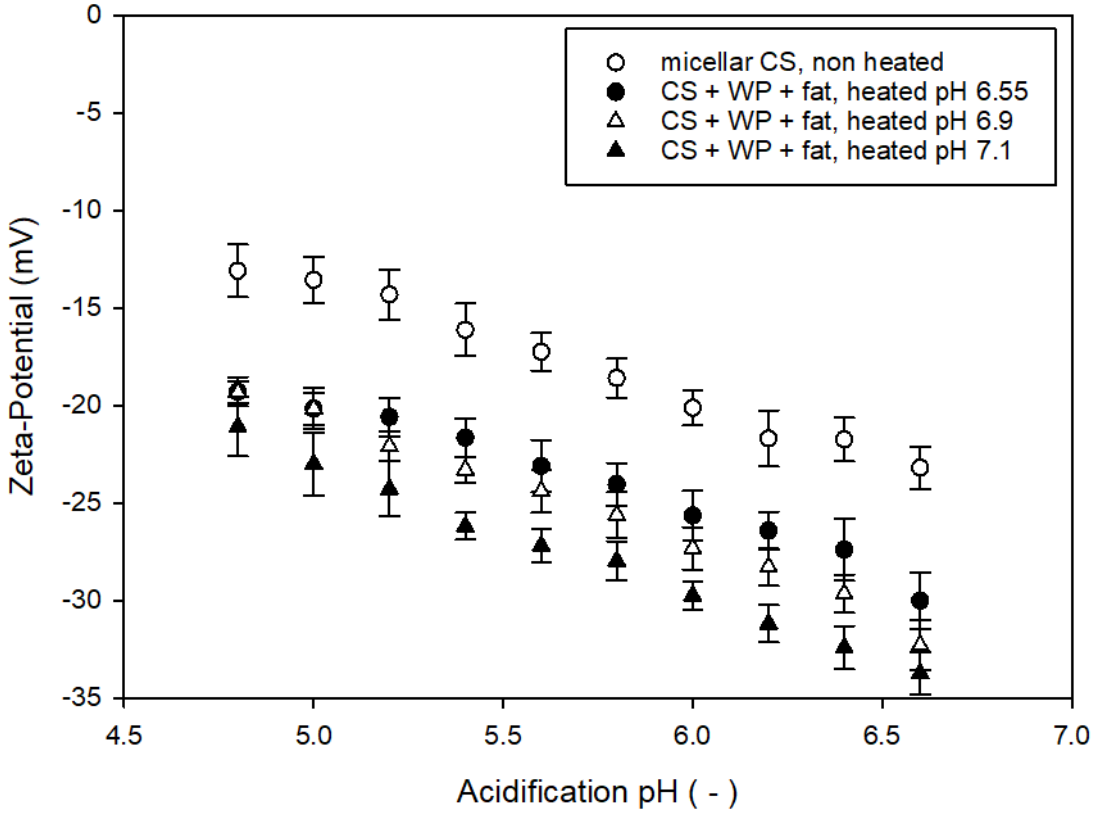

Figure 5-6: Changes in the zeta-potential as a function of the pH of a micellar casein−whey protein suspensions (8.0% (w/w) CS, 2.0% (w/w) WP) mixed with dairy fat (to 1.0% (w/w) total fat), heated at pH 6.55 (●), at pH 6.9 (▲) and at pH 7.1 (Δ). For comparison, the zeta-potential of non-heated micellar casein (○) without any fat is shown. The casein to whey protein ratio was 4:1.

A slight trend to lower ζ-potential values with increasing pH at heating was found. Compared to the pure micellar casein suspensions (non-heated), the addition of fat caused a significant increase in the magnitude of the ζ-potential, similar to previous observations (Daffner et al., 2020a). This could be explained by the coverage of the MFG surface with a more complex range of proteins, including CM, κ-casein−whey protein complexes or denatured whey protein (-aggregates) as a result of the pre-processing treatments applied here.

A lower ζ-potential between –17 mV to –13 mV was found for MFG in whole milk after homogenisation, dependent on the Ca^{2+} concentration (Dalgleish, 1984). For MFG covered with CM after homogenisation at 500 bar, Michalski et al. (2002a) found a similar ζ-potential of –20 mV, compared to –13.5 mV for the native MFG. The ζ-potential of MFG increased with increasing homogenisation pressure, due to the production of smaller MFG and an increase in surface area covered with more CM. Within their research, they concluded that the ζ-potential of a free protein and that of the adsorbed protein on a fat globule surface were the same. It was assumed that the protein charged molecular protuberances on the surface of the carrier were responsible for the mobility of the particles rather than the carrier size (Rajagopalan & Hiemenz, 1997).

5.2.4.1.2 Particle size distribution

The influence of a mechanical input on the particle size distribution of casein−whey protein suspensions with three different fat contents (1.0% (w/w), 2.5% (w/w) and 5.0% (w/w)) after heating at different pH (6.55, 6.9 and 7.1) is illustrated in *Figure 5-7*. The sonication step, followed by high pressure homogenisation, caused a significant decrease in the particle size and resulted in a monomodal particle size distribution, with no changes found dependent on the pH at which heating was conducted. The addition of different amounts of fat to protein suspensions had no significant effect on the particle size distribution, although there was a slight tendency to bigger particles with increasing fat content. The z-average of all the particles captured within the protein−fat suspensions was 275 nm (*Figure 5-7* inset), demonstrating a significant increase of 40 – 50 nm in the particle size compared to casein−whey protein suspensions with the same pH at heating but without any addition of fat (Daffner et al., 2020a). This larger size results from the fat particles being larger than the protein particles, even after homogenisation.

To intentionally induce a fast, local and irreversible sol−gel transition during printing, the particles need to be within a certain size range; this ensures they will move sufficiently fast to successfully collide and aggregate via the pH−T-route (Daffner et al., 2020a; Nöbel et al., 2018; Nöbel et al., 2020). Formulations with no heat- and mechanical treatment contained large, native and emulsified MFG in the protein suspensions (see *Supplementary Figure 5-1*), which slowed down the aggregation and gelation of proteins (data not shown). It is expected that as the size of the MFG approaches the size of the CM, there will be a higher chance that these particles will behave in a similar way (Hammelehle, 1994). It is well known that the rheology of the overall formulations depends on the behaviour of the continuous phase, if the dispersed particles are well separated from each other and do not aggregate (Dickinson, 1998). In this case, the protein suspension will behave as desired if the MFG are sufficiently small and do not associate.

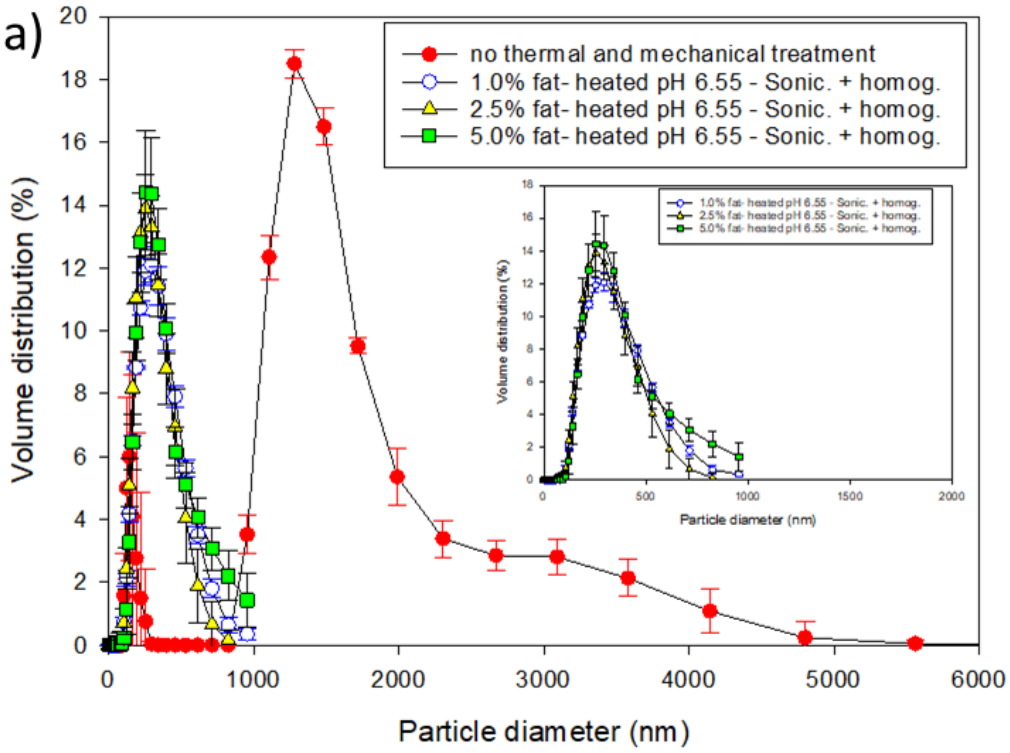

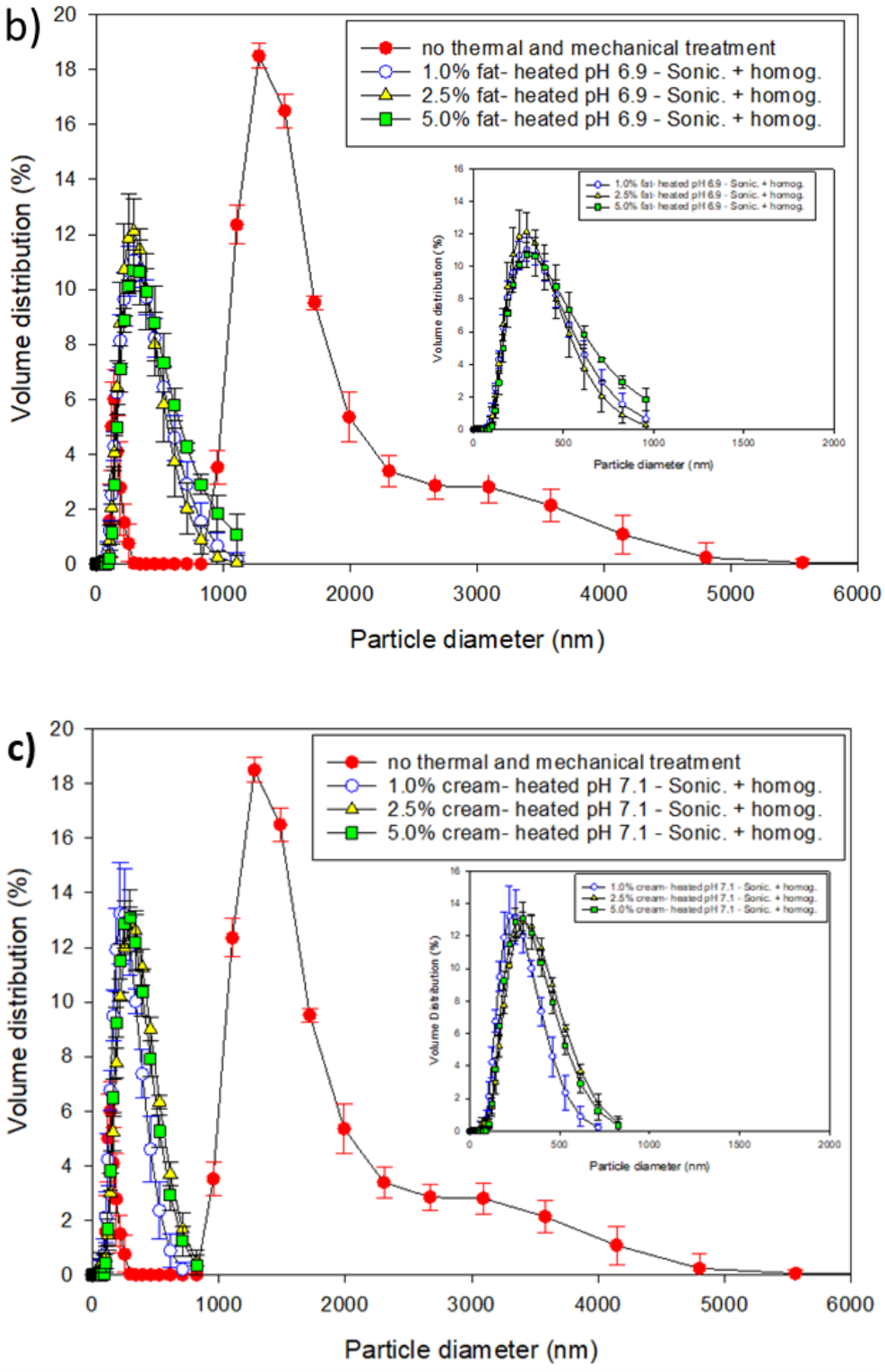

Figure 5-7: Particle size distribution of casein−whey protein suspensions mixed with different amounts of fat to a total fat concentration of 1.0% (w/w), 2.5% (w/w) and 5.0% (w/w)) after a heating step at pH 6.55 (a), 6.9 (b) and 7.1 (c) with either no mechanical input (●/red) or sonication/homogenisation at 500 bar (1.0% (w/w) fat = ○/blue hollow circle; 2.5% (w/w) fat = ▲/yellow triangle; 5.0% (w/w) fat = ■/green square). The inset graphs in all images focus on the particle size distribution of each formulation between 1 – 1000 nm to better see differences as a result of the addition of fat.

5.2.4.1.3 Micrographs from microscopy

5.2.4.1.3.1 CLSM

CLSM was used to investigate the microstructure of casein−whey protein suspensions mixed with fat after a thermal and mechanical treatment (*Figure 5-8,* after heating at pH 7.1) using an intermediate final fat content of 2.5% (w/w). A homogenous distribution of the MFG could be observed in all samples, regardless of the pH adjustment made prior to heating and a representative CLSM image at pH 7.1 is presented in *Figure 5-8*. The MFG, stained red in these images, were distributed relatively evenly between the proteins, which were stained green, with the unstained serum phase appearing black in these images. The size of the MFG, which ranges from 50 – 1000 nm was consistent with the size of ~275 nm observed by light scattering (*Figure 5-7*). Protein particles were also found to be adsorbed on the surface of MFG, where they appear as green particles.

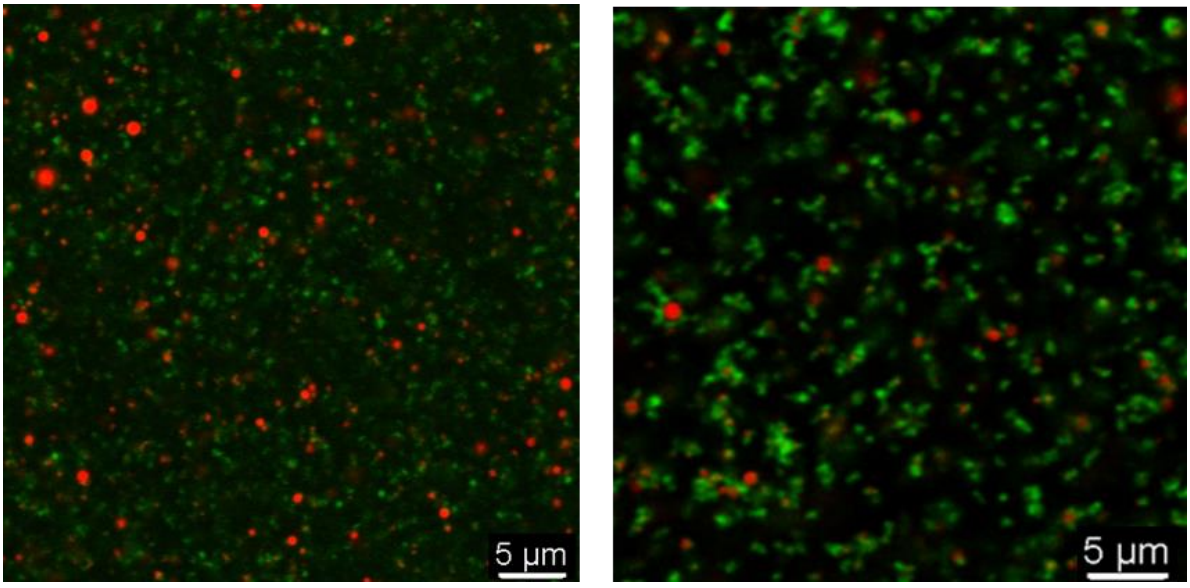

Figure 5-8: CLSM micrographs of casein−whey protein suspensions mixed with milk fat (to a total fat of 2.5% (w/w)) and then thermally (80°C, 10 min, pH 7.1) and mechanically (sonication + homogenisation) treated. Samples were stained with FCF fast green and Nile red fluorescent dyes (fat appears as red and protein as green) as seen on the left. The image after deconvolution with Huygens software is shown on the right. The scale bars are each 5 µm in length.

Independent of the pH at heating, the MFG featured proteins interacting with the membrane surface. After image deconvolution and digital magnification, proteins covering the surface of the MFG could be better observed (*Figure 5-8*, right). Nevertheless, no detailed information of

the specific type of protein, or protein subunits or aggregates covering the MFG surface could be obtained with this standard confocal microscopy due to the resolution limit of this technique.

5.2.4.1.3.2 Cryogenic-EM

A novel technique was recently described for the more detailed visualisation of interactions between the MFG and the proteins in the hydrated state without chemical fixatives or embedding (Daffner et al., 2020b). This method of different time-dependent radiation damage allows differentiation between protein (visible damage > 150 $e^-/Å^2$) and fat (visible damage < 25 $e^-/Å^2$) particles (Daffner et al., 2020b). Previous studies have observed that the mass of casein and whey protein on the surface of MFG after mechanical and thermal input strongly depended on several parameters including homogenisation pressure, heat treatment and casein-fat ratio (Walstra & Jenness, 1984; Sharma & Dalgleish, 1993; Cano-Ruiz & Richter, 1997). The new cryo technique was therefore applied to assess the presence of proteins on the surface of MFG after the processing techniques applied here.

Proteins were observed on MFG after a heating step was applied at different pH (pH 6.55, 6.9 or 7.1) and homogenisation. The images in *Figure 5-9* show small spherical MFG (~ 100 nm) covered with larger CM and smaller proteins. The proteins were distinguished by increasing the beam exposure. Whilst the proteins were clearly present, no differences were observed in the appearance of these structures for the samples with different pH values at heating (6.55, 6.9 or 7.1). This observation is consistent with the finding of intact CM covering the MFG surface under similar conditions (heating at 79°C and a homogenisation pressure of 70 bar), Ye et al. (2008) using the more traditional approach with fixed samples and TEM. The new cryo method is useful for the determination of protein in the hydrated state but does not provide information of the specific type of protein covering the MFG surface. The samples were therefore assessed next by SDS-PAGE analysis.

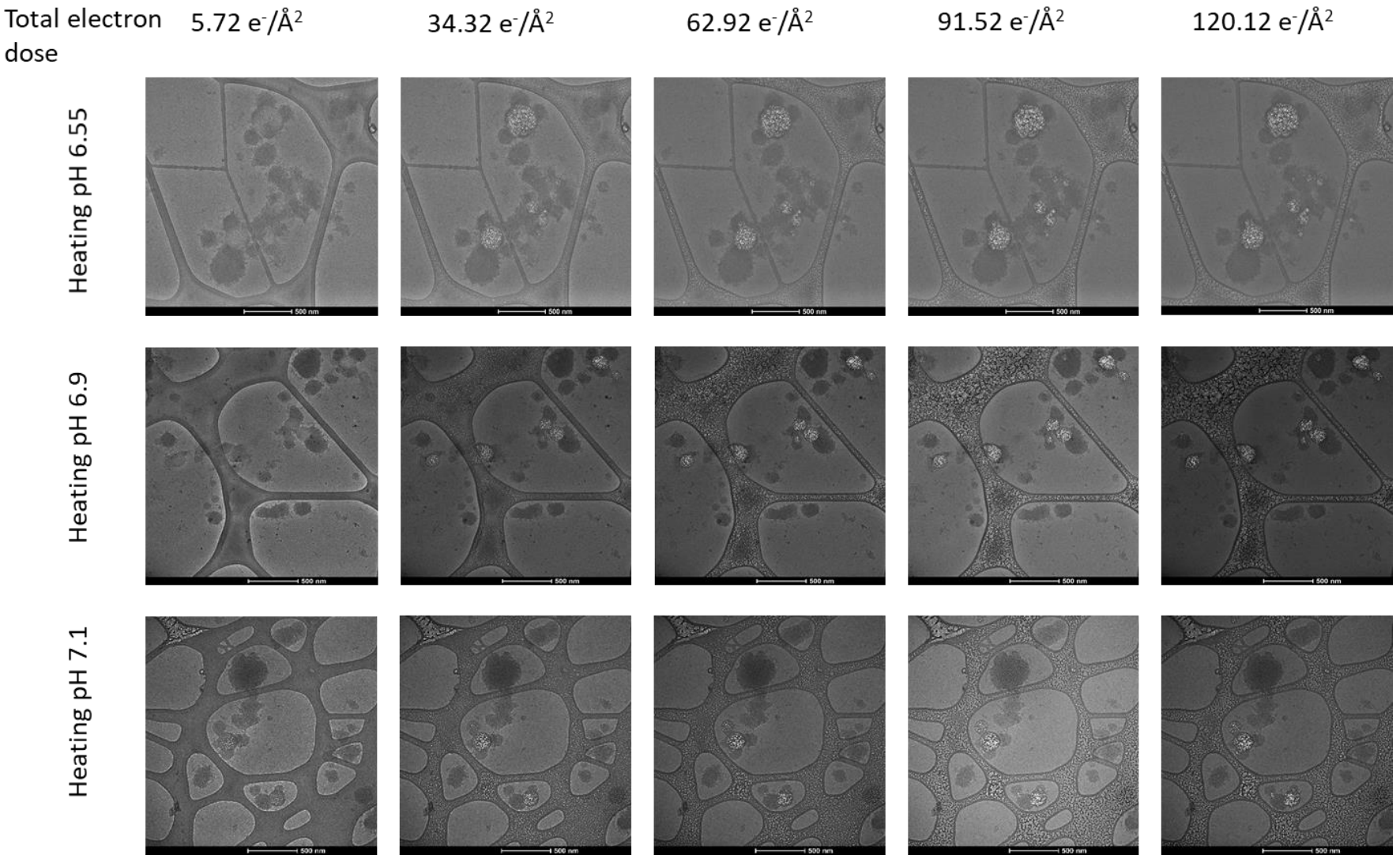

Figure 5-9: Cryo-EM images of casein−whey protein (8.0% (w/w) CS and 2.0% (w/w) WP) suspensions with 2.5 % (w/w) milk fat that have been thermally (80°C, 10 min; adjusted pH 6.55/6/9/7.1) and mechanically (sonication and homogenisation at 500 bar) treated. Samples received a constant dose (5.72 e^-/Å s) but an increasing dose time (moving left to right across the Figure, with the sample after the highest dosage appearing on the far right). A dilution of 1:10 with deionised water was used prior to analysis. The scale bar is 500 nm in length in all images. The increasing contrast between protein and fat particles as a function of exposure was used to differentiate between these two types of particles.

5.2.4.1.4 Analysis of the surface coverage of the MFG via SDS-PAGE

The thermal and mechanical treatment applied in this study reduced the MFG size (see *Figure 5-7* and *Figure 5-9*) and conversely increased the surface area, allowing proteins to adsorb onto the surface of the smaller MFG. An increase in the pH before heating from 6.55 to 7.1 potentially altered proteins in the samples, without changing the MFG surface area, which may be expected to alter protein composition on the MFG.

An increase in the pH at heating caused an increase in the proportions of α- and β-casein on the surface of the MFG and only very faint bands of κ-casein and β-LG were detected adsorbed to the surface under these conditions, as shown in *Figure 5-10,* where the SDS-PAGE gel shows the protein extracted from the MFG surface and the variation in proteins present for replicate extract samples. Both α_{s1}- and β-casein have a strong tendency to adsorb at hydrophobic surfaces, due to accessible non-polar residues (Dickinson, 1999) and were expected to preferentially cover the surface of the MFG compared to other proteins, as occurred for all conditions examined here.

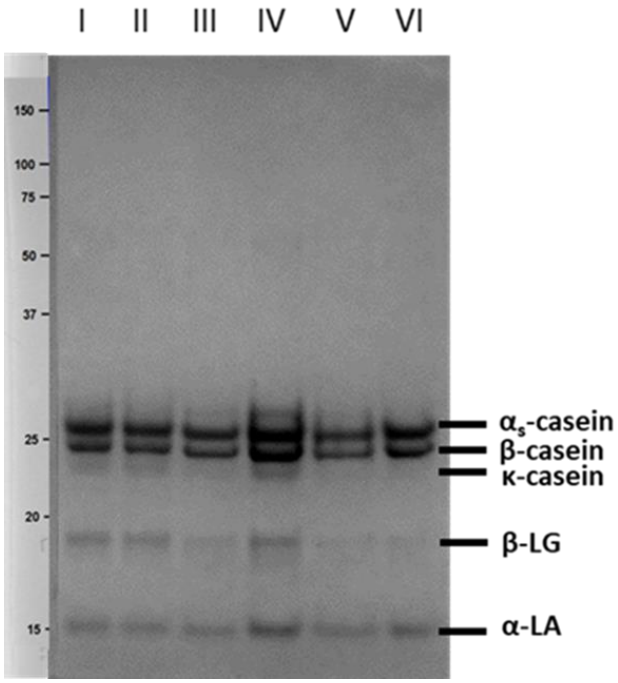

Figure 5-10: SDS-PAGE analysis of proteins covering the milk fat globule surface membrane after thermal (80°C, 10 min) and mechanical treatment. A total fat content of 2.5% (w/w) was analysed for each sample. The molecular weight ladder (kDa) is shown on the left; Lane I-II: heated, pH 6.55; Lane III-IV: heated, pH 6.9; Lane V-VI: heated, pH 7.1.

The increase in casein adsorption as a function of pH at heating also lead to an increase in the casein−whey protein ratio on the MFG surface from 6.6 to 14.7 as the pH at heating was increased, as shown in *Table 5-1*.

Table 5-1: Proportions of individual proteins covering the milk fat globule surface after thermal (80°C, 10 min; pH at heating adjusted to 6.55, 6.9 and 7.1) and mechanical treatment (sonication and homogenisation).

pH at heating	Individual protein (%, w/w of total fat)					Casein-WP ratio
	α_s-CN	β-CN	κ-CN	β-LG	α-LA	
6.55	39.8 ± 2.0 [a]	29.4 ± 2.9 [a]	18.4 ± 1.2 [a]	9.3 ± 1.0 [a]	3.1 ± 1.0 [a]	6.6
6.9	39.6 ± 0.7 [a]	37.9 ± 1.6 [b]	13.7 ± 0.3 [b]	7.7 ± 1.3 [a]	1.2 ± 0.2 [b]	10.1
7.1	49.7 ± 0.8 [b]	44.0 ± 0.8 [c]	n.d.	n.d	6.3 ± 0.1 [c]	14.7

n.d.: non detectable

Values with different superscript letters in one column are significantly different ($P < 0.05$).

The dissociation of κ-casein from the CM at higher pH at heating (6.9, 7.1) has been reported previously (Anema & Klostermeyer, 1997; Daffner et al., 2020a), changing the characteristics of the CM, as well as the aggregates found in the milk serum. This could explain for the preferential adsorption of CM depleted of κ-casein and high in α- and β-casein observed in this study. This dissociation was also confirmed at higher solid concentrations (up to 25%), with increasing pH (6.5 – 7.1) and increasing concentrations causing an increase in the extent of κ-casein dissociation (Singh & Creamer, 1991). For the same pure protein-based system, increasing the pH at heating to 6.9 or 7.1 caused increasing amounts of κ-casein dissociating from the CM into the serum, resulting in κ-casein−whey protein complexes in the serum and decreased levels of CM covered with whey proteins (Daffner et al., 2020a). For concentrated milk systems after a heating step (120°C, 10 min), Singh & Creamer (1991) found that the dissociated protein was composed of 70% κ-casein, 20% β-casein and 10% α-casein.

Other studies have not observed whey proteins on the surface of MFG, as occurred here, due to the difference in processing conditions, highlighting the potential for protein composition to be systematically altered. Only casein (α, β and κ) and no whey or native membrane proteins (e.g. xanthinoxidase) were found on the surface of the MFG after homogenisation (Ong et al., 2010a), potentially due to low heating temperatures and a lack of denaturation of the whey

proteins. Similarly, whey proteins were absent on the surface of the MFG after microfluidization, if the temperature was less than 70°C (Sharma & Dalgleish, 1993).

Other processing variables appear to have less effect on the composition of proteins adsorbed to the MFG. Homogenisation pressure was found to have no effect on the composition of the proteins on the surface of the MFG, with 70% of the material characterised as casein and the rest being whey and native membrane proteins for all conditions examined (Cano-Ruiz & Richter, 1997). Sharma et al. (1996b) found the amount of κ-casein covering the surface of the MFG independent of the heat treatment performed and the order of the heating and homogenisation steps. They concluded that the deposition of κ-casein depended only on the homogenisation step. The κ-casein−whey protein complexes in the serum and on the MFG surface were proposed to be similar after heating and homogenisation (Sharma et al., 1996a).

Similar to the results of our work (compare *Table 5-1*), Sharma et al. (1996a) found increasing amounts of α_s- and β-casein, but decreasing amounts of κ-casein and β-LG covering the surface of MFG after mechanical input, if the pH before a heating step was adjusted from 6.3 to 7.3, which also resulted in an increase in the casein to whey protein ratio from 4.62 (pH 6.3) to 8.01 (pH 7.3) on the surface of the MFG.

5.2.4.2 Rheological characterisation of sol−gel transition

The sol−gel transition temperatures ($T_{sol-gel}$) of all formulations were determined with temperature sweeps at a heating rate of 1 K/min. The goal was to investigate the effect of additional dairy fat on the rheological behaviour of the protein-based systems (Daffner et al., 2020a). $T_{sol-gel}$ of cold acidified casein−whey protein suspensions (8.0% (w/w) CS, 2.0% (w/w) WP) with added fat (to final fat contents of 1.0-, 2.5- and 5.0% (w/w)) after heating (pH 6.55, 6.9, 7.1) and mechanical input are shown in *Figure 5-11*. It was proposed that homogenised MFG can mimic the behaviour of CM and potentially coagulate in a manner similar to CM (Ji et al., 2016; Walstra & Jenness, 1984).

To enable comparison the behaviour of casein−whey protein suspensions without fat (Daffner et al., 2020a) was added as a baseline to all figures. The sol area lies below this line and the gel area above the line. The two most promising formulations using acidifications pH of 4.8 and 5.0, were chosen in the current study, based on previous studies (Daffner et al., 2020a; Nöbel et al., 2018), which reported more promising characteristics, including higher aggregation rates for these formulations, consistent with the desired application of 3D-printing via the pH−T-route.

$T_{sol-gel}$ of casein−whey protein suspensions with fat after heating at pH 6.55 are illustrated in *Figure 5-11* (A). Independent of the amount of fat, formulations showed lower values for $T_{sol-gel}$ with decreasing pH value (4.8 compared to 5.0), which was in accordance with results for casein−whey protein suspensions (Daffner et al., 2020a) and casein-based systems (Nöbel et al., 2020). Apart from one sample (pH 5.0, 5.0% (w/w) fat content), higher $T_{sol-gel}$ ($2-5$°C) were found. The more fat added, the closer the $T_{sol-gel}$ were to those of formulations without any additional fat (*Figure 5-11* (A)). Increasing the pH at heating (6.9) for formulations with fat resulted in lower $T_{sol-gel}$ compared to results after a pH of 6.55 at heating (*Figure 5-11*, (B)). While 1.0- and 2.5% (w/w) of fat caused a slight increase in $T_{sol-gel}$, a tendency to decreased values with 5.0% (w/w) fat was found, independent of the acidification pH, which could potentially be explained with an increasing amount of particles per unit area capable to aggregate and form a gel.

The tendency to lower $T_{sol-gel}$ with increased pH at heating for casein−whey protein formulations with fat was further confirmed by results at pH 7.1 at heating. A decrease (2°C after addition of 1.0- and 2.5% (w/w) fat and more than 4°C after addition of 5.0% (w/w) fat) of $T_{sol-gel}$ at an acidification pH of 5.0 compared to the formulation without any fat added is illustrated in *Figure 5-11* (C). If these formulations (pH 7.1 at heating) were acidified to pH 4.8, pre-gelation characteristics ($G' > 1$ Pa) occurred, making them unsuitable for printing.

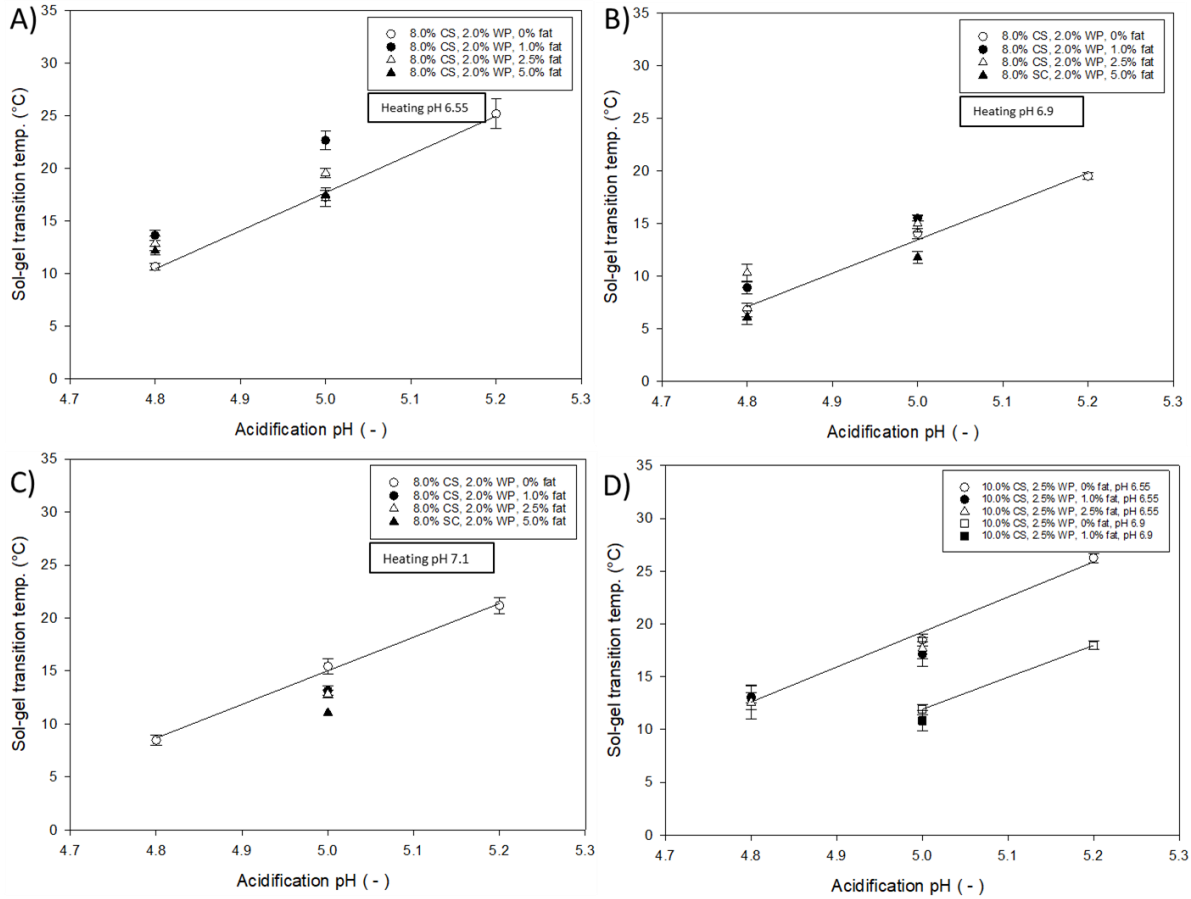

Figure 5-11: Sol−gel transition temperatures of cold acidified casein−whey protein suspensions (8.0% (w/w) CS and 2.0% (w/w) WP) with different amounts of fat added (to final fat contents of 1.0% (●), 2.5% (Δ), 5.0% (▲) and 0% (w/w) as comparison (○)) after heating at pH 6.55 (A), 6.9 (B) and 7.1 (C) and cold acidified casein−whey protein suspensions (10.0% (w/w) CS and 2.5% (w/w) WP) with different amounts of fat added after heating at pH 6.55 and 6.9 (D). A heating rate of 1 K/min was applied.

The decrease in $T_{sol-gel}$ at higher pH at heating (7.1) is likely due to changes of the protein composition of the MFG membrane, shown via gel electrophoresis (compare *Figure 5-10*). For acid gelation, 40% of the membrane had to be coated by serum proteins to significantly change the storage modulus (Michalski et al., 2002b). In contrast to the finding of Hammelehle (1994) who did not find a shift in the coagulation after heating the formulations, our study showed significant changes in the $T_{sol-gel}$ for protein-fat suspensions (8.0% (w/w) casein and 2.0% (w/w) whey protein), strongly dependent on the pH at heating.

The results for $T_{sol-gel}$ of formulations with 10.0% (w/w) casein and 2.5% (w/w) whey protein with additional fat are shown in *Figure 5-11* (D). Due to the increased amount of protein plus additional fat, the overall total solid content increased. As a result, fewer formulations could be

analysed and the results of formulations after pH values of 6.55 and 6.9 at heating were summed up in one figure, which resulted in two coagulation lines. Pre-gelation (G' > 1 Pa) was found for all formulations with a pH of 7.1 at heating and no further analysis was conducted. A slight tendency to lower $T_{sol-gel}$ at both pH values at heating (6.55 and 6.9) was found for all formulations.

At this higher protein content and the lower acidification pH values of 4.8 and 5.0, the influence of additional fat on $T_{sol-gel}$ was less distinct compared to results with the lower protein content. Pre-gelation characteristics (G' > 1 Pa) were found for several formulations after the addition of fat (e.g. pH 4.8, 5.0% (w/w) fat, heated pH 6.55 or pH 5.0, ≥ 2.5% (w/w) fat, heated pH 6.9), explained with the increase in the total solid content and a higher amount of particles per unit volume.

5.2.4.3 Aggregation rate of casein−whey protein suspensions mixed with milk fat

As described in Daffner et al. (2020a), the aggregation rate (represented by the evolution of the storage modulus G' after reaching the sol−gel transition temperature) of the formulations was used to analyse the aggregations kinetics of casein−whey protein suspensions mixed with fat. For a simplified comparison, a solid line was added in all images which represented the aggregation rate of pure protein-based suspensions. The horizontal dashed line for the aggregation rate was used as a positive indicator from printing tests towards future printing applications of casein−whey protein suspensions, if values of 250 Pa/ 10 K were reached or exceeded (compare *4.4.3*).

The influence of three different amounts of fat on formulations with 8.0% (w/w) casein and 2.0% (w/w) whey protein followed by thermal (pH 6.55, 6.9 and 7.1) and mechanical input is shown in *Figure 5-12* (A-C). Increased values for the aggregation rate (Storage Modulus G') with decreasing acidification pH (5.0 to 4.8) were found for formulations after a heating step at pH 6.55. If 1.0% (w/w) fat was added, independent of the acidification pH, the aggregation rate

significantly decreased (47.7% at pH 5.0 and 29.0% at pH 4.8) compared to formulations without fat. While no change in G‘ was found after the addition of 2.5% (w/w) fat acidification pH 4.8 and 5.0, the 5.0% (w/w) additional fat increased the values for the storage modulus G‘, with maximum values of around 300 Pa at pH 4.8. The formulations with 2.5 and 5.0 % (w/w) fat reached around 250 Pa/ 10 K for the aggregation rate and simple printing tests were conducted. As shown in *Figure 5-12* (A), a stable and firm 3D-printed gel was only found for the formulation with 5.0% (w/w) fat at an acidification pH of 4.8, while the one at pH 5.0 (not shown) could not maintain the rectangular shape.

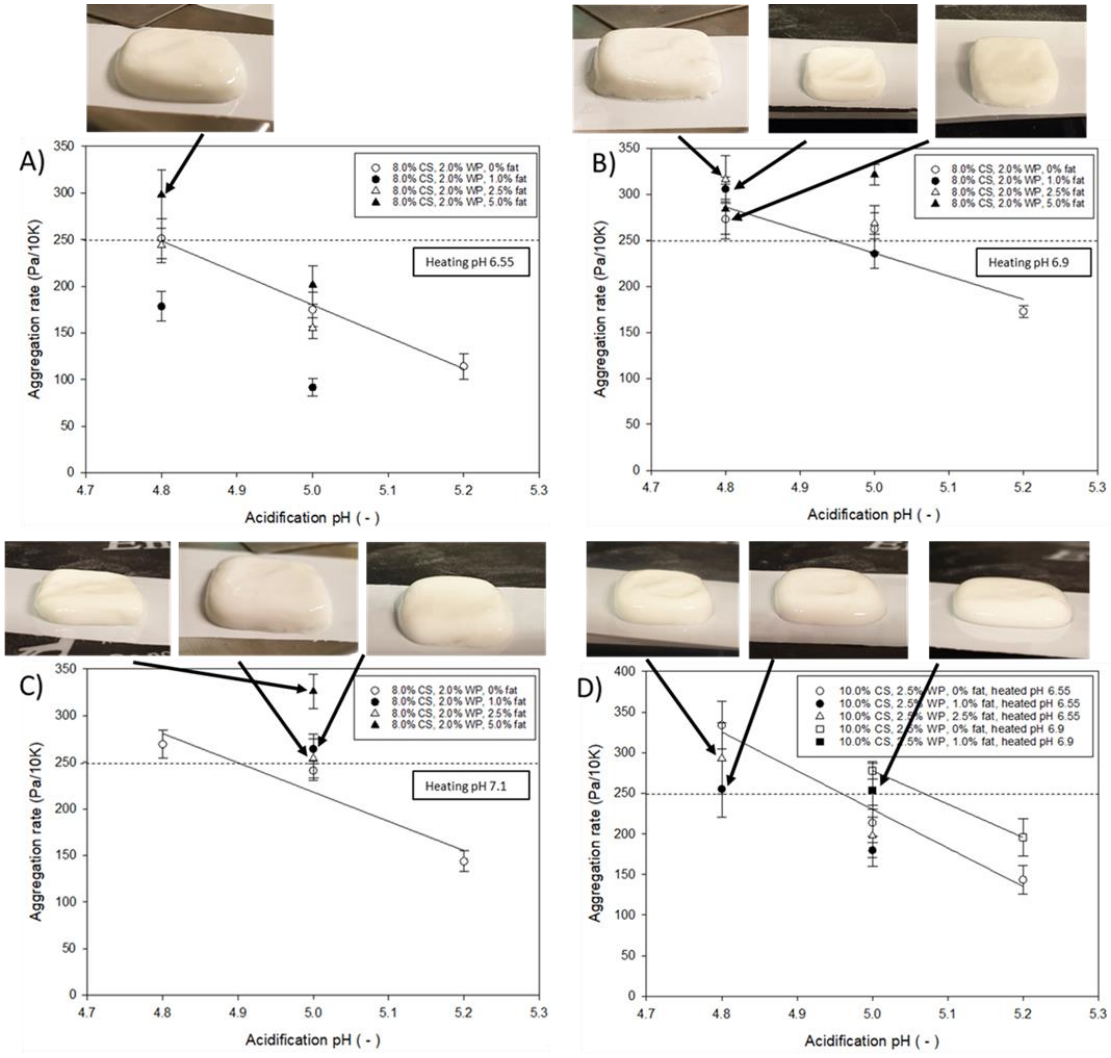

Figure 5-12: Aggregation rate (Pa/ 10 K) of heated samples (80°C, 10 min, pH 6.55 (A), 6.9 (B) and 7.1 (C)) with constant protein content (8.0% (w/w) CS and 2.0% (w/w) WP) and with higher protein content (10.0% (w/w) CS and 2.5% (w/w) WP, (D)) at different pH values (4.8 – 5.2) with different amounts of fat added (to final fat contents of 1.0, 2.5 and 5.0% (w/w)) at 10°C after/higher than sol−gel transition temperature obtained by temperature sweeps with a heating rate of 1 K/min. The solid line in all images represents the aggregation rate of pure protein-based formulations and is added to simplify comparisons to protein−fat suspensions. The dotted line indicates the threshold where above 250 Pa/10 K the aggregation rate was used as a positive indicator towards printability in a simple printing tests as shown by images of the printed samples.

The results for the aggregation rate of the formulations after an increased pH of 6.9 at heating and different amounts of fat added are illustrated in *Figure 5-12* (B). The values for the storage modulus G‘ increased with decreasing acidification pH and increasingly amount of additional fat (one exception at pH 5.0 and 1.0% (w/w) fat), with the highest increase for G‘ of 22.5% (pH 5.0, 5.0% (w/w) fat). A significant increase of G’ (pH 6.9 at heating) compared to formulations heated at lower pH (6.55) was demonstrated, evidenced by reaching or exceeding an aggregation rate of around 250 Pa/10 K for all formulations with milk fat addition. Although all formulations with fat addition showed promising aggregation rates after being heated at pH 6.9, only those acidified to pH 4.8 resulted in firm and very stable 3D-printed gels when heated during conveying (see printed gels related to aggregation rate in *Figure 5-12* (B)).

At a slightly alkaline pH of 7.1 at heating and after the addition of fat, fewer casein−whey protein formulations could be analysed (cf. *Figure 5-12* (C)), as an acidification pH value of 4.8 resulted in pre-gelation characteristics (G‘ > 1 Pa), preventing a temperature-triggered sol−gel transition. At an acidification pH of 5.0, a trend towards increased values of G‘ in samples with 1.0 and 2.5% (w/w) fat content was found, which became significant in the sample with 5.0% (w/w) fat content. All the formulations reached or exceeded an aggregation rate of 250 Pa/ 10 K with the highest value of 325.9 Pa/ 10 K ± 18.3 Pa/ 10 K (5.0% (w/w) fat). Independent of the amount of fat added, all three formulations, which were heated at pH 7.1 and cold acidified to pH 5.0, could be printed into small rectangular gels (*Figure 5-12* (C)). A linear increase of the firmness after addition of amounts of 2.0 – 10.0% (w/w) fat to protein gels (4.3% (w/w)), manufactured via the pH-T route, was found after penetration tests with the final gel (Hammelehle, 1994). Such high fat contents could not be used in these experiments due to pre–gelation characteristics (G’ > 1 Pa) after more than 5.0% (w/w) addition of fat.

The influence of the addition of 1.0 and 2.5% (w/w) fat on the aggregation rate of formulations with an increased overall protein content of 12.5% (w/w), consisting of 10.0% (w/w) casein

and 2.5% (w/w) whey protein, followed by thermal (pH 6.55, 6.9) and mechanical input is shown in *Figure 5-12* (D). Due to pre-gelation (G‘ > 1 Pa) after the addition of fat at the higher protein content (total solid content increased), several samples could not be produced and no formulations with a pH of 7.1 at heating was further investigated. This included the formulation with a pH of 6.55 at heating and 5.0% (w/w) fat) which could not be further processed. The results of the aggregation rate of formulations after both pH values at heating were combined in one figure (*Figure 5-12* (D)). At higher protein contents, a significant decrease in the storage modulus was demonstrated for all formulations after the addition of fat, independent of the pH at heating and the acidification pH. This was proposed to be the result of the increased amount of total solids (fat and protein) in the same unit volume compared to formulations without any fat, therefore slowing down the aggregation kinetics of the protein particles, if an increase in the temperature (pH–T-route) triggered collision and gelation of the particles. All three formulations at this higher protein content were tested for printing and resulted in firm gels.

5.2.4.4 Tailored casein micelle and MFG surface characteristics towards printing applications

Having applied the same thermal treatment (80°C, 10 min), CM with different composition and surface characteristics occurred, depending on the pH adjusted before heating to denature the whey proteins (Daffner et al., 2020a). The CM and protein subunits/ aggregates, which covered the MFG after thermal and mechanical treatment in this study, provided electrostatic and steric repulsion forces hindering coalescence of the fat particles. The small changes in the pH adjusted before heating allowed tailoring of the surface characteristics of the MFG, changing the sol−gel transition temperature (*Figure 5-11*) as well as the aggregation rate (*Figure 5-12*) of the protein suspensions mixed with fat compared to pure casein−whey protein suspensions of our previous study (Daffner et al., 2020a). Therefore, the pH sensitive CM as well as the MFG covered with proteins reacted to changes in the acidification pH and contributed to the gelation process via the pH−T-route. A schematic illustration (*Figure 5-13*) shows the effect of heating (80°C,

10 min) at the three adjusted pH values (6.55, 6.9, 7.1) and a mechanical 526 input (sonication and homogenisation at 500 bar) on the casein−whey protein suspensions mixed with dairy fat, as well as the proposed interactions between proteins and fat globules. Walstra & Jenness (1984) found that MFG after homogenisation could behave like CM and could be coagulated in the same way as pure proteins, although their experiment was conducted under resting conditions. In this study, the MFG, which were coated with different types of dairy proteins on the surface after mechanical input, showed a similar behaviour.

During high pressure homogenisation, CM adsorb faster to droplet surfaces than individual casein molecules (McClements, 2004). Results of the SDS-PAGE (*Figure 5-10*) showed that κ-casein depleted CM (pH of 7.1 at heating) covered the surface of MFG, which resulted in MFG more prone to aggregation compared to MFG covered with protein (CM with whey protein on the surface) after heating at pH 6.55, evidenced by a lower sol−gel transition temperature (compare *Figure 5-11* (C) to (A)). This was proposed to occur due to a decrease of the steric repulsion forces on the surface of the MFG covered with κ-depleted CM, as parts of κ-casein dissociated into the serum which resulted in a less dense hairy layer protruding into the serum phase.

The different surface characteristics of the MFG after mechanical treatment changed the microstructure of protein-fat formulations. As the aggregation rate was used as a positive indicator towards printability with simple printing tests, not all formulations reaching or exceeding 250 Pa/ 10 K were found to be printable or resulted in firm and stable gels. We assume that MFG, which were heated at pH 6.55, were covered with CM, CM with whey protein on their surface as well as denatured whey protein aggregates, as shown from SDS-PAGE (*Figure 5-10*). Those MFG were proposed to have stronger steric repulsion forces due to κ-casein on the outside of the CM, protruding into the serum. On the other hand, in-creased pH values at heating (6.9, 7.1) resulted in κ-casein depleted CM which covered the MFG, demonstrated by a decrease of κ-casein found during SDS-PAGE (*Figure 5-10*). It is assumed that this decrease

in the amount of κ-casein on the outside of the CM and on the surface of the MFG caused lower steric repulsion forces, shown by higher aggregation rates of those formulations.

At a total protein content of 10.0% (w/w), consisting of 8.0% (w/w) casein and 2.0% (w/w) whey protein, only one formulation with additional fat after a pH of 6.55 at heating was found to be printable. On the other hand, three formulations at each pH value at heating (6.9 and 7.1) could be printed, although a lower acidification pH was necessary at pH of 6.9 at heating. As CM were most depleted in κ-casein after being heated at pH 7.1 and therefore, steric repulsion forces of CM on their own and on the surface of MFG decreased, those formulations were the only ones being able to be printed at pH 5.0.

The effect of heating at three adjusted pH values on the casein−whey protein suspensions mixed with dairy fat and the proposed interactions between protein and fat particles depending on the pH at heating (6.55/6.9/ 7.1 at 80°C, 10 min) after mechanical input (sonication and homogenisation at 500 bar) are schematically illustrated in *Figure 5-13*. A similar increase of adsorbed caseins (α_s and β) with increasing pH at heating, but decreasing amounts of κ-casein and β-lactoglobulin were found elsewhere (Sharma et al., 1996a).

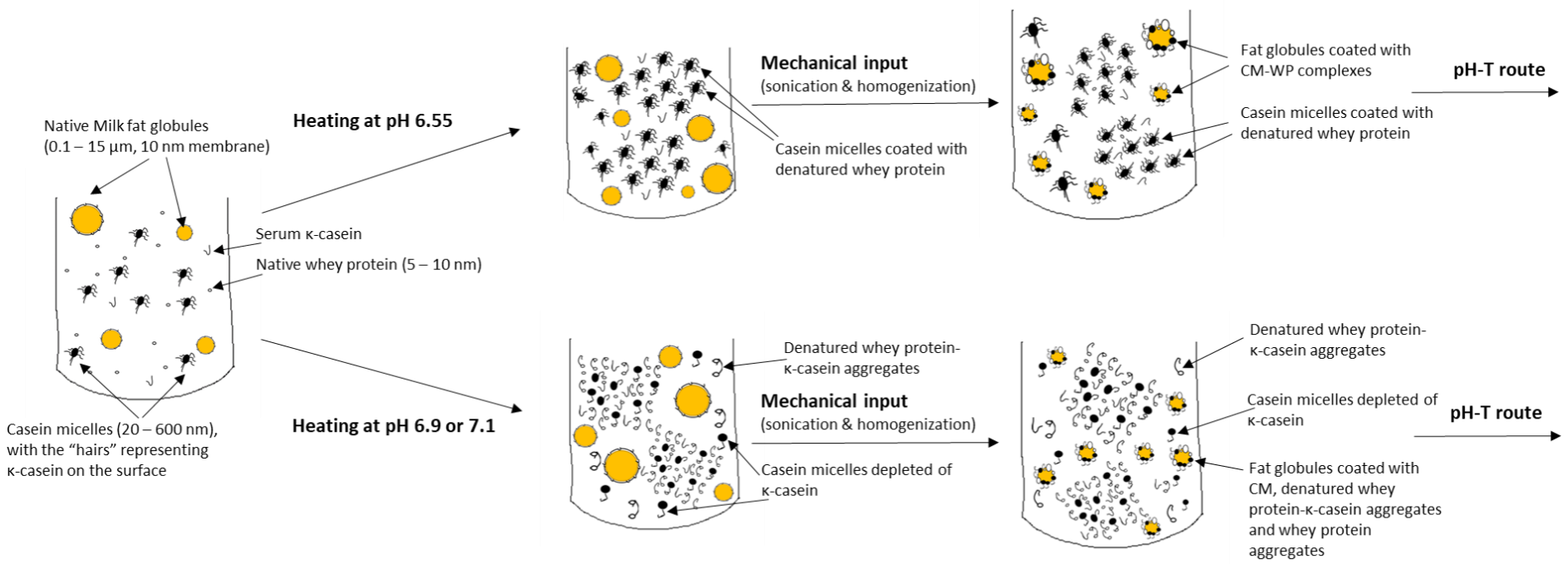

Figure 5-13: Schematic presentation depicting the preparation of casein−whey protein suspensions mixed with milk fat globules, which can then further be used for extrusion-based 3D-printing via the pH−T-route. After a thermal (80°C, 10 min, pH 6.55/ 6.9/ 7.1) and mechanical energy input, the newly created MFG membrane surface is covered by different types of proteins or protein subunits/ aggregates.

5.2.5 Conclusion

The effect of dairy fat on casein−whey protein suspensions was characterised regarding the potential use for extrusion-based 3D-printing applications via the pH–T-route. Small fat particles in the nano metre range were mechanically produced and covered with different protein particles to mimic protein behaviour during gelation. For promising formulations, sol–characteristics after cold acidification (pH 4.8/5.0), independent of the pH at heating but dependent on the protein content, were evidenced by ζ-potential (~ –20 mV) and rheology (G' = 0.1 Pa) and a steep increase of G' above 1 Pa (sol−gel transition temperature) was found.

For protein-fat formulations heated at a lower pH (6.55) followed by mechanical input, an increase in the sol−gel transition temperature and a decrease in the aggregation rate, independent of the amount of fat added, was found. In contrast, a higher pH at heating caused similar (pH 6.9) respectively lower (pH 7.1) sol−gel transition temperatures. For those higher pH values at heating, increased aggregation kinetics compared to casein−whey protein based suspensions without fat were found, resulting in promising material characteristics (G' ≥ 250 Pa/ 10 K) for printing purposes. Dairy fat could thus be added to casein−whey protein suspensions which were considered to be printable via the pH−T-route, if the thermal and mechanical treatments tailored the material properties accordingly. Extrusion-based 3D-printing of protein-fat formulations inclusive a sol−gel transition was found to be more favourable at higher pH values at heating.

5.2.6 Appendix

5.2.6.1 Supplementary data 1

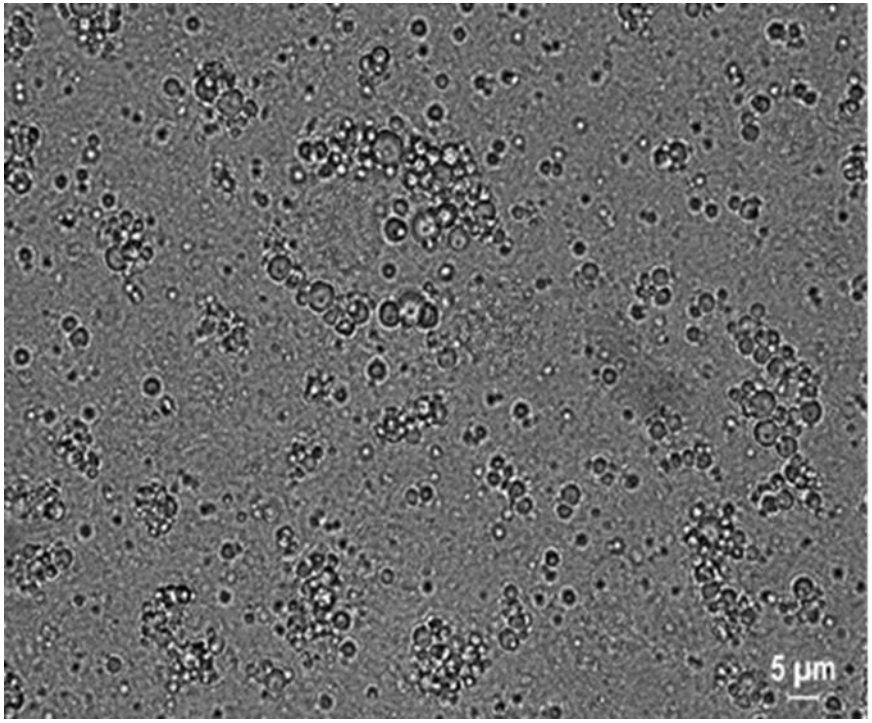

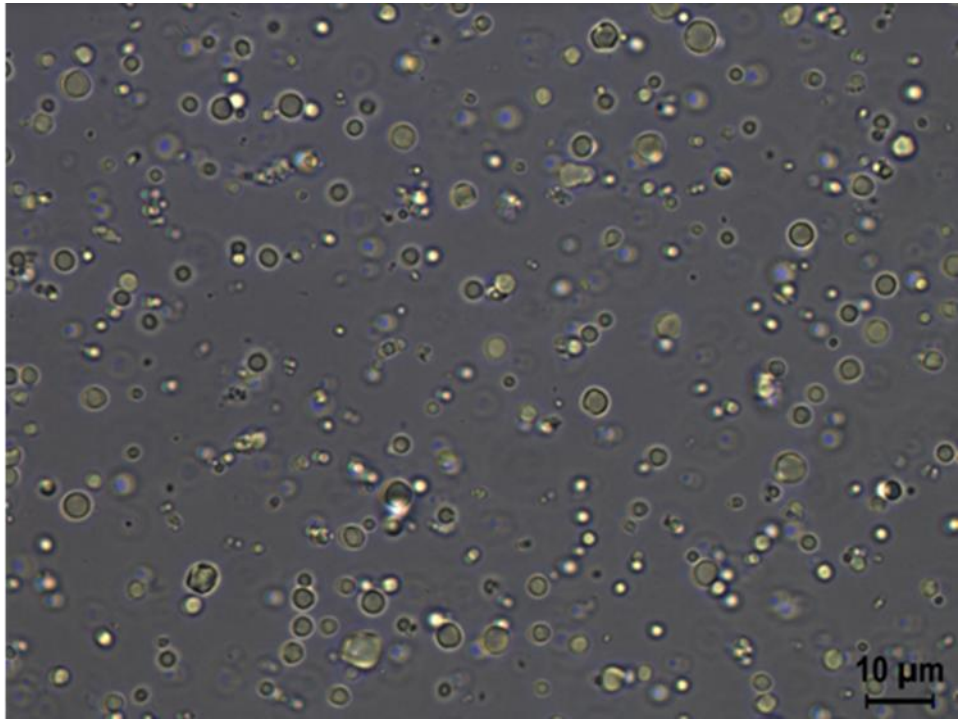

Supplementary Figure 5-1: Optical microscopy of a casein−whey protein suspension inclusive added **fat** with native milk fat globules without any mechanical treatment (100x magnification). Big particles all represent milk fat globules. Scale bar = 5 µm and 10 µm.

5.2.6.2 Supplementary data 2

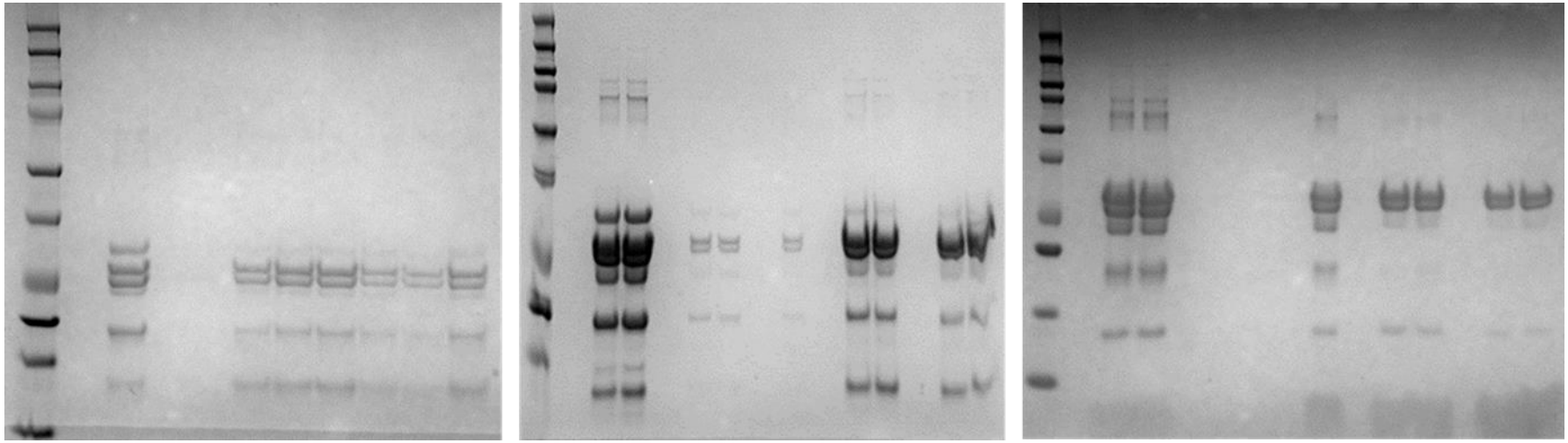

Supplementary Figure 5-2: SDS-PAGE analysis of proteins covering the milk fat globule surface membrane after thermal (80°C, 10 min) and mechanical treatment. Heated at three pH values of 6.55 (left), 6.9 (middle) and 7.1 (right). K-CN and β-LG are visible as bands after pH values at heating of 6.55 (lane VI-XII) and 6.9 (lane XII-XIII and XIV-XV), but not after a pH at heating of 7.1 (lane XII-XIII and XIV-XV). Bis-Tris 4-12 (pH 6.55) – and 12% polyacrylamide gels (pH 6.7, 7.1) were used for pre-experiments while developing the method.

5.2.7 References

Aguilera, J. M., & Kessler, Hg. (1988). Physicochemical and rheological properties of milk-fat globules with modified membranes. Milchwissenschaft 43 (1988), 411-415.

Anema, S. G., & Klostermeyer, H. (1997). Heat-induced, pH-dependent dissociation of casein micelles on heating reconstituted skim milk at temperatures below 100 C. Journal of Agricultural and Food Chemistry, 45(4), 1108-1115.

Buchheim, W. (1986). Membranes of milk fat globules ultrastructural biochemical and technological aspects. Kieler Milchwirtschliche Forschungsberichte, 38, 227-246.

Cano-Ruiz, M. E., & Richter, R. L. (1997). Effect of homogenisation pressure on the milk fat globule membrane proteins. Journal of Dairy Science, 80(11), 2732-2739.

Daffner, K., Vadodaria, S., Ong, L., Nöbel, S., Gras, S., Norton, I., & Mills, T. (2020). Design and characterisation of casein–whey protein suspensions via the pH–temperature-route for application in extrusion-based 3D-printing. Food Hydrocolloids, 112, 105850.

Daffner, K., Hanssen, E., Norton, I. T., Mills, T., Ong, L., & Gras, G. L. (2020b). Imaging of dairy emulsions via a novel approach of cryogenic transmission electron microscopy using beam exposure. Soft Matter, 16(34), 7888-7892.

Dalgleish, D. G. (1984). Measurement of electrophoretic mobilities and zeta-potentials of particles from milk using laser Doppler electrophoresis. Journal of Dairy Research, 51(3), 425-438.

Derossi, A., Caporizzi, R., Azzollini, D., & Severini, C. (2018). Application of 3D printing for customized food. A case on the development of a fruit-based snack for children. Journal of Food Engineering, 220, 65-75.

Devnani, B., Ong, L., Kentish, S., & Gras, S. (2020). Heat induced denaturation, aggregation and gelation of almond proteins in skim and full fat almond milk. Food Chemistry, 126901.

Dickinson, E. (2012). Emulsion gels: The structuring of soft solids with protein-stabilized oil droplets. Food hydrocolloids, 28(1), 224-241.

Dickinson, E. (1999). Caseins in emulsions: interfacial properties and interactions. International Dairy Journal, 9(3-6), 305-312.

Dickinson, E. (1998). Rheology of emulsions - The relationship to structure and stability. In Modern aspects of emulsion science (pp. 145-174).

Dickinson, E. (1994). Protein-stabilized emulsions. Journal of Food Engineering, 22, 59-74.

Godoi, F. C., Prakash, S., & Bhandari, B. R. (2016). 3d printing technologies applied for food design: Status and prospects. Journal of Food Engineering, 179, 44-54.

Hammelehle, B. (1994). Die Direktsaeuerung von Milch. Untersuchungen zur gezielten Einflussnahme auf Textur und Konsistenz gesaeurter Milchgel. PhD Thessis. Muenchen: Technische Universitaet Muenchen/ Weihenstephan.

Horne, D. S. (1998). Casein interactions: casting light on the black boxes, the structure in dairy products. International Dairy Journal, 8(3), 171-177.

Ji, Y. R., Lee, S. K., & Anema, S. G. (2016). Characterisation of heat-set milk protein gels. International dairy journal, 54, 10-20.

Jørgensen, C. E., Abrahamsen, R. K., Rukke, E. O., Hoffmann, T. K., Johansen, A. G., & Skeie, S. B. (2019). Processing of high-protein yoghurt–A review. Intern. Dairy Journal, 88, 42-59.

Kessler, H. G. (2002). Food and bio process engineering. Dairy Technology, 5th edition (Verlag A. Kessler, Munich, Germany).

Lanaro, M., Forrestal, D. P., Scheurer, S., Slinger, D. J., Liao, S., Powell, S. K., & Woodruff, M. A. (2017). 3D printing complex chocolate objects: Platform design, optimization and evaluation. Journal of Food Engineering, 215, 13-22.

LeTohic, C., O'Sullivan, J. J., Drapala, K. P., Chartrin, V., Chan, T., Morrison, A. P., ... & Kelly, A. L. (2018). Effect of 3D printing on the structure and textural properties of processed cheese. Journal of Food Engineering, 220, 56-64.

Liu, W., Ye, A., Liu, W., Liu, C., & Singh, H. (2013). Stability during in vitro digestion of lactoferrin-loaded liposomes prepared from milk fat globule membrane-derived phospholipids. Journal of dairy science, 96(4), 2061-2070.

Lopez, C., Madec, M. N., & Jimenez-Flores, R. (2010). Lipid rafts in the bovine milk fat globule membrane revealed by the lateral segregation of phospholipids and heterogeneous distribution of glycoproteins. Food Chemistry, 120(1), 22-33.

Malone, E., & Lipson, H. (2007). Fab@ Home: the personal desktop fabricator kit. Rapid Prototyping Journal, 13 (2007), 245-255.

McClements, D. J. (2004). Protein-stabilized emulsions. Current opinion in colloid & interface science, 9(5), 305-313.

Michalski, M. C., Michel, F., Sainmont, D., & Briard, V. (2002a). Apparent ζ-potential as a tool to assess mechanical damages to the milk fat globule membrane. Colloids and Surfaces B: Biointerfaces, 23(1), 23-30.

Michalski, M. C., Cariou, R., Michel, F., & Garnier, C. (2002b). Native vs. damaged milk fat globules: membrane properties affect the viscoelasticity of milk gels. Journal of Dairy Science, 85(10), 2451-2461.

Michalski, M. C., Michel, F., & Geneste, C., (2002c). Appearance of submicronic particles in the milk fat globule size distribution upon mechanical treatments. Le Lait, 82(2), 193-208.

Nöbel, S., Seifert, B., Schäfer, J., Daffner, K., & Hinrichs, J. (2018). Oral presentation Food Colloids, Leeds 2018 - Session - Processing of Novel Structures for Functionality. Temperature-triggered gelation of milk concentrates applied to 3D food printing.

Nöbel, S., Seifert, B., Daffner, K., Schäfer, J., & Hinrichs, J. (2020). Instantaneous gelation of acid milk gels via customized temperature-time profiles: Screening of concentration and pH suitable for temperature triggered gelation towards 3D-printing. Food Hydrocolloids, 106450.

Ong, L., Dagastine, R. R., Kentish, S. E., & Gras, S. L. (2010a). The effect of milk processing on the microstructure of the milk fat globule and rennet induced gel observed using confocal laser scanning microscopy. Journal of food science, 75(3), E135-E145.

Ong, L., Dagastine, R. R., Kentish, S. E., & Gras, S. L. (2010b). Transmission electron microscopy imaging of the microstructure of milk in cheddar cheese production under different processing conditions. Australian Journal of Dairy Technology, 65(3), 222.

Rajagopalan, R., & Hiemenz, P. C. (1997). Principles of colloid and surface chemistry. Marcel Dekker, New-York, 8247, 8.

Rios, R. V., Pessanha, M. D. F., Almeida, P. F. D., Viana, C. L., & Lannes, S. C. D. S. (2014). Application of fats in some food products. Food Science and Technology, 34(1), 3-15.

Roefs, P. F. M. (1986). Structure of acid casein gels: A study of gels formed after acidification in the cold (Doctoral dissertation, Roefs). Wageningen University & Research Centre.

Ross, M. M., Kelly, A. L., & Crowley, S. V. (2019). Potential Applications of Dairy Products, Ingredients and Formulations in 3D Printing. In Fundamentals of 3D Food Printing and Applications (pp. 175-206). Academic Press.

Schäfer, J., Läufle, I., Schmidt, C., Atamer, Z., Nöbel, S., Sonne, A., Kohlus, R. & Hinrichs, J. (2018). The sol−gel transition temperature of skim milk concentrated by microfiltration as affected by pH and protein content. International journal of dairy technology, 71(3), 585-592.

Sharma, S. K., & Dalgleish, D. G., (1993). Interactions between milk serum proteins and synthetic fat globule membrane during heating of homogenized whole milk. Journal of Agricultural and Food Chemistry, 41(9), 1407-1412.

Sharma, R., Singh, H., & Taylor, M. W. (1996a). Recombined milk: factors affecting the protein coverage and composition of fat globule surface layers. Australian journal of dairy technology, 51(1), 12.

Sharma, R., Singh, H., & Taylor, M. W. (1996b). Composition and structure of fat globule surface layers in recombined milk. Journal of Food Science, 61(1), 28-32.

Singh, H., & Creamer, L. K. (1991). Influence of concentration of milk solids on the dissociation of micellar κ-casein on heating reconstituted milk at 120° C. Journal of dairy research, 58(1), 99-105.

Van Vliet, T., & Dentener-Kikkert, A. (1982). Influence of the composition of the milk fat globule membrane in the rheological properties of acid milk gels. Netherlands Milk and Dairy Journal, 36, 261-265.

Walstra, P., & Jenness, R. (1984). Dairy chemistry & physics. John Wiley & Sons. New York.

Wegrzyn, T. F., Golding, M., & Archer, R. H. (2012). Food Layered Manufacture: A new process for constructing solid foods. Trends in Food Science & Technology, 27(2), 66-72.

Ye, A., Singh, H., Taylor, M. W., & Anema, S. (2002). Characterization of protein components of natural and heat-treated milk fat globule membranes. International Dairy Journal, 12(4), 393-402.

Ye, A., Anema, S. G., & Singh, H. (2008). Changes in the surface protein of the fat globules during homogenisation and heat treatment of concentrated milk. Journal of dairy research, 75(3), 347-353.

6 Chapter:

Set-up and retrofitting of a plastic printer into a customised 3D food printer

6.1 Abstract

The set-up of a customised 3D food printer was created to specifically print dairy-based formulations via the pH−T-route, including a sol–gel transition. A commercially available plastic printer was retrofitted and subsequently used for printing different casein−whey protein suspensions with and without fat. Customisation included removal of needless parts of the plastic printer followed by adding specific parts which were generated via CAD software and plastic printed. A special focus during retrofitting was placed on a reduction of the weight of the moving parts during printing, a temperature control of different sections, a simple set-up to allow a fast cleaning procedure of the pipe and the nozzle as well as changes within the software. The most promising formulations from oscillatory measurements (G' > 250 Pa/ 10 K) were tested on the customised printer regarding their extrusion-based printability.

6.2 Introduction

Additive layer manufacturing (ALM) is a digitally controlled, robotic construction technology which deposits materials layer-by-layer to build a three-dimensional shape. For food layer manufacturing (FLM) of dairy-based materials, extrusion is the most widely adopted technology (Sun et al., 2018), as recently used for e.g. melted cheese (Le Tohic et al., 2017), sodium caseinate (Schutyser et al., 2018), protein pastes (Lille et al., 2018), casein-based milk concentrates (Nöbel et al., 2018) or semi-hard model cheese (Kern et al., 2018). Different extrusion-based printed food objects, obtained either via HME or SME, were presented in section *2.2.3.1 (Table 2-4)*. In general, extrusion allows to manufacture solid or semi-solid objects with particular shapes and textures (Cheyne et al., 2005) and to modify the microstructure via the effects of shear, temperature and local temperature changes induced by shear (Matz, 1991). According to Tan et al. (2018), an ideal 3D food printer has to match certain features, including

a) an easy and quick refill process

b) a high storage capacity

c) a potential for a continuous printing process, which can incorporate printing and cooking at the same time

d) an easy cleaning procedure (even a cleaning in place process)

e) an automated layer defect correction

f) an independent temperature control for the storage unit and the extrusion nozzle

Compared to customised printers in the laboratories of research institutions, plenty of commercial printers are available nowadays, especially extrusion-based food printers, some of which were presented in recent reviews (Sun et al., 2018; Toh et al., 2018). So far, all these printers provide different advantages and disadvantages, none of them offering a single solution which can be applied to all different types of foods. For extrusion-based food printing, chocolate is

frequently used as a feed material, with the first commercially available chocolate printer - the Choc Creator V2.0 Plus (Choc Edge Ltd. UK) - containing a 30 ml syringe and a heated jacket which prevents solidifying of the material, being able to print 2D and 3D shapes of chocolate. Other research groups have also constructed customised chocolate printers, e.g. the 3Drag (Open Electronics, Online), the QiaoKe (3DCloud, Beijing, China) or the CocoJet (3D Systems, Rock Hill, USA). Currently commercially available printers include the

- BeeHex (BeeHex®, USA) which has a patent on a self-cleaning technology, an important tool for future applications.

- Procusini 3.0 Dual (Print2Taste GmbH, Germany) for chocolate, marzipan and fondant, which can hold up to 85 grams of food paste material.

- Foodini (Natural Machines, Spain) which consists of five 100 mL stainless steel capsules with an independent temperature control.

- Barilla Food Printer (TNO, The Netherlands) which was created to deposit dough layer-by-layer.

So far, few scientific studies have focused on printing of dairy-based foods. Therefore, little is known about optimising the feedstock as well as the printing parameters of dairy suspensions, and no current-generation 3D-printer is specifically engineered to print these materials (Ross et al., 2019). To create objects of high quality via extrusion, the understanding of the interplay between ingredients, process parameters and equipment design (printer set-up) is necessary (Cheyne et al., 2005).

The first dairy-based material printed was melted cheese (Le Tohic et al., 2017) on a retrofitted plastic printer (RepRap Pro Ormerod 1, RepRap Professional Ltd, UK). A syringe (12 ml) was fixed in a mount and driven by a motor to deposit the material. Additional plastic parts were created with CAD-software, printed and mounted to fix syringe and motor. Microstructure

and firmness of melted 3D-printed cheese were compared to normal industrial processed cheese. It was found that 3D-printed cheese samples had almost 50% less hardness than normal untreated cheese. By using confocal laser scanning microscopy they also showed that higher extrusion flow rates (12 ml/min compared to 4 ml/min) resulted in a smaller fat globule size and a more uniform fat particle size distribution.

Schutyser et al. (2018) printed sodium caseinate dispersions mixed with pectin, sucrose and starch. Their printing apparatus consisted of a fluid dispensing robot (model 2203, Nordson EFD, USA) which moved in the xyz-direction, and a dispenser control device (Performus III, Nordson EFD, USA) which was necessary as a driving force ($0 - 5.5$ bar) to dispense the feed material from the dispenser. The temperature of the dispenser and the feed material was adjusted to $5 - 15$°C higher than the gelation temperature to induce a fast solidification process after depositing the dispersion.

Nöbel et al. (2018) retrofitted a plastic printer into a food printer capable of cooling, heating and transporting milk concentrates to a nozzle. Their set-up consisted of several sections and hoses in hoses (mono tube heating system) with counter-current flow conditions to cool or heat up formulations, respectively. They were the first to successfully implement 3D-printing of concentrated milk via the pH−T-route, using pure, liquid casein-based formulations as a feedstock, which were transferred into a gel under dynamic conditions.

So far, most of the extrusion-based printers used for food printing were customised plastic printers. Within this study, a plastic printer was fully retrofitted into a food printer and formulations differing in product and process parameters were printed if promising characteristics (compare *4.4.3*) were obtained during linear temperature ramps (heating rate of 1 K/min).

6.3 Material and methods

6.3.1 Retrofitting a plastic printer into a 3D food printer

In this section, the whole set-up and retrofitting process of a plastic printer into a customised 3D food printer capable of cooling, heating and transporting the feedstock is shown. Step by step, all changes are depicted and the appropriate advantages are explained. A customised extrusion-based 3D-printer was created by retrofitting a commercially available Creality Ender 3 Printer (Creality Ender 3 Printer; Creality, Shenzhen, China). The requirements for the printer were taken with the aim to print dairy protein-based formulations inclusive a sol−gel transition of the feedstock. The set-up of the original plastic printer, including the printing head and plastic cables, is illustrated in *Figure 6-1*.

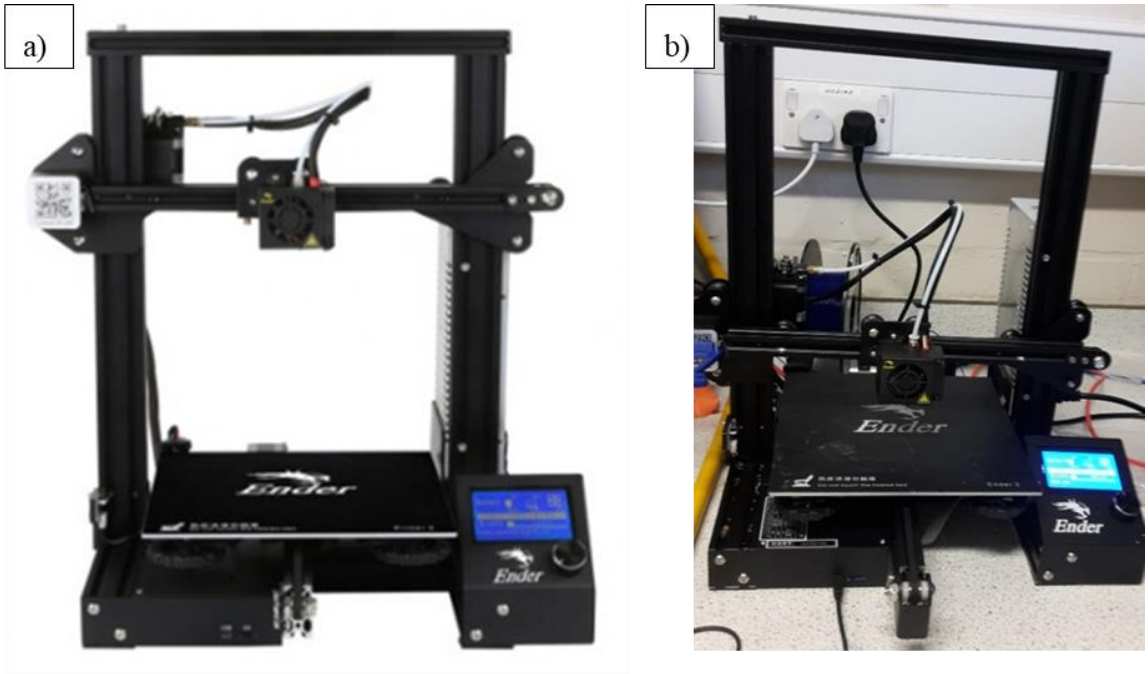

Figure 6-1: Set-up of the commercially available plastic printer "Creality Ender 3" for plastic printing with a) the plastic printer as shown online and b) the plastic printer after the successful set-up and testing in the lab.

Printing of plastic relies on a fast melting process of the material (e.g. ABS or PLA) in the heating section with high temperatures, e.g. 180°C for PLA. The melted PLA is deposited after extrusion onto the heated printing bed (60°C). Due to no need for food printing, the printing head, fan, cables and plastic material were all removed from the original set-up. After removal

of all dispensable parts, the major parts for the design of a food printer were taken into consideration, as shown before for a printer for pure-casein based formulations (Nöbel et al., 2018).

The retrofitted printer had to

1) include a “feed tank”/ syringe which could be cooled to maintain sol−characteristics of the dairy-based formulations before printing

2) have a cooling/ insulating pipe transporting the feedstock from the chilled syringe to a nozzle to maintain sol−characteristics of the feedstock

3) be capable of a heating step in the nozzle to induce a transition from sol to gel

4) have thermistors/ thermocouples at selective places, e.g. at the beginning and at the end of the nozzle to control the temperature of the formulations and to adjust the temperature within the firmware

The completely modified version of the set-up of the printer is shown in *Figure 6-2*. For a better control of all the additional weight of the new parts, the motor and the syringe with the double walled cooling jacket were fixed on top of the printer (*Figure 6-2* and *Figure 6-3*). This facilitated the printing process by moving less weight, which could otherwise affect the print quality (Warner, 2019). The stepper motor, connected to a screw plunger, controlled and powered the syringe to perform the extrusion-based printing (retraction speed). The motor driven syringe on the top of the printer was a contradictory design compared to Nöbel et al. (2018) whose apparatus had to move all the cables and hoses during the printing process, driven by a syringe pump next to the printer itself.

Several more parts were considered to be necessary to fix the syringe and the stepper motor on top of the printer to enable a continuous movement of the syringe controlled by the computer software. Two 30 cm long stainless steel bars held all the parts in line and several CAD-printed parts supported the straight attachment of the motor, the syringe and the double walled cooling

jacket (1) on the top of the printer. The syringe was driven forward by the stepper motor, shown on the left of the upper part of the printer (*Figure 6-2*, part 7). A 60 ml syringe, which was placed within the double walled cooling jacket, was used for all experiments to store enough material for the printing process (*Figure 6-3*). The cooling jacket was connected to a water bath (water−ethylene glycol solution (20%)) to maintain sol−characteristics of the feedstock at around 2°C. The tip of the syringe was connected to a transport hose (inner diameter temperature control hose = 8×10^{-3} m) which was covered by nitrile foam to maintain the cold temperature of the feedstock.

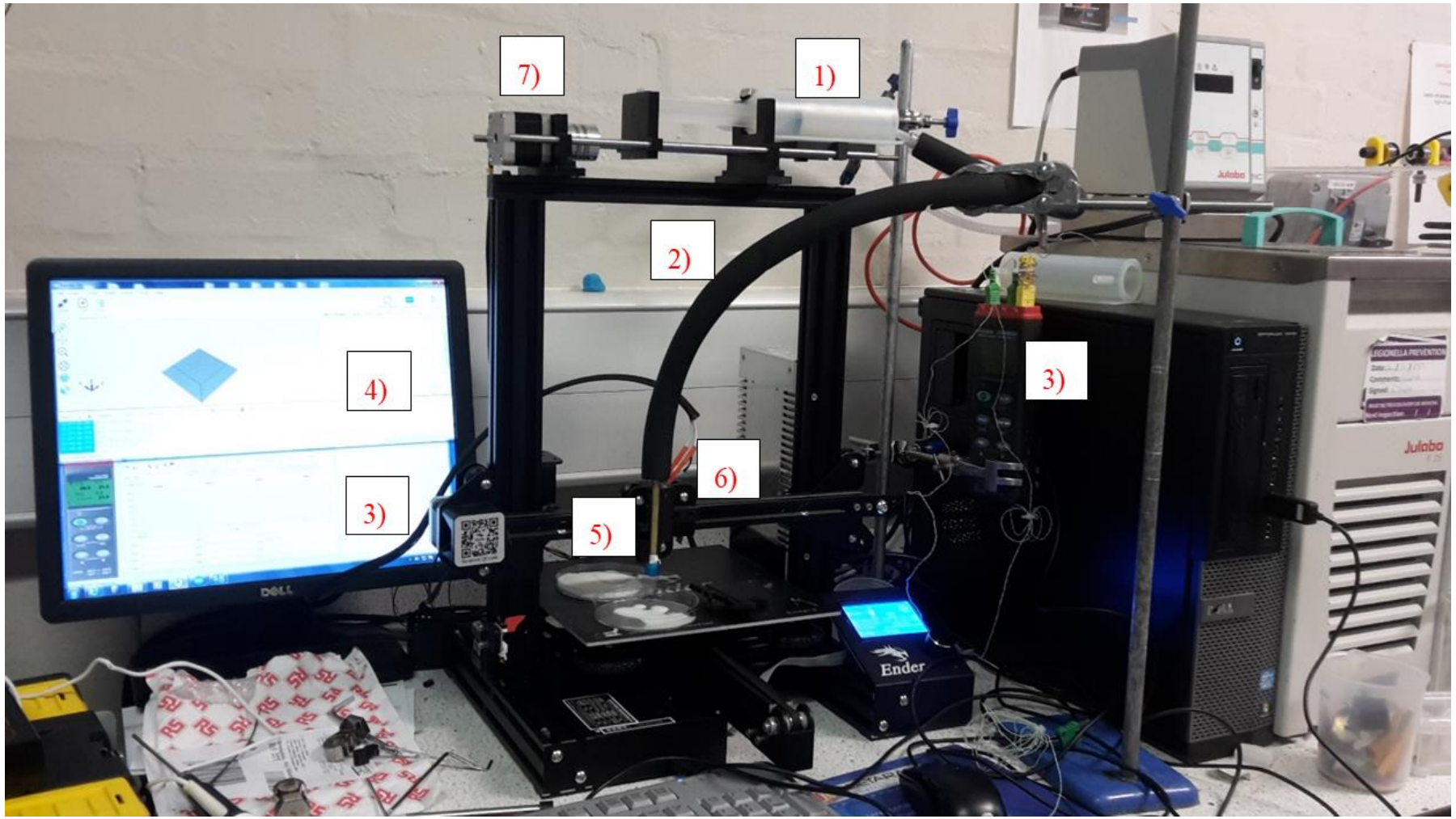

Figure 6-2: Labelled set-up of the customised 3D-food printer inclusive 1) syringe in double walled cooling jacket, 2) insulated pipe for transport of feed material to nozzle, 3) thermometer, thermo-couples and software, 4) firmware of Ender 3 printer, 5) nozzle with die at the end, 6) heating element for nozzle and 7) stepper motor.

Adjusting and maintaining the temperature (2°C) of the feed material in the syringe was a pre-requisite for the pH−T-route to maintain sol−characteristics and to avoid pre−gelation before the nozzle during conveying. A flat plastic 3D-printed mounting (1) was fixed with the stainless steel bars (2) below the double walled cooling jacket to avoid any material movements during the printing process (*Figure 6-3*). Before the dairy suspensions were printed layer-by-layer, a transition from a sol to a gel had to be conducted within the length of the nozzle (*Figure 6-4*). The feed material entered the nozzle (brass pipe) on the top, maintaining sol−characteristics. As shown in *Figure 6-4* (b), the original heating element of the plastic printer was placed in the mounting construction next to the brass pipe to ensure heating of the feed material through the brass pipe. An increase in the temperature of the feed material caused collision and aggregation of the protein particles to trigger a fast and irreversible gelation process.

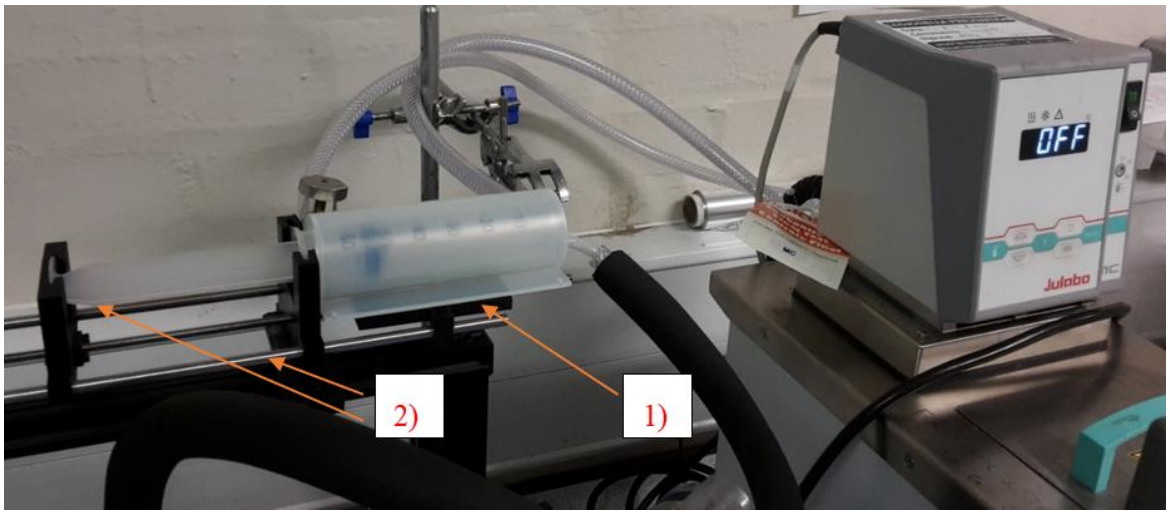

Figure 6-3: Presentation of the upper part on top of the printer, exclusively showing the syringe placed in a double-walled cooling jacket, connected to a water bath. The tip of the syringe is connected to a hose to transport the feed material to the nozzle. The flat plastic 3D-printed mounting (1) was fixed with the stainless steel bars (2) below the double walled cooling jacket.

The final version (d) of the die offered two orifices at the sides to have thermocouples in contact with the brass pipe to control the outlet temperature of the feed material, as demonstrated in *Figure 6-4* (c). The holes were big enough to hold the thermocouples and a small amount of heat transfer paste (Keratherm KP 97, KERAFOL – Keramische Folien GmbH, Germany). The two thermocouples (Labfacility Ltd, Bognor Regis, UK) were used to measure the temperature

and were placed each on one side of the die, connected to a 4-channel data logger thermometer (HH309A, Omega) which could display and record four channels simultaneously. Adjustment of the temperature of the heating element via the software allowed quick changes over a certain temperature range.

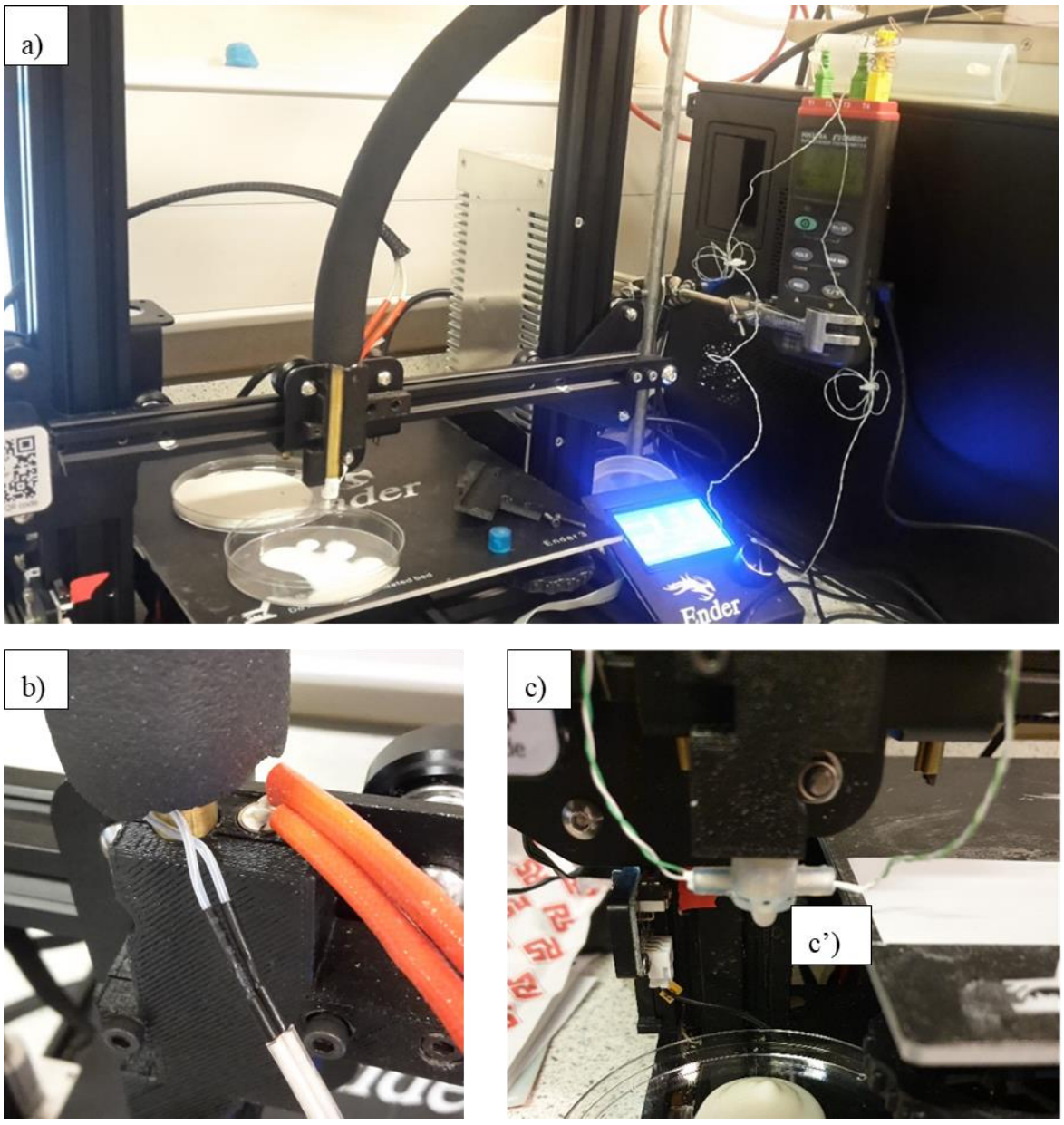

Figure 6-4: Focus on the nozzle of the customised printing set-up with a) the brass pipe in the CAD design to induce the sol−gel transition, b) the heating element on the top of the nozzle in contact with the brass pipe and c) the die (c‘) at the end of the nozzle extruding the material, with heating elements on the side in contact with the brass pipe.

The construction process of the die at the end of the nozzle in shown in *Figure 6-5* (a-d). The prerequisites for the die were to fit into the nozzle (brass pipe) and to be fixed in this position during the printing process, but also to be easily removable for cleaning afterwards. Firstly, it was ensured that the brass pipe could be placed into the die (compare (a)) and fitted. Secondly, the outlet of the die had to be constructed (compare (b) and (c)) in the correct size (1.15 mm) to enable depositing of the feed material and avoid clogging (if too small outlet size).

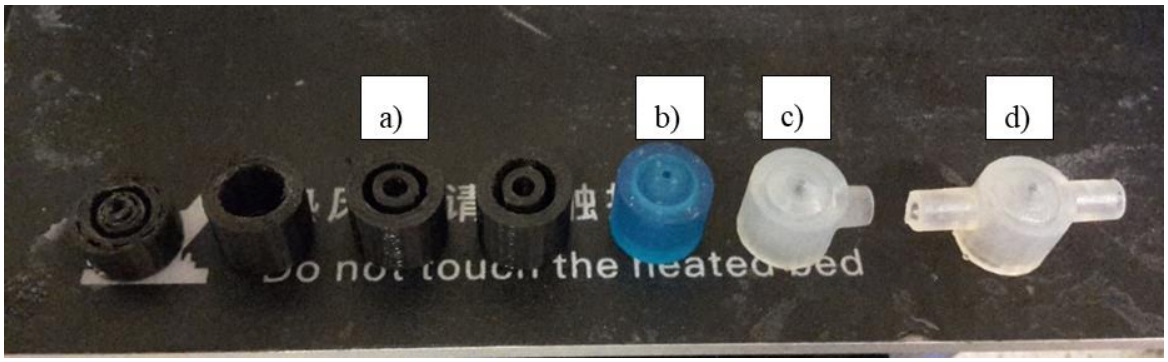

Figure 6-5: Process of creating the die for the end of the nozzle to print the dairy formulations with the final version on the right, providing two orifices for thermocouples.

6.3.2 Electrical and software

The software used to control the printer was Repetier (Host V2.1.3). To create a printed object, a CAD model (25 x 25 x 3 mm, rectangle slice) of the object was created in the software. This object was sliced by the software into three layers, and a path was calculated for printing. During printing, the nozzle followed this path and extruded the feedstock to create the desired rectangular shape.

6.3.3 CAD-design of plastic parts and 3D-printing of CAD-models

The virtual models (*Figure 6-6*) were designed by using the software Tinkercad (Autodesk Inc.) and printed using polylactic acid (PLA) on a plastic printer, with some of the printed pieces used for the design of the nozzle shown in *Figure 6-4*. The final printed pieces made of PLA are shown in *Figure 6-2* on top of the printer. The double walled cooling jacket (see *Figure 6-2 (1)* and *Figure 6-3*) was printed using a Formlabs Form 2 SLS Printer (Somerville, MA), which used Formlabs standard clear resin for printing.

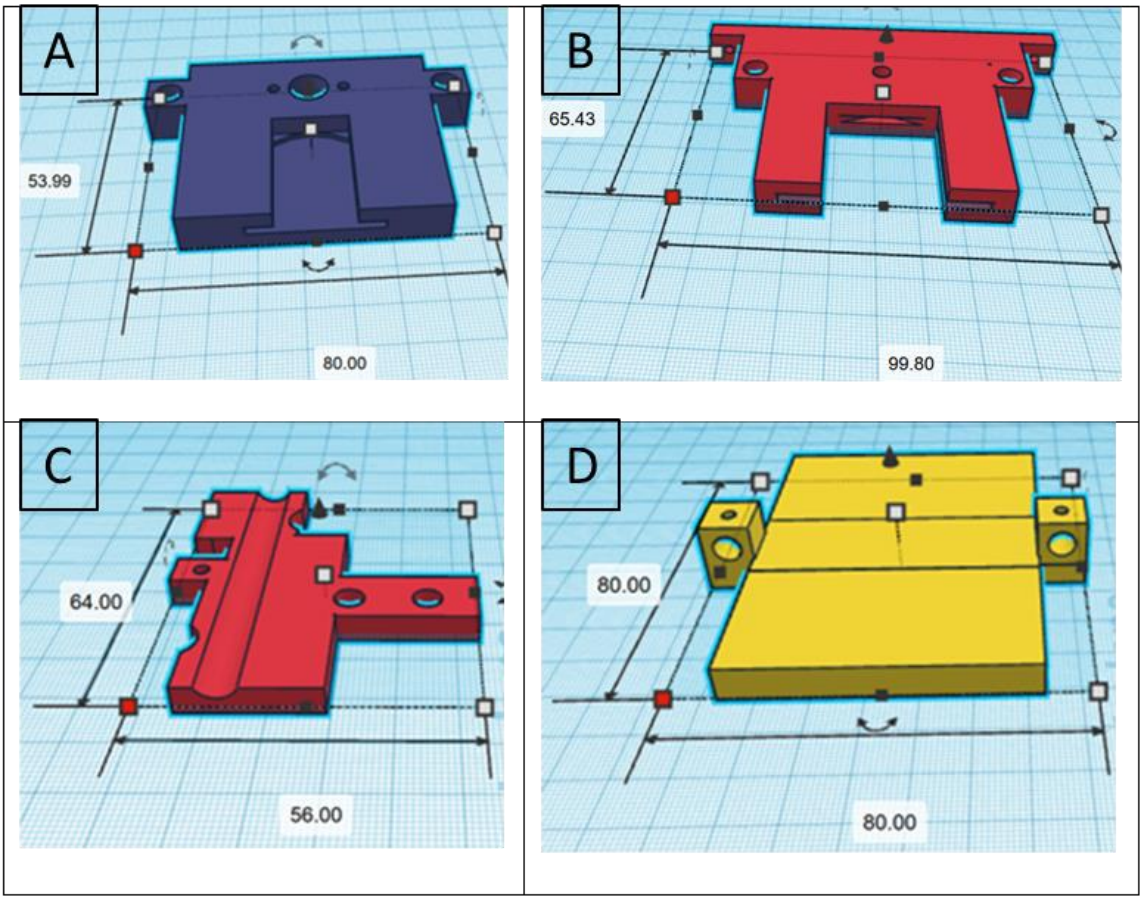

Figure 6-6: Technical drawings of the syringe holders (A) and (B) on top of the printer, the nozzle holder (C) for the brass pipe and the mounting (D) that was used to hold the stainless steel bars on top of the printer.

6.3.4 Adjusting parameters for 3D-printing of dairy formulations

In order to prove design rules and print small rectangular shapes, several parameters had to be adjusted in the software Repetier Lines were printed next and subsequently above each other to create a three-dimensional object, in this study limited to rectangular shapes. The printing line speed was adjusted between 20 – 40 mm/s, with a non-printing line speed at 30 mm/s, with the

same speed set for the inner and outer perimeter. The retraction speed during extrusion was set to 30 mm/s. The temperature of the extruder was set in dependence of $T_{sol–gel}$ and was adjusted during printing depending on the sol/gel state of the feedstock.

The layer height was adjusted to 1 mm for all three layers, which were printed subsequently above each other, with a first layer extrusion width of 100%. Before each print, the bed level had to be calibrated manually. Printing was performed on a hydrophobic printing paper (10 x 10 cm; Legamaster International B.V., The Netherlands) to prevent spreading of the first layer. As no complex objects were printed, the shell thickness, the infill overlap, the support filaments etc. were not adjusted. No temperature for the printing bed was set and as the fan was removed during retrofitting, no temperatures were adjusted, respectively.

6.4 Conclusion

A plastic printer was retrofitted to print dairy protein-based formulations inclusive a sol−gel transition of the feedstock differing in the protein and fat content, as well as the heating and acidification pH. Prerequisites were considered to adjust printing parameters according to the pH−T-route, with conveying, cooling (sol−characteristics) and heating (trigger gelation) in different sections of the set-up.

Cold acidified dairy formulation showing sol−characteristics ($G \sim 0.1$ Pa, $T_{sol–gel} < 5$ K) were conveyed as a sol from the cooled syringe over an insulated hose to the temperature-controlled nozzle, where the sol−gel transition of the feedstock was triggered via a temperature increase. The use of high dairy protein-based formulations differing in product (e.g. protein content) and process parameters (e.g. the pH at heating) showed the suitability of the food printing set-up to induce temperature-triggered gelation under dynamic conditions via the pH−T-route. Small rectangular shapes were printed, if the previously established design rules from formulation engineering of the feedstock were adhered to.

6.5 References

Cheyne, A., Barnes, J., & Wilson, D. I. (2005). Extrusion behaviour of cohesive potato starch pastes: I. Rheological characterisation. Journal of food engineering, 66(1), 1-12.

Hao, L., Mellor, S., Seaman, O., Henderson, J., Sewell, N., & Sloan, M. (2010). Material characterisation and process development for chocolate additive layer manufacturing. Virtual and Physical Prototyping, 5(2), 57-64.

Kern, C., Weiss, J., & Hinrichs, J. (2018). Additive layer manufacturing of semi-hard model cheese: Effect of calcium levels on thermo-rheological properties and shear behavior. Journal of food engineering, 235, 89-97.

Le Tohic, C., O'Sullivan, J. J., Drapala, K. P., Chartrin, V., Chan, T., Morrison, A. P., ... & Kelly, A. L. (2018). Effect of 3D printing on the structure and textural properties of processed cheese. Journal of Food Engineering, 220, 56-64.

Lille, M., Nurmela, A., Nordlund, E., Metsä-Kortelainen, S., & Sozer, N. (2018). Applicability of protein and fiber-rich food materials in extrusion-based 3D printing. Journal of Food Engineering, 220, 20-27.

Matz, S. A. (1991). Chemistry and technology of cereals as food and feed. Springer Science & Business Media.

Nöbel, S., Seifert, B., Schäfer, J., Daffner, K., & Hinrichs, J. (2018). Oral presentation Food Colloids, Leeds (2018) - Session - Processing of Novel Structures for Functionality. Temperature-triggered gelation of milk concentrates applied to 3D food printing.

Ross, M. M., Kelly, A. L., & Crowley, S. V. (2019). Potential Applications of Dairy Products, Ingredients and Formulations in 3D Printing. In Fundamentals of 3D Food Printing and Applications (pp. 175-206). Academic Press.

Schutyser, M. A. I., Houlder, S., de Wit, M., Buijsse, C. A. P., & Alting, A. C. (2018). Fused deposition modelling of sodium caseinate dispersions. Journal of Food Engineering, 20, 49-55.

Sun, J., Zhou, W., Yan, L., Huang, D., & Lin, L. Y. (2018). Extrusion-based food printing for digitalized food design and nutrition control. Journal of Food Engineering, 220, 1-11.

Tan, C., Toh, W. Y., Wong, G., & Lin, L. (2018). Extrusion-based 3D food printing–Materials and machines.

Toh, W. Y., Li, L., Chua, C. K., & Wong, G. (2018). Comparison of existing 3D food printers.

Warner, E (2019). Design and characterisation of edible biopolymer mixtures for use in additive manufacturing (Doctoral dissertation, University of Birmingham).

7 Chapter:

Conclusions and suggestions for future work

7.1 Conclusion

The objective of this research was to investigate dairy protein-based formulations regarding applications for extrusion-based 3D-printing via the pH−T-route, inclusive a sol−gel transition of the feedstock. Rheological results were applied to mimic extrusion behaviour during potential printing applications and formulations differing in product and process parameters were analysed. In-depth characterisation of high dairy protein-based formulations was conducted to expand the available feedstock of printable materials for thermal extrusion printing.

This study aimed to determine design rules, which allow to asses formulations regarding their printability to avoid a time- and resource-intensive trial-and-error approach. Detailed conclusions were presented at the end of each of the peer-reviewed result chapters within this work. This final chapter summarises the overall findings of this work and aims to highlight ideas for future work.

7.1.1 Development of novel dairy protein-based formulations

Most of the current extrusion printing of dairy-based formulations relies on pastes/gels, which maintain their shape after extrusion due to a yield stress, depending on their overall composition. On the contrary, this study aimed to develop formulations which undergo a thermal sol−gel transition of the feedstock. As casein was well investigated over the last decades and represents the main protein contributing to gelation and firmness in dairy-based products, it was chosen as the key material for this work.

The addition of whey protein and the change in process parameters allowed to modify the composition of the casein micelle, to change the type of casein−whey protein complexes and to manipulate the sol−gel transition temperature as well as the aggregation rate. Formulations differing in the concentration of the two main proteins as well as of the additional product parameter dairy fat, the pH at heating and the acidification pH were investigated in order to find novel edible and printable feedstock.

7.1.2 Design rules to create dairy protein-based formulations for applications in extrusion-based 3D-printing

The whole interplay of product and process parameters during the formulation engineering approach was necessary to characterise and understand dairy-based formulations regarding thermal extrusion printing. A suitable gelation mechanism as well as the precise adjustment of product and process parameters allowed to create and to tailor suitable formulations, as shown below in *Figure 7-1*.

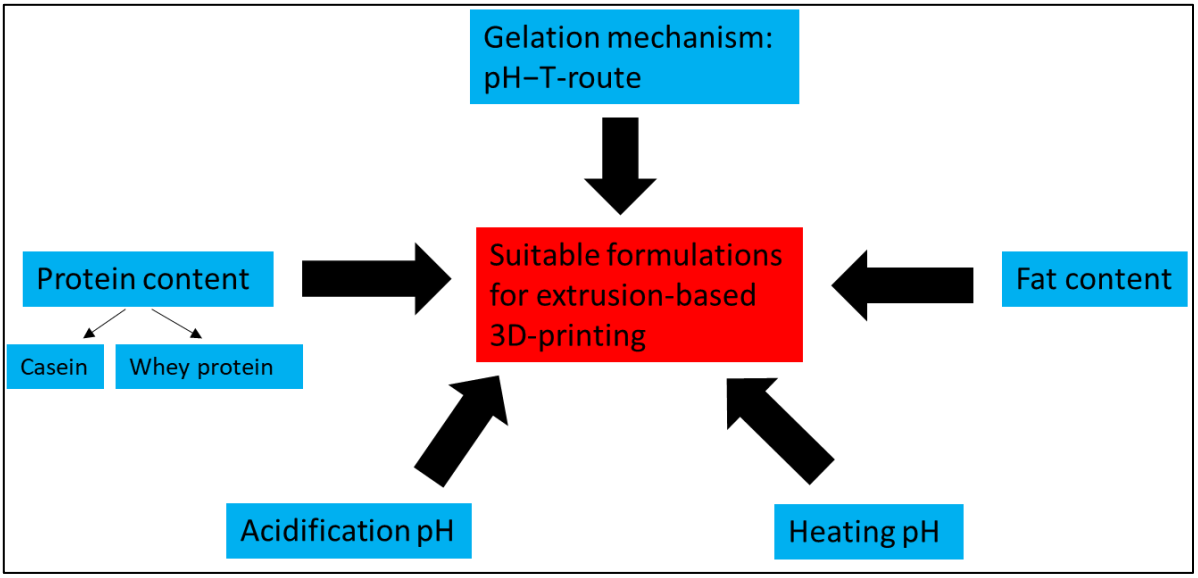

Figure 7-1: Interplay of a suitable gelation mechanism as well as product and process parameters to create dairy-based formulations for applications in thermal extrusion printing.

To formulate for structure and texture via 3D-printing inclusive a sol−gel transition, the following **set of design rules** has been determined in order to characterise casein-based formulations via the pH−T-route:

- The temperature–time profile from quasi steady−state heating (1 K/min) was found to be comparable to 3D-printing but without superimposed flow. The change in the temperature, demonstrated by a steep increase (approx. 30 K/min) of the casein-based formulations, was induced on a Peltier plate in order to mimic the printing set-up in the nozzle. Therefore, these results provided clear evidence that the pH−T-route is a suitable mechanism to trigger gelation under dynamic conditions.

- Casein−whey protein suspensions have to be prepared at a minimum overall protein content of 10.0% (w/w), consisting of 8.0% (w/w) casein and 2.0% (w/w) whey protein, to ensure that enough protein is available to entrap the serum phase during a fast and irreversible gelation process via the pH−T-route. To conclude, all formulations containing equal or less than 6.0% (w/w) casein and 1.5% (w/w) whey protein hinder a fast gelation and cannot be printed.

- Casein−whey protein suspensions can only be prepared at a maximum overall protein content of 12.5% (w/w), consisting of 10.0% (w/w) casein and 2.5% (w/w) whey protein, depending on the pH value at heating during whey protein denaturation, to maintain sol−characteristics. Formulations containing of 15.0% (w/w) protein, 12.0% (w/w) casein and 3.0% (w/w) whey protein, result in gel−characteristics (G' > 1 Pa) at low pH values of 4.8 and 5.0; therefore, no sol−gel transition can be induced and none of these formulations can be printed.

- For a successful implementation of the pH−T-route for thermal extrusion printing, high dairy protein-based formulations have to be cold acidified at 2°C to pH values of 4.8 or 5.0. At a pH ≥ 5.2, the gelation process is significantly decelerated, shown by a decrease in the aggregation rate (< 250 Pa/ 10 K), independent of the protein content or the pH at heating adjusted for denaturation of the whey proteins. To conclude, dairy-based formulations with an acidification pH ≥ 5.2 cannot be printed via the pH−T-route.

- If the pH at heating during denaturation of the whey proteins is adjusted to 6.55, casein−whey protein suspensions have the same sol−gel transition temperature as pure micellar casein-based formulations. On the other hand, if the pH at heating is increased to 6.9 or 7.1, sol−gel transition temperatures were found to decrease, shown by a shift of the coagulation line. This information is crucial to convey results from resting to

dynamic conditions and therefore has to be applied to adjust the temperature during a printing process to trigger particles to aggregate and to cause gelation, as well as to avoid clogging in the nozzle.

- If the pH at heating is increased to 6.9 or 7.1, dissociation of κ-casein results in casein micelles partly depleted of κ-casein, therefore providing less steric repulsion forces. It was concluded that formulations with κ-casein depleted casein micelles mostly show faster aggregation rates than those heated at pH 6.55, resulting in more promising formulations for thermal extrusion printing.

- Casein−whey protein suspensions were printable if values of 250 Pa/ 10 K for the aggregation rate (represented by the storage modulus G') were reached or exceeded, independent of the pH at heating adjusted for each formulation before denaturation.

- Dairy fat at total concentration of 1.0, 2.5 or 5.0% (w/w) can be added to protein-based suspensions to create more complex and novel formulations. If dairy fat is added to casein−whey protein suspensions, mechanical treatment has to be applied to reduce the particle size of the milk fat globules to less than 1 µm to guarantee a) sol−characteristics of the formulations and b) a fast and irreversible gelation process via the pH−T-route. A novel screening protocol for protein-fat suspensions in the nanometre range combined with SDS-PAGE allowed visualisation and in-depth characterisation via degrading protein and fat particles with the use of a dose-dependent radiation damage obtained by a controlled electron dose.

- If dairy fat is added to casein−whey protein suspensions, not all formulations reaching or exceeding 250 Pa/ 10 K were found to be printable or resulted in firm and stable gels. After heating at pH 6.55, milk fat globules had stronger steric repulsion forces due to κ-

casein/ κ-casein-β-lactoglobulin complexes on the outside of the CM, protruding into the serum, thereby hindering fast gelation under dynamic conditions. It was concluded that if formulations were heated at pH 6.9 or 7.1, κ-casein depleted CM covered the milk fat globules, which caused higher aggregation rates and formulations were found to be more suitable for printing.

By following these design rules presented, it was possible to create novel soft matter gels (dairy protein-based formulations) which could be used for extrusion-based printing of simple rectangular squares (25 x 25 x 3 mm). In the future, a more sophisticated printing set-up will help to print more complex formulations based on the design rules established in this study. Nevertheless, food printing will never replace the current mass production (like current manufacturing methods), but will allow to create small amounts of customised food, e.g. for special needs (soft matter gels for people with dysphagia) or for special creations in high class restaurants. The pH−T-route will therefore be suitable for extrusion-based printing of dairy-based products with certain amounts of protein and fat.

7.2 Suggestions for future work

The goal of this work was to understand the interplay of a solidification mechanism combined with product and process parameters towards printing under dynamic conditions, which could be successfully implemented. Additional changes in the product and process parameters to create more complex formulations will provide further evidence if the pH−T-route is a viable route to print multicomponent feedstock, and if as well as how far the current dairy-based formulations can be changed and tailored while maintaining their printability. This would further prove that the current solidification mechanism is the most suitable tool to print dairy protein-based formulations mixed with additional ingredients, resulting in novel, complex and individualised food products, if a sol−gel transition is conducted.

Having investigated dairy protein-based formulations in great depth, it would be interesting to see how the addition of hydrocolloids (e.g. xanthan) or enzymes (e.g. transglutaminase) changes the overall (micro-) structure and the extrusion-based printability. The addition of hydrocolloids to protein-based formulations could on the one hand help to further tailor formulations and trigger gelation and on the other hand to increase the feedstock of edible and printable materials. While tertiary protein-hydrocolloid systems were well analysed in the past, the specific type of hydrocolloid, the overall amount and the addition of these ingredients at a particular time/ process step will still be crucial to find suitable formulations for extrusion-based thermal printing. Based on results and design rules established in this study, more work would be necessary to characterise these formulations, to tailor their material properties and to trigger a fast and irreversible gelation via the pH−T-route.

Moving away from the formulation engineering approach and the in-depth characterisation of the feedstock, the whole set-up of food printers will require more detailed work, as e.g. the current printing speed cannot satisfy consumers' needs. The creation of a 100% reliable and reproducible printer will be important, as most of the research is conducted with customised equipment which complicates reproducibility. Creation of an extrusion-based printer with a printing unit (movement of print head to control the printing speed) and a feed tank (extrusion of material to control the volume flow) working independently controlled from each other would result in a continuous flow of material and prevent clogging of the material in the nozzle during breaks of printing. Although such a set-up will increase the amount of lost material, the accuracy of printing and the overall reproducibility would become better.

Moreover, working with different nozzle sizes and geometries will further help to achieve novel textures and shapes. Depending on the formulation and its particle size distribution, a minimum nozzle/ die size will be given. As dairy-based formulations were characterised in-depth, configuration of the printing parameters should be optimised in the next step.